N-containing Polyaryl Ligands in Coordination and Supramolecular Chemistry

Angelika Graczyk
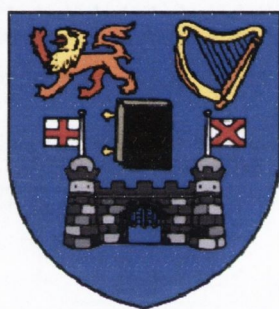
A thesis submitted to the University of Dublin for the degree of

Doctor of Philosophy

School of Chemistry

Trinity College Dublin
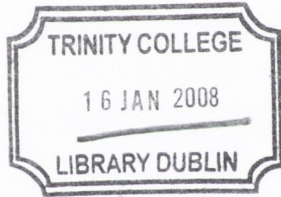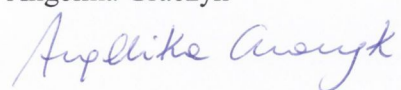
January 2007

Declaration

This thesis has not been submitted as an exercise for a degree at this or any other university. Except where acknowledgement is given, all work is original and was carried out by the author alone. I agree that the library may lend or copy this thesis upon request.

Angelika Graczyk

Summary

Part 1 describes the synthetic route and the characterisation of a family of nitrogen heterosuperbenzene compounds. Those polyaromatic ligands, which contain a fused dipyrimidine unit possess unusual photophysical properties and are ideal for transition metal coordination. The novel homoleptic Ru(II) complexes and their photophysical properties are presented.

Part 2 The supramolecular ability of novel pyridine-centered compounds is presented in this chapter. The ligands are analogues of pyterpy and possess two or four independent coordination units. New Ln(III), Cd(II) and Cu(II) coordination polymers have been synthesised and six of them are structually characterised by single crystal X-ray analysis. In the case of Ln(III) and Sm(III) a hydrogen-bonded and coordination polymer is former. The cooper coordination polymers show very unique structures involving Cu(II) and the I^- counterion situated on the face of the central pyridine ring. There are three different environments for Cd(II) and bridging SO_4^{2-} anions in the three dimensional polymer involving this metal.

Part 3 shows the synthesis of new terpyridine type of compounds. The [2+4] Diels-Alder reaction between acetylene substituted terpyridine and substituted tetraphenylcyclone gave two novel compounds. Those pentaphenylbenzene substitued terpyridines are ideal ligands for transition metal complexes. The oxidative cyclodehydrogenation reaction gave the partially cyclised ligand, which combines the properties of both terpyridine and highly delocalised platform of nine fused aromatic rings. The novel homo and heteroleptic complexes with Ru(II) were synthesised and their photophysical properties were tested and discussed.

Part 4 involves the synthesis of Fe(II), Pt(II) and Pd(II) complexes with ligands synthesised in Part 3. The analysis of ^{1}H NMR spectra are present. The photophysical properties of these complexes were tested and discussed.

Part 5 gives the experimental details of this work.

Acknowledgement

Table of Contents

List of figures

xiii

List of schemes

List of tables

Abbreviations

1D	one-dimensional
2D	two-dimensional
abs	absorption
AcO	acetate
An	anthracene
Anal	elemental analysis
Ar	aryl
binap	2,2'-bi-1,8-naphthyridine
biq	2,2'-biquinoline
bpy	2,2'-bipyridine
br	broad
Bu	butyl
Calcd	calculated
CCDB	Cambridge Crystallographic Data Base
COSY	Correlation spectroscopy
d	doublet
dibneil	dibenzoeilatin
dd	doublet of doublets
DMF	dimethylformamide
DMPD	1,4-dimethylpiperazine-2,3-dione
DMSO	dimethylsulfoxide
eil	eilatin
em	emission
ESI-MS	electro spray mass spectrometry

EtO	ethoxy
Gs	ground state
HBC	hexa-peri-hexbenzocoronene
HOMO	highest occupied molecular orbital
IR	infrared
J	coupling constant
L	ligand
LC	ligand centred
LMCT	Ligand-to-metal-charge transfer
LUMO	lowest unoccupied molecular orbital
m	multiplet
M	metal
M	molarity
m.p.	melting point
m/z	mass to charge ratio
MALDI-TOF MS	Matrix-assisted laser desorption/ionisation – time of flight mass spectrometry
max	maximum
MC	metal centered
Me	methyl
MHz	megahertz
MLCT	metal to ligand charge transfer
MO	molecular orbital
MS	mass spectrometry
N-½HSB	half-cyclised N-heterosuperbenzene
N-HSB	N-heterosuperbenzene

nBuli	Lithium-1-butanide
nm	nanometer
NMR	nuclear magnetic resonance
nOe	nuclear Overhouser effect
OTf	Trifluoromethanesulfonate
PAH	polycyclic aromatic hydrocarbon
Ph	phenyl
phen	1,10-phenantroline
PIFA	phenyliodine(III) bis(trifluoroacetate)
ppm	part per million
PPP	poly(p-phenylene)
s	singlet
t	triplet
t or *tert*	tertio
taphen	dipyrido[3,2-c:2',3'-e]-pyridazine
THF	tetrahydrofuran
TLC	thin layer chromatography
TOCSY	Total correlation spectroscopy
tpt	2,4,6-tris(2-pyridyl)-1,3,5-triazine
UV-vis	ultraviolet-visible
δ	chemical shift
ν	stretching frequency

Part 1: Synthesis of N-heterosuperbenzenes and their Ru(II) complexes

1.1. Introduction

1.1.1. Superbenzenes

Polycyclic aromatic hydrocarbons (PAHs), which can be formally regarded as a two-dimensional graphite section, represent one of the most intensively investigated class of compounds with materials application.

Alkyl substituted derivatives of such large aromatic molecules form discotic liquid crystals with unusual properties (Figure 1).[1,2] They have the potential to undergo one-dimensional transport processes facilitating energy migration, electrical conductivity and photoconductivity.
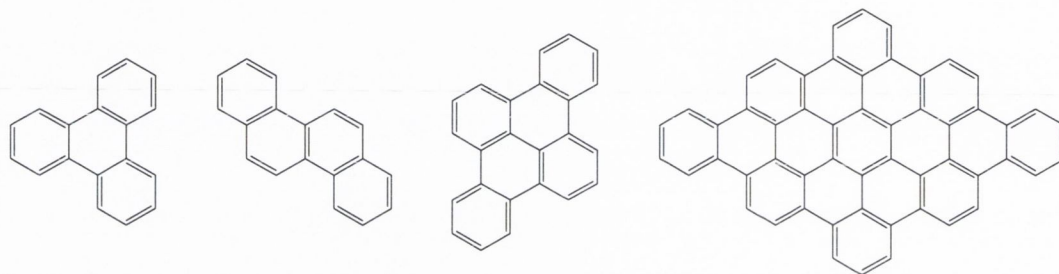
Figure 1: Examples of polyaromatic hydrocarbons.

In 1960s Kovacic *et al.* polymerized benzene and its derivatives to poly(*p*-phenylene) (PPP) under mild reaction conditions (Scheme 1). They employed copper(II) chloride as an oxidant and aluminum(III) chloride.[3,4] The PPPs reported by Kovacic were non-selective in terms of the size and the shape. This pioneering reaction demonstrated multiple C-C bond formation and opened the way for creating a highly selective oxidative dehydrogenation process to convert oligophenylenes to polyaromatic hydrocarbons.
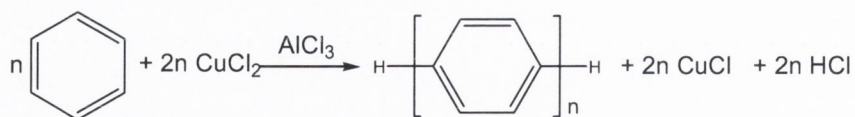
Scheme 1: Oxidative polymerization of benzene under Kovacic conditions.[1]

Müllen *et al.* have developed a route to a series of predefined all-carbon framework PAHs, the "superbenzenes" *via* the cyclodehydrogenation of a polyphenylene precursor. The molecules, such as: hexa-peri-hexabenzocorenene (HBC)

(superbenzene) (**1**) and supernaphthalene (**2**) (Figure 2)[5] are two members of this great family of compounds. The soluble derivatives of HBC and its higher homologues were synthesised by substitution in the free para possitions with long chains or with bulky *tert*-butyl groups. The substituted molecules are less disposed to graphite-like stacking.
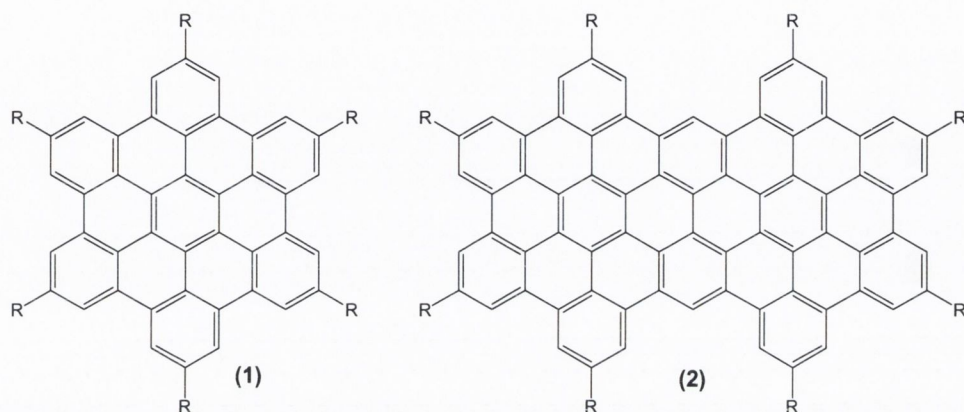
Figure 2: Two members of the PAHs family, R: H, t-butyl.[5]

1.1.2. Müllen's hexa-peri-hexabenzocoronene, HBC

Due to its hexagonal symmetry, and extended aromatic framework, HBC serves as an intriguing homologue of benzene with unique electronic properties. Using HBC as a starting point for investigating the benzene-like chemistry of molecular graphite subunits, a large number of structural modifications have been performed. Increasing the size, and varying the peripheral substitutents of disk-like PAHs molecules influences not only their two-and three-dimensional superstructures,[2] but also their electronic properties. The all-benzenoid hydrocarbons can have different numbers of C_6 rings, each aromatic sextet possessing six π-electrons. Electrons originating in the unhybridised p-orbital on the C atoms are free to move within the sheets in delocalised π-orbitals. As a consequence of their extensive delocalisation, it is believed that polycyclic aromatic hydrocarbons (PAHs) will find extensive and valuable applications in the area of molecular electronics. The synthesis of large PAHs molecules consists of two main steps: the synthesis of nonplanar and soluble oligophenylene precursors and their subsequent oxidative cyclodehydrogenation. Generally the preparation of the nonplanar precursors is achieved either by the

cyclotrimerisation of diarylacetylenes or Diels-Alder reaction between tetraarylcyclopentadienone and diarylacetylene (Scheme 2).[1]
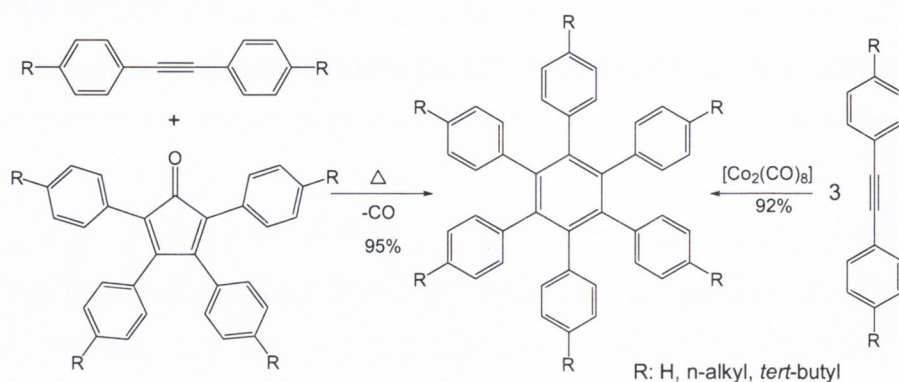
Scheme 2: Route to oligophenylene by intermolecular Diels-Alder reaction, or cyclotrimerization catalysed by dicobaltoctacarbonyl.[1]

Müllen and coworkers use a variety of oxidant compounds for cyclodehydrogenation, including Kovacic conditions copper(II) chloride/aluminum(III) chloride,[6] then copper(II) trifluoromethanesulfonate/aluminum(III) chloride,[7] iron(III) chloride[8] and molybdenum(V) chloride.[9]

A new method to achieve the soluble hexaperi-hexa benzocoronene was discovered by Rathore and Burns.[10] To omit the multi-step synthetic route for substituted polyphenylene precursors they developed a simple and practical synthesis of a soluble HBC. The substitution of the para positions with *tert*-butyl groups and the oxidative cyclodehydrogenation are done in a one-pot reaction. Iron(III) chloride was used both as an oxidant and a Lewis acid catalyst (Scheme 3).
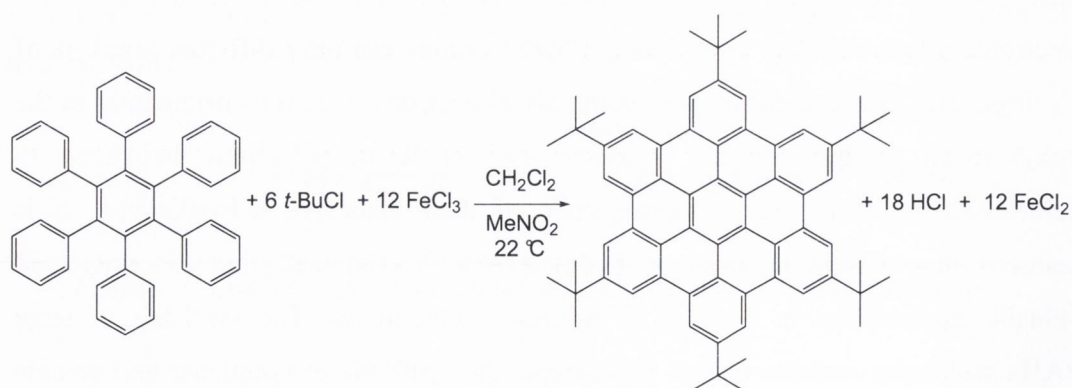
Scheme 3: Synthesis of t-butyl substituted HBC.[10]

1.1.3. N-heterosuperbenzene family

N-heterosuperbenzene is a nitrogen-containing analogue of Müllen's more classical all-carbon "superbenzene". Like superbenzene, it comprises 13 fused aromatic rings; unlike superbenzene two of these rings are functionalized with two nitrogen atoms in a pyrimidine-like substitution patern.[11,12] N-HSB retains the high thermal stability which also characterizes the superbenzenes, with decomposition occuring at approximately 450°C with loss of the *tert*-butyl groups. As a consequence of nitrogen functionalisation, N-HSB also has increased solubility in comparison with its all-carbon analogues. N-HSB is soluble in common organic solvents like benzene, chloroform, acetone and methanol.

The synthesis of N-heterosuperbenzene (Scheme 4) is based on Müllen's route to obtain superbenzene *via* the cyclodehydrogenation of a polyphenylene precursor.

The synthetic route to N-HSB involves a number of steps. The precursor (**7**) for heterosuperbenzene is generated in a stepwise manner by Diels-Alder reaction of di-(pyrimidin-3,5-yl) ethyne (**6**) with 2,3,4,5-tetra-(4-tert-butylphenyl) cyclopenta- dien-1-one (**5**). The choice of starting materials and the established stereochemistry of the [2+4] cycloaddition reaction ensures the ortho-arrangement of the pyrimidine subunits on the benzene core of (**7**). The oxidative cyclodehydrogenation of (**7**) using two different sets of oxidising agents gives both fully cyclised N-HSB (**8**) and its half-cyclised daughter N-½HSB (**9**).
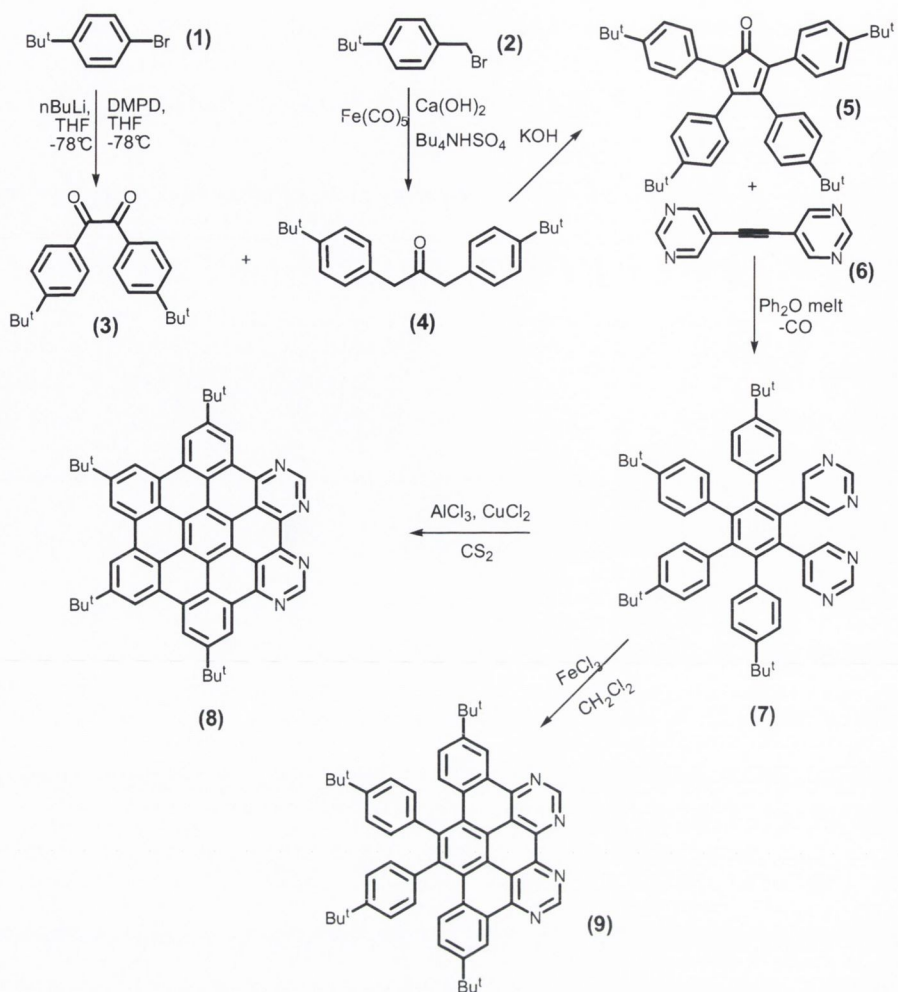
Scheme 4: Synthesis of N-HSB (8) and N-½HSB (9).[11]

N-heterosuperbenzene (**8**) is a fusion of both superbenzene and bipyrimidine, giving it physical, electrochemical and photochemical properties, which supersede both. The enhanced π-electron mobility of N-HSB is due to the polar nature of the molecule, which results from the structural opposing of the electronegative nitrogen atoms and weakly donating *tert*-butyl groups.[11]

(a) The UV-vis absorption spectra of (**8**) (conc.6.66*10⁻⁷M) in toluene, (i-v) sequential addition of (i) 0 µL, (ii) 5 µL, (iii) 10 µL, (iv) 50 µL, (v) 110 µL of trifluoroacetic acid (0.1 M).

b) The fluorescence spectra of (**8**) (conc.6.66*10⁻⁷M) in toluene, (i-vii) sequential addition of (i) 0 µL, (ii) 5 µL, (iii) 10 µL, (iv) 50 µL, (v) 110 µL, (vi) 200 µL, (vii) 450 µL of trifluoroacetic acid (0.1 M).
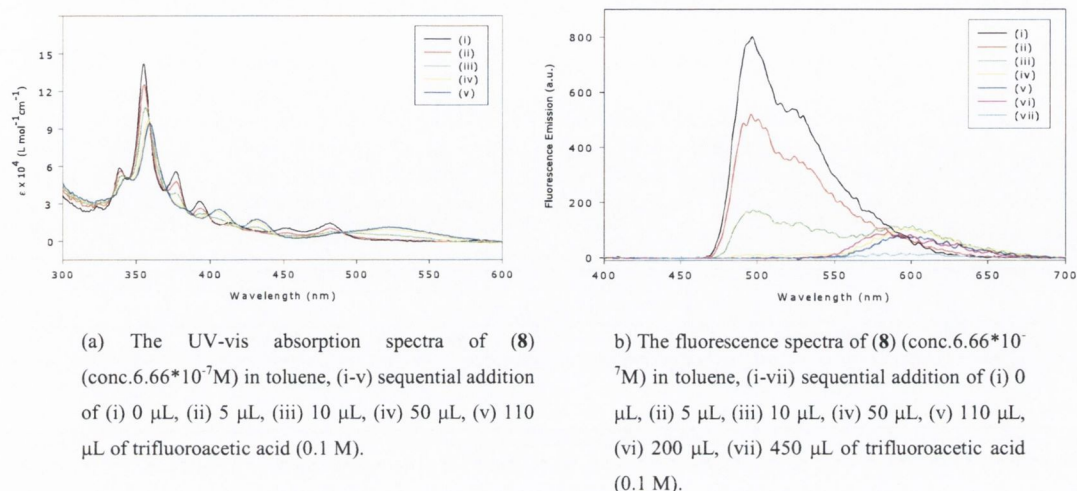
Figure 3: The absorption (a) and fluorescence (b) spectra of 8 on addition of trifluoroacetic acid. [11]

The UV-visible spectrum of N-heterosuperbenzene displays the characteristic absorptions of hexa-peri-coronene with two weak bands at 450 nm and 490 nm, which are $\pi \rightarrow \pi^*$ transitions Figure 3(a).[11] The spectrum also contains a new band at 372 nm, which is an $n \rightarrow \pi^*$ transition[11] resulting from the introduction of nitrogen. N-HSB exhibits a strong green emission in toluene under both visible and UV light. A very strong fluorescent band is observed in toluene at 494 nm, Figure 3(b). Protonation of the peripheral nitrogen atoms by the gradual addition of acid quenches the fluorescence and changes the UV/vis spectrum. The decrease in intensity of the 355 nm absorption band along with the disappearance of the 372 nm band in the UV/vis spectrum indicates that nitrogen protonation has a profound electronic effect on the π-electron density of the system.

The second member of the N-heterosuperbenzene family is half-cyclised N-HSB (N-½HSB) (**9**). N-½HSB was discovered when a different oxidative cyclodehydrogenation catalyst was used.[13] AlCl₃/CuCl₂ was replaced by FeCl₃. The N-½HSB daughter molecule possesses eight fused aromatic rings and two uncyclised phenyl rings, which can rotate out of the plane. The UV-vis absorption spectrum of N-

½HSB is shifted to the blue compared to N-HSB (Figure 4), this is due to the reduced aromaticy of N-½HSB. The λ_{max} in the spectrum of N-½HSB (291 nm) appeared at higher energy with respect to N-HSB (355 nm). The lowest energy absorption for N-½HSB is present at 429 nm, for N-HSB at 481 nm. The same type of behaviour was observed for the emission spectrum. The λ_{max}^{em} for N-½HSB is blue shifted compared to N-HSB (474 nm compared to 494 nm respectively).[11,13]
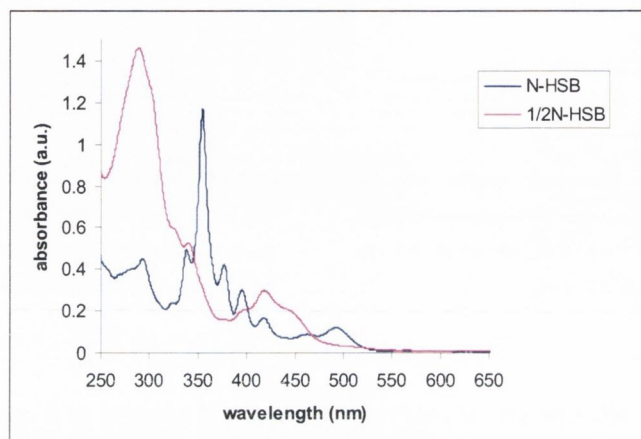
Figure 4: The UV-vis spectra of N-HSB and N-½HSB in chloroform.

The mechanism of the oxidative cyclodehydrogenation reaction of oligophenylene precursors is still under investigation. There are few examples of the theoretical study presented in the literature.[9,14,15] The fact that each oligophenyl precursor with a different oxidising agent has to be verified individually makes the problem even more complicated. C-C bond formation requires the elimination of two protons, which are evolved as HCl molecules. Analogous conditions to those proposed by Kovacic (Scheme 1) can be used, except for the fact that the reaction in this case is intramolecular. In practice it means each bond created will increase the size of the PAH being formed.

The cyclisation of oligophenylenes when successful allows for the generation of topologically complex graphite sheets. Two main pathways based on the School reaction have been proposed.[15] In 1910, Scholl investigated the acid-catalysed oxidative condensation of aryl groups. Scheme 5 shows two mechanisms, which have since been examined by computational and experimental chemistry. The C-C bond generation in the arenium-cation mechanism (Scheme 5a) is due to the reaction between electrophilic complex (**11**) with another aromatic core. Compound (**11**) was

8

created by the protonation of (**10**). The intermediate (**12**) was obtained by deprotonation and later dehydrogenation gave the fully aromatic product (**13**).
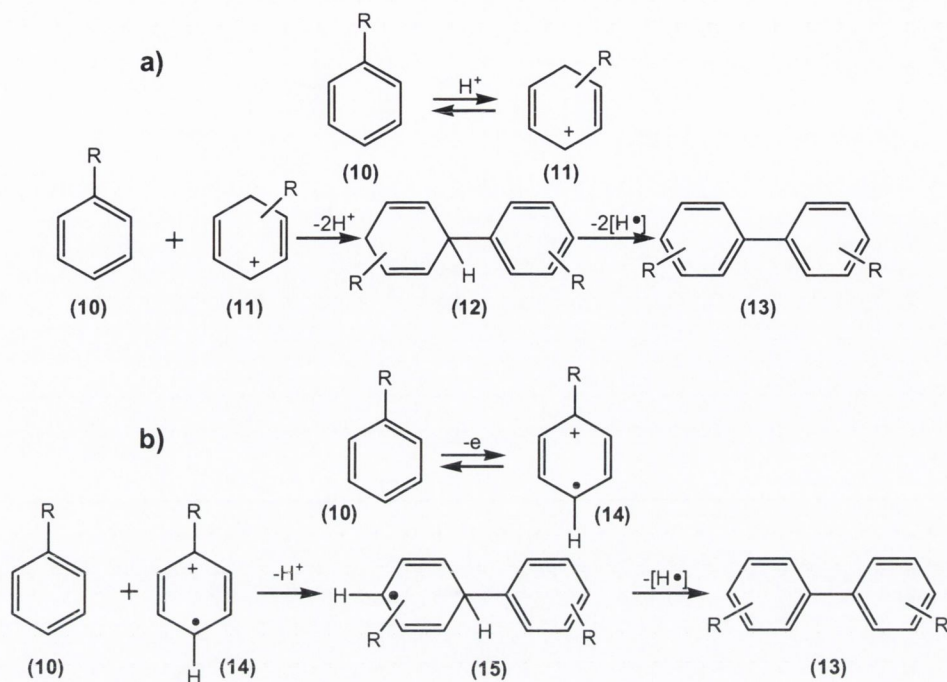
Scheme 5: Proposed mechanisms of the Scholl reaction: a) arenium-cation mechanism, b) radical-cation mechanism.[15]

The second pathway proposed is a radical cation mechanism (Scheme 5b). The starting material gave a radical cation (**14**) by one-electron oxidation. The radical cation reacted with another aromatic core to generate the C-C bond and deprotonation reaction occurred at the same time. The loss of the proton from the intermediate (**15**) gave aromatic dimer (**13**).

A comparison of these mechanisms shows that the arenium cation mechanism involves lower energy transition states than the radical cation mechanism. In large systems, like oligophenylene the arenium cation mechanism is more favoured. Acidic media do not promote radical cation formation. It is believed that the School reaction of unsubstituted oliphenylenes occurs by an arenium cation mechanism.

In the case of N-HSB, due to the presence of four nitrogen atoms the situation is more unclear, but it is believed that the oxidative cyclodehydrogenation of 1,2-dipyrimidyl-3,4,5,6-tetra(4-*tert*-butylphenyl)benzene (**7**) also proceeds by the arenium cation mechanism. The precursor for N-HSB, on protonation the pyrimidine ring can act as an electrophile. This might explain the bond formation *ortho* to the N atoms in

pyrimidine rings. The protonation of the phenyl ring is anticipated to be more difficult; the basic nitrogens will gain the protons as a first step and bare the positive charge. Different oxidative agents result in a variety of products, probably due to dissimilar metal coordination.

The functionalisation of N-HSB and N-½HSB with nitrogen donor atoms offers one further property on the molecule: it can be used as a ligand for coordination chemistry.

1.1.4. Ruthenium(II) complexes.

Ruthenium(II) complexes are the object of investigation as they can interact with light by absorbing, emitting and transmitting light as photons or as electronic excitation. Particular attention has been paid to complexes with aromatic ligands containing donor atoms for example polypyridine complexes.

In the field of coordination chemistry, Ru(II) polypyridine complexes play an important role, especially in the development of photochemistry,[16] photophysics, electro-chemistry[6] and electron and energy transfer.[17]

The properties of such complexes can be tuned by the right choice of ligand. The most satisfactory ligands are polypyridine derivatives with extended aromatic cores, such as: N-HSB (**8**),[18] N-½HSB (**9**),[13] eilatin (eil) (**16**),[19] 1,12-diazaperylene (**17**),[20] 1,10-phenanthroline (phen) (**18**)[21] (Figure 5). They have drawn attention due to advantages of rigid, delocalised aromatic planes in the electronic communication between metal and ligand.
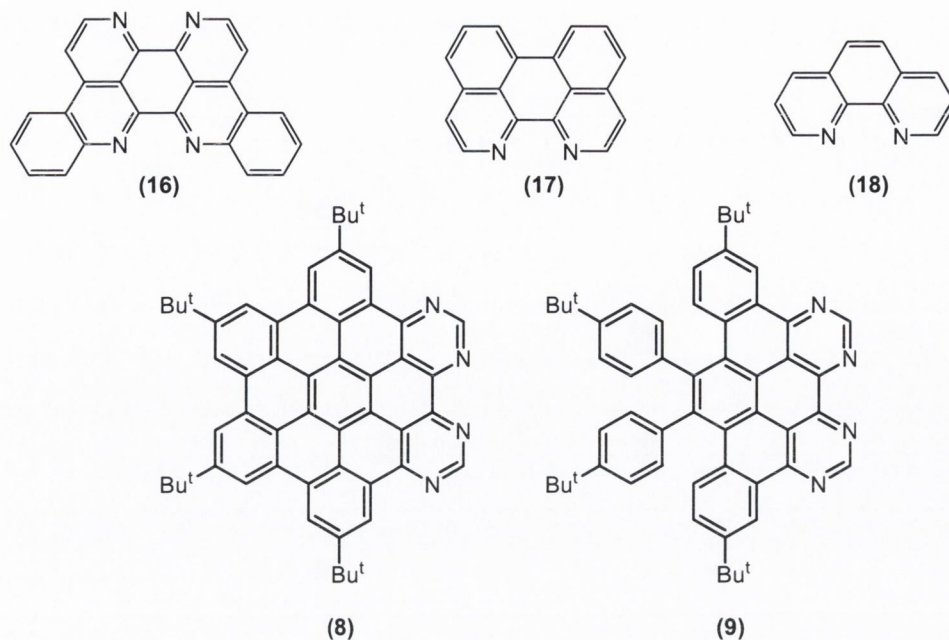
Figure 5: Examples of bidentate polyaromatic ligands.

The spectroscopic, redox and kinetic properties of transition metal complexes are usually discussed with the assumption that the ground states and the redox species can be described in an approximate way by a localized molecular orbital configuration according to Scheme 6.[22]
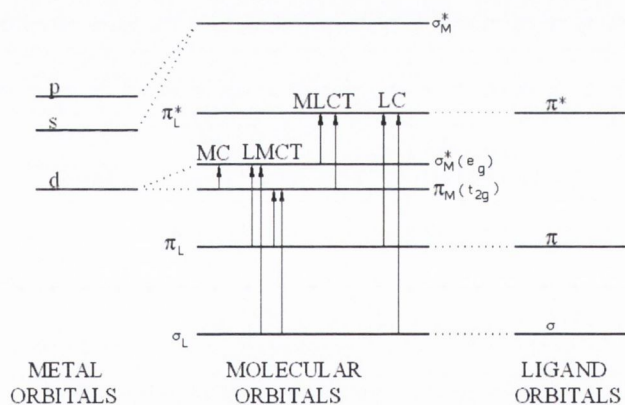
Scheme 6: Schematic energy-level diagram for an octahedral transition metal complex.[22]

In this diagram each molecular orbital (MO) is labelled as metal (M) or ligand (L). The low energy σ-bonding MO is a result of the combination of metal and ligand orbitals. Light absorption or a change in redox state causes the energy of the molecular orbitals to change; hence each excited state and redox state is described by

a unique MO configuration. In the ground state transition metal complexes have their σ_L and π_L orbitals completely filled, π_M orbitals partially or completely filled and higher orbitals which are usually empty.

A transition between MO localized on the central metal is called a metal-centered (MC), ligand field or d-d transition. A transition between MO localized on the ligands is a ligand-centered transition. The interactions within the complex are weak enough that both metal and ligand properties are seen, yet are strong enough that complex transitions such as metal-to-ligand charge-transfer (MLCT) or ligand-to-metal charge transfer (LMCT) can occur.

Ruthenium(II) complexes are characterized by MLCT transitions. Ru^{2+} is a d^6 system and polypyridine ligands possess σ-donor orbitals localized on the nitrogen atoms and π donor and π^* acceptor orbitals delocalized on aromatic rings. The promotion of an electron from a π_M metal orbital to the π_L^* ligand orbitals gives rise to the metal-to-ligand charge transfer (MLCT) excited states. The promotion of an electron from π_M to σ_M^* orbitals gives rise to metal centered (MC) excited states. Ligand centered (LC) excited states can be obtained by promoting an electron from π_L to π_L^*. These excited states then have singlet or triplet multiplicity.

The most common examples of bidentate ligands in the literature are 2,2'-bipyridine (bpy) and 1,10-phenanthroline.[23,24] They have been used extensively to study the photoinduced electron and energy transfer in transition metal complexes. The introduction of large-surface nitrogen containing ligands, such as: N-HSB (**8**) and N-½HSB (**9**) plays a significant role in modifying the lowest ^{1}MLCT absorption and ^{3}MLCT emission bands in Ru(II) complexes. The Ru(II) complexes of large-aromatic ligands, with low lying π^* orbitals have great potential as "black MLCT" absorbers and near IR-emitters. The highly delocalised coordinated ligand N-HSB in the complex [Ru(bpy)$_2$(N-HSB)](PF$_6$)$_2$ (**19**) indicated an unusually low energy absorption band 615 nm, which was assigned to a MLCT transition to the H-NSB ligand (Figure 8).[18] For comparison λ_{max}^{abs} for [Ru(bpy)$_3$]$^{2+}$ appeared at 450 nm.[24] The lowest energy absorption for complex [Ru(bpy)$_2$(N-½HSB)](PF$_6$)$_2$ (**20**) is the MLCT band absorption due to the N-½HSB, λ_{max}^{abs} 591 nm.[13] The absorption band is shifted to the blue compared to (**19**) due to the less planar and less delocalised N-½HSB ligand.

The typical approach used to prepare polypyridine complexes is reacting ruthenium trichloride and an excess of ligand in aqueous ethanol followed by precipitation of the complex by PF_6^- counterion metathesis. Depending on the nature of the ligand, its solubility or sensitivity variations have been made to this synthetic procedure, including the use of solvents such as ethylene glycol, DMF, diethylene glycol ethyl ether and ethanol.[25] High temperatures can be required.[26] As an alternative to $RuCl_3 \cdot 3H_2O$ the more labile precursor $Ru(DMSO)_4Cl_2$[27] has been used.

The synthesis of [Ru(bpy)$_2$(N-HSB)](PF$_6$)$_2$ (**19**)[18] and [Ru(bpy)$_2$(N-½HSB)](PF$_6$)$_2$ (**20**)[13] extends the scope of coordination chemistry. These photoactive transition metal complexes have been prepared using the novel heterosuperbenzenes; N-HSB and N-½HSB, as ligands.

Figure 6 shows self-association of the Ru(II) complex (**19**) featuring a wide range of π-stacking. Due to the large, rigid aromatic core of N-HSB complex, (**19**) creates dimers by an offset π-stack. The π-stacking interaction between coordinated N-HSB has a big influence on the ^{1}H NMR spectroscopic analysis.
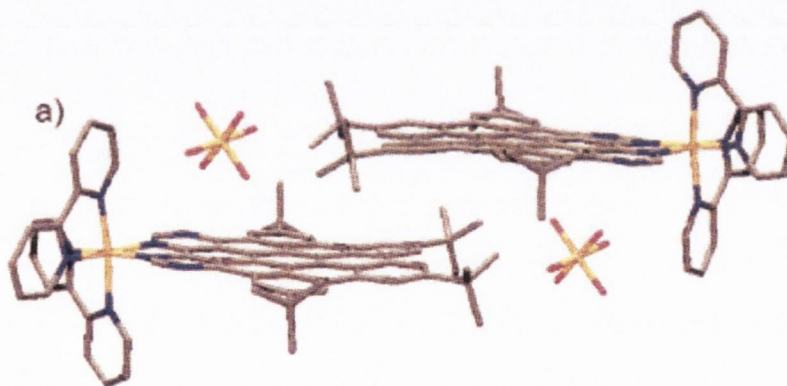
*Figure 6: Picture showing the aggregation of two molecules of complex [Ru(bpy)$_2$(N-HSB)](PF$_6$)$_2$ (**19**) and two PF$_6^-$ anions.[28]*

The ^{1}H NMR spectrum of (**19**) shows both temperature (Figure 7) and concentration dependence. The changes in chemical shifts and resolutions are consistent with extensive aggregation generating solution species held together by π-stacking.
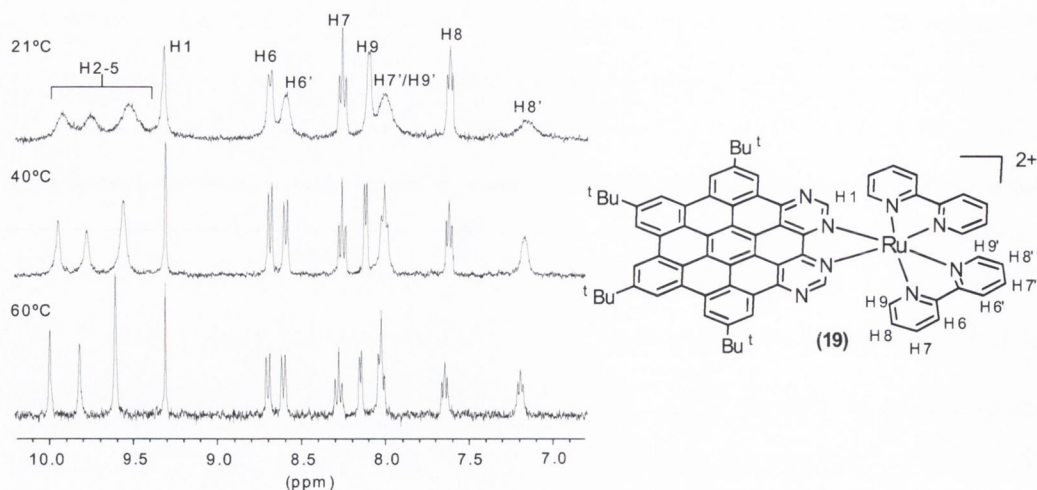
Figure 7: The ^{1}H NMR spectra of [Ru(bpy)$_2$(N-HSB)](PF$_6$)$_2$ (19), with assigned proton numbers at 21°C, 40°C and 60°C.[18]

The same behaviour was observed in Ru(II) complexes of other large ligands, such as eilatin, isoeilatin, 1,12-diazaperylene.[19,20,42] The complex (20) does not show temperature or concentration dependence in its ^{1}H NMR spectrum. This is due to the reduced aromaticy on N-½HSB, which possesses two uncyclised and flexible phenyl rings. Extended π/π^* frameworks of large aromatic ligands are known to decrease the energy gap between the ground and excited state, and stabilize the excited electron. This can shift the emission into the near IR. The enlarged π system of the N-½HSB and N-HSB in the Ru(II) complexes (20) and (19) result in the near infrared emissions, with the λ_{max}^{em} 868 nm and 880 nm respectively. ^{3}MLCT emission for (19) and (20) is shifted considerably to the red with respect to [Ru(bpy)$_3$]$^{2+}$ and the lifetimes are much shorter. This is a consequences of the reduced energy gap.[29,30]
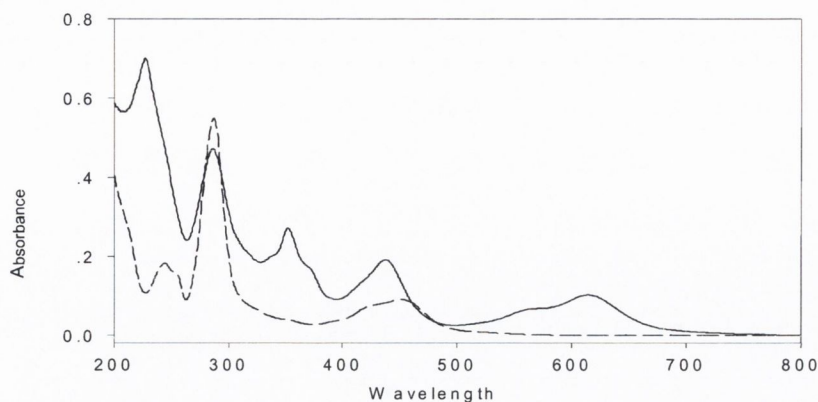
Figure 8: The UV-vis absorption spectra of [Ru(bpy)₂(N-HSB)](PF₆)₂ (solid line) and [Ru(bpy)₃]²⁺ (dashed line) in acetonitrile.[18]

Kol *et al*. developed eilatin-type of ligands and their octahedral Ru(II) complexes.[19] Eilatin-type ligands possess large fused aromatic surface and their complexes were found to exhibit interesting photophysical and electrochemical properties. Eilatin (**16**) possesses two types of binding sites: a bpy-type and biq-type (biq-2,2'-biquinoline), which are fused rigidly back to back. Isoeilatin (ieil) is a structural isomer of eilatin (eil) (Figure 9).
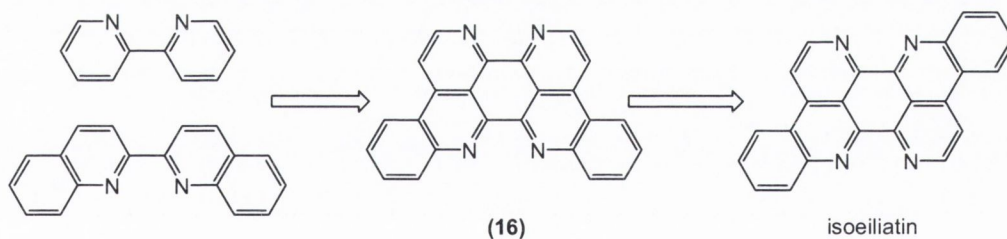
*Figure 9: The structures of eilatin (**16**) and isoeilatin ligands.*[19,42]

A series of eilatin complexes have been synthesized. In these complexes the ligand binds to the metal via its bpy-type side. Reacting [Ru(bpy)₂Cl₂] with eilatin in methanolic solution, and precipitation using NH₄PF₆ yielded the green solid of [Ru(bpy)₂(eil)][PF₆]. In the synthesis of the bis eilatin complex [Ru(bpy)(eil)₂][PF₆] [Ru(bpy)₂Cl₃]ₙ was used as a source of the metal. The [Ru(py)₄Cl₂] was used as a precursor for homoleptic complex [Ru(eil)₃][PF₆]. Due to the low-lying π^* orbital of eilatin ligand these complexes exhibit low-energy absorption attributed to a d_π (M)→π^* MLCT transition. The UV-vis absorption spectra (Figure 10) show that the

15

sequential replacement of bpy ligand by eil ligands moves the MLCT transition to lower energy. The MLCT band for heteroleptic complex $[Ru(bpy)_2(eil)]^{2+}$ appears at λ_{max} 583 nm, for $[Ru(bpy)(eil)_2]^{2+}$ at 594 nm and for homoleptic complex $[Ru(eil)_3]^{2+}$ at 596 nm. Upon the addition of eil ligand the intensity of the transition involving bpy ($\pi \rightarrow \pi^*$, 200-350 nm range) decreases, while the intensity of those transitions involving eil ligands increases.
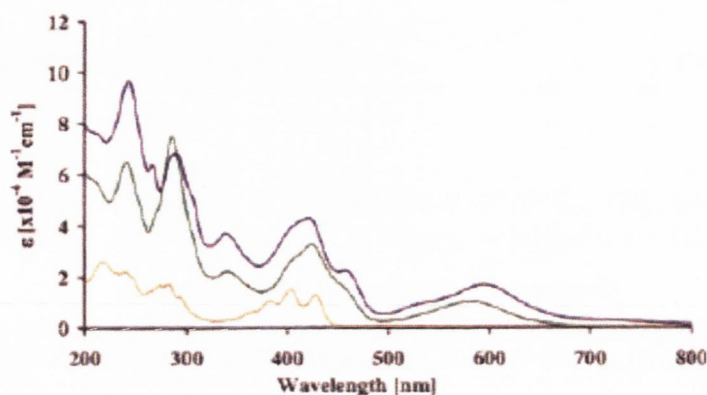
Figure 10: Absorption spectra of [Ru(bpy)(eil)₂][PF₆] (blue line),

[Ru(bpy)₂(eil)][PF₆] (green line) and eilatin (red line), recorded in acetonitrile.[19]

Ru(II) complexes of the eilatin-type of ligands can create dimers in solution and in the solid state. These dimers are formed by intermolecular π-π interaction between the molecules of eil.[19] The ^{1}H NMR spectra of Ru(II) eilatin-type complexes show the temperature and the concentration dependence and this effect increases due to the presence of additional eil molecules. Increasing dilution and the raising of temperature can break the intermolecular interactions. The isoeilatin complexes exhibit similar self-aggregation phenomena. Figure 11 shows the crystal packing of $[Ru(bpy)_2(ieil)][PF_6]$. The crystal lattice consists of dimers formed by a face-to-face π-stacking interaction through the isoelatin moiety. There is an interaction between isoeilatin molecules and molecules of toluene.[43]
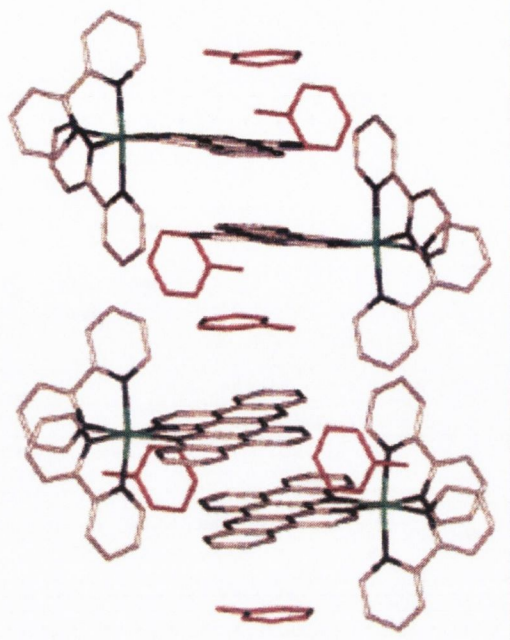
Figure 11: Crystal packing of [Ru(bpy)$_2$(ieil)][PF$_6$] complex. Counterion and acetonitrile solvent molecules are omitted for clarity.[43]

The aim of the first part of my research was to optimize the synthesis of N-HSB and its daughter N-½HSB. Preparing sufficient of each to be able to investigate their material properties. Secondly, novel transition-metal complexes of N-HSB and N-½HSB were synthesized and their photophysical properties established.

1.2. Results and discussion

1.2.1. Optimization of the synthesis of the N-heterosuperbenzene

N-heterosuperbenzene (N-HSB) was synthesized according to the strategy previously described in the introduction (Scheme 4) with a few modifications.

One of the precursors required for the synthesis of N-HSB, di-(pyrimidin-3, 5-yl)ethyne (**6**), was prepared *via* the scheme below (Scheme 7).
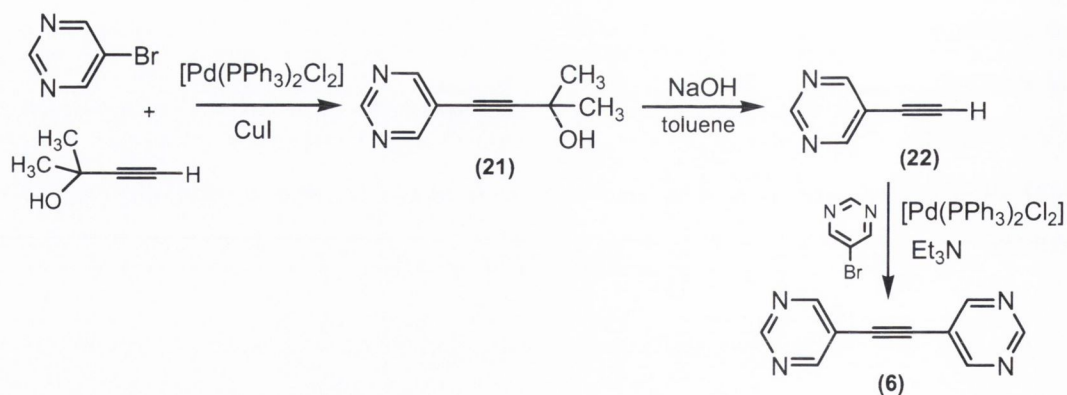
Scheme 7: Synthesis of di-(pyrimidin-3,5-yl)ethyne (6).

The first step in this synthesis is the Sonogashira coupling reaction, catalyzed by bis(triphenylphosphine)palladium(II) dichloride. This reaction gave the protected acetylene (**21**) in 54% yield. This product was then deprotected with the strong base, NaOH. The problem with the purification of 5-ethynylpyrimidine (**22**) was that it was obtained in a high boiling solvent, toluene. Since (**22**) is very volatile, attempts to remove the solvent resulted in considerable loss of product, therefore a modification was introduced. Rather then evaporating the solvent, the reaction mixture was chromatographed (SiO$_2$), and the product was further purified by sublimation. A yield of 64%, higher than the literature value was obtained.[11]

The second precursor 2, 3, 4, 5-tetra-(4-tert-butylphenyl)cyclopentadienone (**5**) was synthesized in a two-fold Knövenagel condensation reaction by heating (**3**) with (**4**) in ethanol with KOH (Scheme 4). By reducing the amount of KOH to a quarter of the amount, used in the literature and by decreasing the quantity of solvent, product (**5**) was isolated in better yield (73%) (compared with literature).[11,31] The next step in the synthesis of heterosuperbenzene was the Diels-Alder [2+4]-cycloaddition of (**6**) and (**5**) to give the precursor to N-HSB (**7**) (Scheme 8).

The final step, cyclodehydrogenation of (**7**) with CuCl$_2$ and AlCl$_3$ as oxidative reagents was carried out and gave a deep orange product, N-heterosuperbenzene (**8**). The oxidative cyclodehydrogenation reaction was a significant problem for the synthesis of heterosuperbenzene (**8**) and gave an unsatisfactory yield of 34%. The cyclisation of the graphite sheet, which contains four heteroatoms, is very sensitive to the reaction conditions. Different reagents such as Cu(CF$_3$SO$_3$)$_2$[7] with AlCl$_3$ were used. The amounts of reagents and time of reaction were changed. Following

Müllen's reported synthesis routes 36 equivalents of Cu(CF$_3$SO$_3$)$_2$ and AlCl$_3$ were applied to create the necessary 6 bonds. The reaction was carried out for 5 days, but only starting material was recovered. In separate reactions the number of equivalents of Cu(CF$_3$SO$_3$)$_2$ and AlCl$_3$ was decreased to 20 and then to 15. In both cases the reaction gave a mixture of several partially cyclised products, which were impossible to separate, no fully-cyclised product was obtained. A few more attempts were made by altering the number of equivalents of CuCl$_2$ and AlCl$_3$, no better results were obtained.

Iron(III) trichloride was applied as an alternative catalyst as per the literature. It can act as both a Lewis acid and oxidative agent. This time the fully and the half-cyclised products were obtained in different yields (Table 1). In all trials the applied reaction conditions were exactly the same.
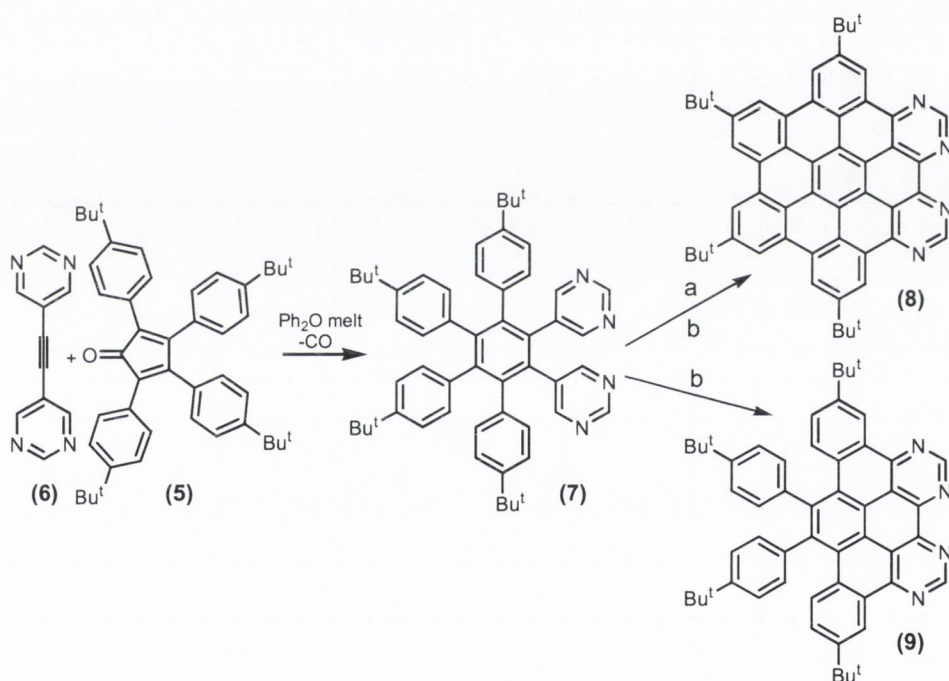
Scheme 8: Synthesis of N-HSB and N-½HSB with a) AlCl$_3$, CuCl$_2$ and b) FeCl$_3$ as an oxidising agent.

N-HSB Yield (%)	N-½HSB Yield (%)
9	0
45	17
22	9
19	11

Table 1: The different yields for oxidative cyclisation of (7) with FeCl₃.

The proton ^{1}H NMR shifts obtained for N-HSB and N-½HSB matched the shifts reported for both products (Table 2).

^{1}H NMR shifts (ppm)			
N-HSB (8)	N-HSB (8)[11]	N-½HSB (9)	N-½HSB (9)[11]
9.81	9.76	10.13	10.14
9.44	9.42	9.68	9.65
9.09	9.07	7.84	7.82
9.03	9.01	7.40	7.39
8.96	8.94	7.29	7.25
1.96 (-CH₃)	1.95 (-CH₃)	7.06	7.05
1.88 (-CH₃)	1.87 (-CH₃)	1.50 (-CH₃)	1.51 (-CH₃)
-	-	1.36 (-CH₃)	1.36 (-CH₃)

Table 2: The ^{1}H NMR shifts for N-HSB (8) and N-½HSB (9) and the comparison with the literature, in CDCl₃, 25°C, 400 MHz.[11]

1.2.2. Synthesis of a new N-containing superbenzene

According to the literature a new method for the synthesis of substituted polyaromatic hydrocarbons was available.[10] In the simple one pot reaction, starting from the new precursor (**24**) it was expected that both the substitution and oxidative cyclodehydrogenation would occur. In our case this route would be even easier due to

the commercial availability of cyclopentadienone. Scheme 9 below shows the synthetic route for the new precursor.
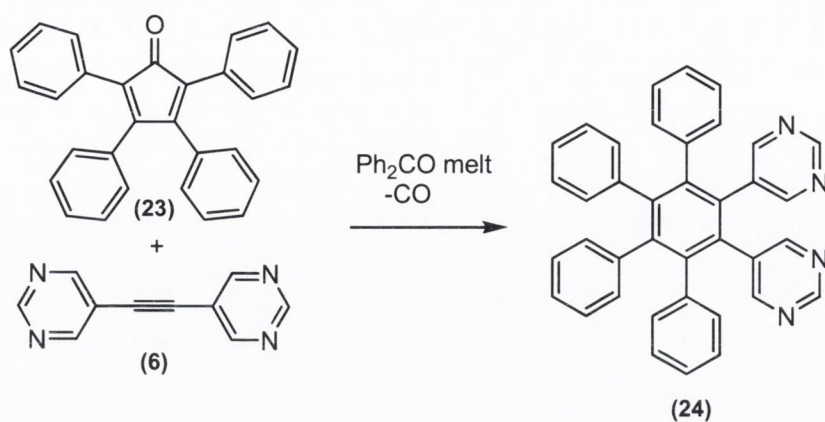
Scheme 9: The synthesis of a new precursor for N-HSB.

Compound (24) was generated in a stepwise manner by the Diels-Alders reaction of di(pyrimidin 3,5 yl)ethyne (6) and tetraphenyl-cyclopentadienone (23). The first time the reaction mixture, with benzophenone as a solvent, was refluxed at 280°C for 6 hrs, in air. After work up, TLC chromatography showed no remaining starting materials and a new product. The new compound obtained in this reaction was a side product, a lacton created by the reaction between the cyclone and atmospheric oxygen.[32] To avoid this process the reaction was carried out under an argon atmosphere. This allowed us to obtain the right product with a good yield of 59%.

Figure 12 shows the ^{1}H NMR spectrum of precursor (24) signal. The most shifted downfield signal at δ 8.78 is assigned to the H1 protons situated between the N heteroatoms and integrates for two hydrogen atoms. The signal at δ 8.25 assigned to proton H2 integrates for four atoms. The multiplet at δ 6.95-6.85 integrates for 20 hydrogen atoms and corresponds to the aromatic signals of the remaining four phenyl rings.
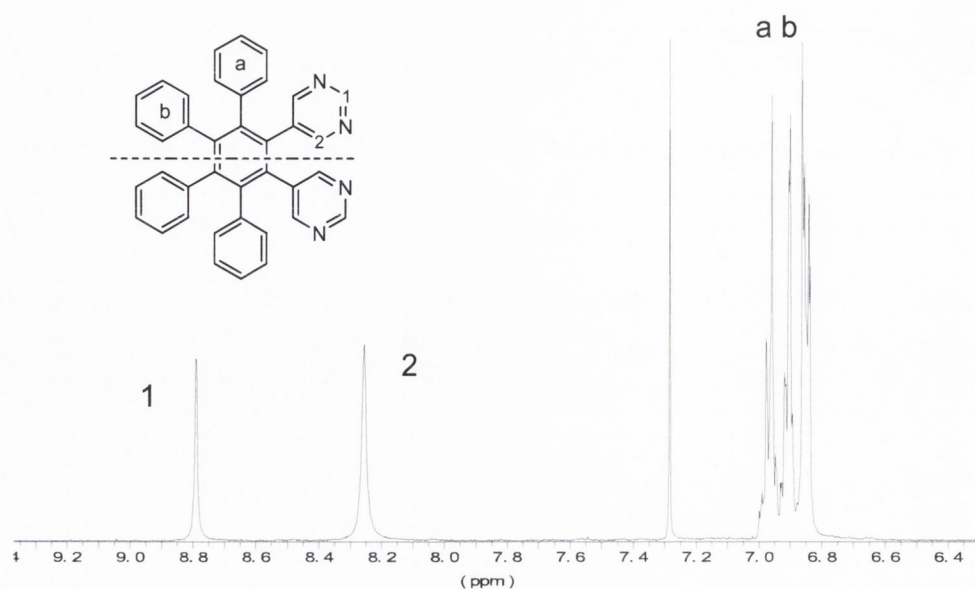
Figure 12: The ¹H NMR spectrum of the precursor (24), CDCl₃, 25°C, 400 MHz.

The ¹H NMR shifts in the aromatic region for both precursors with and without *t*-butyl groups are almost identical (Table 3).

protons	¹H NMR shifts for precursor (24) (ppm)	¹H NMR shifts for precursor (7) (ppm)
H1	8.78	8.78
H2	8.25	8.26
phenyl rings	6.95-6.85	6.95-6.69

Table 3: The ¹H NMR shifts for (24) and (7).

The solubility of precursor **(24)** in common solvents such as chloroform, dichloromethane, toluene or methanol is high and comparable to the *t*-butyl N-HSB precursor. The final, delicate step was to use iron(III) trichloride to achieve fully cyclised N-HSB (Scheme 10). The precursor and *t*-butyl chloride were dissolved in dichloromethane and a solution of anhydrous ferric chloride in nitromethane was added in two portions, with argon bubbling. Pre-dissolving the oxidizing agent in nitromethane speeds-up the desired reaction, while bubbling with argon helps to remove the evolving hydrochloric acid. After quenching with methanol and extraction

22

with chloroform the starting material was recovered. Unfortunately, precursor (**24**) with four nitrogens in the dipyrimidine did not react under the reaction conditions used successfully for the all-carbon analogue. [10]
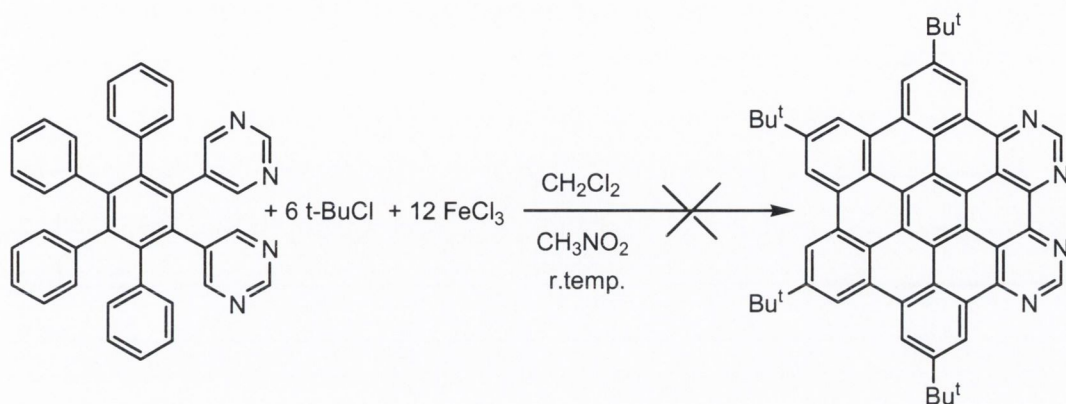
Scheme 10: Proposed synthetic route for fully cyclised N-HSB.

At this point it was decided to test if iron(III) trichloride is a suitable oxidising agent for the dehydrogenation of precursor (**24**) (Scheme 11). The solution of (**24**) in dichloromethane was treated with eighteen equivalents of $FeCl_3$ previously dissolved in nitromethane. After an hour of stirring the reaction mixture was quenched with methanol. After extraction and chromatography TLC the white starting material was recovered. The ^1H NMR spectrum showed no signs of cyclodehydrogenation.
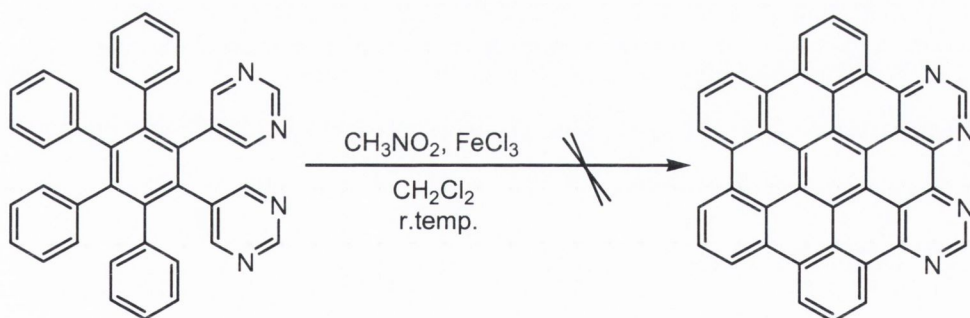
Scheme 11: Oxidative cyclodehydrogenation reaction of precursor (24).

It was clear that a change of oxidative cyclodehydrogenation catalyst was required. The aluminium(III) trichloride and copper(II) chloride combination is the second most common mixture used for polyaromatic dehydrogenation. The mixture of precursor (**24**) and 16 equivalents of $AlCl_3$ and $CuCl_2$ in carbon disulfide was stirred for three days in an argon atmosphere. The reaction was quenched by 10% ammonia solution and one product extracted into chloroform. The dark orange precipitate was filtered

off and the bright yellow filtrate was chromatographed. The compound was separated by column chromatography in 5% yield and identified as a half-cyclised product (**25**), with fused pyrimidine rings (Scheme 12). The remaining orange precipitate failed to dissolve in all available solvents, or acid or base solution. Due to the extremely low solubility the successful cyclisation could not be proven by conventional analysis methods. The product (**26**) was characterized by MALDI-TOF spectrometry, which analyses samples in solid state. The MALDI-TOF spectrum shows peak *m/z* at 526 which corresponds to the fully cyclised product. Also a peak at 592 was found to correspond to $[M+Cu]^+$. The full cyclisation gave a completely planar, disk like molecule. Due to π-stacking interactions the fully cyclised product was extremely insoluble even in solvents like benzene or chlorobenzene.

The solubility of the second product (**25**) allowed identification by conventional analysis methods. Figure 13 shows the ^{1}H NMR spectrum for compound (**25**). The lowest field signal in the spectrum at δ 10.12 is related to the two hydrogen atoms situated between the two nitrogen atoms. The signal is very broad and assigned to H1. The next signal in the low field area is a doublet at δ 9.54, integrated for two hydrogen atoms and it is assigned to H2. The protons H5 appear as a doublet at δ 7.80 and integrate for two. Signals at δ 7.68 and δ 7.38 are triplets and they integrate for two hydrogen atoms each, and are assigned to H3 and H4. Two phenyl rings, which remain uncyclised appeared as a multiplet at δ 7.26-7.20 integrating for ten hydrogen atoms (H6). The assignments were made by using the well-resolved coupling information from ^{1}H NMR, H-H TOCSY NMR spectra and nOe experiments. The accurate mass ESI-spectrum of (**25**) showed a single isotopic envelope at *m/z* 533.1946 assigned to $(C_{38}H_{21}N_4)^+$ and in agreement with the calculated value.

24
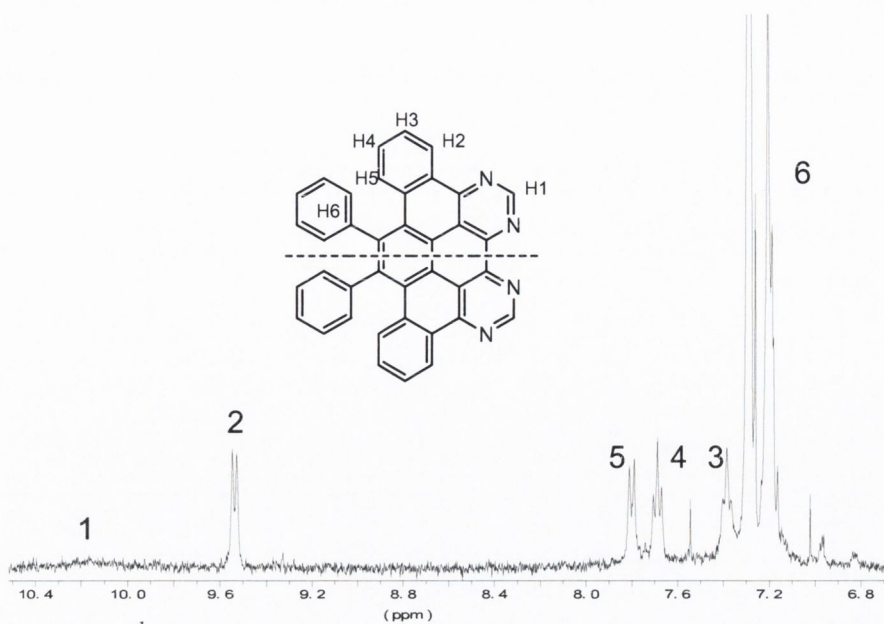
Figure 13: The ^1H NMR spectrum for the half-cyclised compound (25), CDCl$_3$, 25°C, 400 MHz.

Figure 14 shows aromatic region of two ^{1}H NMR spectra for the half-cyclised products ½ N-HBS (top) and product (25) (bottom). It is important to notice that in both compounds, the signals that correspond to protons situated between the two heteroatoms are very broad. Having characterized N-½HBS helped a lot to identify half cyclised (25). Comparison of the spectra allows the assignment of the signals in (25).
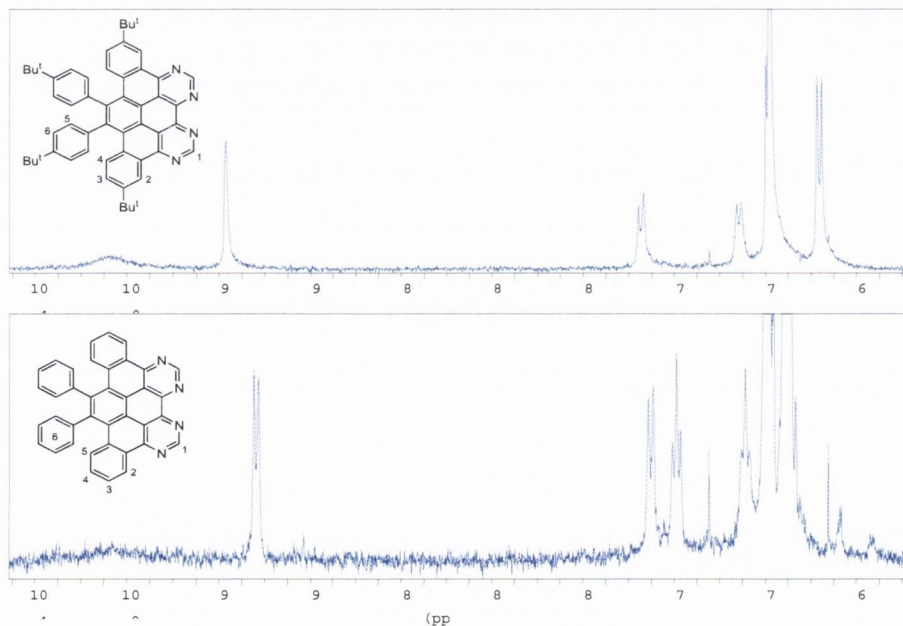
Figure 14: The ^1H NMR spectrum of the aromatic region for N-½HSB (9) (top) and (25) (bottom), CDCl$_3$, 25°C, 400 MHz.

The proton ^{1}H NMR shifts for the half-cyclised product (**25**) and (**9**) are colected in table 4. As was mentioned before the most shifted downfield signals are assigned to H1 in both cases. The shifts for the other signals are given in Table 4.

Proton	^{1}H NMR shifts (ppm) for half cyclised (25)	proton	^{1}H NMR shifts (ppm) for N-½HSB
H1	10.12 (br.s)	H1	10.13 (br.s)
H2	9.54 (s)	H2	9.64 (d)
H3/4	7.68(d)	H4	7.84 (d)
H3/4	7.38 (d)	H3	7.40 (t)
H5	7.81 (d)	H5/6	7.29 (br.t)
H6	7.26 (d)	H5/6	7.06 (m)

Table 4: A comparison of the ^{1}H NMR shifts for N-½HSB (9) and (25).

The half-cyclised products (**25**) and N-½HSB possess very similar bright yellow fluorescent colours (Figure 15).

Figure 15:The chloroform solutions of N-½HSB (9) (left) and (25) (right).

The UV-vis absorption spectra of (**25**) and (**9**) in chloroform are presented in Figure 16. The overall shape of the absorption bands is similar for both. The maximum absorption (λ_{max} 287 nm) for (**25**) appears at slightly higher energy than that of N-½HBS (λ_{max} 289 nm). The lowest energy band at 415 nm is blue shifted with respect

26

to N-½HBS (418 nm). In general it can be said that the absence of *t*-butyl groups does not influence the electronic spectrum.
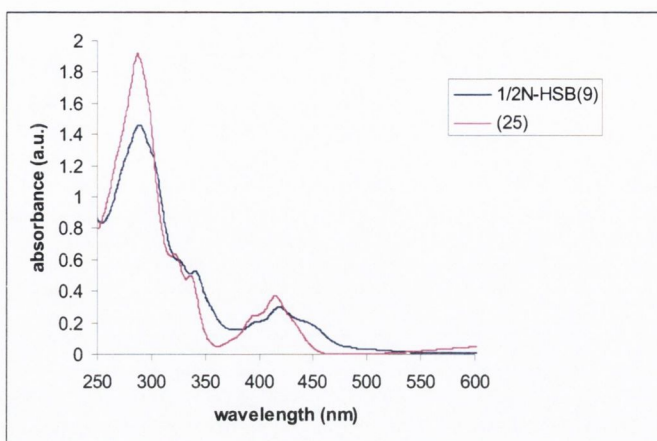
Figure 16: The UV-vis spectra of (25) and (9) in chloroform.

From the successful dehydrogenation with aluminium(III) trichloride/copper(II) dichloride two products were purified and characterized, but the yields were not very satisfactory. Looking for better results, a third oxidizing agent was introduced for the cyclisation reaction of precursor (**24**). This time the Lewis acid molybdenium(V) pentachloride was used (Scheme 12). A mixture of precursor and 12 equivalents of molybdenium(V) pentachloride[33,34] were dissolved in dichloromethane and stirred under an argon atmosphere for 3 days. The reaction mixture was washed with water and extracted with dichloromethane. TLC chromatography showed two main products with very similar R$_f$. Purification by silica preparative plates was repeated a few times and finally allowed the separation of a pale yellow compound (**27**) and the canary yellow product (**25**), in reasonable yields (15% and 20% respectively).
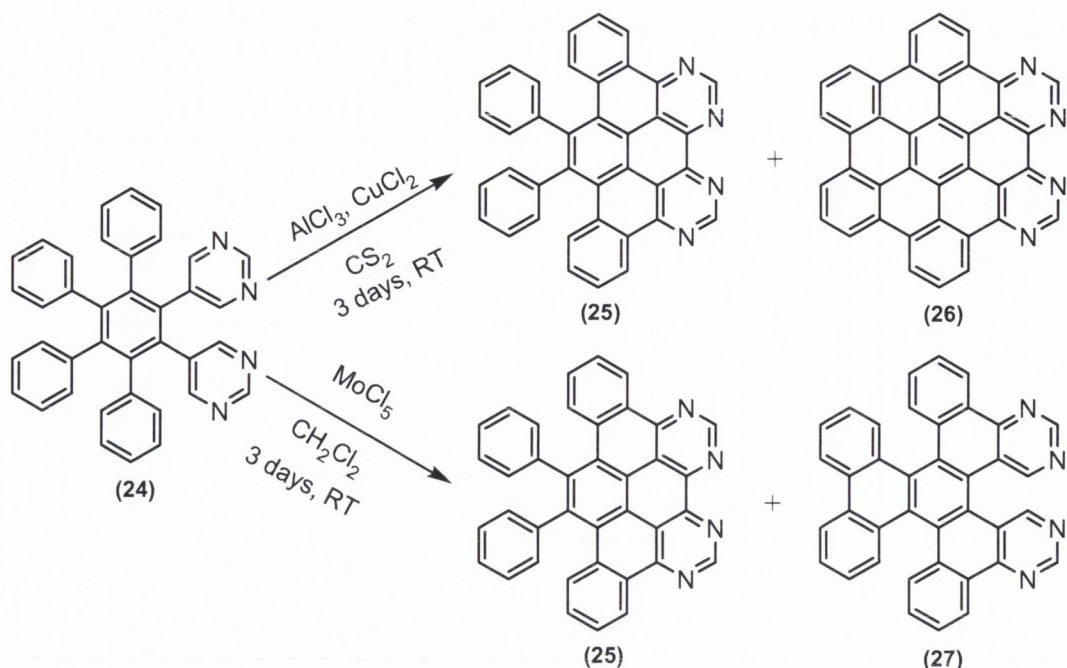
Scheme 12: The oxidative cyclodehydrogenation reaction of (24).

The oxidative dehydrogenation with molybdenum pentachloride as a Lewis acid was a more efficient reaction for precursor (24) than iron(III) trichloride or aluminium(III) trichloride. The darker yellow product was charcterised by ^{1}H NMR spectroscopy and mass spectrometry and identified as the half-cyclised product (25), also produced in the cyclisation with aluminium trichloride but with improved yield.

The partially cyclised product (27), less planar than (25), runs on the preparative plate faster than (25). Figure 17 shows the ^{1}H NMR spectrum of this molecule. The most downfield signal at δ 9.42 integrates for two hydrogen atoms corresponding to proton H1. The singlet at δ 9.37 integrates for two hydrogen atoms and is assigned to H2. The doublet at δ 9.32 integrates for two atoms and corresponds to protons H3. The triplet at δ 7.68 and the doublet at δ 7.43 integrate for two hydrogen atoms each and are assigned respectively to protons H4 and H6. The triplet corresponds to proton H5 and is overlapping with the doublet for H7 at δ 7.28. Both integrate for four hydrogen atoms. The two overlapping triplets at δ 7.19 integrate for four protons and they correspond to protons H8 and H9. The most upfield signal is a doublet, which integrates for two hydrogen atoms and is assigned to H10.

28

The assignment was made using the information from ^{1}H NMR and H, H TOCSY NMR spectra and an nOe experiment. The accurate mass ESI-spectrum of (**27**) showed a single isotopic envelope at *m/z* 533.1777 assigned to $(C_{38}H_{21}N_4)^+$ and in accordance with the calculated value.
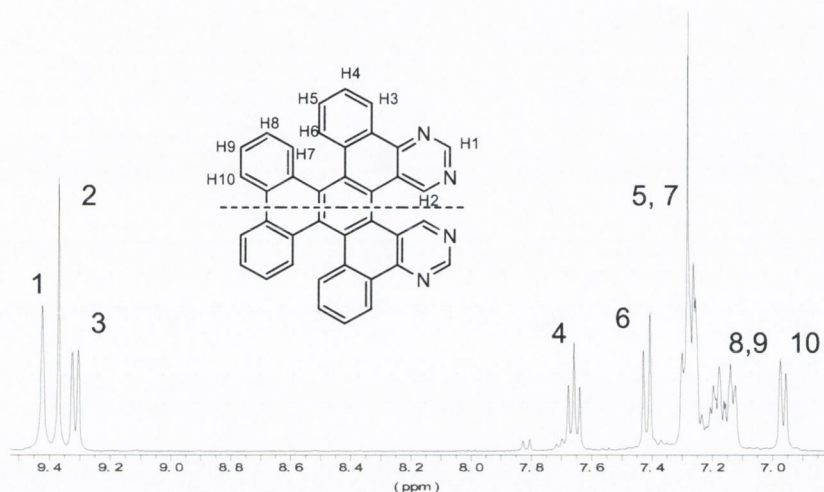
Figure 17: The^{1}H NMR spectrum of the (27), CDCl$_3$, 25°C, 400 MHz.

The ^{1}H NMR spectrum of the hexabenzotriphenylene (**27a**)[35,36,37] the all-carbon analogue (Figure 18) to partially cyclised (**27**) possesses only four aromatic signals due to its D_{3h} symmetry. All proton signals in this case integrate for six hydrogen atoms.
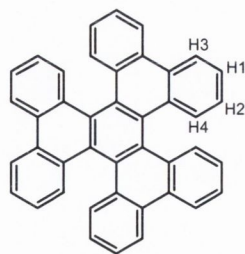
Figure 18: The labeling for the ^{1}H NMR protons in dibenzo[f,j]phenanthro[9,10-s]-picene (27a).

Proton	^{1}H NMR shifts (ppm) for partially cyclised (27)	^{1}H NMR shifts (ppm) for all carbon analogue (27a)
H1/2	9.42 (s)	8.54 (br.d)
H1/2	9.37 (s)	8.15 (br.d)
H3/4	9.32 (d)	7.55 (br.t)
H3/4	7.66 (t)	7.21 (br.t)
H6	7.43 (d)	
H5, H7	7.28 (m)	
H 8, H9	7.19 (m)	
H 10	6.97 (d)	

Table 5:The ^{1}H NMR shifts for partially cyclised (27) and its all-carbon analogue (27a).

The introduction of four nitrogen atoms in a pyrimidine like pattern has lowered the symmetry to C_2 and increased the number of signals in the ^{1}H NMR spectrum (Table 5) contains the proton NMR shifts for both partially cyclised (27) and its all-carbon analogue (27a). The protons assigned to H1, H2 and H3 for (27) are shifted downfield with the respect to (27a) due to the deshielding effect of the nitrogen atoms. The protons which are located furthest from the nitrogen atoms appear upfield δ 7.66–6.97, compared to (27a) δ 8.54–7.21.

In general the ^{1}H NMR shifts for partially cyclised product (27) are shifted upfield compared to its half-cyclised analogue (25). The characteristic proton assigned as H1 appeared at δ 9.42 for (27) and is shifted upfield with respect to the same proton in (25) δ 10.12. This is due to the larger deshielding effect of extending the aromatisation of the product. The proton H3 δ 9.32 for (27) was affected the same way with the respect to H2 (25) δ 9.54. It is interesting that the proton H10 (27) δ 6.97 appeared upfield compared to that of the uncyclised phenyl rings H6 in (25) δ 7.26. The influence of the planar, cyclised-side of the molecule is significant, and has a big deshielding effect.

30

(25)   **(27)**
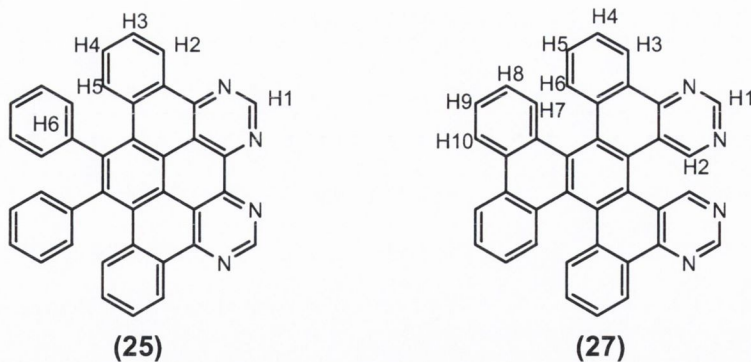
Figure 19: The numbering for the proton ^1H NMR for (25) and (27).

Figure 20 shows the electronic absorption spectrum of (**27**) in chloroform. The maximum absorption band appeared at 302 nm and is shifted to lower energy compared to the half-cyclised (**25**).
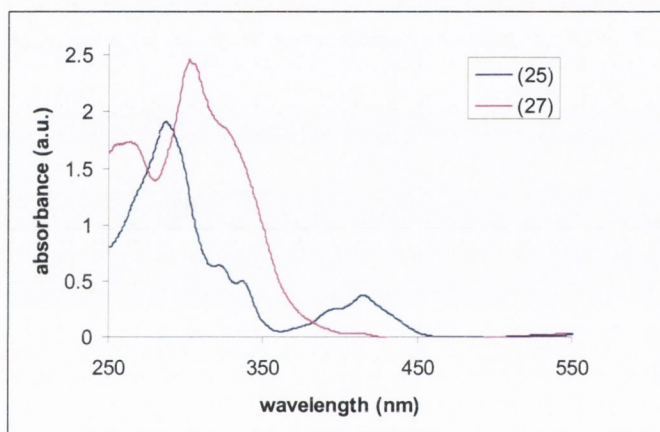
Figure 20: The UV-vis absorption spectra of (27) and (25) in chloroform.

The UV-vis spectrum of (**27**) is broader than that of (**25**) (Figure 20) and a broad shoulder can be seen at 325 nm. The lowest energy band of (**25**) at 427 nm is red shifted with respect to (**27**), which shows the tail of an absorption at 330 nm. This is due to the reduction of conjugation and the depletion of π electron density in (**27**), which possesses pockets of four fused rings while (**25**) has eight.

1.2.3. Ruthenium complexes

The intriguing properties of N-heterosuperbenzene make it ideal for further investigation as a ligand in ruthenium complexes. With this aim in mind a ruthenium heteroleptic and homoleptic complex of N-heterosuperbenzene was synthesized.

In order to check the synthetic conditions of the complexation reaction for N-heterosuperbenzene the synthesis of complex [Ru(bpy)$_2$(N-HSB)](PF$_6$)$_2$ **(19)** was repeated using the literature procedure.[18] [Ru(bpy)$_2$(N-HSB)](PF$_6$)$_2$ **(19)** was prepared by heating [Ru(bpy)$_2$Cl$_2$] with N-heterosuperbenzene in diethylene glycol ethyl ether for 20 h at 127°C. Addition of NH$_4$PF$_6$ and chromatography gave a green precipitate of the product with a satisfactory yield of 58%.

The ^{1}H NMR shifts gave a good agreement with results given in the literature; Table 6 shows the result with the proton assignment (Figure 21).
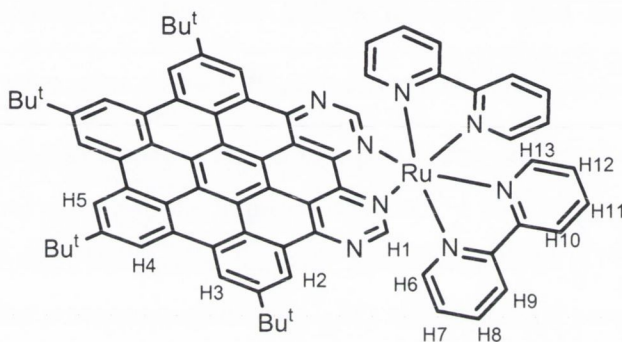
Figure 21: The protons labelling for the ^{1}H NMR spectrum of [Ru(bpy)$_2$(N-HSB)](PF$_6$)$_2$

(19).

Proton	^{1}H NMR shifts (ppm) for [Ru(bpy)$_2$(N-HSB)](PF$_6$)$_2$ (19)	^{1}H NMR shifts (ppm) [Ru(bpy)$_2$(N-HSB)](PF$_6$)$_2$ (19)[18]
H2, H3,	9.89	9.94
	9.73	9.80
H4, H5	9.50	9.60
H1	9.31	9.31
H9	8.67	8.67
H10	8.58	8.58
H8	8.28	8.25
H6	8.08	8.10
H11, 13	8.01	8.00
H7	7.62	7.63
H12	7.16	7.17
CH$_3$	1.89	1.88
CH$_3$	1.84	1.83

Table 6: Comparison of the proton ^{1}H NMR shifts for [Ru(bpy)$_2$(N-HSB)](PF$_6$)$_2$ (CD$_3$CN at 25°C, 400 MHz) with literature data.

1.2.3.2. Synthesis of [Ru(N-HSB)$_3$](PF$_6$)$_2$

The synthesis of [Ru(N-HSB)$_3$](PF$_6$)$_2$ (Scheme 13) was carried out under an argon atmosphere, in the same high boiling point solvent as for the synthesis of complex (**19**), diethylene glycol ethyl ether.[38,39,40]

Initially [Ru(N-HSB)$_3$](PF$_6$)$_2$ (**28**) was synthesised by heating ruthenium trichloride with 4 equivalents of heterosuperbenzene (**8**) in the presence of N-ethylmorpholine[40] as the reducing agent (Scheme 13A). The reaction mixture was heated at 149°C for 44 h and upon PF$_6^-$ ion exchange a khaki precipitate formed. By TLC it was clear that 6 fractions were present including some unreacted ligand. Chromatography (Al$_2$O$_3$, 3:1 toluene:acetonitrile) allowed the separation of the unreacted ligand and some fractions, but insufficient product was obtained to allow isolation. The synthesis of [Ru(N-HSB)$_3$](PF$_6$)$_2$ (**28**) in a different set of conditions was investigated (Scheme 13B). The more labile Ru(II) precursor [Ru(DMSO)$_4$Cl$_2$] (**29**) was used.[41]

The precursor (**29**) was prepared from ruthenium trichloride hydrate in refluxing DMSO in yield 58%. To test the reactivity of the [Ru(DMSO)$_4$Cl$_2$] precursor, it was first reacted with 1,10-phenanthroline in refluxing ethanol, giving [Ru(1,10-phen)$_3$](PF$_6$)$_2$ in 79% yield after 72 h.
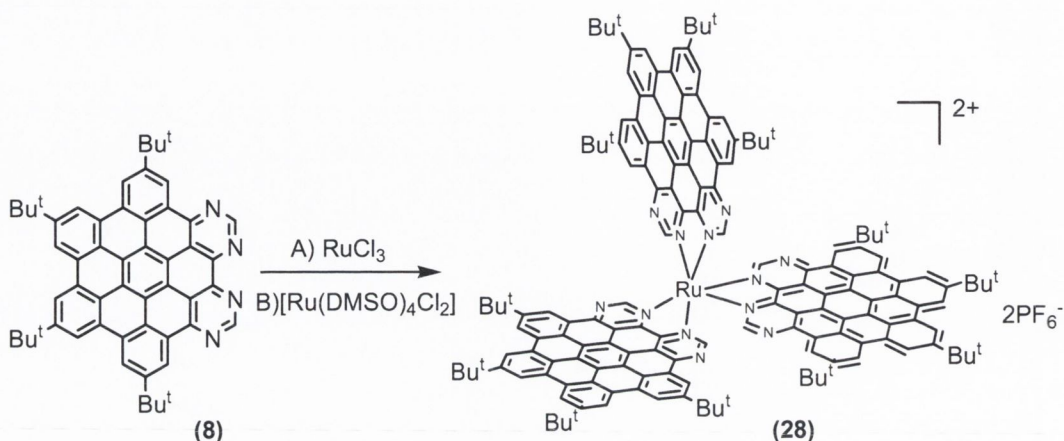
Scheme 13: The synthesis routes A and B for formation of [Ru(N-HSB)$_3$](PF$_6$)$_2$ complex (28).

[Ru(DMSO)$_4$Cl$_2$] was then used for the synthesis of [Ru(N-HSB)$_3$](PF$_6$)$_2$ (**28**). A diethylene glycol diethyl ether solution containing 4 equivalents of heterosuperbenzene (**8**) and 1 equivalent of [Ru(DMSO)$_4$Cl$_2$] (**29**)[41] was heated for 74 h at 182°C. The solution changed colour from dark orange to khaki. Following counterion metathesis, numerous solvent systems were investigated to purify the crude product by chromatography. Eventually chromatography on alumina, in (12:4:0.5 THF:acetonitrile:KNO$_{3(aq)}$) was selected and gave enough product (**28**) for characterization, however the isolated yield was quite low (15%).

1.2.3.3. Characterisation of [Ru(N-HSB)$_3$](PF$_6$)$_2$.

The ruthenium tris-heterosuperbenzene complex was characterised by ^{1}H NMR spectroscopy and electrospray mass spectrometry. Analysis was possible only at high temperatures. The ^{1}H NMR spectrum of [Ru(N-HSB)$_3$](PF$_6$)$_2$ (Figure 22) shows temperature dependent behaviour. In the spectrum at room temperature, the proton signals are very broad, but at 40°C sharp proton peaks can be seen, which can be assigned to the five N-HSB protons environments. This temperature effect is

consistent with the aggregation of [Ru(N-HSB)$_3$](PF$_6$)$_2$ in solution. The highly planar ligand N-HSB is expected to result in π-stacking. It was shown (Figure 6) that complex [Ru(bpy)$_2$(N-HSB)](PF$_6$)$_2$ (**19**) can create discrete dimers by the off-set stack of molecules of N-HSB. (**28**) might show a higher degree of aggregation compared to (**19**), due to the presence of three molecules of N-HSB in the complex. The degree of aggregation can be reduced by increasing the temperature of the NMR sample.
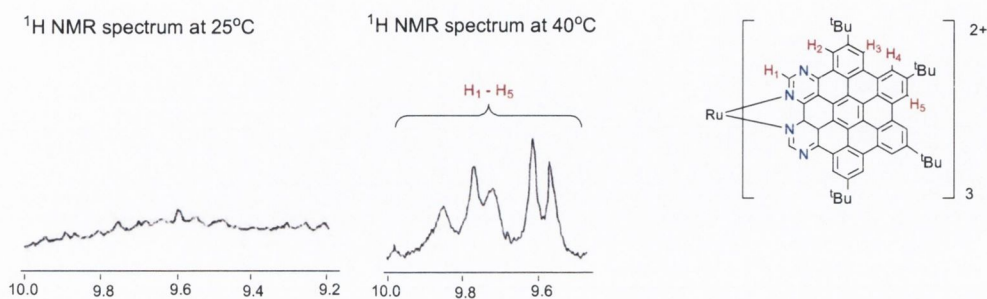
Figure 22: The aromatic region of the ^{1}H NMR spectrum (400 MHz) of [Ru(N-HSB)$_3$](PF$_6$)$_2$] (28) at 25°C and 40°C in CD$_3$CN.

Figure 23 shows a comparison of the ^{1}H NMR spectra of free ligand (**8**) (top) and of [Ru(N-HSB)$_3$](PF$_6$)$_2$ (**28**) (bottom). The complexation of N-HSB considerably changes the position of its aromatic protons in the spectrum. They are shifted downfield, from δ 8.94-9.79 to δ 9.61-9.91. This behaviour is observed for other ruthenium(II) complexes such as [Ru(bpy)$_2$(N-HSB)](PF$_6$)$_2$,[18] [Ru(bpy)$_2$(biq)](PF$_6$)$_2$, [Ru(bpy)$_2$(binap)](PF$_6$)$_2$ [25] and is considered normal for ligand complexation. The N-HSB protons appear downfield in the complex because metal coordination reduces electron density within the N-HSB ring system. The protons between the two nitrogen atoms of coordinated N-HSB would be expected to resonate upfield of the free ligand because they must point directly toward the shielding face of another N-HSB ligand.
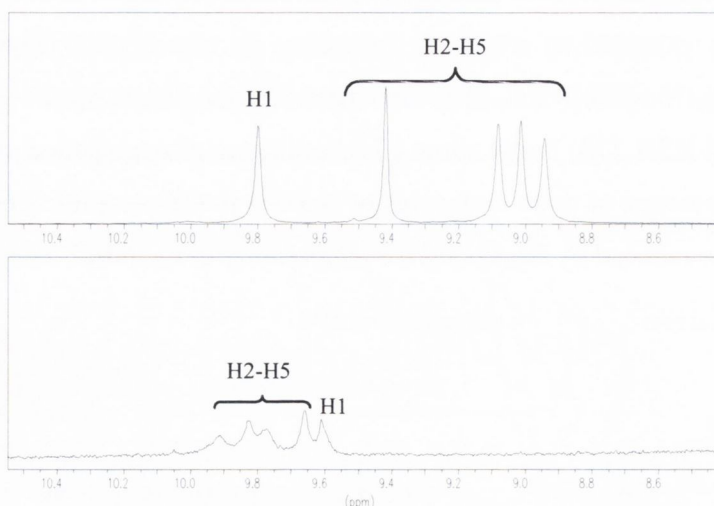
Figure 23: The aromatic region of the ^1H NMR spectrum (400 MHz, CD₃CN) of N-HSB ligand (top) and [Ru(N-HSB)₃](PF₆)₂ (28) (bottom).

The electrospray mass spectrometric characterization of [Ru(N-HSB)₃](PF₆)₂ in acetonitrile was carried out at high desolvation temperature (180°C). This was necessary because no signals were observed in the spectrum at lower desolvation temperature (120°C). This finding suggests the aggregation of (28) in the solution, *via* the overlap of π orbitals from ligand molecules. Due to the lack of single crystal X-ray analysis it can be only speculated that (28) creates dimers similar to (19) or [Ru(bpy)₂(eil)](PF₆)₂.[46]

The ESI-mass spectrum (Figure 24) shows the molecular ion at *m/z* 1177.15 assigned to [M-2PF₆]²⁺ and the ½ m.u. intervals of the isotopic distribution which confirms the 2+ charge of the molecular ion. The peak at *m/z* 391.19 is assigned to [Ru(PF₆)₂], peaks at *m/z* 454.19 and 803.31 were found to be an artefact of the solvent, by running the ESI-mass spectrum for pure solvent-CH₃CN. Peaks at *m/z* 507.19 and 683.31 were not found as a fragmentation of [Ru(N-HSB)₃](PF₆)₂.

Electrospray mass spectrum at 180°C
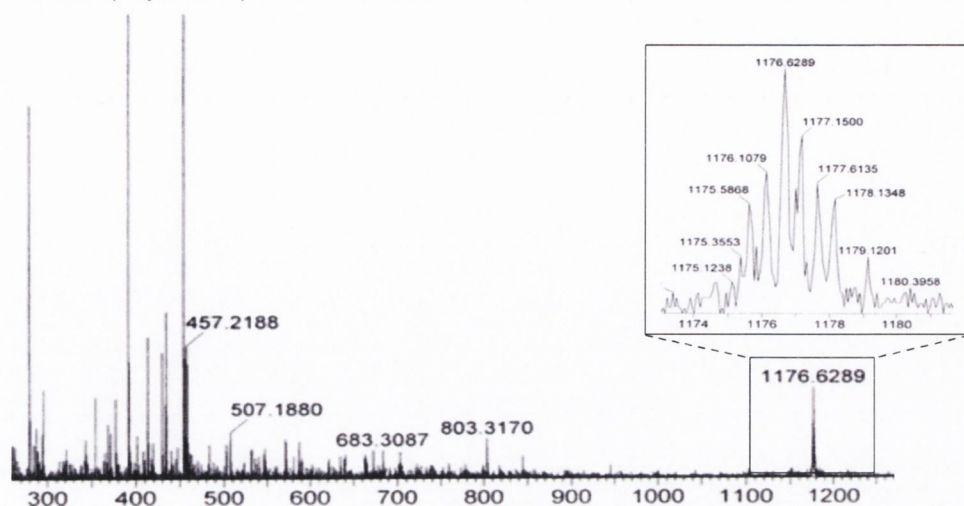
Figure 24:The 300-1200 m. u. region of ESI-mass spectrum of [Ru(N-HSB)₃](PF₆)₂.

UV-vis absorption spectroscopy.

The absorption spectrum of $[Ru(N-HSB)_3]^{2+}$ (Figure 25) shows six characteristic bands. Three of these are in the ultraviolet region: 227 nm, 278 nm and 352 nm assigned to LC $\pi \rightarrow \pi^*$ transitions of N-HSB. In the visible region two broad bands can be observed. The transition at 439.5 nm is also assigned to a LC $\pi \rightarrow \pi^*$ transition of N-HSB having shifted into a visible region of the spectrum on coordination to Ru(II). The peak at low energy is absorption at 630 nm with an extinction coefficient of 3.3×10^3 mol^{-1} dm^3 cm^{-1}. This is the MLCT $d \rightarrow \pi^*$ transition between ruthenium and the coordinated heterosuperbenzene molecules. This transition occurs at lower energy compared to $[Ru(bpy)_2(N-HSB)]^{2+}$ (λ_{max} 615 nm with an extinction coefficient 26×10^3 mol^{-1} dm^3 cm^{-1}). The unusual low energy of this transition is indicating the presence of low-lying π^* acceptor orbitals in the highly delocalised N-HSB ligand. It is this absorption which is responsible for the colour of the N-HSB containing complex, which is red-shifted compared to $[Ru(bpy)_3]Cl_2$. Complex (**28**) possesses a green colour as a solid and when dissolved in common solvents (Figure 25). Similar behaviour was observed for eilatin complexes which show a low energy absorption, for example $[Ru(bpy)_2(eil)]^{2+}$ with a MLCT transition at 580 nm.[20]

37
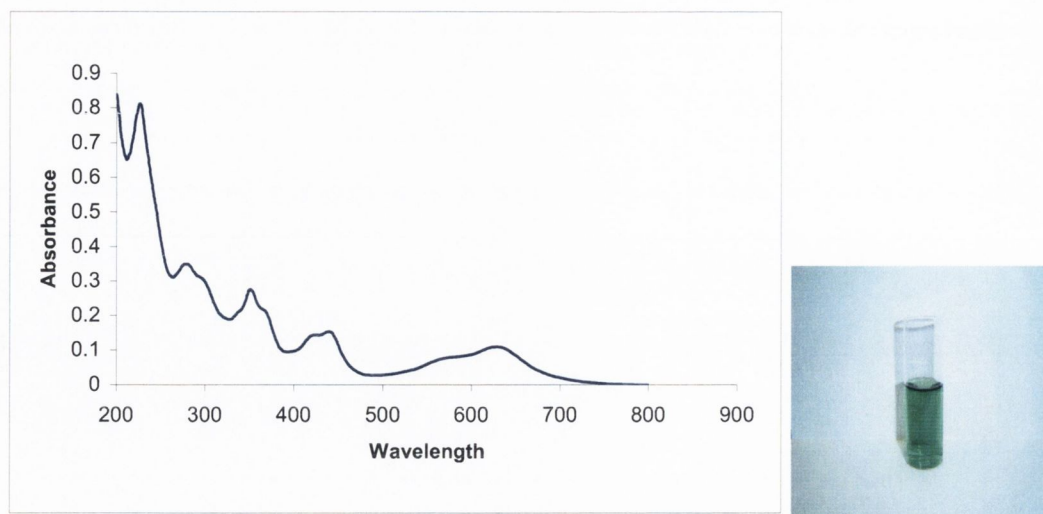
Figure 25: Absorption spectrum of [Ru(N-HSB)$_3$](PF$_6$)$_2$ (conc. 4.27*10^{-5} M) in acetonitrile and a sample of the complex in chloroform.

Table 7 contains the absorption bands for both [Ru(N-HSB)$_3$]$^{2+}$ and [Ru(bpy)$_2$(N-HSB)]$^{2+}$. In general, the both absorption spectra are similar. The bands in the UV region for [Ru(bpy)$_2$(N-HSB)]$^{2+}$ (Figure 8) are more intense due to the ligand-centered π-π^* transition of the bpy ligands. In the visible region bands assigned to the complexed N-HSB are apparent. In both cases N-HSB centered π-π^* transitions occur at similar wavelengths, except the lowest energy one, assigned to the metal to N-HSB charge transfer.

Compound	Wavelength λ_{max} (nm)								
[Ru(N-HSB)$_3$]$^{2+}$		273	336	352		415 shoulder	437	562 shoulder	628
[Ru(bpy)$_2$(N-HSB)]$^{2+}$	227	286	335	352	370	416 shoulder	437	565 shoulder	615

Table 7: The wavelengths of the absorption maxima in the spectra of [Ru(N-HSB)$_3$]$^{2+}$ (28) and [Ru(bpy)$_2$(N-HSB)]$^{2+}$ (19) in acetonitrile.[18]

The Figure 26 shows the absorption spectra of N-HSB and its homoleptic complex [Ru(N-HSB)$_3$]$^{2+}$ in chloroform. The absorption spectra of the ligand shows the most intense band at λ_{max} 351 nm in chloroform. The UV-vis spectrum of complex in

38

chloroform shows the most intense bands at 256, and 340 nm. The low energy MLCT transition is a result of the very low lying π^*-acceptor orbitals on the highly delocalised N-HSB.

Only one band is attributed to this MLCT absorption. The same is true of other Ru(II) tris complexes such us $[Ru(eil)_3]^{2+19,42,43,44}$ and $[Ru(taphen)_3]^{2+}$ (tephen-dipyrido[3,2-c:2',3'-e]-pyridazine).[45]
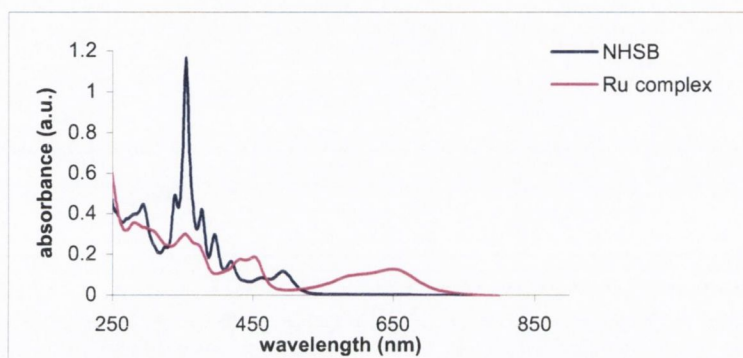
Figure 26: Absorption spectrum of $[Ru(N\text{-}HSB)_3](PF_6)_2$ (28) (pink) and ligand (blue) in chloroform.

In general the solvatochromic behaviour is not observed for complex $[Ru(N\text{-}HSB)_3]^{2+}$(28). The absorption spectra in acetonitrile, methanol, toluene and tetrahydrofuran are shown in Figure 27. The graphs show slight differences (1-4nm), which become more pronounced at lower energy (Table 8). The UV-vis spectra for heteroleptic N-HSB complex $[Ru(bpy)_2(N\text{-}HSB)]^{2+}$(19) show solvent dependence. The MLCT transition for (19) moves to higher energy, when the polarity of solvent increases (620 nm in CHCl$_3$, 615 nm in CH$_3$CN and 609 nm in MeOH).[18]

39
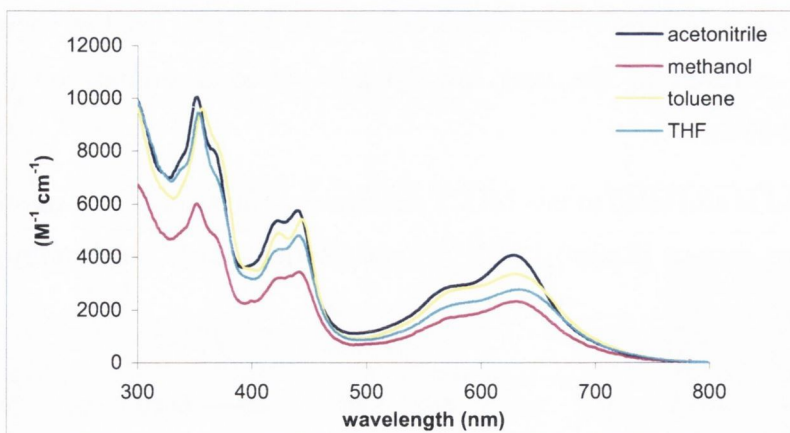
Figure 27: The absorption spectra of $[Ru(N\text{-}HSB)_3]^{2+}$ in various of solvents.

Emission spectroscopy.

The electronic excitation of Ru(II) polypyridine complexes gives rapid relaxation to create an emissive ^{3}MLCT state. The complex $[Ru(N\text{-}HSB)_3]^{2+}$ shows very strong emission in the 700 – 900 nm range and exhibits red shifts with respect to the uncoordinated ligand, which emits in the 500-600 nm range. The irradiation of the MLCT absorption band of (**28**) at 628 nm in acetonitrile gave a broad emission band with the λ_{max}^{em} at 773 nm. The emission of (**28**) was observed in a variety of solvents, such as acetonitrile, methanol, toluene and tetrahydrofuran (Figure 28). All the results are collected in Table 8.
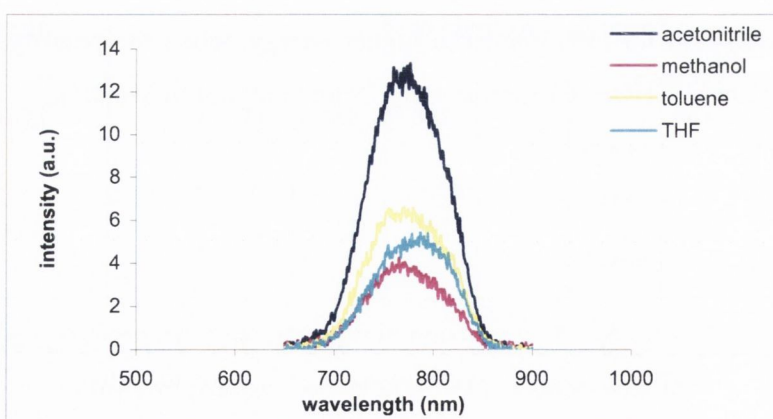
Figure 28: Emission spectra of $[Ru(N\text{-}HSB)_3]^{2+}$ in various solvents at room temperature.

40

The maximum emission intensity is observed in acetonitrile. The emissio spectra for [Ru(N-HSB)$_3$]$^{2+}$ show solvatochromic behaviour. The polarity of the solvent has consequence on the order of λ_{max}^{em}.

The MLCT absorption of [Ru(N-HSB)$_3$]$^{2+}$ (628 nm) appeares at lower energy compared to [Ru(bpy)$_2$(N-HSB)]$^{2+}$(615 nm).[18] This behavior would be expected to be reflected in the emission spectrum, however λ_{max}^{em} (773 nm) for [Ru(N-HSB)$_3$]$^{2+}$ is blue-shifted compared to λ_{max}^{em} (816 nm) for [Ru(bpy)$_2$(N-HSB)]$^{2+}$. This behaviour has been reported in the literature for other combinations of ligands, such as (taphen)[45] and phenanthroline (phen), but those ligands are structually less extensive than N-HSB.

Bergman *et al.* have examined series of Ru(II) eilatin complexes.[19] It has been shown that the substitution of bpy ligand for eil results in blue-shifting of the emission maxima compared to [Ru(bpy)$_3$]$^{2+}$. The emission maxima appear at 945 nm, 932 nm and 926nm for [Ru(bpy)$_2$(eil)]$^{2+}$, [Ru(bpy)(eil)$_2$]$^{2+}$ and [Ru(eil)$_3$]$^{2+}$ respectively. Upon the replacing bpy for eil the nature of the emission changes from Ru→bpy to Ru→eil.

Complex	Solvent	λ_{max}^{abs} (nm)	λ_{max}^{em} (nm)
[Ru(N-HSB)$_3$]$^{2+}$	THF	634	790
[Ru(N-HSB)$_3$]$^{2+}$	methanol	632	765
[Ru(N-HSB)$_3$]$^{2+}$	toluene	630	758
[Ru(N-HSB)$_3$]$^{2+}$	acetonitrile	628	773
[Ru(bpy)$_2$(N-HSB)]$^{2+}$	acetonitrile	615	816
[Ru(bpy)$_2$(N-HSB)]$^{2+}$	methanol	609	813

Table 8: UV-vis and emission maxima for [Ru(N-HSB)$_3$]$^{2+}$ and [Ru(bpy)$_2$(N-HSB)]$^{2+}$ in various solvents at room temperature.

A good π-acceptor ligand bearing a low lying π^* orbital can lead to a red shifted MLCT absorption band. Such a ligand can lead to increased aggregation via π stacking interactions, which is not very helpful for the characterization of single molecule of complex. It has been found that complex [Ru(bpy)$_2$(N-HSB)]$^{2+}$ creates dimers in solution via π-stacking of the N-HSB ligand (Figure 6). However, because the complex [Ru(N-HSB)$_3$]$^{2+}$ contains three N-HSB ligands, there is potential to form

higher-aggregates. The photophysics of a tris homoleptic complex of N-HSB shows a complex mixture, which is challenging to understand fully its behaviour in the solution.

1.2.3.4. Synthesis of [Ru(N-½HSB)₃](PF₆)₂

The homoleptic tris ruthenium complex of N-½HSB was synthesized in a similar way as its tris-fully cyclised N-HSB analogue (**28**). The synthetic route is shown in Scheme 14. The complex [Ru(N-½HSB)₃](PF₆)₂ (**30**) was obtained by heating 1 molar equivalent of ruthenium(III) trichloride with four equivalents of N-½HSB (**9**), in degassed diethylene glycol ethyl ether under an argon atmosphere. A few drops of N-ethylmorpholine as a reducing agent were added. The mixture was stirred at 130°C for three days and formed a grey suspension, which was filtered and the product was precipitated out with a saturated solution of KPF₆.
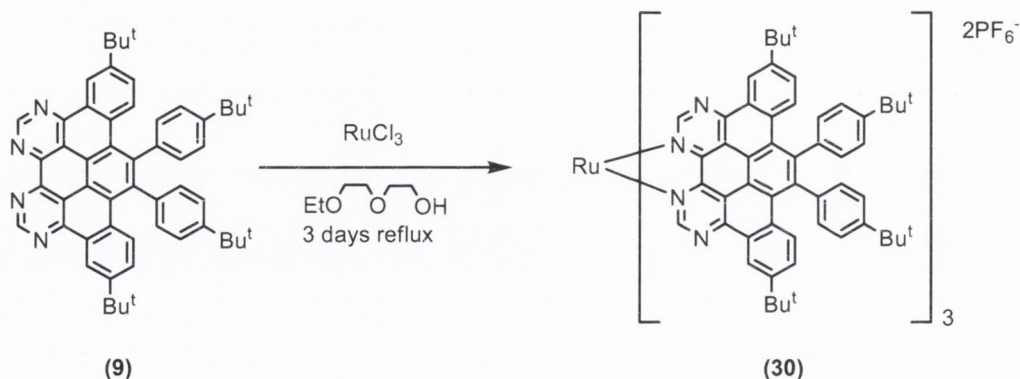
Scheme 14: The synthetic route for [Ru(N-½HSB)₃](PF₆)₂.

The TLC of the crude mixture showed unreacted ligand, a few new products one of which was a major blue compound. This blue product was successfully separated by silica column chromatography, followed by preparative silica plates using (12: 4: 0.5; THF : acetonitrile : KNO₃(aq)) as the system of solvents. The anion exchange gave a blue powder of [Ru(N-½HSB)₃](PF₆)₂ in a 32% yield.

1.2.3.5. Characterisation of Ru(N-½HSB)₃J(PF₆)₂

The lower level of planarity in N-½HSB, meant that analysis techniques could be performed at lower temperature, at room temperature for ^{1}H NMR spectroscopy and 120°C desolvation temperature for electrospray mass spectrometry. Similar behaviour was observed for [Ru(bpy)₂(N-½HSB)](PF₆)₂ **(20)**, which shows no temperature or concentration dependence in its ^{1}H NMR spectra. This is an effect of the reduced aromatic framework of N-½HSB and two non-planar phenyl rings, which are expected to rotate out-of-the plane.

The ESI-mass spectrum of **(30)** (Figure 29) shows a base peak at *m/z* = 1185.96 assigned to [M-2PF₆]$^{2+}$. The ½ m.u. intervals confirmed the 2+ charge of the molecular ion.
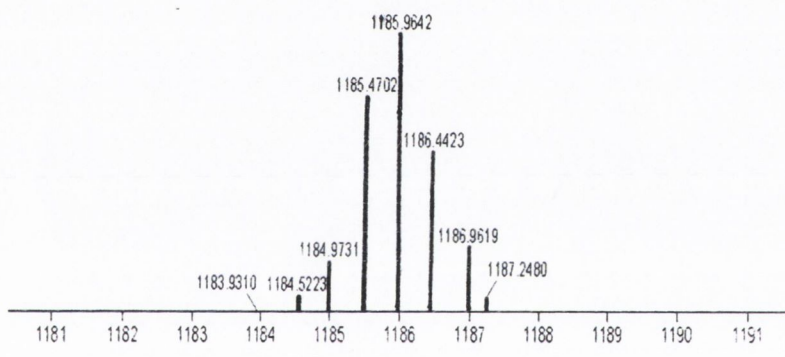
Figure 29: The ESI-mass spectrum of [Ru(N-½HSB)₃](PF₆)₂ (30).

In the room temperature ^{1}H NMR spectrum of **(30)**, two aliphatic signals are observed at δ 1.37 and δ 1.35 each integrating for 18 hydrogen atoms. The six aromatic signals were assigned using the coupling information from the ^{1}H, H TOCSY spectra. The aromatic region for **(30)** is shown in Figure 30. In general, the signals for coordinated N-½HSB are shifted downfield with respect to free N-½HSB. The most downfield signal which is a singlet corresponding to the two hydrogen atoms H1, is one of the exception in this regard (Figure 30). Due to the shielding effect of the pyrimidine ring on the other coordinated ligand signals H1 (δ 9.56), and H2 (δ 9.41) are shifted upfield with respect to H1 (δ 10.13) and H2 (δ 9.64) in the free ligand. The same effect was observed for [Ru(bpy)₂(N-HSB)]$^{2+}$ and [Ru(bpy)₂(N-½HSB)](PF₆)₂.[13,18]

Two doublets assigned to H3 and H4, integrating for two hydrogen atoms each are moved downfield compared to uncoordinated ligand. The signals for protons H5 and H6 also integrating for two hydrogen atoms each, moved downfield about 0.1 ppm with respect to the ligand. The proton shifts for complex (**30**) and ligand (**9**) are collected in the Table 9.

Proton	^{1}H NMR shifts for complex (**30**) (ppm)	^{1}H NMR shifts for ligand (**9**) (ppm)
H1	9.56 (s)	10.13 (br.s)
H2	9.41 (s)	9.64 (d)
H4	7.92 (d)	7.84 (d)
H3	7.56 (dd)	7.40 (t)
H5/6	7.39 (dd)	7.29 (br.t)
H5/6	7.19 (dd)	7.06 (m)

*Table 9: The ^{1}H NMR spectral shifts for [Ru(N-½HSB)₃](PF₆)₂ (**30**) (CD₃CN) together with N-½HSB ligand (CDCl₃).*
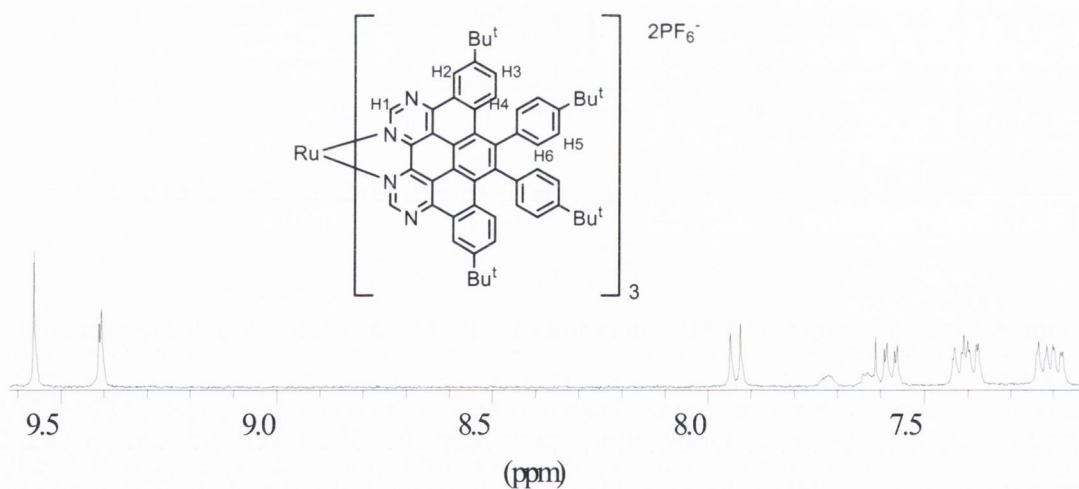
*Figure 30: The aromatic region of the ^{1}H NMR spectrum of [Ru(N-½HSB)₃](PF₆) (**30**) (400 MHz, CD₃CN, 25°C).*

44

UV-vis absorption spectroscopy.

The UV-vis absorption spectrum of [Ru(N-½HSB)$_3$](PF$_6$) (**30**) and of ligand (**9**) are shown in Figure 31. The spectrum of (**30**) shows three characteristic bands. In the ultraviolet region two bands appeared at 279 nm and 363 nm both attributed to ligand localized transitions of N-½HSB, the band at 279 nm is the most intense one. The absorption band for the free ligand (412 nm) in the visible region shifts to the UV when coordinated to the ruthenium. A new broad band is observed in the visible region at 605 nm (with a shoulder at 536 nm). This absorption is assigned as [1]MLCT d-π* transition between ruthenium metal and the ligand.
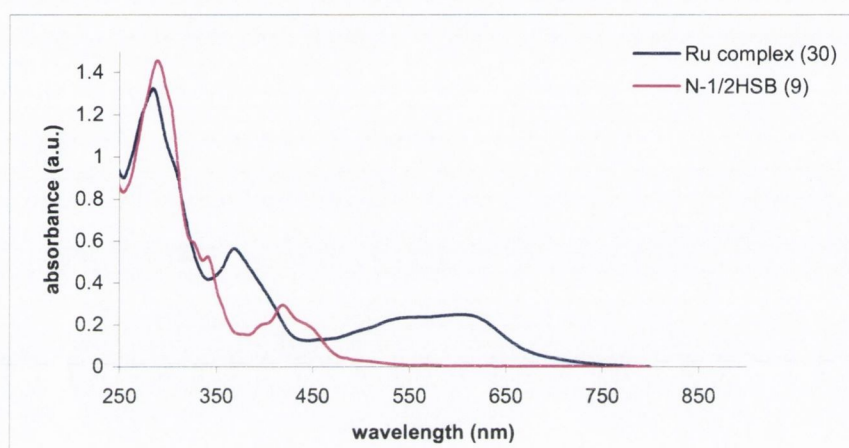
*Figure 31: The UV-vis spectrum of [Ru(N-½HSB)$_3$](PF$_6$) (**30**) and ligand N-½HSB in chloroform.*

The [1]MLCT transition for [Ru(N-½HSB)$_3$]$^{2+}$ (605 nm in chloroform) appeared at the higher energy with respect to [Ru(N-HSB)$_3$]$^{2+}$ (640 nm in chloroform). This blue shift effect of λ_{max} is due to the reduced π electron density on the N-½HSB, which has less fused rings. The shifted [1]MLCT as a consequence of the decrease in aromaticy in N-½HSB has an influence on the colour of the complex. (**30**) possesses an unusual blue colour (Figure 32) in contrast to green [Ru(N-HSB)$_3$]$^{2+}$. This behaviour was not observed in the two heteroleptic complexes [Ru(bpy)$_2$(N-HSB)]$^{2+}$ and [Ru(bpy)$_2$(N-½HSB)]$^{2+}$, which are both green.
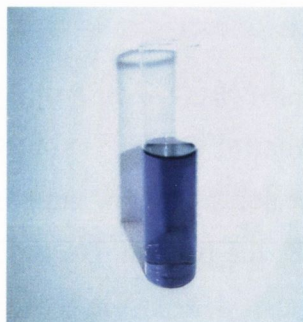
Figure 32: A sample of a solution of [Ru(N-½HSB)₃](PF₆) (30) in d₃-chloroform.

The UV-vis absorptions spectra of (**30**) were run in a variety of solvents, such as acetonitrile, methanol, toluene and tetrahydrofuran. $[Ru(N\text{-}\frac{1}{2}HSB)_3]^{2+}$ does not exhibit the solvatochromic behaviour. This is different compared to absorption spectra of $[Ru(bpy)_2(N\text{-}\frac{1}{2}HSB)]^{2+}$ which are strongly solvent dependent.[13] Mostly λ_{max} (MLCT) appeared around 598 nm. Only in THF was a red shift of 8 nm observed. The absorption spectra for (**30**) in the range of solvents are shown in Figure 33. The complex shows the most intense absorption peaks in acetonitrile, and lower intensity in methanol. The same tendency was noticed for $[Ru(N\text{-}HSB)_3]^{2+}$. In Table 10 are collected λ_{max} absorption and λ_{max} emission for $[Ru(N\text{-}\frac{1}{2}HSB)_3]^{2+}$ together with the literature data for $[Ru(bpy)_2(N\text{-}\frac{1}{2}HSB)]^{2+}$. The ^{1}MLCT absorption for $[Ru(N\text{-}\frac{1}{2}HSB)_3]^{2+}$ was at lower energy with respect to $[Ru(bpy)_2(N\text{-}\frac{1}{2}HSB)]^{2+}$ as expected, due to the presence of the three rigid, highly delocalised molecules of N-½HSB in the complex (**30**).
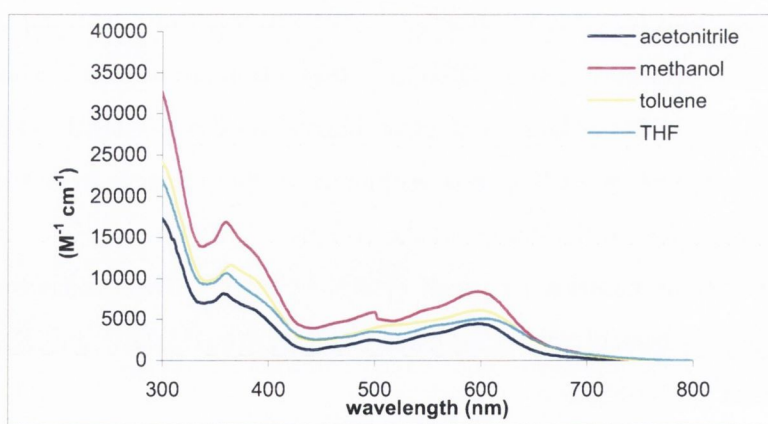
Figure 33: TheUV-vis absorption spectra of $[Ru(N\text{-}\frac{1}{2}HSB)_3]^{2+}$ in various solvents.

Emission spectroscopy

The complex $[Ru(N-\frac{1}{2}HSB)_3]^{2+}$ (**30**) exhibits a very strong emission in the range 700-850 nm and this is shifted to lower energy compared to free ligand (**9**). The emission for $[Ru(bpy)_2(N-\frac{1}{2}HSB)]^{2+}$, $[Ru(bpy)_2(N-HSB)]^{2+}$ are in the range 700-900 nm.[13,18] This emission is red shifted compared to $[Ru(bpy)_3]^{2+}$ as a result of the effect of the low energy of the ^{3}MLCT state stabilized by the extended aromatic ligand N-HSB family. The electronic excitation by the irradiation of the ^{1}MLCT absorption band of (**30**) at 597 nm in acetonitrile shows a broad emission at λ_{max}^{em} at 779 nm. The complex (**30**) exhibits emission in acetonitrile, methanol, toluene and tetrahydrofuran. The most intense emission for this complex was observed in acetonitrile, the least intense in methanol and toluene. In the variety of solvents the λ_{max}^{em} of complex (**30**) is the most blue-shifted (771 nm) in methanol as was expected for the most polar solvent and the emission in tetrahydrofurane is the most red-shifted with λ_{max}^{em} at 800 nm (Figure 34). Similar behaviour was observed for $[Ru(bpy)_2(N-\frac{1}{2}HSB)]^{2+}$ λ_{max}^{em} in methanol (851 nm) when is blue-shifted by 17 nm with respect to acetonitrile solution. For (**30**) this shift is smaller only 8 nm.
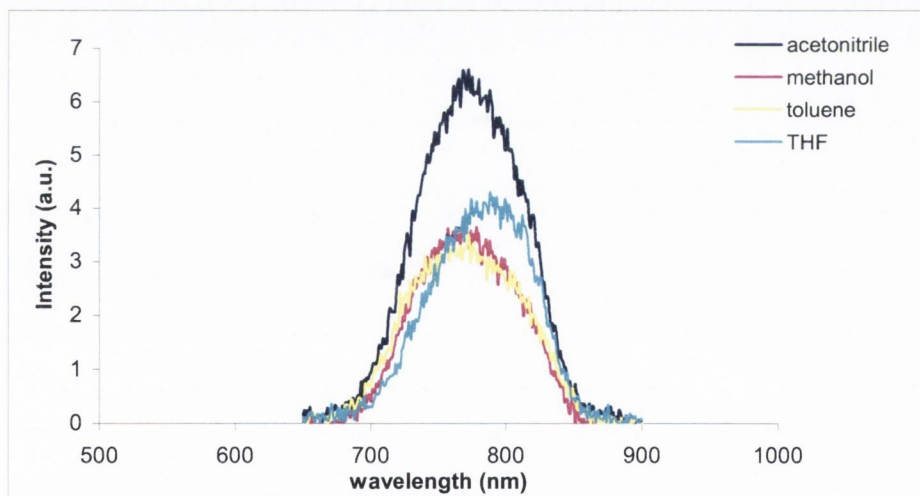
Figure 34: The emission spectra of $[Ru(N-\frac{1}{2}HSB)_3]^{2+}$ (30) in range of solvents

Complex	Solvent	λ_{max}^{abs} (nm)	λ_{max}^{em} (nm)
$[Ru(N-\frac{1}{2}HSB)_3]^{2+}$	THF	606	800
$[Ru(N-\frac{1}{2}HSB)_3]^{2+}$	methanol	598	771
$[Ru(N-\frac{1}{2}HSB)_3]^{2+}$	toluene	598	775
$[Ru(N-\frac{1}{2}HSB)_3]^{2+}$	acetonitrile	597	779
$[Ru(bpy)_2(N-\frac{1}{2}HSB)]^{2+}$ [18]	acetonitrile	591	868
$[Ru(bpy)_2(N-\frac{1}{2}HSB)]^{2+}$ [18]	methanol	583	851

Table 10: Spectroscopic shifts for $[Ru(N-\frac{1}{2}HSB)_3]^{2+}$ in various of solvents together with $[Ru(bpy)_2(N-\frac{1}{2}HSB)]^{2+}$ (room temp).

It is interesting that irrespective of solvent all λ_{max}^{em} in for $[Ru(bpy)_2(N-\frac{1}{2}HSB)]^{2+}$ (**20**) are at lower energy than $[Ru(N-\frac{1}{2}HSB)_3]^{2+}$ (**30**). The same effect was observed for $[Ru(N-HBS)_3]^{2+}$, compared to $[Ru(bpy)_2(N-HSB)]^{2+}$. This effect has been reported in the literature for different ruthenium complexes such as $[Ru(elatin)_3]^{2+}$,[19] $[Ru(taphen)_3]^{2+}$.[45] The sequential replacement of the bpy ligand of $[Ru(bpy)_3]^{2+}$ with taphen or elatin moves λ_{max}^{em} to the higher energy.

A study of the electrochemical behaviour of mono-N-HSB and mono-N-$\frac{1}{2}$HSB complexes was made, but the high level of aggregation of the tris-complex $[Ru(N-HBS)_3]^{2+}$ (**28**) did not allow the redox characterization. A few tests were attempted with 0.1M BuNPF$_6$ as a supporting electrolyte, but no results were obtained. There are a few examples in the literature of the electrochemical behaviour of $[Ru(bpy)_3]^{2+}$ complexes where the bpy are systematically replaced.

Complex or ligand	Reduction potential (V vs Fc/Fc$^+$)^a
[Ru(bpy)$_2$taphen]$^{2+}$.	-0.72
[Ru(bpy)(taphen)$_2$]$^{2+}$.	-0.74
[Ru(taphen)$_3$]$^{2+}$.	-0.70
[Ru(bpy)$_2$eil]$^{2+}$,	-0.88
[Ru(bpy)(eil)$_2$]$^{2+}$,	-0.84, -0.96
[Ru(bpy)$_2$(N-HSB)]$^{2+}$.	-0.93, -1.43
[Ru(bpy)$_2$(N-½HSB)]$^{2+}$	-0.95, -1.47
bpy	-2.22
taphen	-1.26
N-HSB	-1.56, -2.00
N-½HSB	-1.59, -2.04

Table 11: The reduction potentials for Ru(II) complexes, literature examples. $^{a.\ reduction}$
potentials for bpy in the complexes are omitted

The reduction potentials for free ligands such as: taphen, eil, N-HSB and N-½HSB are much less negative than for the free bpy ligand because they have low-lying π^* orbitals rendering reduction easier. The same is true for the reduction of the complexed ligands so that systems containing sequential replacement of bpy for more aromatic ligands see the ligand reduction occurring at less negative potential. It can be postulated that the same trend would have been observed for the redox behaviour of [Ru(N-HSB)$_3$]$^{2+}$ had it been measurable.

1.3. **Conclusion.**

In this work five N-containing polyaromatic compounds have been synthesized, three of them are novel. N-HSB (**8**) and its daughter N-½HBS (**9**) have been obtained according to the literature procedure with satisfactory yields.[11,13] The synthetic route for (**8**) and (**9**) involves a lot of steps, a few modifications were introduced and some purifications methods were changed, which improved the yields of these reactions.

The new precursor (24) analogous to (7) without substituted alkyl chains was obtained. The oxidative cyclodehydrogenation of (24) resulted in three novel ligands. In the cyclisation reaction with AlCl$_3$ and CuCl$_2$ two products were obtained, fully cyclised (26) and half-cyclised (25). In the reaction with MoCl$_5$ (24) gave a half-cyclised product (25) and partially cyclised (27). Compounds (25) and (26) are analogues to N-HSB and N-½HSB, respectively. (27) represents the new member of N-heretosuperbenzene family in the way of cyclisation arrangement. Due to the lack of the t-butyl groups these three new compounds are low in solubility compared to (8) and (9). (26) is not soluble in any common solvent and only solid-state analysis allowed its characterization.

Novel homoleptic Ru(II) complexes of (8) and (9) have been synthesised and fully characterised. The tris-complex of (8) [Ru(N-HSB)$_3$]$^{2+}$ (28) shows π-stacking in the solution which affects the spectroscopic and spectrometry analysis. The high temperature ^{1}H NMR and MS are required to characterise (28). Due to two uncyclised rings, which are free to rotate in N-½HSB complex [Ru(N-½HSB)$_3$]$^{2+}$ (30) does not show aggregation in solution. Polyaromatic ligands (8) and (9) with extended electron density possess low-lying π* orbitals and play an important role in the modifying the lowest energy ^{1}MLCT absorption and ^{3}MLCT emission in Ru(II) complexes.

The UV-vis absorption and emission analysis have been studied in a variety of solvents. The electronic absorption spectra for (28) and (30) in all solvents are similar in terms of overall shape. In general the absorption spectra of (28) and (30) do not show solvatochromic behaviour, but the polarity of solvent has an influence on the emission.

The ^{1}MLCT absorption for (30) is blue-shifted with respect to (28), due to the reduction of electron density on (9). Compared to [Ru(bpy)$_3$]$^{2+}$ ^{1}MLCT absorption for (28) and (30) is red-shifted and appear at 630 nm and 597 nm, respectively. Both complexes show intensive emission in the range 700-900 nm. The emission maxima are blue shifted compared to mono-complex [Ru(bpy)$_2$(N-HSB)]$^{2+}$. This phenomena was reported previously in the literature.[19]

As future work, from the photophysical point of view the homoleptic Osmium(II) complexes of N-HSB and N-½HSB would be very interesting to develop. In general Os(II) analogues to Ru(II) complexes exhibit MLCT transition at lower energy, due to

the higher-lying d-orbitals of Os compared to Ru. According to the literature example the MLCT transition for $[Os(eil)_3]^{2+}$ at 632 nm moves by 33 nm to the lower energy, compared to $[Ru(eil)_3]^{2+}$ at 599 nm.[46]

1.4. <u>References</u>

[1] M. Müller, C. Kübel, K. Müllen, *Chem. Eur. J.*, **1998**, 4, 2099-2109

[2] F. Dötz, J. D. Brand, S. Ilo, L. Gherghel, K. Müllen, *J. Am. Chem. Soc.*, **2000**, 122, 7707-7717

[3] P. Kovacic, A. Kyriakis, *J. Am. Chem. Soc.,* **1963**, 20, 454-458

[4] P. Kovacic, M. Jones, *Chem. Rev.,* **1987**, 87, 357-379

[5] M. Wehmeier, M. Wagner, K. Müllen, *Chem. Eur. J.*, **2001**, 7, 2197-2205

[6] S. Iyer, M. Wehmeier, J. Diedrich, K. Müllen, *Angew. Chem., Int. Ed.*, **1997**, 36, 1603-1610

[7] . F. Barigelletti, L. de Cola, V. Balzani, P. Belser, A. von Zalewsky, F. Vöglte, F. Ebmeyer, S. Gramenudi, *J. Am. Chem. Soc.*, **1989**, 111, 4662-6668

[8] M. D. Watson, A. Fechtenkötter, K. Müllen, *Chem. Rev.*, **2001**, 101, 1267-1300

[9] P. Rempala, J. Kroulik, B. T. King, *J. Am. Chem. Soc.*, **2004**, 126, 15002-15003

[10] P. Rathore, C. Burns, *J. Org. Chem. Synth.*, **2003**, 68, 4071-4074

[11] S. M. Draper, D. Gregg, R. Madathil, *J. Am. Chem. Soc.*, **2002**, 124, 3486-3487

[12] D. J. Gregg, C. M. A. Ollagnier, C. M. Fitchett, S. M. Draper, *Chem. Eur. J.*, **2006**, 3043-3052

[13] D. J. Gregg, E. Bothe, P. Höfer, P. Passaniti, S. M. Draper, *Inorg. Chem.,* **2005**, 44, 5654-5660

[14] M. Di Stefano, F. Negrii, P. Carbone, K. Müllen, *Chem. Phys.,* **2005**, 314, 85-99

[15] P. Rempala, J. Kroulik, B. T. King, *J. Org. Chem.*, **2006**, 71, 5067-5081

[16] B. Durham, J.V. Cacpar, J. K. Nagle, T. J. Meyer, *J. Am. Chem. Soc.*, **1982**, 104, 4003-4810

[17] P. R. Aston, R. Ballardini, V. Balzani, E. C. Constable, A. Credi, O. Kocian, S. J. Langford, J. A. Preece, L. Prodi, E. R. Schofield, N. Spencer, J. F. Stoddart, S. Wanger, *Chem. Eur. J.*, **1998**, 12, 2413-2422

[18] S. M. Draper, D. J. Gregg, E. R. Schofield, W. R. Browne, *J. Am. Chem. Soc.*, **2004**, 126, 8694-8701

[19] S. D. Bergman, D. Gut, M. Kol, C. Sabatini, A. Barbieri, F. Barigelletti, *Inorg. Chem.*, **2005**, 22, 7943-7950

[20] E. C. Glazer, Y. Tor, *Angew. Chem. Int. Ed.*, **2002**, 41, 4022-4026

[21] N. Kakegawa, A. Yamagishi, *Chem. Mater.,* **2005**, 17, 2997-3003

[22] V. Balzani, A. Juris, M. Venturi, *Chem. Rev.*, **1996**, 96, 759-833

[23] A. Sardarian, B. J. Coe, K. T. Douglas, *Tran. Metal Chem.*, **2003**, 28, 905-907

[24] R. J. Watts, *J. of Chemical Education*, **1983**, 60, 10, 834-842

[25] R. P. Thummel, F. Lefoulon, *Inorg. Chem.*, **1987**, 26, 675-680

[26] E. Barranoff, J. P. Collin, Y. Furusuho, A. C. Laemmel, J. P. Sauvage, *Chem. Commun.*, **2000,** 1935-1936

[27] E. Alessio, G. Mestroni, G. Nardin, W .M. Attia, M. Calligaris, G. Sava, S. Zonet, *Inorg. Chem.*, **1988**, 27, 4099-4106

[28] D. J. Gregg, C. M. Fitchett, S. M. Draper, *Chem. Commun.*, **2006**, 3090-3092

[29] . V. Caspar, T. J. Meyer, *Inorg. Chem.*, **1983**, 22, 2444-2453

[30] G. d. Danzer, J. A. Golus, J. R. Kincaid, *J. Am. Chem. Soc.*, **1993**, 115, 8643-8648

[31] J. R. Johnson, O. Grummit, *Org. Synth.,* III, N.Y., **1955**, 806

[32] R. Singh, M. P. S. ishar, N. K. Girdhar, D. Velmurugan, A. S. Pandi, *Eur. J. Org. Chem.*, **2002**, 3734

[33] B. Kramer, A. Averhoff, S. R. Waldvogel, *Angew. Chem. Int. Ed.*, **2002**, 41, 2981-2982

[34] B. Kramer, R. Fröhlich, S. R. Waldvogel, *Eur. J. Org. Chem.*, **2003**, 3549-3554

[35] L. Barnett, D. M. Ho, K. K. Baldridge, R. A. Pascal Jr, *J. Am. Chem. Soc.*, **1999**, 121, 727-733

[36] . N. P. Hacker, J. F. W. McOmie, J. Meunier-Piret, M. Van Meerssche, *J. C. S. Perkin I*, **1982**, 19-23

[37] D. Pena, A. Cobas, D. Perez, E. Guitian, L. Castedo, *Org. Letters*, **2000**, 11, 1629-1632

[38] E. Barranoff, J. P. Collin, Y. Furusuho, A. C. Laemmel, J. P. Sauvage, *Chem. Commun.*, **2000,** 1935-1936

[39] S. Bernard, J. A. Bomon, P. L. Huston, H. D. Abruna, J. L. Guglovsky, X. Gao, G. G. Malliaras, *J.Am.Chem.Soc.*, **2002**, 124, 13624-13628

[40] S. E. Encinas, L. Flamigni, F. Barigelletti, E. C. Constable, C. E. Housecroft, E. R. Schofield, E. Foggemeier, P. Fenske, M. Neuburger, J.G. Vos, M. Zehnder, *Chem. Eur.,* **2002**, 8, 137-150

[41] I. P. Evans, A. Spencer, G. Wilkinson, *J. Chem. Soc., Dalton Trans.*, **1972**, 204-209

[42] A. Rudi, Y. Kashman, D. Gut, F. Lellouche, M. Kol, *Chem. Commun.,* **1997**, 17-18

[43] S. D. Bergman, D. Reshef, L. Frish, Y. Cohen, I. Goldberg, M. Kol, *Inorg. Chem.*, **2004**, 43, 3792-3794

[44] S. Bergman, M. Kol, *Inorg. Chem.*, **2005**, 44, 1647-1654

[45] A. Juris, P. Belser, F. Barigelletti, A. Von Zelewsky, V. Balzani, *Inorg. Chem.,* **1986**, 25, 256-259

[46] D. Gut, A. Rudi, J. Kopilov, I. Goldberg, M. Kol, *J. Am. Chem. Soc.*, **2002**, 5449-5456

Part 2: Pyridine-centred ligands and their complexes

2.1. Introduction

2.1.1. Synthesis of terpyridine ligands

The literature shows a great number of interesting supramolecular structures based on multidentate terpyridine ligands. The first tridentate ligand 2,2':6', 2"-terpyridine was discovered in 1933 by Morgan and Burstall. Since then the chemistry of terpyridine has been intensively investigated, due to its interesting coordination chemistry.

It has been shown that a wide range of terpyridine derivatives can be synthesised via simple synthetic routes. The first synthetic approach for terpyridine derivatives is shown in Scheme 15.[1] There are many examples of the use of this route in the literature, some of which are shown in the Scheme 15. The synthetic route includes two steps.[1] The base catalysed aldol condensation between two equivalents of 2-acetylpyridine and one equivalent of adequately substituted aldehyde forms an intermediate diketone. The cyclisation reaction of this intermediate, using ammonium acetate gives the corresponding cyclised ligand. The formation of the central pyridine ring is achieved in the presence of an oxidising agent. With this synthetic pathway a great number of terpyridine ligands can be obtained.
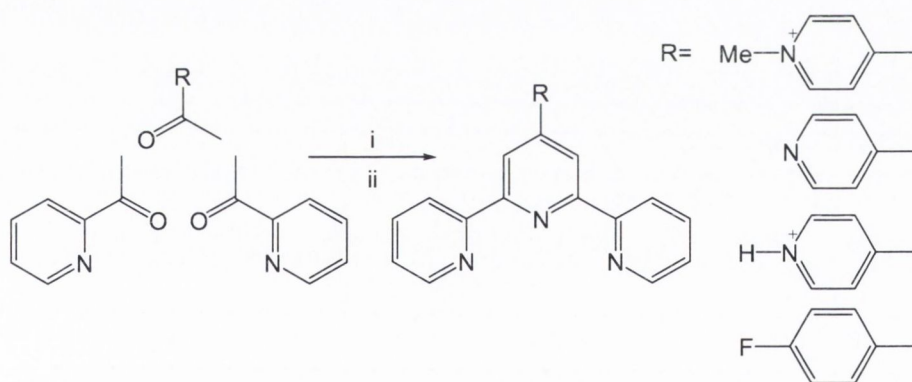
Scheme 15: The synthetic route for substituted terpyridine derivatives, i) NaOH, ii) [NH4][OAc][1,2]

The second synthetic pathway to form multidomain ligands employs 4'-chloro substituted terpyridine.[3,4] Cltpy (4'-chloro-2,2':6',2"-terpyridine) is obtained in a three-step reaction (Scheme 16). The reaction of two equivalents of ethyl-pyridine-2-carboxylate and one equivalent of acetone in the presence of NaH, followed by

cyclisation with ammonium acetate gives a keton. Prolonged reaction of this keton with PCl_5 in $POCl_3$ yields Cltpy.
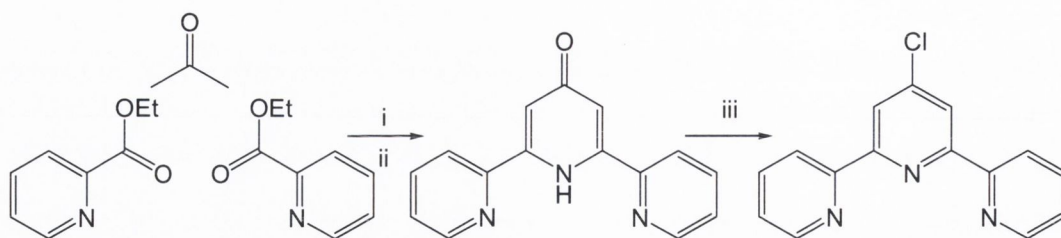
Scheme 16: The synthesis of 4'-chloro-2, 2':6', 2"-terpyridine, i) NaH, ii) [NH₄][OAc], iii) POCl₃, PCl₅.[3,4]

Substitution of the chloride of Cltpy using appropriate reagents allows the formation of a wide range of substituted terpyridines. They can contain a variety of electron-withdrawing or electron-accepting groups such as EtO-, HO-, Me_2N-, to form the following ligands: EtOtpy (4'-ethoxy-2,2':6',2"-terpyridine), HOtpy (4'-hydroxy-2,2':6',2"-terpyridine or Me_2Ntpy (4'-(N,N-dimethylamino)-2,2':6',2"-terpyridine. [3,4]

The Cltpy plays an important role in the synthesis of "back-to-back" terpyridines or potentially binucleating ligands, for example 6', 6"-bis(2-pyridyl)-2,2':4',4":2",2"'-quaterpyridine (Figure 35). This binucleating ligand was obtained through the formation of a C-C bond at the 4' positions between two terpyridines, using [Ni(Ph₃)₂Cl₂] as a catalyst to remove the chlorine atoms. This novel bridging ligand, which behaves as a "back to back" ligand, is ideal for di-transition metal complexes or for the tailoring of new supramolecular architectures.[4]
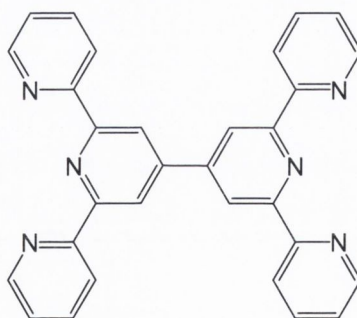
Figure 35: The structure of "back to back" ligand 6', 6"-bis(2-pyridyl)-2,2':4',4":2",2"'-quaterpyridine.[4]

2.1.2. Terpyridine ligands in supramolecular chemistry

The rapid development of crystal design and the engineering of coordination polymers have created novel materials with a variety of structural features and properties. The construction of various novel polymers such as molecular strings, helicates, grids and boxes involves carefully designed multidentate ligands and metal ions with appropriate stereoelectronic preferences. The formation of supramolecular polymers is based on the self-assembled generation of compatible monomeric compounds (Scheme 17).[5]
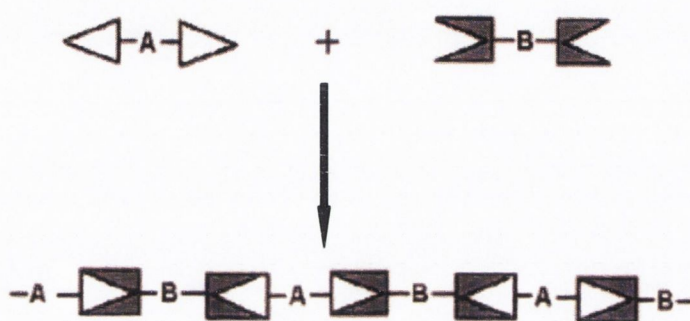
Scheme 17: Association of molecular blocks leading to the formation of a polymeric supermolecule.[5]

Multidomain, nitrogen-containing ligands are very attractive for the construction of supramolecular architectures. The ligands 4'-(4-pyridyl)-2,2':6',2"-terpyridine (pyterpy) (31), 4'-(2-pyridyl)-2,2':6',2"-terpyridine (32) and 4'-(pyridylethynyl)-2.2':6'2"-terpyridine (33) contain two metal binding domains (Figure 36)[6,7,8,9,10].
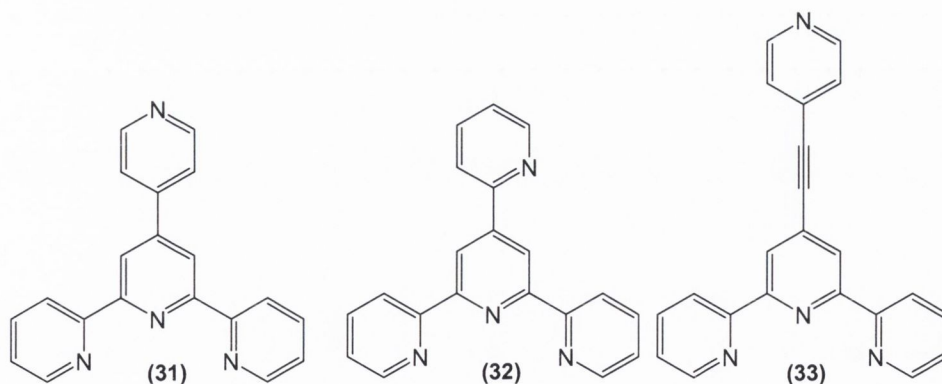
Figure 36: Examples of multlidentate ligands.

These compounds can act as bridging ligands, because they possess a tridentate terpy on one side and a monodentate pyridyl on the opposite side. This allows them to create macrocyclic oligomers or linear polymers. The reaction of ligands (**31**) and (**32**) with the same metal salt (saturated KSCN solution containing CuSCN), can build different supramolecular architectures. These ligands present a very good example of how the design of the ligand can greatly affect the product of the reaction. Hou *et al.* prepared mixed valence $Cu^{I} Cu^{II}$ compounds based on ligands (**31**) and (**32**)[11,12] with SCN as a linker. They obtained polymers with two independent structures $[Cu_2(\mathbf{31})(\mu1,3\text{-}SCN)_{2.5}]_n \cdot 0.5n SCN$ (**34**) and $[Cu_2(\mathbf{32})(\mu1,3\text{-}SCN)_3]_n$ (**35**). The influence of the terpyridyl moiety on the structure is shown in (Figure 37 and Figure 38). Ligand (**31**) forms a 2-D brick-wall-like layer structure. The asymmetric unit of (**34**) consists of two copper atoms, one molecule of (**31**) and four thiocyanates. Divalent Cu2 and monovalent Cu1 are linked with ligand (**31**) by a tridentate and monodentate pyridyl site, respectively. Cu2 possesses square-pyramidal geometry, which is completed by two nitrogen atoms from SCN⁻ ions. Cu1 has a distorted tetrahedral geometry created by the pyridyl nitrogen and three sulfur atoms from different SCN⁻ ions.
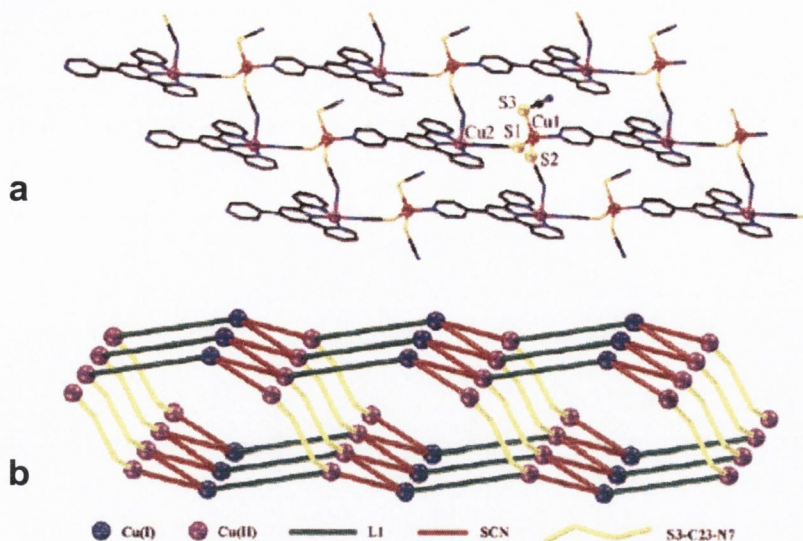
Figure 37: a) 2-D brick-like layer structure of compound (34), b) 2-D brick-wall like bilayer structure connected by S3-C23-N7 groups between two monolayers in (34).

The asymmetric unit of (**35**) contains two mixed-valence copper atoms, one molecule of (**32**) and three SCN⁻ ions. The geometry of the coordination environment divalent Cu2 is similar to that of (**34**) except that one of the SCN⁻ ions is linked by sulfur instead of nitrogen in SCN⁻. The distorted tetrahedral geometry of the monovalent Cu1 is composed of two nitrogen atoms and two sulfur atoms from four SCN⁻ groups. In (**35**) the pendant pyridine is uncoordinated and no grid-type building was observed. In (**35**) the [Cu^{II}(**32**) (SCN)$_2$] unit is linked to two Cu^{I} by two bridging SCN⁻ ions with a N-1,3-SCN coordination mode, this gives a sixteen member Cu^{II}NCSCu^{I}NCSCu^{II}NCSCu^{I}NCS ring (Figure 38).
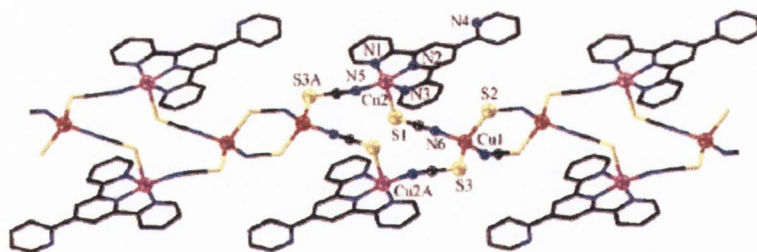
Figure 38: Perspective view of the structure (35).

Potentially bridging ligands (pyridyl–terpy) (**31**) and (**33**) are popular for the creation of linear coordination networks in the "head-to-tail" fashion.

Hayami *et al.* synthesised the spin transition compound [Co(pyterpy)Cl$_2$]·MeOH,[13] which forms a 1-D network. The intermolecular arrangement shows π-stacking between terpy units forming a quasi 3-D network, with molecules of MeOH in the inter-chain position (Figure 39).
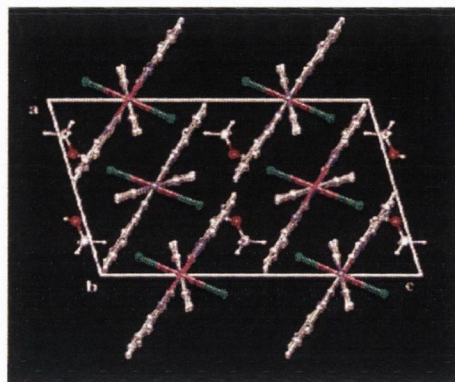
Figure 39: Molecular packing of [Co(pyterpy)Cl$_2$]·MeOH along the b-axis, (Co in pink, O in red).

The self-assembly of CoCl$_2$ and ligand (**33**) resulted in the formation of a 1-D directional network, with the single unit defined as [py-CoCl$_2$-terpy].[14] The 1-D networks are organised parallel to each other with opposite directionality (Scheme 18).
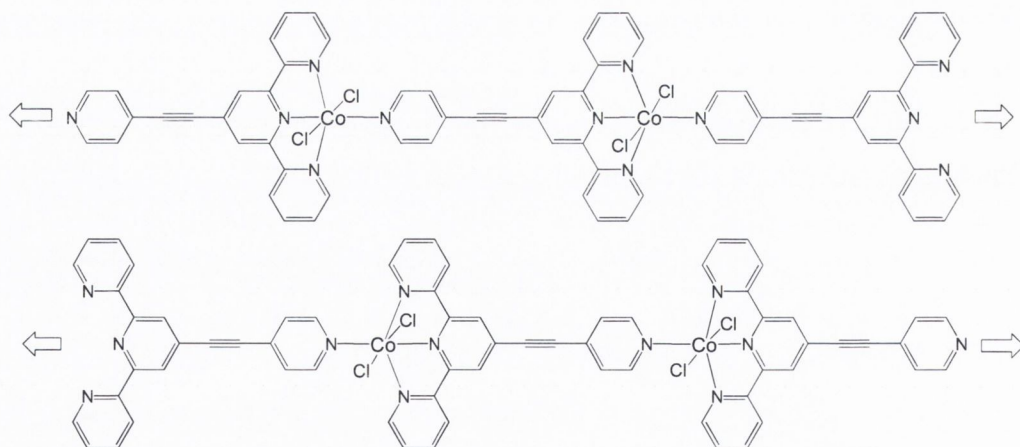
*Scheme 18: Scheme of the chains of 1-D network of [Co(**33**)Cl$_2$].*

Lanthanide metal ions, such as Eu(III), Sm(III), Yb(III) and La(III), due to their high coordination numbers, are very likely to form supramolecular architectures. There are a lot of examples of lanthanide polymers based on mono- and bidentate nitrogen

containing bridging ligands,[15,16] but only a few supramolecular networks with tridentate terpy-like ligands are reported.[17,18]

Schröder *et al.* obtained interesting framework structures based on 4,4'-bipyridine and its derivatives. Highly-connected nets using lanthanide(III) metals and 4,4'-bipyridine-N,N'-dioxide (**36**) as the ligand L were synthesised.[19,20] Figure 40 shows a net of the 4-connected complex of $[La(36)_2(NO_3)_3]_\infty$. This is formed by reacting $La(NO_3)_3$ with L in methanol, the La(III) metal is 10-coordinated.
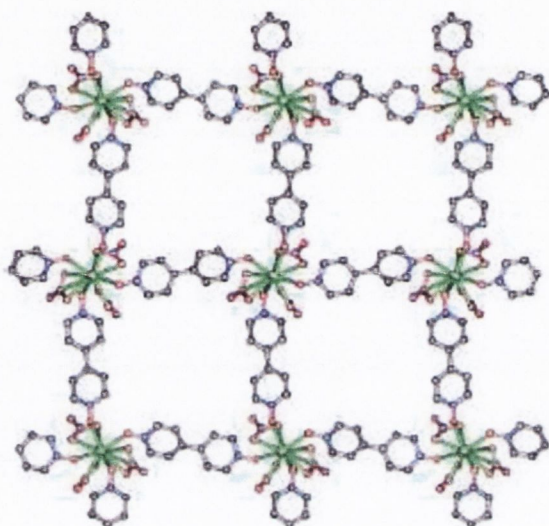
Figure 40: View of the 4^4 grid of compound $[La(36)_2(NO_3)_3]_\infty$[19].

Other complexes based on (**36**) have been formed; $[Yb(36)_3(CF_3SO_3)_3]_\infty$, $[Er(36)_5(I)_3(36)_{0.5} \cdot MeOH]_\infty$ and $[La(36)_4(ClO_4)_3 \cdot C_6H_5Cl \cdot CH_3OH]_\infty$.[19] Due to the flexible bridging N-oxide ligand these complexes can create highly connected bilayer topologies, which are shown in Figure 41.
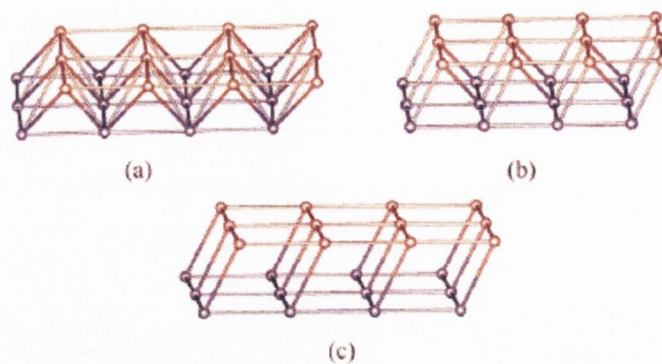
Figure 41: Topological networks of (a) 8-connected bilayer, (b) 6-connected bilayer, (c) 5-connected bilayer. The 4^4 nets are shown in red and blue.[19]

The two different coordinating moieties in pyterpy type ligands allow the generation of heteronuclear coordination networks. The group of Sun synthesised heterometallic complexes with general formula {*fac*-Br(CO)$_3$Re[μ-(pyterpy)$_2$M]}$_4$(PF)$_8$ (M=Fe, Ru or Os) (Figure 42).[21] Transition metal-based macrocycles are interesting due to their photophysical properties. They can be used as hosts for a variety of guest molecules. The bridging ligand has a big influence on the geometries and physical properties of self-assembly macrocyclic complexes.[22] The M(II) square-like structures due to the high possitive charge have potential as hosts for inorganic anionic species.
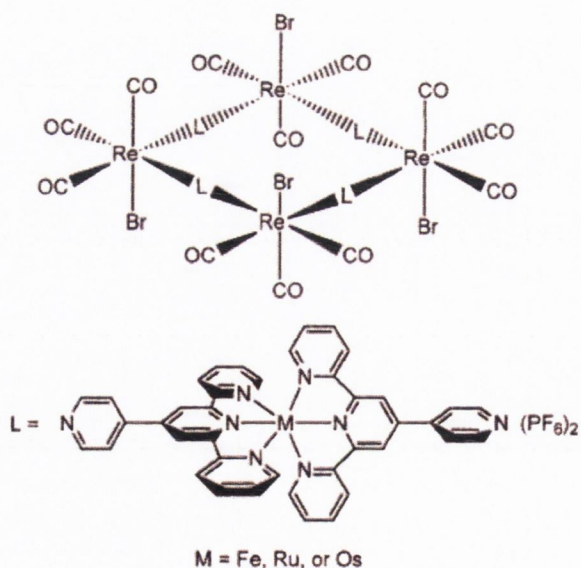
Figure 42: The structure of {fac-Br(CO)$_3$Re[μ-(pyterpy)$_2$M]}$_4$(PF)$_8$.

The aim of our work was to synthesise novel pyridine-centered ligands. The new compounds contain two or four coordination sites. A tri-dentate terpy on one side and a monodentate species on the opposite side of these ligands make them ideal to act as a bridging ligands. New ligands were reacted with a range of metals, such as Cu, Cd, La and Sm to create interesting coordination polymers.

2.2. Results and discussion

2.2.1. Synthesis of pyridine-centered ligands

The pyridine-centered ligands are based on a combination of pyridine and terpyridine units. The synthetic method for 3', 4' and 5'-substituted 2.2':6',2''-terpyridines involves several steps. Substituted aldehydes and ketones are required as precursors.

The [1-(2-pyridyl)-2-phenyl]ethanone was prepared by Grignard reaction (Scheme 19), following a literature procedure.[23] Benzyl magnesium chloride was reacted with 4-cyanopyridine under an argon atmosphere. A yellow precipitate was formed. The reaction mixture was treated with a saturated solution of NH_4Cl. Column chromatography of the yellow crude oil gave product (39) in satisfactory yield (56%).
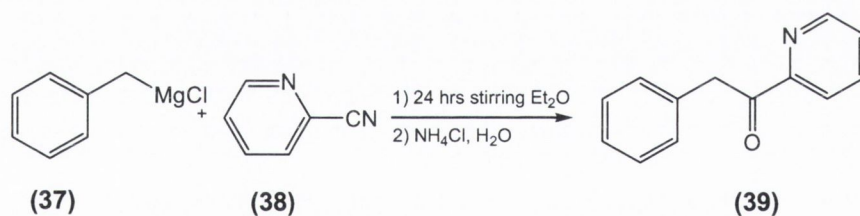
Scheme 19: The synthesis of ketone (39).

Scheme 20 shows the synthetic pathway for the novel binucleating ligands (41) and (42). This reaction is based on the Hantzsch synthesis. This reaction allows the preparation of the new pyridine-centered ligands by the condensation of an aldehyde and two equivalents of keton in the presence of ammonia.

Scheme 20: The synthetic route for ligands (41) and (42), with reaction conditions: 1)
KOH, EtOH, H₂O; 2) CH₃COONH₄, acetic acid.

The base catalysed aldol condensation between 4-pyridine carboxaldehyde (or 3-pyridine carboxaldehyde) and (39), followed by Michael reaction gave an intermediate diketone (40a) (or 40b). The cyclisation reaction of (40a,b) with an excess of ammonium acetate in ethanol resulted in the formation of the corresponding cyclised products (41), (42). Both ligands were obtained in good yields (75% and 60% respectively).

Compound (42) is a new bridging ligand in the family of multi-functional ligands, while (41) was synthesised before in our group.[29] The only difference between them is the position of the nitrogen on the pyridine ring, opposite to the terpy. The position of the monodentate species 3' or 4' respectively for (42) and (41) had a dramatic effect on the metallosupramolecular architectures obtained with these ligands.

The synthesis of the next multidomain ligand (51) is also based on the Hantzsch synthesis. The mechanism and conditions were similar to those for ligands (41) and (42). The aldehyde used for this reaction was commercially available 4-pyridine-carboxaldehyde; the keton had to be synthesised. At first the synthesis of the ketone precursor 1-pyrimidin-2-yl-2-pyridin-4-yl-ethanone (46) was attempted to allow the same synthetic pathway as for (42) (Scheme 21).[23] The problem was that the commercially available starting material (43) was in the acidic form. In order to neutralise the 4-picocyl chloride hydrochloride (43) was washed with a solution of NaOH. Then (44) was reacted with magnesium to form a Grignard reagent. But only part of the magnesium reacted and after the addition of 2-cyanopyridine there was no sign of product (46). After washing with NH₄Cl and extraction with chloroform the

64

reaction mixture turned to a purple gel, which might suggest that the molecules of (**44**) react with itself and create polymer of $[C_5H_4NCH_2Cl]_n$.

Scheme 21: The synthetic route for ketone (46) based on Grignard reaction.

Finally the substituted ethanone (**46**) was synthesised according to a literature procedure (Scheme 22).[24] The reaction of one equivalent of ethylpicolinate (**47**) with 4-picoline (**48**) in a lithiation reaction gave (**46**) as a yellow precipitate in good yield (80%).
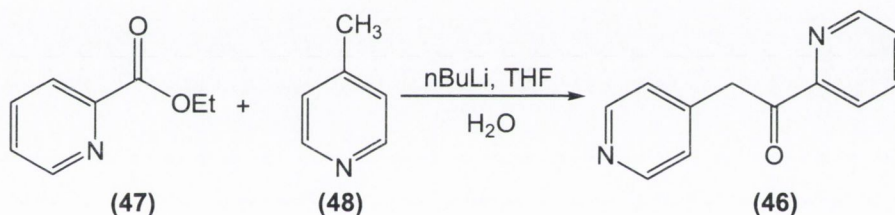
Scheme 22: The synthetic route for ketone (46).

The base-catalysed aldol condensation between (**46**) and 4-pyridinecarboxaldehyde (**49**) followed by Michael reaction provided the diketone intermediate (**50**). This was in turn reacted with ammonium acetate in the presence of acetic acid to give a new terpy ligand (**51**), substituted with three 4-pyridyl groups (Scheme 23).
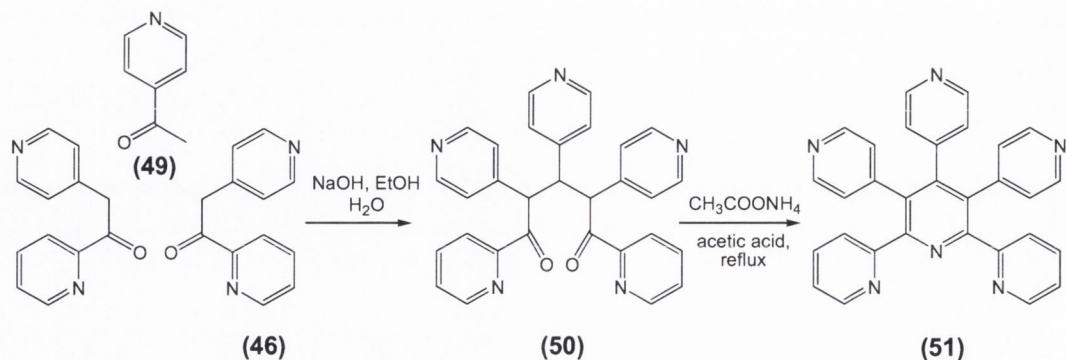
Scheme 23: Synthesis of multidomain ligand (51).

2.2.2. Characterisation of pyridine centered ligands

The ^{1}H NMR spectra for ligands (41), (42) and (51) were assigned using H, H and C, H COSY experiments, and the nOe spectra. All the ligands possess a C_2 axis of an symmetry, which simplifies their spectra.

The ^{1}H NMR spectrum for ligand (41), together with assigned hydrogen atoms, is shown in Figure 43. All peaks are situated in the aromatic region between δ 8.51 and δ 6.75. The most downfield peak integrates for two hydrogen atoms and appears at δ 8.51. It is a doublet corresponding to the proton assigned to H9. The next signal is a doublet of doublets allocated to proton H19 at δ 8.21, which is situated on ring D. The downfield shift of these peaks was expected due to the deshielding effect of the neighbouring nitrogen atoms in each case. The next three signals are located on ring B and they are a triplet of doublets, a doublet and a multiplet assigned to H7 (δ 7.53), H6 (δ 7.38) and H8 (δ 7.12) respectively. All integrate for two hydrogen atoms. Multiplets at δ 7.02 and δ 6.92 integrate for six and four hydrogen atoms respectively; both are related to protons on ring C. The most upfield signal of all is a doublet of doublets that integrates for two protons and is assigned to H18 (δ 6.75).
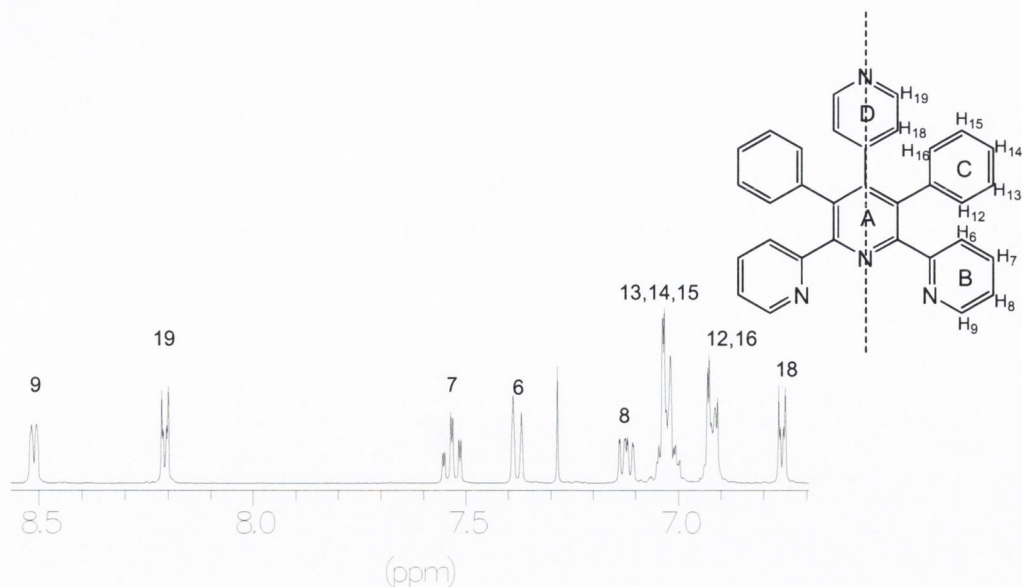
Figure 43: The ^1H NMR spectrum of the ligand (41), 400 MHz, CDCl$_3$, 25°C.

Due to the rotation of the 3-pyridyl ring (42) also possesses C$_2$ symmetry. The ^{1}H NMR spectrum of (42) (Figure 44) contains eight signals. The most downfield signal δ 8.52 is assigned as expected to H9 and integrates for two hydrogen atoms. Upfield of this signal appears proton H20 (δ 8.21), integrating for one hydrogen atom, it is situated on ring D. Proton H18 (δ 8.09) also integrates for one proton. The characteristic triplet of doublets and doublet for protons H7 and H6 of ring B are situated at δ 7.53 and 7.40 respectively, both integrate for two protons each. The fourth signal H8, of ring B is overlapped with the signal correlated to proton H22 at δ 7.13; this multiplet corresponds to four hydrogen atoms. The last two signals, integrating for six protons in total appear at δ 7.04 and 6.99, and are attributed to H13, H14, H15 and H12, H16 and H21, respectively.
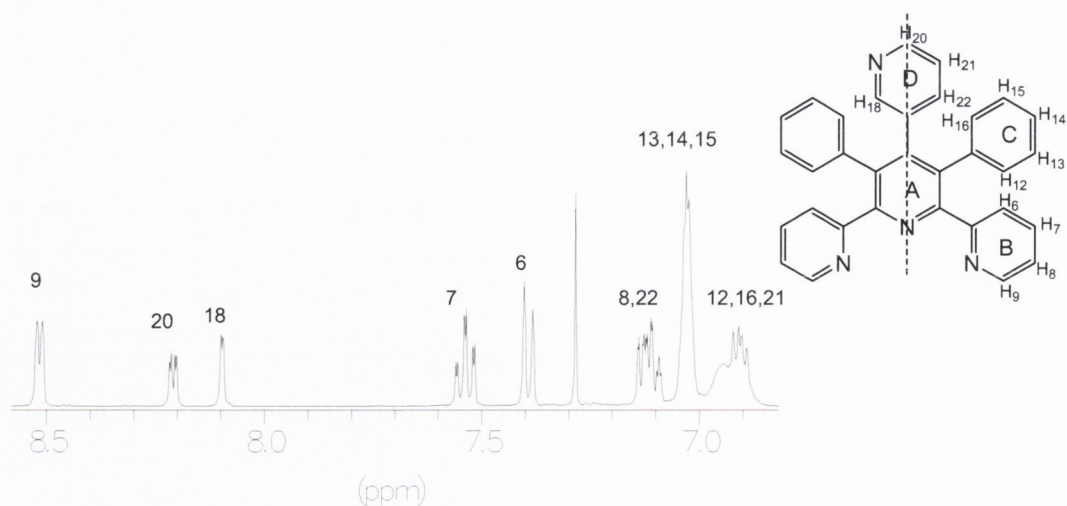
*Figure 44: The ^1H NMR spectrum of the ligand (**42**), 400 MHz, CDCl$_3$, 25°C.*

The last compound synthesised in this series of bridging ligands is the multifunctional compound (**51**). Figure 45 shows the proton ^1H NMR spectrum for this ligand. The seven signals altogether integrate for 20 hydrogen atoms. The signal correlated with proton numbered H9 is the lowest field signal (δ 8.30), the same as for ligands (**41**) and (**42**). Due to the shielding effect of the nitrogen atoms on the pyridine rings the next downfield signals are for protons H13, H15 and H19 (δ 8.24). Signals for proton H6, H7 and H8 appear as a doublet, triplet of doublets and a multiplet respectively at δ 7.72, 7.66 and 7.14. The two doublets at δ 6.83 (H12, 16) and 6.73 (H18) are integrated for four and two hydrogen atoms respectively.
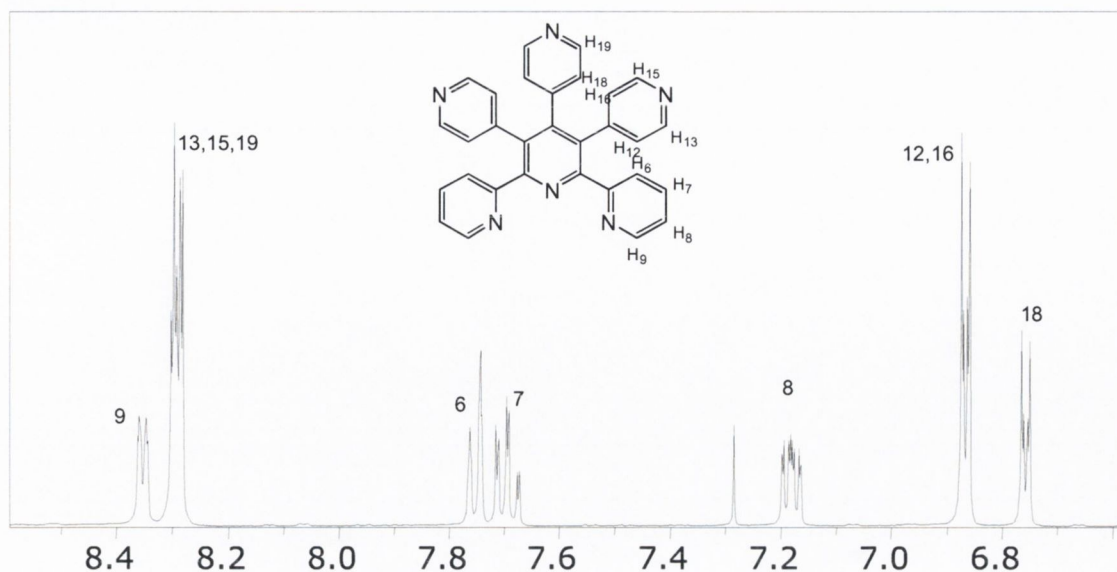
Figure 45: The ^1H NMR spectrum of the ligand (51), 400 MHz, CDCl₃, 25°C.

In assigning the spectra the coupling constants were very useful. The couplings $J_{6,7}$ are bigger (7.5-8.0 Hz) than $J_{8,7}$ (4.0-5.5 Hz) and the comparable values for (41), (42) and (51) are almost identical (Table 12).

Coupling Constants (Hz)	Compound		
	(41)	(42)	(51)
$J_{9,8}$	5.04	5.04	5.04
$J_{9,7}$	1.56	1.52	1.48
$J_{8,6}$	1.00	1.00	2.00
$J_{6,7}$	7.56	7.52	8.04
$J_{8,7}$	7.56	7.52	7.52

Table 12: Coupling constants for (41), (42) and (51).

The X-ray crystal structure of compound (51) was obtained. Crystals of (51) suitable for analysis were grown by slow evaporation of solvent from the chloroform solution

of the ligand. Ligand (51) crystallised in the monoclinic space group P2₁/c. The asymmetric unit contains one molecule of (51) and one molecule of chloroform.
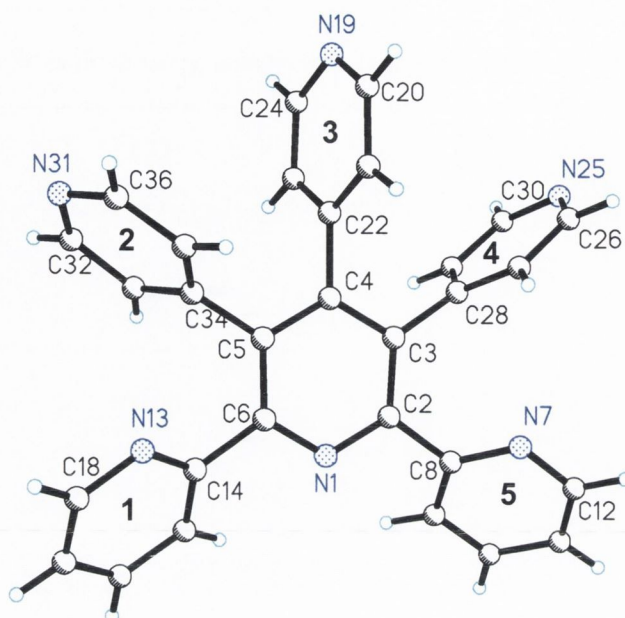
Figure 46: The X-ray crystal structure of [2,6-di(2-pyridyl)-3,4,5-tri-(4-pyridyl)]-pyridine (51) showing the selected atomic labeling. The chloroform molecule of the asymmetric unit has been omitted for clarity.

Selected bond lengths (Å): N1-C2 1.341(2), N1-C6 1.334(2), C6-C14 1.498(2), N13-C14 1.333(2), N13-C18 1.338(2), C2-C8 1.493(2), N7-C8 1.339(2), N7-C12 1.337(2), C2-C3 1.409(2), C3-C28 1.498(2), N25-C26 1.327(2), N25-C30 1.328(2), C3-C4 1.399(2), C4-C22 1.496(2), N19-C20 1.333(2), N19-C24 1.335(2), C4-C5 1.398(2), C5-C34 1.492(2), N31-C32 1.329(3), N31-C36 1.329(3), C5-C6 1.407(2). Selected bond angles (°): C2-N1-C6 119.9(13), C8-N7-C12 116.8(15), C14-N13-C18 117.1(15), C32-N31-C36 116.7(16), C24-N19-C20 116.4(15), C30-N25-C26 115.6(17).

Compound	Ring numbering				
	1(N13)	2(C34)	3(C22)	4(C28)	5(N7)
51	35.3°	69.1°	75.3°	86.7°	43.3°
41	39.7°	72.9°	89.8°	69.9°	43.3°

Table 13: Tilt angles of the peripheral rings with respect to the central pyridine ring.

The tilt angles of the peripheral rings of ligand (51) are shown in Table 13. The values of the angles are compared with the literature data for ligand (41). The tilt angles for

the 4-pyridyl rings (ring 2,3,4) for compound (**51**) vary between 69.1°-86.7°, with the most distorted being ring 4. The tilt angles for phenyl rings (ring 2,4) and 4-pyridyl ring (ring 3) for compound (**41**) vary between 69.9°-89.8°, with the largest angle for ring 3. The tilt angles for the 2-pyridyl rings of both compounds are very similar and vary between 35.3°-43.3°.

The peripheral rings tilted with respect to the central ring create the propeller-like shape of (**51**). Due to this effect (**51**) possesses racemic character. The ligand presents as two enatiomers Λ or Δ in equal amounts. The picture of the asymmetric unit (Figure 46) shows only one of these.

2.2.3. Cyclodehydrogenation of pyridine-centred ligands

The polyaromatic hydrocarbons presented by Müllen *et al.* possess unique electro-optical and photophysical properties. The most intriguing step in the synthesis of PAHs is the oxidative cyclodehydrogenation reaction (Scheme 24)[25], which allows the production of extended flat molecules. The cyclised compounds formed as rigid and planar sheets with extended electron density. Functionalised PAHs like N-HSB (Chapter 1) have great potential as ligands to modify the properties of photochemically active metal centres. The substituted pyridine-centered ligands (**41**, **42** and **51**) are ideal candidates for the generation of rigid, fully-cyclised polyaromatic ligands.
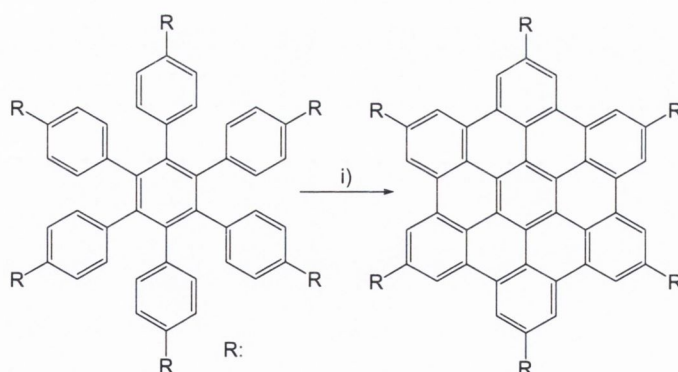
Scheme 24: The cyclodehydrogenation reaction R: H or tert-butyl, i) FeCl$_3$/CH$_2$Cl$_2$.[26]

Ligands **41**, **42** and **51** have been tested as potential precursors for cyclised products. The multidomain compounds, once cyclised, would be very attractive as bridging

71

ligands with a high electron density level. Several attempts at oxidative cyclodehydrogenation were made for all three compounds **41**, **42** and **51.** The dehydrogenation reaction was carried out with various oxidising agents, such as: iron(III) trichloride, aluminium(III) trichloride/copper(II) dichloride and molybdenum(V) pentachloride.[26,27] None of them gave satisfactory results; in all cases the starting material was recovered. All previously mentioned oxidising agents used in the synthesis of N-HSB compounds were tested. The pyridine centre in the skeleton of the ligands **41**, **42** and **51**, compared to benzene-centred N-HSB appears to be the cause of the problem.

A different oxidising reagent was introduced, as per Churruca *et al.* in the cyclisation of a derivative of isoquiniline.[28] In the synthesis of (**52**) (Scheme 25) the iodine phenyliodine(III) bis(trifluoroacetate) (PIFA) reagent was used for cyclisation reaction.
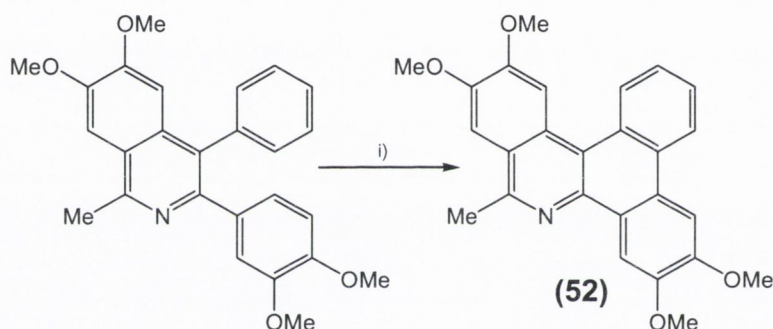
Scheme 25: The synthesis of 10-methyl-6,7,12,13-tetrametoxydibenzo[a,c]-phenanthridine (52); i) PIFA, BF₃Et₂O, CH₂Cl₂, -40°C, 2h.[28]

The same procedure was used for the cyclisation reaction for (**41**). A solution of PIFA in dry dichloromethane was added to a stirred solution of precursor (**41**) in dry dichloromethane at -40°C, under argon. After adding BF₃Et₂O, a blue solution of a radical intermediate should have appeared, but no colour change was observed. After quenching with Na₂CO₃ solution and extracting with dichloromethane the starting material was recovered. This method was not found successful for any of the pyridine-centred compounds (**41, 42** and **51**).

The reason behind the difficulty in forming the cyclised product resulting from (**41**), (**42**) or (**51**) is hard to determine, as the mechanism of the cyclodehydrogenation in

heteroatom graphens has not yet been elucidated. The failure of the reaction may be due either to the deactivating effect of a central pyridine ring or the lack of electron-donating groups on the phenyl rings. The substitution of the aromatic rings with electron donating groups, for example with methoxy groups, might help to cyclise compounds (**41**), (**42**) or (**51**).

2.2.4. Complexes of pyridine-centred ligands.

2.2.4.1. Reaction of (*42*) and CuI

A warm acetonitrile solution of copper(I) iodine was added in 1:1 ratio to a warm solution of ligand (**42**) dissolved in methanol. Green crystals suitable for single crystal X-ray diffraction were obtained overnight after the slow evaporation of the solvents. The asymmetric unit contains one molecule of ligand (**42**) coordinated to a copper atom, one molecule of methanol also coordinated to the copper atom and one iodide (Figure 47).
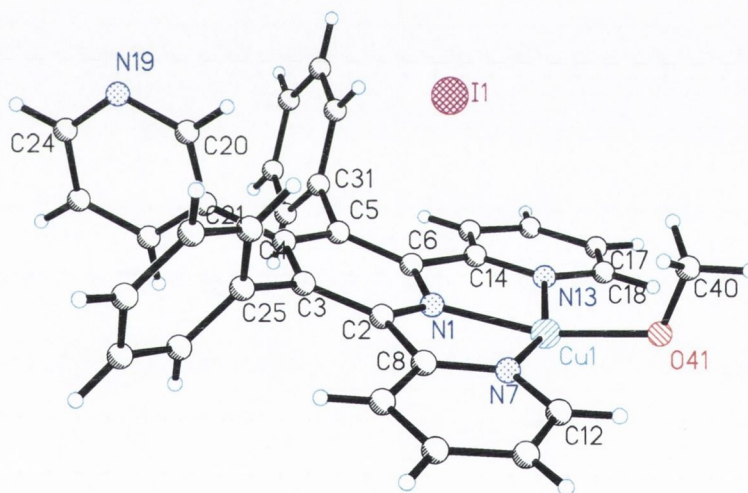
Figure 47: The structure of polymer [Cu(42)MeO](I)·MeOH-(53), showing the selected atomic labelling. Solvent molecule is omitted for clarity.

Selected bond lengths (Å): Cu1-N1 1.961(4), Cu1-N7 2.014(5), Cu1-N13 2.009(5), Cu1-O41 1.897(4), N1-C2 1.358(8), N1-C6 1.340(7), C6-C14 1.490(8), N13-C14 1.353(8), N13-C18 1.332(8), C2-C8 1.486(8), N7-C8 1.343(8), N7-C12 1.327(7), C2-C3 1.398(8), C3-C25 1.490(8), C3-C4 1.389(8), C4-C21 1.501(7), N19-C20 1.342(7), N19-C24 1.317(7), C4-C5 1.403(8), C5-C31 1.487(8), C5-C6 1.402(8). Selected bond angles (°): C2-N1-C6 123.6(4), C8-N7-C12 121.4(5), C14-N13-C18 120.11(6), C24-N19-C20 117.3(5).

73

The reaction of (**42**) and CuI gave polymer (**53**). The copper(II) metal ion is chelated in a five-coordination environment, the Cu(II) coordination geometry is square-pyramid. While the tridentate side of the ligand (N1, N7, N13) is coordinated to Cu1 from the same asymmetric unit, the monodentate 3-pyridyl (N19) is coordinated to the Cu1 from an adjacent asymmetric unit. The two negative charges are provided by the iodide ion and the ligand MeO⁻. The iodide anion is positioned in a very unique way on the face of the central pyridine (N1) ring with distance (py....I⁻) 3.59 Å, while the MeO⁻ is coordinated to the copper atom. The copper(I) has been oxidised to copper(II), by exposure to atmospheric oxygen.

Polymer (**53**) is constructed such that the iodide is sandwiched between two molecules of ligand. The whole polymeric chain has a zig-zag like character (Figure 48). Two chains are evident in the structure with a methanolate pointing along the x-axis, but in a different direction; looking at the top (orange) chain and the chain below (green) (Figure 48).
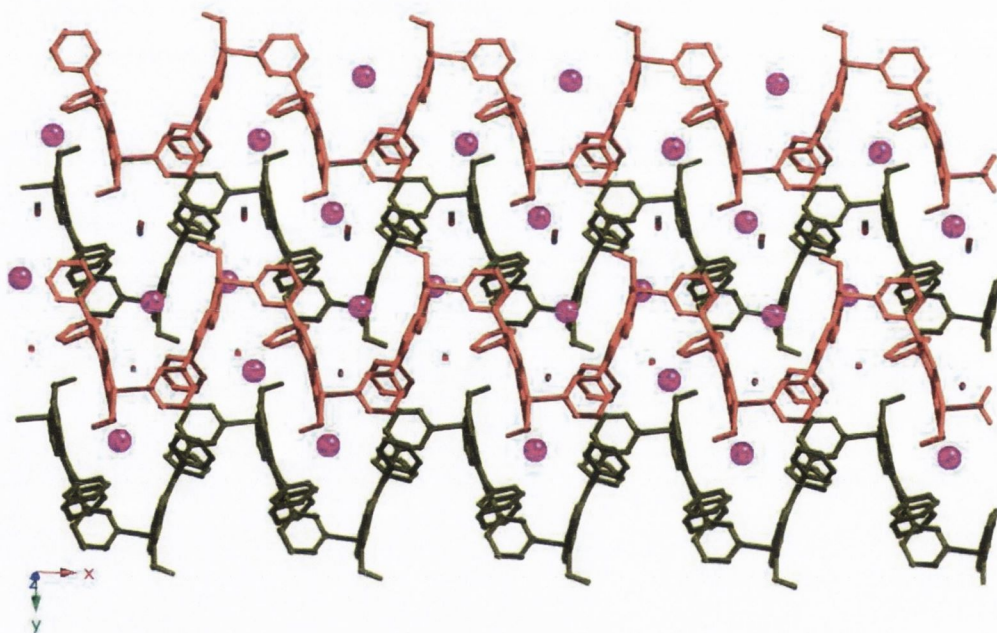
*Figure 48: View of polymer (**53**) down the z- axis.*

The view of the polymer (**53**) down the x-axis shows another interesting feature (Figure 49). The perspective view of the chains shows cavities; each cavity is filled

74

with two molecules of methanol. The packing of the structure of (**53**) is well organised.
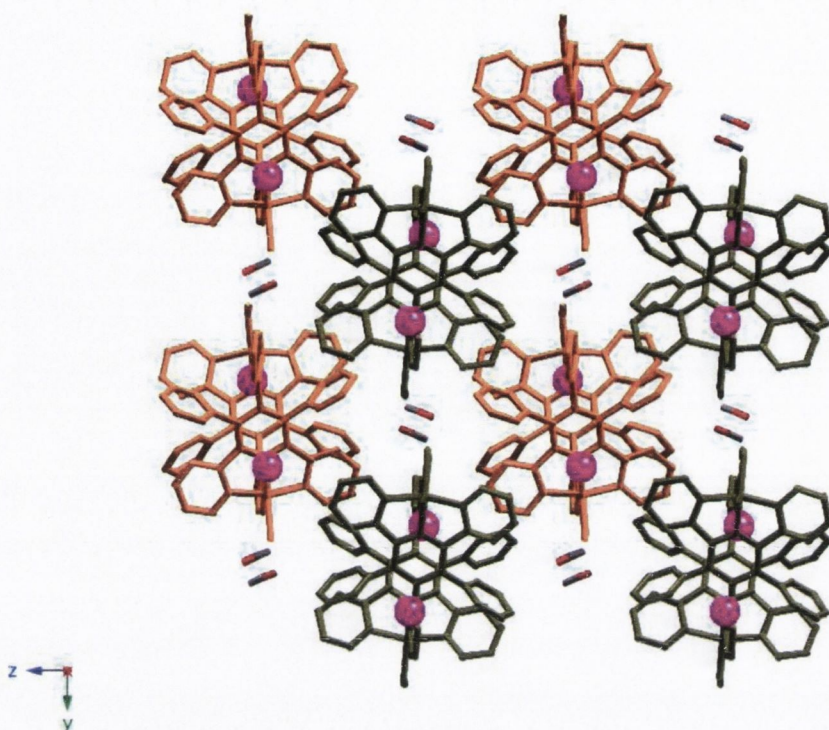
*Figure 49: View of the polymer (**53**) down the x- axis.*

In the generation of supramolecular architectures the design of the ligand plays a very important role. In the case of polymer (**53**) the position the monodentate species (3-pyridyl) in the ligand has a dramatic effect on the results of the reaction.

This is clearly demonstrated by the fact that the complexation reaction between CuI and ligand (**41**) in methanol results in the formation of monomer [Cu(**41**)I$_2$·MeOH] (**54**)[29] (Figure 50). As for (**53**) copper(I) has been oxidised to copper(II), but this time both counterions are provided by iodide I⁻ and coordinated to the metal ion. The tridentate moiety of coordinated ligand (**41**) is flat, while (**42**) is bent with an angle of 169.4°.
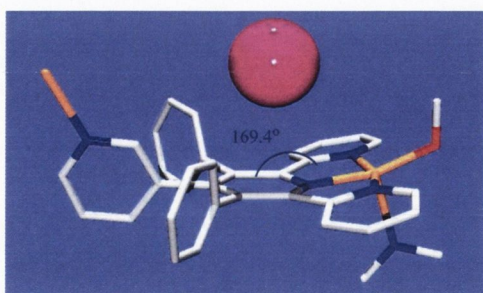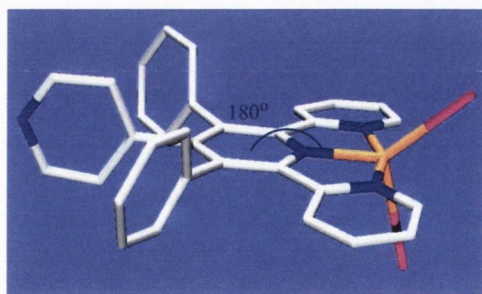
(53)   (54)

Figure 50: The structures of Cu(II) complexes (53) and (54), (Cu, in orange, N; in
blue; O, in red; I, in pink).

[Cu(**41**)I$_2$] has a similar structure to the complex obtained by the reaction between 4'-phenyl-2.2';6',2''-terpyridine and CuI which gave   [Cu(phterpy)I$_2$] (Figure 51).[30] Copper(I) ion has again been oxidised to Cu(II), the metal ion is chelated by the ligand and coordinated by two iodide ions. In both (**54**) and [Cu(phterpy)I$_2$] the five-coordinate copper has square-pyramidal geometry.
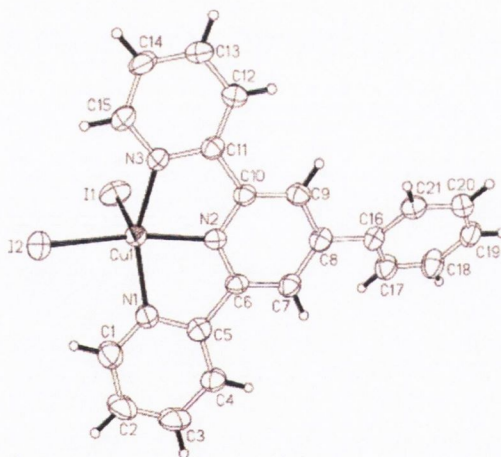
Figure 51: X-ray structure of [Cu(phenterpy)I$_2$].[30]

The small difference in the structure of ligands (**41**) and (**42**), namely the position of the nitrogen atom of the pyridyl ring, resulted in two completely different assemblies.

2.2.4.2. Reaction of (51) and CuI

A warm solution of CuI in methanol was added to a dichloromethane solution of ligand (51). The slow evaporation of solvents gave green crystals of copper(II) polymer (55) suitable for X-ray analysis. The complex (55) crystallised in the monoclinic space group C2/c. The asymmetric unit consists of one molecule of ligand (51) coordinated on the terpy-side (N1, N7, N13) to copper(II), half a molecule of CO_3^{2-}, one iodide counterion, and several molecules of solvent, 0.5 molecule of methanol and 4 molecules of water. Copper(I) has been oxidised to copper(II) due to the air oxygen. Figure 52 shows the CO_3^{2-} unit which bridges two molecules of complex by the coordination to copper atoms. Two molecules of iodide I⁻ provide the remaining counter ions.
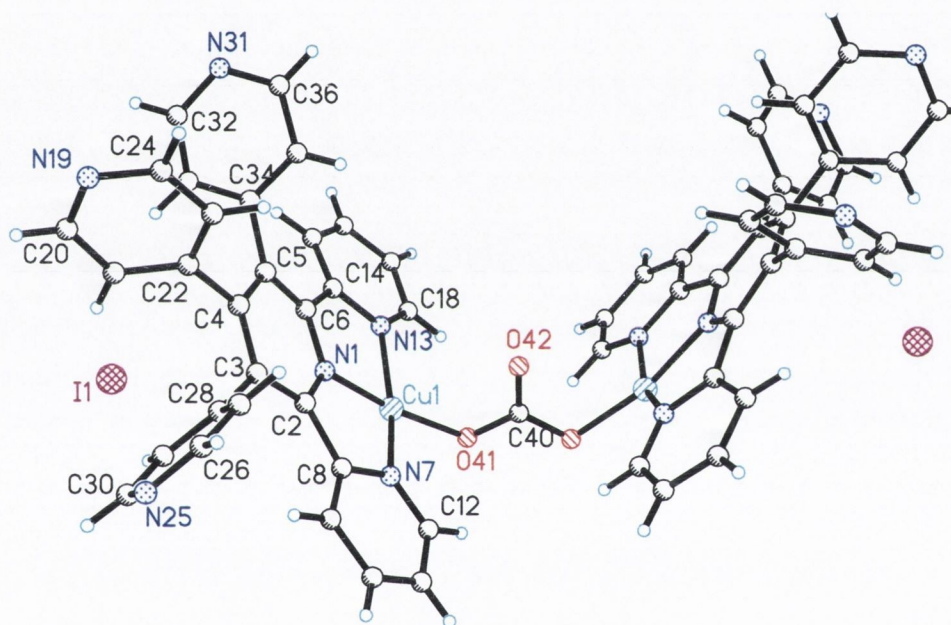
Figure 52: The structure of copper complex [Cu₂(51)₂(CO₃)](I⁻)₂·MeOH-(55) showing selected atomic labelling. Solvent molecules are omitted for clarity.

Selected bond lengths (Å): Cu1-N1 1.947(5), Cu1-N7 2.011(5), Cu1-N13 2.006(5), Cu1-O41 1.918(4), O41-C40 1.294(5), O42-C40 1.239(5), N1-C2 1.331(8), N1-C6 1.336(7), C6-C14 1.489(8), N13-C14 1.352(8), N13-C18 1.327(8), C2-C8 1.496(8), N7-C8 1.349(8), N7-C12 1.341(8), C2-C3 1.394(8), C3-C28 1.503(8), N25-C26 1.327(10), N25-C30 1.305(10), C3-C4 1.405(8), C4-C22 1.493(8), N19-C20 1.339(8), N19-C24 1.338(7), C4-C5 1.403(8), C5-C34 1.490(9), N31-C32 1.324(2), N31-C36 1.311(2), C5-C6 1.399(8). Selected bond angles (°): C2-N1-C6 123.9(5), C8-N7-C12 120.2(6), C14-N13-C18 119.6(5), C32-N31-C36 117.0(8), C24-N19-C20 118.1(5), C30-N25-C26 117.2(6).

The copper (Cu1) is five-coordinate (Figure 53). The Cu(II) coordination geometry is square-pyrimid. Three coordination sides are provided by the terpy position of the ligand (N1, N7, N13) (**51**), the others from the monodentate (N19) of another molecule of (**51**) and the oxygen (O41) from the CO_3^{2-} unit.
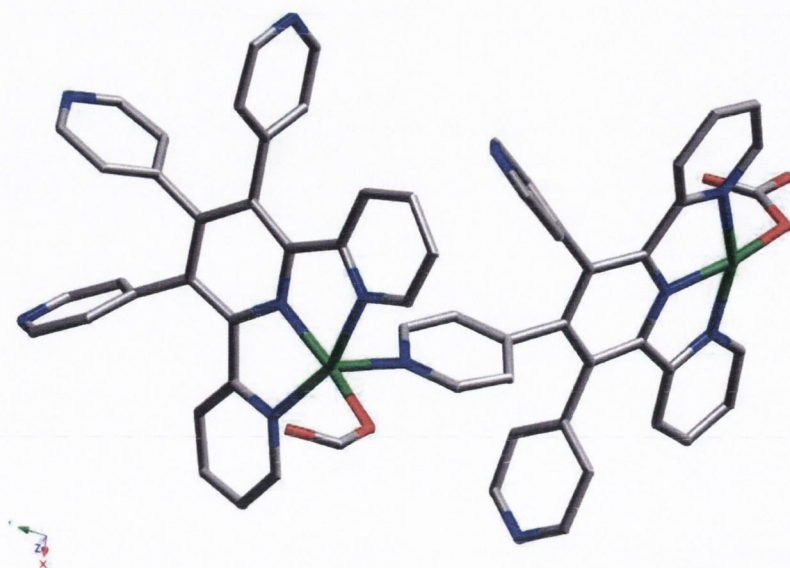
*Figure 53: View of copper (Cu1) environment in (**55**).*

The fixation of atmospheric CO_2 is a known effect.[31,32] There are a lot of examples in the literature of the insertion of CO_2 from the atmosphere to a coordination compound. The carbonate bridging anion can bind in different ways to generate complex supramolecular systems. Kickelbick obtained a dimeric carbonato-bridged copper(II) bipyridine complex (Figure 54).[33] CuBr was used as a source of copper. Each copper atom is square-pyramidal, with the basal plane formed by three N atoms from two chelating ligands and one oxygen atom from the CO_3^{2-} group. A similar structural motif was reported by Kruger *et al.*,[34] after recrystallisation of a (μ_2-carbonato) copper(II) bipyridine complex.
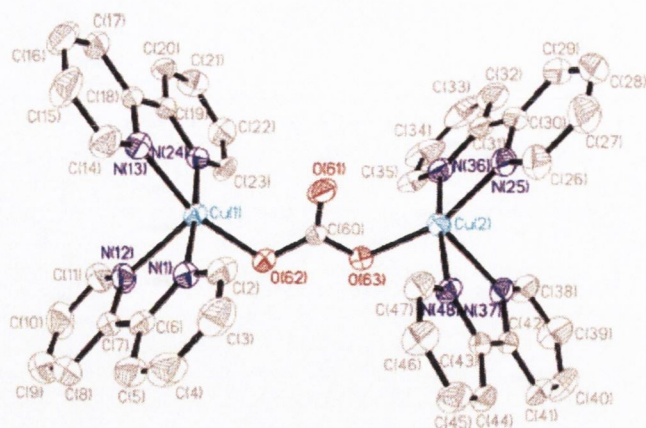
Figure 54: Example of CO_2 fixation to a Cu(II) complex.[33]

Table 14 shows the tilt angles of the peripheral rings with respect to the central pyridine ring for the free ligand (**51**) and the coordinated ligand in complex (**55**). Due to the coordination to the copper ion the tilt angles for the rings on the terpy side for (**55**) are smaller compared to (**51**), but the terpy unit is not flat: rings coordinated to Cu1 are bent with angles of 15.6° (N13) and 12.8° (N7), with respect to the central pyridine ring. The angle between the centroid of the central pyridine ring (N1, C2, C3, C4, C5, C6), N1 and Cu1 is 166°. The coordinated terpy is therefore more distorted than in complex (**53**) where the equivalent angle was 169°.

Compound	The ring numbering				
	1(N13)	2(C34)	3(C22)	4(C28)	5(N7)
55	15.6°	86.1°	81.9°	79.1°	12.8°
51	35.3°	69.1°	75.3°	86.7°	43.3°

Table 14: The tilt angles of the peripheral rings with respect to the central pyridine ring in complex (55) and ligand (51).

Figure 55 shows the structure of a layer of the 2D polymer (**55**). We can see two copper ions (in green) bridged by CO_3^{2-}, as well we can see both ligands coordinated by the monodentate moiety (N19). N19 is linked to the copper from the row below; the copper is already coordinated to the terpy-side of another molecule of ligand. This arrangement is repeatable and creates a net with cavities.
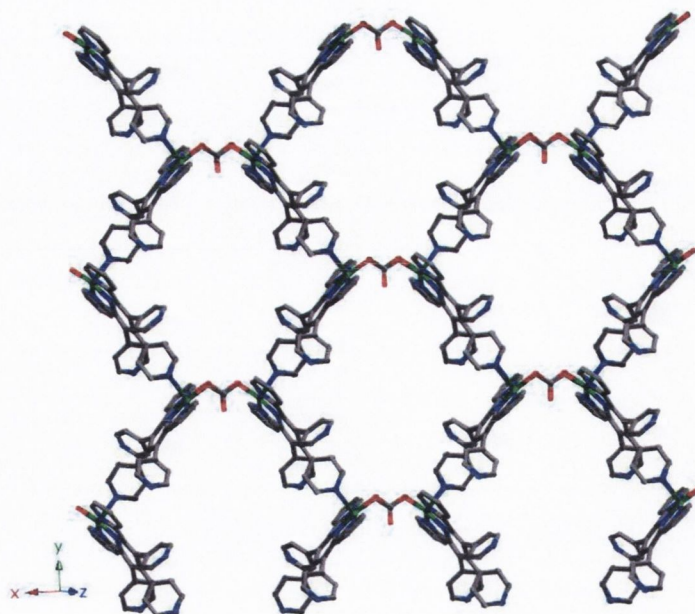
Figure 55: The view of polymer (55) showing the cavities created between molecules of the complex.

Figure 56 shows the organisation of two consecutive layers down the z-axis. The pink system is the layer shown on Figure 55. The blue and the pink layers are lyaing in [001] direction. The blue sheet is similar to the pink one. They are rotated by the mirror plane. Each cavity is filled with four molecules of methanol and four iodide ions. Half of the methanol and iodide molecules belong to the pink layer, and half to the blue.
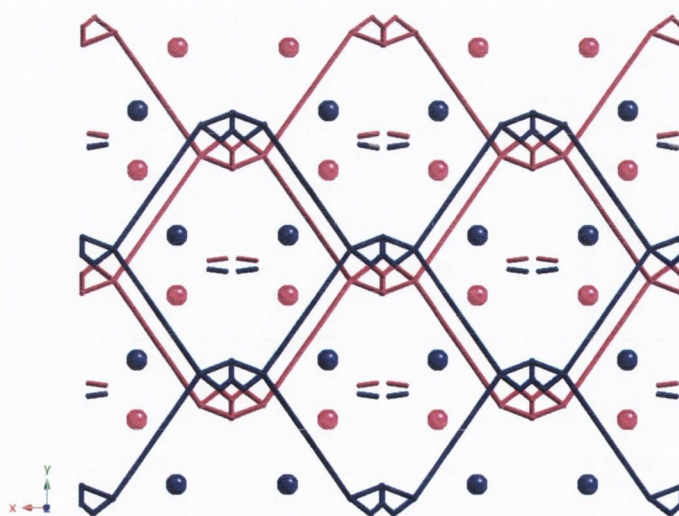
Figure 56: Cartoon representation of polymer (55), down the z- axis.

Figure 57 shows two views of polymer (**55**). Part (**a**) is a view down the x-axis and (**b**) is a view down the y-axis, both show the arrangement of the two types of layer with surrounding molecules of solvent and ions.

(a)   (b)
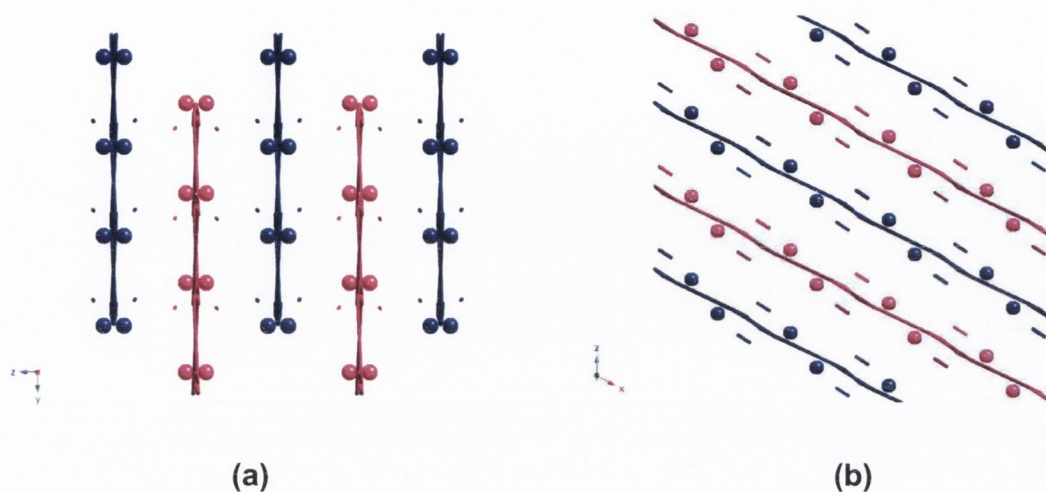
Figure 57: Cartoon representation of polymer (55), a) view down the x- axis, b) view down the y- axis.

2.2.4.3. The reaction of (51) and CdSO₄

A warm methanol-water solution of two equivalents of $CdSO_4$ was mixed with a methanolic solution of one equivalent of ligand (**51**). The slow evaporation of methanol gave white crystals suitable for X-ray analysis.

The results and discussion in this paragraph are based on the preliminary data refining.

The reaction between $CdSO_4$ and ligand (**51**) resulted in the three-dimensional polymer (**56**). The complex crystalised in P2(1)/c space group. Figure 58 shows the asymmetric unit of complex (**56**). The molecules of solvent are omitted. The important distances and angles are given.
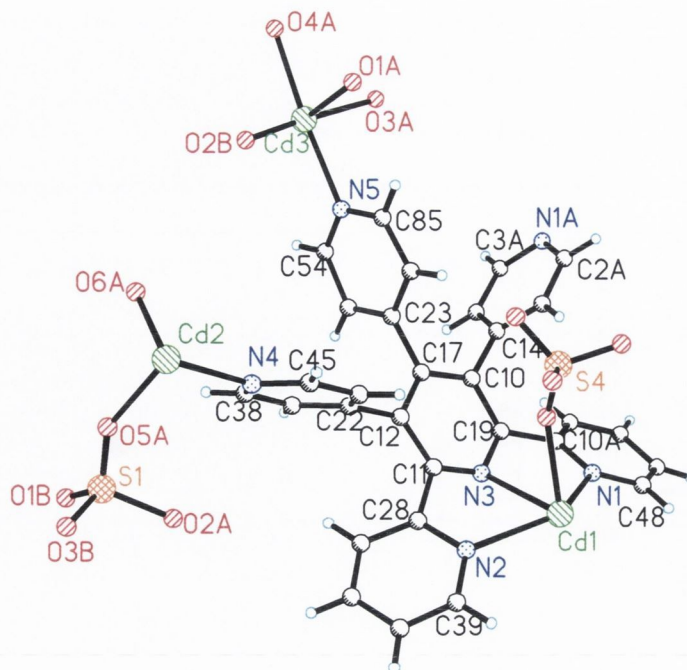
*Figure 58: The structure of complex [Cd$_{2.5}$(**51**)(SO$_4$)$_2$OH]-(**56**) showing the selected atomic labelling. The molecules of solvents are omitted for clarity.*

Selected bond lengths (Å): Cd1-N1 2.369(7), Cd1-N2 2.342(7), Cd1-N3 2.446(6), Cd2-N4 2.296(8), Cd3-N5 2.302(8), N3-C19 1.313(10), C10-C17 1.385(11), C17-C12 1.409(10), C12-C11 1.390(10), C11-N3 1.329(10), C11-C28 1.507(11), C19-C10A 1.483(11), C10-C14 1.479(11), C17-C23 1.490(11), C12-C22 1.493(12), N1-C48 1.332(11), N1-C10A 1.345(11), N2-C28 1.361(11), N2-C39 1.341(11), N4-C38 1.323(13), N4-C45 1.340(13), N5-C54 1.313(18), N5-C85 1.296(16). Selected bond angles (°): C10A-N1-C48 118.7(8), C11-N3-C19 120.9(7), C39-N2-C28 117.1(7), C38-N4-C45 118.6(8), C54-N5-C85 117.9(9), C3A-N1A-C2A 117.4(7).

The design of the ligand (**51**) plays a significant role in the product of this reaction. The structure of polymer (**56**) possesses three different environments for the cadmium atoms. Cd1 (coloured pink in Figure 59) is six-coordinated by the tridentate moiety (N1, N2, N3) of one molecule of ligand, monodentate to the 4-pyridyl ring at the 3'-position of another ligand (1NA) and the last two coordination sides are occupied by two monodentate ions of SO$_4^{2-}$. The sulfate ions are creating double bridges between two atoms of Cd1; the bridges are linked to the metal by O2 and O3. Figure 59 shows this very clearly, with the sulfur (S4) from the bridging SO$_4^{2-}$, which is shown in yellow. The second cadmium atom Cd2 (colour black in Figure 59) is four coordinate. Cd2 links two molecules of ligand through the monodentate moiety N4. However, two groups of SO$_4^{2-}$ are coordinated to Cd2 as well, by their 5OA and 6OA oxygen

atoms. The sulfate ions (sulfur in light pink-S1) create the bridge between Cd2 and the third atom of cadmium Cd3 (in purple in Figure 59). Each molecule of the ligand has the same arrangement around its coordination sites. Six molecules of ligand coordinated to seven ions of cadmium together with SO_4^{2-} counter ions form the ring with the linkage crossing in the middle. This ring arrangement is the smallest unit of this polymer. Three cadmium ions give the overall charge (+5); Cd2 and Cd3 possess 100% occupancy while Cd1 50%. Two SO_4^{2-} ions give charge (-4). To balance the charge one of the oxygen atoms coordinated to Cd2 is required to be an OH⁻ group.
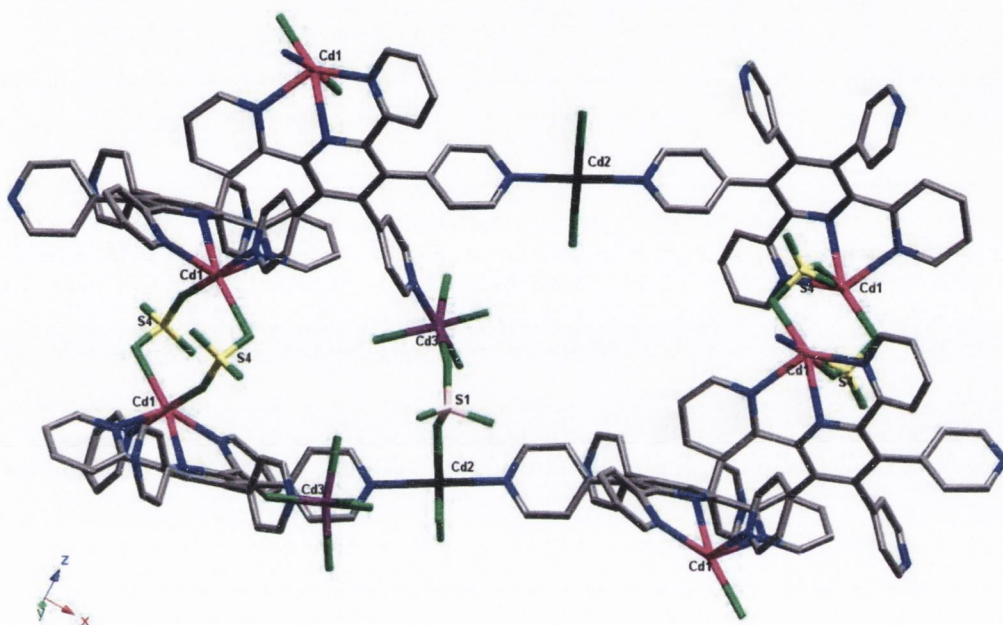
Figure 59: The smallest unit of polymer (56).

In polymer (**56**) there are two types of metal-sulfato species. According to the Cambridge Crystallographic Data Base,[35] the polymer (**56**) prefers the mode III for Cd2-Cd3 arrangement and mode IV for Cd1-Cd1 (Figure 60).[36]
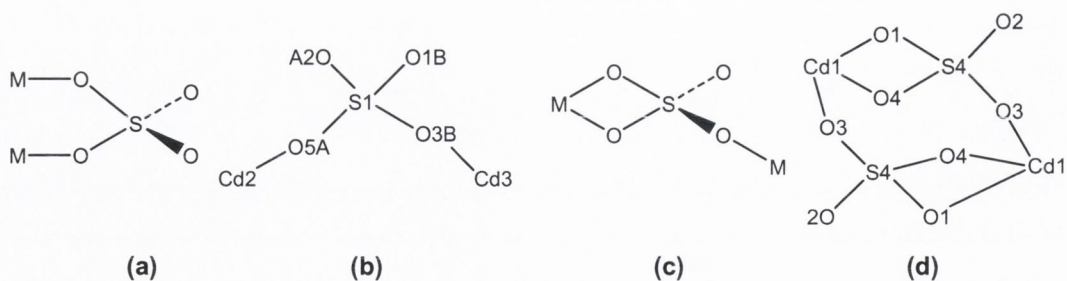
Figure 60: a) coordination mode III from CCDB[36] b) metal-sulfato arrangement for Cd2 and Cd3 in (56), c) coordination mode IV from CCDB,[36] d) metal-sulfato arrangement for Cd1 in (56).

According to CCDB (October 2006) the mode III is popular for cadmium complexes, but there are only two examples of cadmium-sulfato complexes with mode IV. One of these is $[Cd(SO_4)_2(tpt)_2(H_2O)_2]$ tetrahydrate[39](Figure 64) and the second $[Cd(SO_4)_2(Py_2C_3H_6)_3(H_2O)_{2.7}]\cdot4.5H_2O$ $(Py_2C_3H_6$-1,3-bis(4-pyridyl)-propane).[37] There is one more example of the cadmium complex with mode IV, $\{[Cd(41)(SO_4)]\cdot5CH_3OH\cdot3H_2O\}_\infty$[29], this polymer has been synthesised in our group and is unpublished.

Complex (56) gives a 3D polymer. Figure 61 shows a view of the complex (56) down the x-axis. The ring unit shown in Figure 59 builds a comb type structure with big cavities.
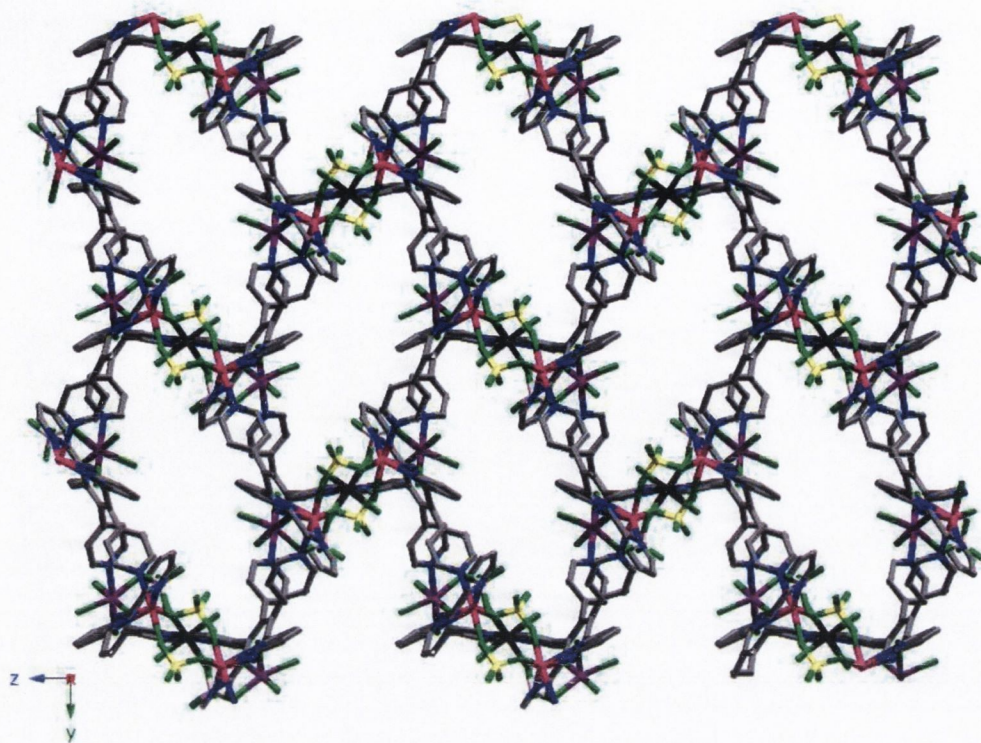
Figure 61: The view of the polymer (56) down to the axis x, (Cd1 in pink; Cd2 in black; Cd3 in purple; S1 in light pink; S4 in yellow).

Down the y-axis of polymer (56) (Figure 62) shows how the net layers are connected to create the 3D polymer. The picture shows the organisation between Cd2 (black) and Cd3 (purple). Cd2 links two molecules of ligand through the monodentate moiety N4. The sulfate ions (sulfur in light pink-S1) create the bridge between Cd2 and Cd3 (in purple).
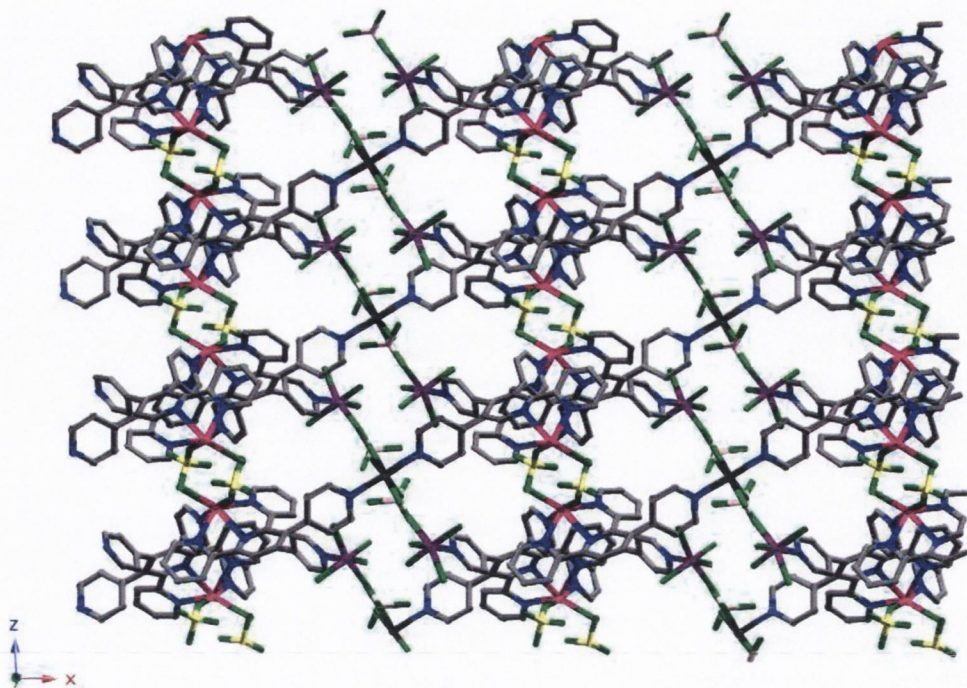
Figure 62: View of the polymer (56) down the y- axis, (Cd1 in pink; Cd2 in black; Cd3 in purple; S1 in light pink; S4 in yellow).

The last view of the (56) structure is down the z-axis (Figure 63). This perspective view mainly shows the arrangement of Cd2-Cd3. The environment of Cd2 (in black) is shown very well. The inorganic part of the polymer (Cd2-SO$_4$-Cd3) creates kind of a zig-zag packing formation.
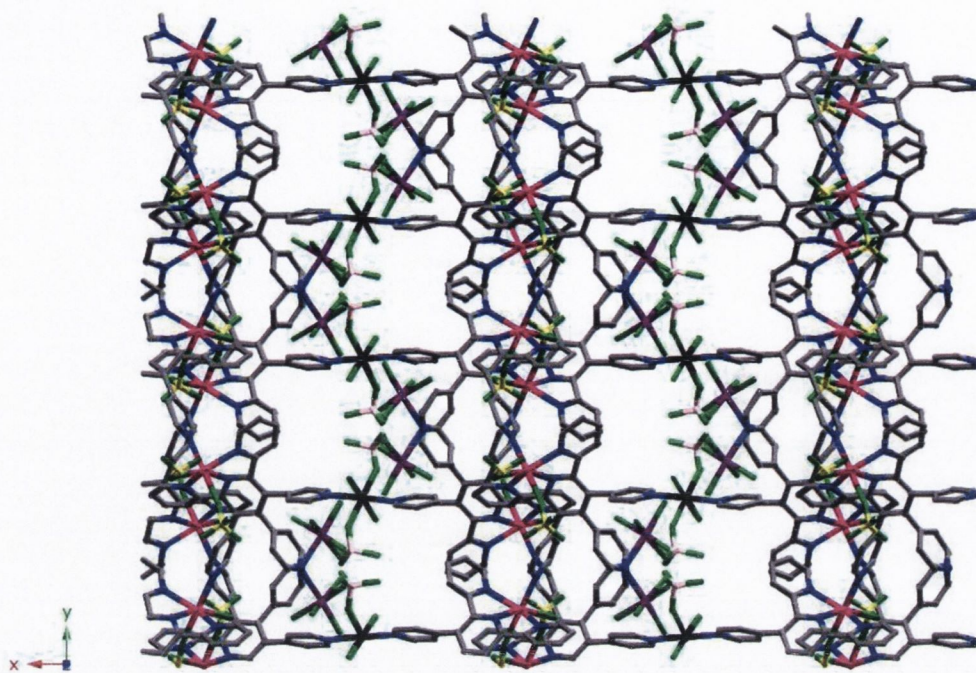
*Figure 63: The view of the polymer (**56**) down the z- axis, (Cd1 in pink; Cd2 in black; Cd3 in purple; S1 in light pink; S4 in yellow).*

Literature examples of cadmium complexes with terpy-bridging ligands are shown in Figure 64. The reaction of pyterpy with $Cd(NO_3)_2*4H_2O$ gave a monomer $[Cd(pyterpy)(H_2O)(NO_3)_2]$ (Figure 64a),[38] where the metal ion is heptacoordinated by tridentate pyterpy ligand, bidentate NO_3^- and one monodentate H_2O and one monodentate NO_3^-. The coordination number for cadmium atom is higher than in (**56**), where Cd1, Cd3 are six-coordinate and Cd2 four.

The rection of $CdSO_4$ and 2,4,6-tris(2-pyridyl)-1,3,5-triazine (tpt) as a ligand gave complex $[Cd(SO_4)_2(tpt)_2(H_2O)_2]$ tetrahydrate[39], with metal-sulfato arrangement the same as for Cd1 in (**56**). The terminal pyridyl remains uncoordinated (Figure 64b).
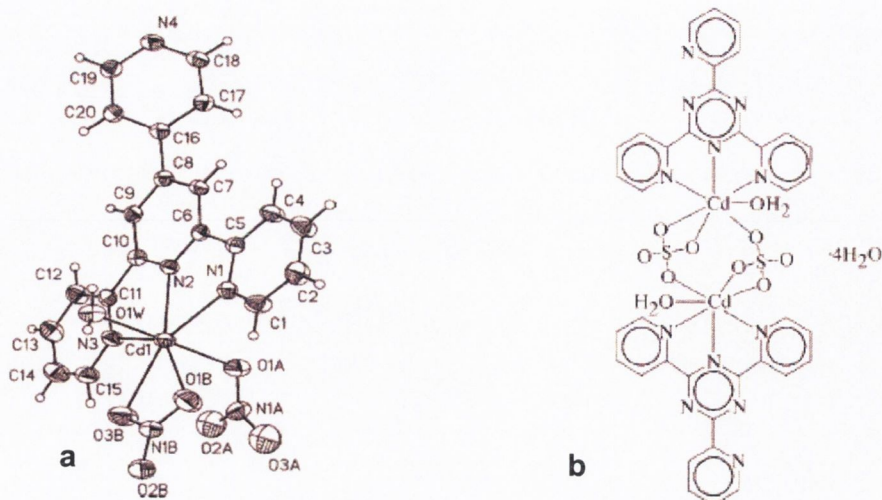
Figure 64: The structures of a) [Cd(pyterpy)(H₂O)(NO₃)₂] and b)
[Cd(tpty)(H₂0)₂(SO₄)₂] 4H₂O.[39]

2.2.4.4. The reaction of ligand (41) and La(NO₃)₃ xH₂O.

To a warm methanol solution of $La(NO_3)_3 \cdot xH_2O$ was added a warm methanolic solution of ligand (**41**). Slow methanol evaporation from the 1:1 mixture gave white crystals of the hydrogen-bonded polymer (**57**). The asymmetric unit (Figure 65) contains one molecule of ligand, $La(NO_3)_3 \cdot xH_2O$ and one molecule of methanol. The tridentate terpy-side of ligand (N1, N7, N13) is coordinated to lanthanum ion together with three ions of NO_3^-, and one molecule of methanol. The metal is ten-coordinate. Hydrogen-bonding is created through the methanol, which is linked to the monodentate (N19) of the ligand from another monomer. Polymer (**57**) crystallised in monoclinic space group $P2_1/n$.

Figure 65: Asymmetric unit of complex [La(41)(NO₃)₃MeOH]-(57) showing selected

atomic labelling.

Selected bond lengths (Å): La1-N1 2.759(3), La1-N7 2.707(3), La1-N13 2.711(3), La1-O61 2.485(2), O61-C60 1.423(4), N1-C2 1.342(4), N1-C6 1.343(4), C6-C14 1.498(4), N13-C14 1.353(4), N13-C18 1.337(4), C2-C8 1.490(4), N7-C8 1.351(4), N7-C12 1.340(4), C2-C3 1.406(4), C3-C25 1.493(4), C3-C4 1.406(4), C4-C22 1.501(4), N19-C20 1.320(5), N19-C24 1.338(5), C4-C5 1.411(4), C5-C31 1.495(4), C5-C6 1.402(4). Selected bond angles (°): C2-N1-C6 119.7(3), C8-N7-C12 117.8(3), C14-N13-C18 118.0(3), C24-N19-C20 117.8(3).

The molecules of complex create a 1D hydrogen-bonded polymer. Figure 66 shows a fragment of the chain of polymer (**57**). The length of the hydrogen bond (H-N19) is 2.65Å. The coordinated terpy-side of the ligand is bent, with a torsion angle of 127.6° with respect to the central ring. The value of this angle is unusually large in comparison to other complexes containing terpy available in the literature.

Figure 66: A fragment of the chain of the 1D hydrogen-bonded polymer (57).

The picture below (Figure 67) shows the organisation of the chains in the structure of (**57**). The chains go in opposite directions, and are rotated by inversion centre.
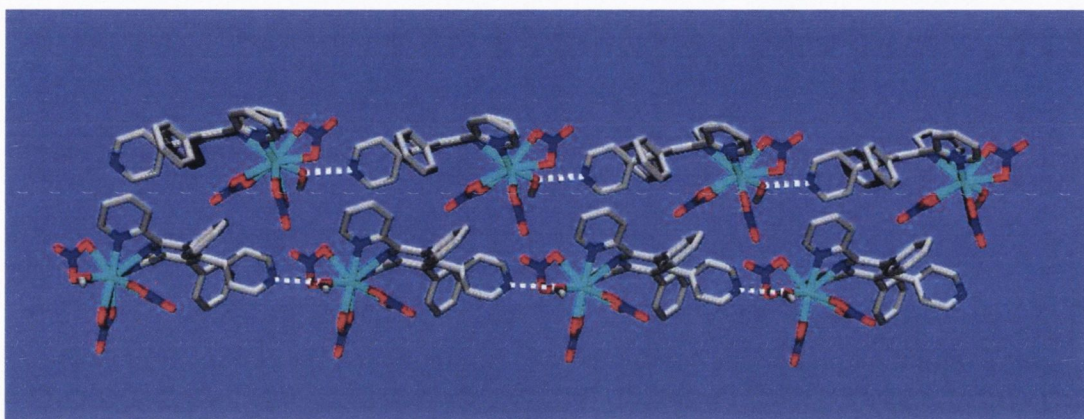
Figure 67: Two directionally opposed chains of polymer (57).

A view down the x-axis (Figure 68) shows that the chains possess four different orientations. The pink and the purple chains go the same direction but they are rotated of 180° with respect to each other. The chains in blue and green go in the opposite directions to pink and purple, and are also rotated with respect to each other by angle of 180°.
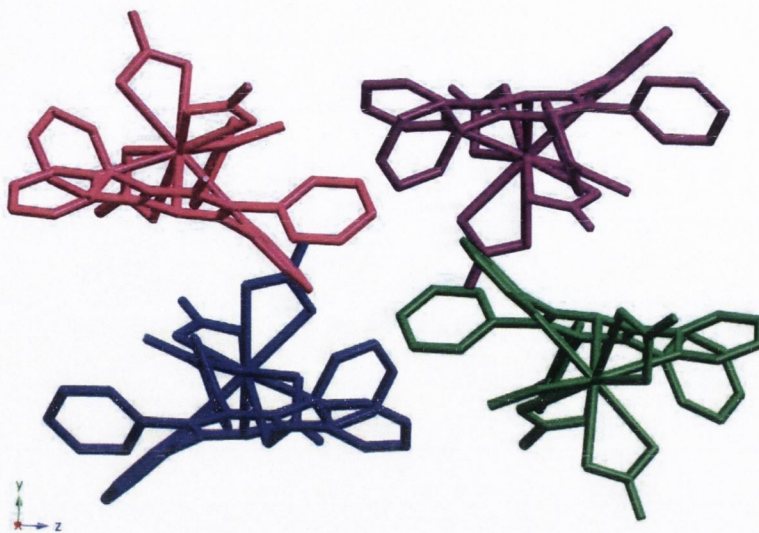
*Figure 68: View of polymer (**57**) down the x- axis.*

2.2.4.5. The reaction of (41) and Sm(NO₃)₃·6H₂O.

Two warm methanolic solutions, one of $Sm(NO_3)_3 \cdot 6H_2O$ and the other of ligand (41) were mixed together. Slow evaporation of the solvent overnight resulted in white crystals suitable for X-ray analysis. The reaction gave a 1D hydrogen-bonding polymer (58), which is iso-structural with (57). An asymmetric unit is shown in Figure 69. The coordination arrangement around the samarium(III) metal is the same as for lanthanum(III) in (57). The samarium metal is 10-coordinate, *via* the tridentate terpy, three bidentate nitrate ions and one molecule of methanol. The hydrogen bond responsible for creating the polymer occurs between the methanol hydrogen from one complex and the monodentate unit (N19) from another. The H-N19 distance is 2.66 Å. Complex (58) crystallised in a monoclinic space group P2₁/n. As complexes (57) and (58) are iso-structural; the packing and the supramolecular organisation are identical (Figure 66, Figure 67,Figure 68). The difference is seen in the distances, which are shorter between the coordinated ligand and samarium than analogous bonds in the lanthanum complex. The values for (58) vary between 2.627(19)-2.667(18) Å (Sm1-N13, -N7, -N1) and for (57) between 2.707(3)-2.759(3) Å (La1-N13, -N7, -N1). This is due to the size of the metal ions Sm^{3+} (1.098 Å) and La^{3+} (1.172 Å).
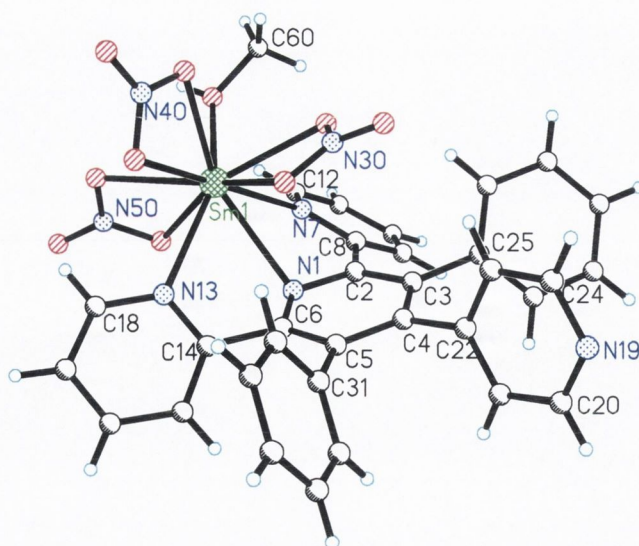
Figure 69: Asymmetric unit of complex [Sm(41)(NO₃)₃MeOH]-(58) showing selected

atomic labelling.

Selected bond lengths (Å): Sm1-N1 2.667(2), Sm1-N7 2.637(2), Sm1-N13 2.627(2), Sm1-O61 2.406(2), O61-C60 1.421(3), N1-C2 1.340(3), N1-C6 1.337(3), C6-C14 1.488(3), N13-C14 1.349(3), N13-C18 1.339(3), C2-C8 1.496(3), N7-C8 1.354(3), N7-C12 1.338(3), C2-C3 1.406(3), C3-C25 1.491(3), C3-C4 1.409(3), C4-C22 1.500(3), N19-C20 1.317(4), N19-C24 1.342(4), C4-C5 1.405(3), C5-C31 1.496(3), C5-C6 1.404(3). Selected bond angles (°): C2-N1-C6 120.0(2), C8-N7-C12 117.9(2), C14-N13-C18 117.8(2), C24-N19-C20 117.7(2).

The tilt angles between the peripheral ring and central pyridine ring in both complexes (**57**) and (**58**) are presented in Table 15. In general the values of tilt angles for (**58**) are higher than those for (**57**), with the average angle 57.5° and 60.4° for (**57**) and (**58**) respectively. In both complexes the 4-pyridyl ring possesses the highest tilt angle: 75.4°and 88.7° for (**57**) and (**58**) respectively.

2.2.4.6. The reaction of (41) and La(NO₃)₃·xH₂O

A warm mixture of (**41**) in dichloromethane was added to a warm solution of La(NO₃)₃·xH₂O in acetonitrile. After three days of slow solvent evaporation white crystals were obtained. Complex (**59**) crystallised in a monoclinic space group P2₁/c. The coordination number of the lanthanum ion was 10. The coordination environment of the metal ion is similar in this complex to that of (**57**), but this time the methanol is

92

replaced by coordination to a 4-pyridyl ring nitrogen (N19) of an adjacent ligand. The distance between the metal and the nitrogen atom of another is 2.675 Å (La1-N19). The asymmetric unit (Figure 70) contains one molecule of ligand, one atom of lanthanum, three ions of nitrate and one molecule of dichloromethane.
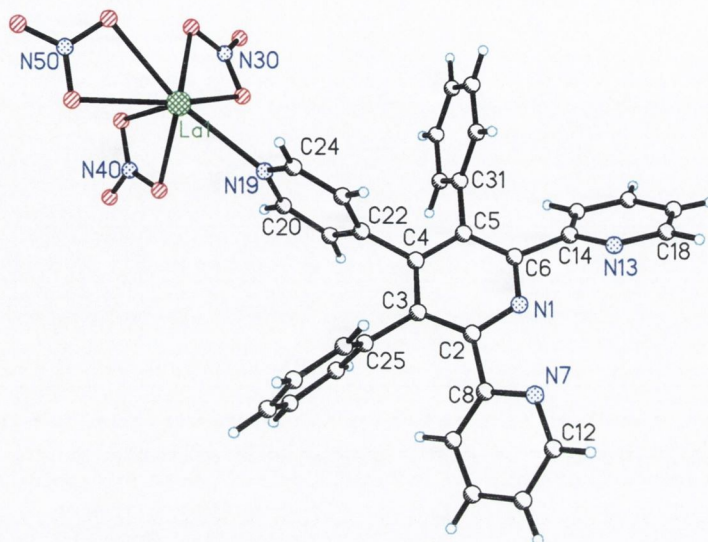
Figure 70: The structure of complex [La(41)(NO₃)₃]·CH₂Cl₂ in (59), showing selected atomic labelling. The solvent molecule is omitted for clarity.

Selected bond lengths (Å): La1-N19 2.675(4), N1-C2 1.343(6), N1-C6 1.349(5), C6-C14 1.498, (6) N13-C14 1.349(6), N13-C18 1.343(6), C2-C8 1.494(6), N7-C8 1.345(6), N7-C12 1.336(6), C2-C3 1.405(6), C3-C25 1.490(6), C3-C4 1.401(6), C4-C22 1.504(6), N19-C20 1.353(6), N19-C24 1.326(7), C4-C5 1.395(6), C5-C31 1.498(6), C5-C6 1.400(6); (when terpy is coordinated to another molecule of lanthanum La1-N1 2.705(4), La1-N7 2.702(4), La1-N13 2.695(4)). Selected bond angles (°): C2-N1-C6 119.9(4), C8-N7-C12 118.6(4), C14-N13-C18 118.4(4), C24-N1-C20 116.6(4).

The tilt angles for the peripheral rings with respect to the central pyridine ring are shown in Table 15. The tilt angles for rings on the terpy side of (59) are smaller than those of (57). In both polymers the biggest tilt angle is observed for the pyridyl ring at 88.7° and 75.4° for (59) and (57) respectively.

Compound	Rings numbering				
	1(N13)	2(C31)	3(N19)	4(C25)	5(N7)
57	40.0°	58.3°	75.4°	69.2°	44.5°
58	44.9°	68.7°	76.0°	58.5°	38.5°
59	35.7°	66.6°	88.7°	74.2°	36.9°

Table 15: Tilt angles of the peripheral rings with respect to the central pyridine ring for (57), (58) and (59).

The chain of polymer (**59**) has a zig-zag-like shape (Figure 71) along the z-axis. The distance between two metal atoms (La-La) is 11.26Å. The coordinated terpy-side of the ligand is bent with a distortion angle 134.6°, with respect to the centroid of the central pyridine ring. The value of the distortion angle is smaller to that of the hydrogen-bondined polymer (**57**).
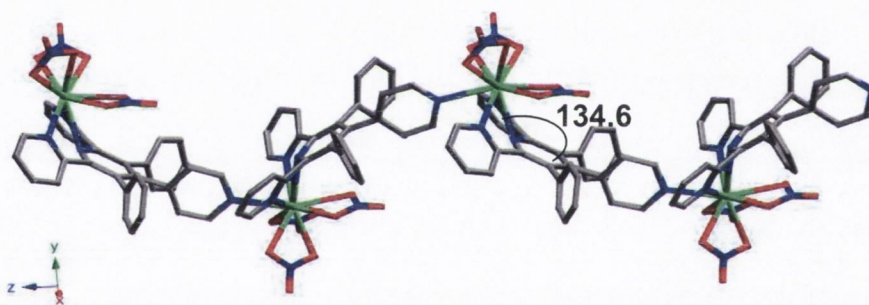
Figure 71: Chain of polymer (59) raised along x axis.

Each polymer chain is surrounded by two others, which go in opposite directions (Figure 72). There is π-π stacking of every second ligand in the chain with a distance of 3.37 Å, which is very close to the interlayer distance in graphite (3.35 Å) (Figure 73). The π-stacking interaction takes place on the terpy-side of the ligand between the 2-pyridyl rings containing N7. Molecules of dichloromethane solvate occupy the space between chains.

94

(a)
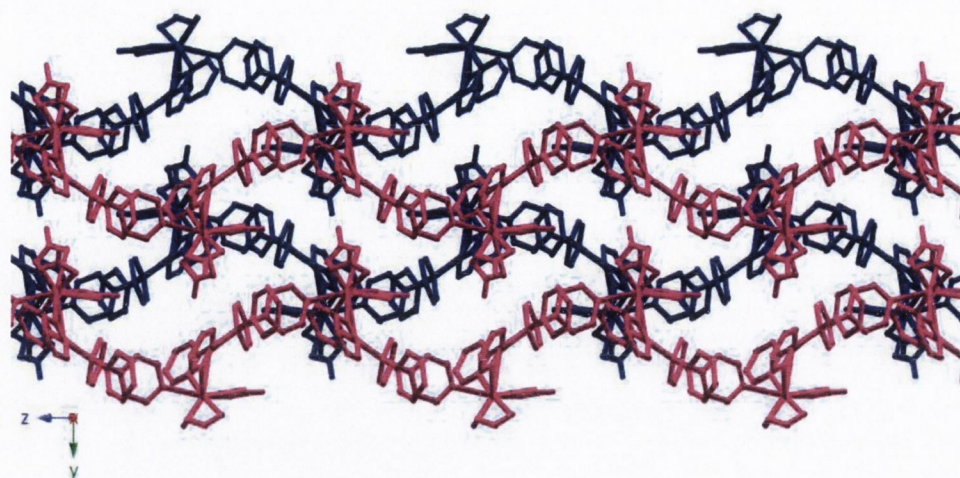
(b)
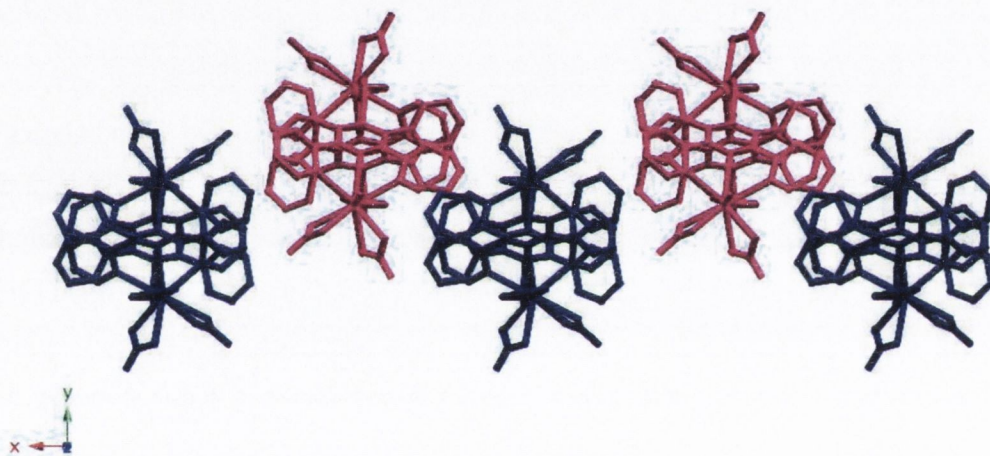
Figure 72: Perspective view of polymer (59): a) view down the x-axis, b) view down the z-axis. Solvent molecules are omitted for clarity.
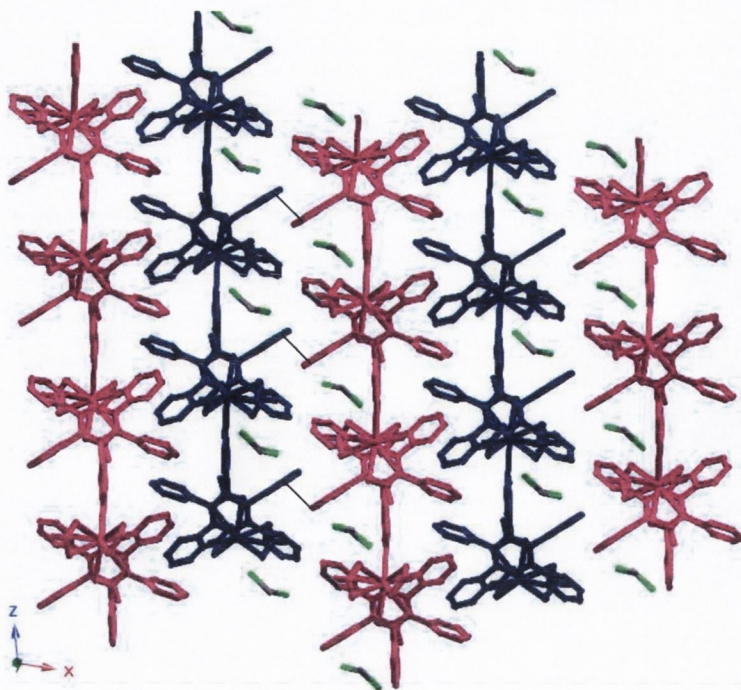
*Figure 73: View of the structure of polymer (**59**) down the y-axis, with the molecules of dichloromethane in green and π-stacking marked in black.*

A literature example for a lanthanide nitrate complex with tridentate ligand shows a different arrangement around the metal ion compared to (**57**) and (**59**).[40] The reaction between $La(NO_3)_3$ and terpy in a 1:1 ratio gave a complex with the formula $[La(terpy)(NO_3)_2(H_2O)_3]NO_3$.[41] The La(III) ion is ten coordinate, as in (**57**) and (**59**), but in the terpy complex only two nitrate groups are coordinated to the metal ion and the third group is replaced by two molecules of water. Water molecules occupy the last free coordination sites. For (**57**) and (**59**) this site is either occupied by a molecule of methanol (hydrogen bonding polymer) or by the monodentate N-pyridyl of the bridging ligand.

Drew *et al.* obtained a very interesting complex of samarium. They mixed one equivalent of $La(NO_3)_3$ with four equivalents of terpy ligand. The experiment gave both a cation and an anion in the asymmetric unit, with the formula $[Sm(NO_3)_2(terpy)_2][Sm(NO_3)_4(terpy)]$ (Figure 74)[41]. Both the cation and the anion are ten-coordinate, the anion possesses a similar configuration to that of (**58**).

The metal is bonded to one molecule of tridentate terpy ligand and three bidentate nitrate anions. The last coordination site in this literature example is occupied by a fourth NO_3^-, which is monodentate.
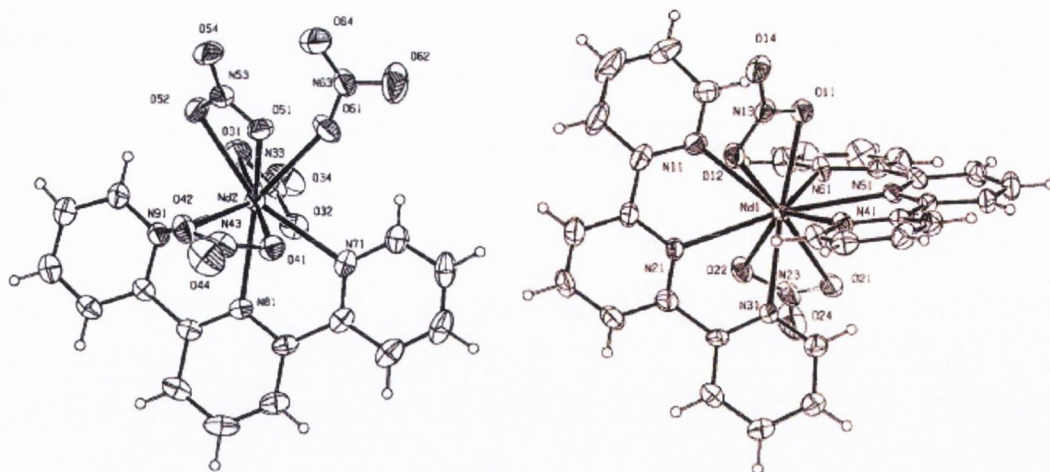
Figure 74: X-ray structure of [Sm (NO₃)₄(terpy)]⁻ and [Sm(NO₃)₂(terpy)₂]⁺. [41]

*2.2.4.7. The synthesis of [Ru(**41**)₂](PF₆)₂*

The synthesis of ruthenium(II) complex [Ru(**41**)₂]$^{2+}$ (**60**) was based on the general procedure for this type of complex (Scheme 26). A solution of two equivalents of ligand (**41**) in ethylene glycol was bubbled with argon for 30 min and 1 equivalent of RuCl₃ was added. The reaction mixture was heated at 110°C for 18 hrs. After cooling a saturated solution of KPF₆ was added, and a deep orange precipitate was formed. Complex (**60**) was purified by chromatography column in 32% yield. The first attempt at this reaction was carried out in ethanol. The reaction mixture was refluxed for 12 hrs, but complex (**60**) did not form. The reaction required a higher temperature, which was achieved by introducing ethylene glycol as a higher boiling point solvent.
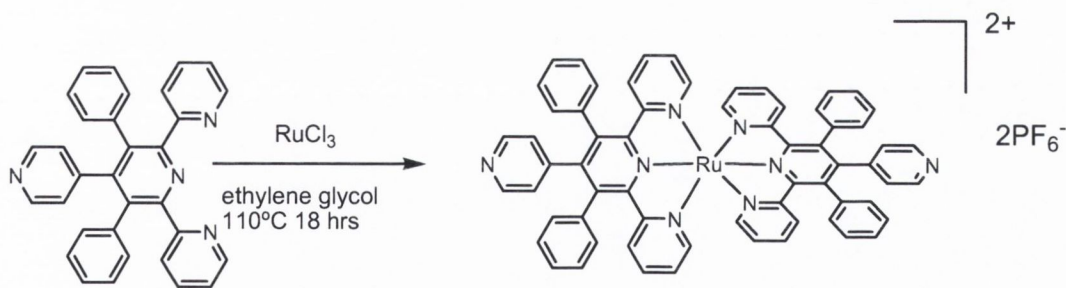
*Scheme 26: Synthesis of the Ru(II) complex (**60**), [Ru(**41**)₂](PF₆)₂.*

Complex (**60**) was characterised by NMR spectroscopy and ESI- mass spectrometry. The proton spectrum was assigned using two-dimensional COSY and nOe

experiments. The proton NMR of (60) (Figure 75) contains seven signals. The most downfield is a broad singlet assigned to proton H19 at δ 8.30, which integrates for two hydrogen atoms. The doublet at δ 7.81 also integrates for two protons and is assigned to H9. The two overlapping signals at δ 7.48-7.43 integrate for twelve hydrogen atoms and are assigned to H7 and a multiplet for H15. The next signal is a triplet of doublets at δ 7.23 and relate to H8 integrating for two protons. The broad singlet at δ 7.11 integrates for two protons and corresponds to the signal for H18. The most upfield signal at δ 6.92 is a doublet, which integrates for two protons and is assigned to H6.

The upfield shifting of H9 (δ 7.81) for (60) with respect to H9 (δ 8.51) for free ligand (41) is explained by the shielding effect of the pyridine ring of the second coordinated ligand. Compared to the literature data for [Ru(pyterpy)$_2$]$^{2+}$ complex (61) the 4-pyridyl ring signals for (60) are shifted upfield, H19 δ 8.30 (8.97 for 61) and H18 δ 7.17 (8.14 for 61) due to the shielding effect of two additional phenyl rings in (41).[1] The same behaviour is observed for the proton assigned to H6.
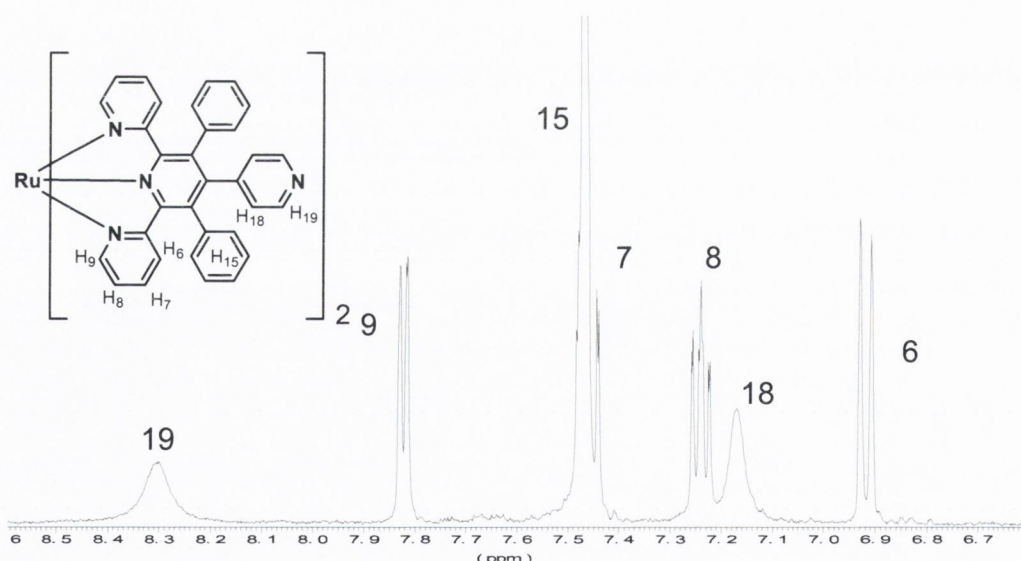
Figure 75: The ^{1}H NMR spectrum of [Ru(41)$_2$]$^{2+}$ complex, CD$_3$CN, 25°C, 400MHz, (atom labelling shown in insert).

The UV-vis absorption spectra for [Ru(41)$_2$]$^{2+}$ in a variety of solvents are shown in Figure 76. Complex (60) does not show solvatochromic behaviour. The spectra for

acetonitrile and methanol (acetone-cut off at 330nm) show three characteristic bands. Those at higher energy in the range 270-325 nm are ligand-centered π-π^* and n-π^* transitions. The red-shifted peak at around 490 nm is assigned in each case to a metal-to-ligand charge transfer (see Table 16).

Complex/solvent	Absorption peaks (nm)		
(60) in acetonitrile	489.5	315.5	277.5
(60) in methanol	489.5	315.0	277.0
(60) in acetone	490.0	326.0	-
[Ru(pyterpy)$_2$]$^{2+}$ (61) in acetonitrile	488.0	312.0	273.0

Table 16: The absorption data for (60) and (61).

Table 16 contains the data for the literature example [Ru(pyterpy)$_2$]$^{2+}$ for comparison with (60). It shows that the two additional phenyl rings on substituted ligand (41) compared to pyterpy did not affect the electronic spectra of (60) significantly. The MLCT band for (60) shifts only 2 nm to lower energy compared to (61).
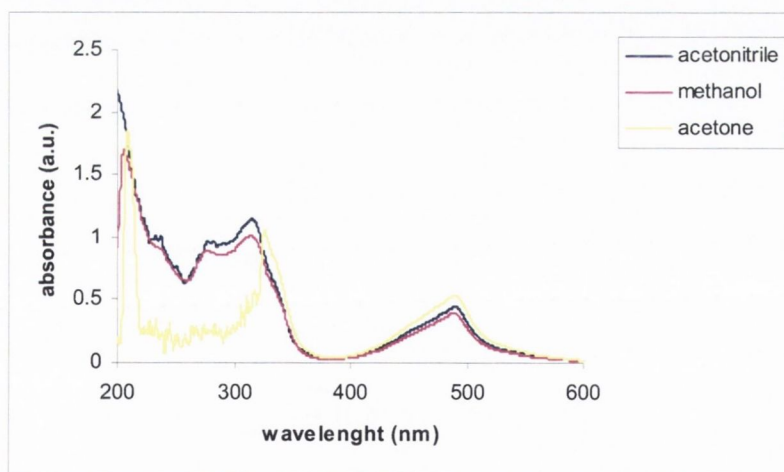
*Figure 76: The UV-vis spectra of (60) in a variety of solvents, concent. 5*10^{-5}M.*

The emission spectra for [Ru(41)$_2$]$^{2+}$ complex were run in acetonitrile, methanol and acetone (Figure 77). In all these solvents, (60) emits in the range 600-650 nm. The maximum λ emission for different solvents varies between 633-638 nm (633 nm-

acetonitrile, 636 nm-methanol, 638 nm-acetone). The spectrum in acetone shows the highest intensity, methanol the lowest.
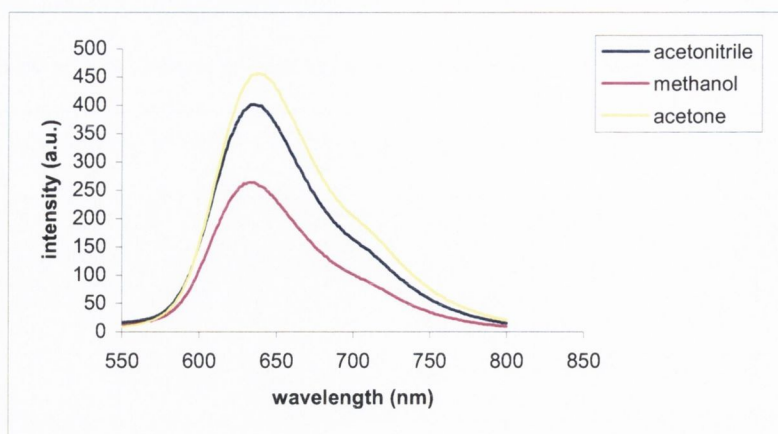
Figure 77: The emission spectra of (60) in a variety of solvents, conc. $5*10^{-5}M$.

Complex (**60**) is an ideal candidate for the formation of mixed metal complexes. The pyridyl monodenate moiety in (**60**) is free to coordinate to other metals. (**60**) was reacted with the $AgNO_3$ in 1:1 ratio. A warm acetonitrile solution of (**60**) was added to a warm methanolic solution of silver nitrate. The orange reaction mixture changed colour immediately to dark red. The mixture was allowed to cool down, and a layer of the diethyl ether was carefully deposited over the mixture. The slow diffusion of ether gave a deep red precipitate; there was no evidence of single crystal suitable for X-ray analysis. Other systems were tried but none of them gave satisfactory results.

As future work complex (**60**) will be tested with other metal ions such as Pd(II), Pt(II) and Cd(II).[42]

2.3. **Conclusion.**

The aim of the work presented in this chapter was to synthesise pyridine-centerd compounds and to investigate them as bridging ligands in new supramolecular architectures. We have successfully synthesised and fully characterised three terpy-type ligands (**41**), (**42**) and (**51**). Ligands (**42**) and (**51**) have not been reported before.

The ligand design plays an important role in the synthesis of coordination polymers. These ligands proved that they could react as bridging ligands. Novel copper(II) complexes (53) and (55) have been synthesised by reacting CuI with (42) and (51), respectively. New polyaromatic ligands due to their flexible aromatic rings can create functional architectures, which can be useful in the storage of solvents and ions.

Ligands (41) and (42) as was expected proved that the different position of the pyridyl nitrogen plays a crucial role in the resulting of the coordination polymer. The change of the position of nitrogen in (42) for the 3'-pyridyl gave the 2-D coordination polymer of Cu(II) (53), while (41) gave a monomer. The analysis was done using X-ray crystallography.

Ligand (41) proved to be an ideal bridging ligand with lanthanides. In methanolic solution, two hydrogen-bonded polymers of La(III) and Sm(III) were obtained, (57) and (58) respectively. The change of solvent for the non-coordinating dichloromethane gave La(III) coordination polymer (59). A similar result was found by reacting $Sm(NO_3)_3$ with 4-pyridine-4'-terpy (pyterpy). The 1-D hydrogen-bonded polymer $[Sm(pyterpy)(NO_3)_3(MeOH)]$[43] (61) was obtained. The two additional phenyl rings on (41) compared to pyterpy do not influence the linear arrangement of the units in (58) and (61), but has an influence on the packing of the polymer chains.

In the literature there are only a few examples of Cd(II) coordination polymers with terpy-type ligands. Some were synthesised in our group. ${[Cd(41)(NO_3)(CH_3OH)]NO_3}_\infty$[29] is the one-dimensional polymer of (41). The reaction between (41) and $CdSO_4$ gave a two-dimensional polymer with the formula ${[Cd(41)(SO_4)]\cdot5CH_3OH\cdot3H_2O}_\infty$[29]. Due to the additional binding sites of (51) compared to (41) and (42) it possesses higher coordination potential. The cadmium sulfate complex of (51) gave a three-dimensional network (56).

The synthesised homoleptic Ru(II) complex (60) of (41) is an ideal candidate for mixed metal polymers. Compared to the coordination polymer of pyterpy ligand ${[Ru(pyterpy)_2]Ag...}$[43], the two additional phenyl rings of (41) and complex (60) might give even more interesting results.

Looking at the satisfactory results obtained with ligands (41), (42) and (51), from the supramolecular point of view, the synthesis of their analogues seems attractive. These ligands are [2,6-di(2-pyridyl)-3,5-di(4-pyridyl)-4-(3-pyridyl)]-pyridine (62), [2,6-di(2-

pyridyl)-3,5-di(3-pyridyl)-4-(4-pyridyl)]pyridine (**63**) and [2,6-di(2-pyridyl)-3,5-di(3-pyridyl)-4-(3-pyridyl)]pyridine (**64**). The syntheses for these ligands should be quite easy by adopting the same method as for (**42**) and (**51**). The result might be further new compounds with unique structural properties.

(62)   **(63)**   **(64)**
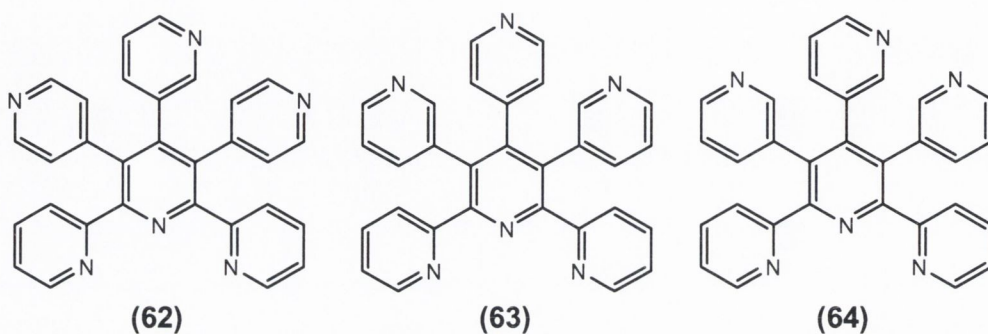
Figure 78: Proposed new ligands.

2.4. References

[1] E. C. Constable, A. M. W. Cargill Thompson, *J. Chem. Soc. Dalton Trans.*, **1994**, 1409-1418

[2] E. C. Constable, M. Neuburger, D. R. Smith, M. Zehnder, *Inorg. Chim. Acta*, **1998**, 359-365

[3] E. C. Constable, A. M. W. Cargill Thompson, *New J. Chem.*, **1992**, 16, 855-867

[4] E. C. Constable, M.D. Ward, *J. Chem. Soc. Dalton Trans.* **1990**, 1405-1409

[5] A. N. Khlobystov, A. J. Blake, N. R. Champness, D. A. Lemonovski, A. G. Majouga, N. V. Zyk, M. Schröder, *Coord. Chem. Rev.*, **2001**, 155-192

[6] E. C. Constable, *Advances in Inorganic chemistry and Radiochemistry*, **1986**, 30, 69-216

[7] C. Metcalfe, S. Spey, H. Adams, J. A. Thomas, *J. Chem. Soc., Dalton Trans.*, **2002**, 4732-4739

[8] J. P. Lopez, W. Kraus, G. Reck, A. Thünemann, D. G. Kurth, *Inorg. Chem. Commun.*, **2005**, 281-284

[9] J. P. Lopez, W. Kraus, G. Reck, A. Thünemann, D. G. Kurth, *Inorg. Chim. Acta*, **2005**, 3384-3390

[10] S. K. Padhi, V. Manivannan, *Inorg. Chem.*, **2006**, 7994-7996

[11] L. Hou, D. Lin, W. J. Shi, Y. G. Yin, S. W. NG, *Inorg. Chem.*, **2005**, 44, 7825-7832

[12] J. Y. Lu, *Coord. Chem. Rev.*, **2003**, 327-347

[13] S. Hayami, K. Hashiguchi, G. Juhasz, M. Ohba, H. Okawa, Y. Maeda, K. Kato, K. Osaka, M. Takata, K. Inoue, *Inorg. Chem.*, **2004**, 43, 4124-4126

[14] A. Jouaiti, V. Jullien, M. W. Hosseini, J. M. Planeix, A. De Cian, *Chem. Commun.*, **2001**, 1114-1115

[15] M. G. B. Drew, M. R. Foreman, M. J. Hudson, K. F. Kennedy, *Inorg. Chim. Acta*, **2004**, 4102-4112

[16] X. J. Zheng, L. P. Jin, *Polyhedron*, **2003**, 2617-2624

[17] A. M. Arif, F.A. Hart, M. B. Hursthouse, M.Thornton-Pett, W. Zhu, *J. Chem. Soc. Dalton Trans.*, **1984**, 2449-2454

[18] S. A. Cotton, P. R. Raithby, *Inorg. Chem. Commun.,* **1999**, 86-88

[19] R. J. Hill, D. L. Long, M. S. Turvey, A. J. Blake, N. R. Champness, P. Hubberstey, C. Wilson, M. W. Schröder, *Chem. Commun.*, **2004**, 1792-1793

[20] D. J. Long, A. J. Blake, N. R. Champness, C. Wilson, M. W. Schröder, *Angew. Chem. Int. Ed.*, **2001**, 40, 2444-2447

[21] S. S. Sun, A. J. Lees, *Inorg. Chem.*, **2001**, 3154-3160

[22] R. V. Slone, D. I. Yoon, R. M. Calhoun, J. T. Hupp, *J. Am. Chem. Soc.*, **1995**, 117, 11813-11814

[23] G. M. McCann, R. A. More O'Ferrall, S. M. Walsh, *J. Chem. Soc. Perkin Trans. 2*, **1997**, 2761

[24] B. D. Wade, R. Bonjouklian, L. Junkai, W. T. McMillen, P. B. Lee, S. J. Scott, J. M. Yingling, Y. J. Schulenburg, **2004**, patent number:WO2004026871

[25] P.T. Herwing, V.Enkelmann, O. Schmelz, K. Müllen, *Chem. Eur. J.*, **2006**, 1834-1839

[26] M. D. Watson, A. Fechtenkötter, K. Müllen, *Chem. Rev.*, **2001**, 1267-1300

[27] M. Müller, H. Mauermann-Düll. M. Wagner, V. Enkelmann, K. Müllen, *Angew. Chem. Int. Ed. Engl.*, **1995**, 1583-1586

[28] F. Churruca, R. SanMartin, M. Carril, M. K. Urtiaga, X. Solans, I. Tellitu, E. Dominguez, *J. Org. Chem.*, **2005**, 70, 3178-3187

[29] Cecile Ollagnier, PhD thesis, New N-and S-containing polyaryl compounds as ligands in transition metal complexes, **2005**, Trinity College Dublin

[30] L. Hou, D. Li, T. Wu, Y. G. Yin, S. W. Ng, *Acta Crystall. Sec. E*, **2004**, E60, m1181-m1182

[31] E. G. Espana, P. Gavina, J. Latorre, C. Soriano, B. Verdejo, *J. Am. Chem. Soc.*, **2004**, 126, 5082-5083

[32] G. A. Van Albada, I. Mutikainen, O. S. Roubeau, U. Turpeinen, J. Reedijk, *Eur. J. Inorg. Chem.*, **2000**, 2179-2184

[33] G. Kickelbick, *Acta Crystall. Sec. E*, **2001**, E57, m475-m477

[34] P. E. Kruger, G. D. Fallon, B. Moubaraki, K.J. Berry, K. S. Murray, *Inorg. Chem.*, 1995, 34, 4808-4814

[35] F. H. Allen, *Acta Crystall. Sec. B*, **2002**, B58, 380-388

[36] G. Tamasi, R. Cini, *Dalton Trans.*, **2003**, 2928-2936

[37] M. J. Plater, M. R. Foreman, T. Gelbrich, S. J. Coles, M. B. Hursthouse, *J. Chem. Soc. Dalton Trans.*, **2000**, 3065

[38] J. Granifo, M. T. Garland, R. Baggio, *Inorg. Chem. Commun.*, **2004**, 77-81

[39] M. Harvey, S. Baggio, S. Russi, R. *Baggio, Acta Crystallography. Sec. C*, **2003**, C59, m171-m174

[40] B. Ahrens, S. A. Cotton, N. Feeder, O. E. Noy, P. R. Raithby, S. J. Teat, *J. Chem. Soc., Dalton Trans.*, **2002**, 2027-2030

[41] M. G. B. Drew, P. B. Iveson, M. J. Hudson, J. O. Liljenzin, L. Spjuth, P.Y. Cordier, A. Enatsson, C. Hill, C. Madic, *J. Chem. Soc., Dalton Trans.*, **2000**, 821-830

[42] R. V. Slone, K. D. Benkstein, S. Belanger, J. T. Hupp, I. A. Guzei, A. L. Rheingold, *Coord. Chem. Rev.*, **1998**, 221-243

[43] D. Nolan, S. M. Draper, C. Fitchett, C. Ollagnier, *Poster,* Trinity College Dublin, **2006**

Part 3: Terpyridine-type ligands and their Ruthenium complexes

3.1. Introduction

3.1.1. Terpyridine-type of ligands

Tridentate ligands, derivatives of 2,2':6',2"-terpyridine have been employed extensively in coordination chemistry and as metal-binding domains in metallosupramolecular systems.[1,2,3]

The general method for the synthesis of appropriate substituted terpy-type ligands, was described in Chapter 2, Scheme 6. This involves the reaction of an enone (or equivalent) with an enolate (or equivalent) to generate a dione that can be cyclised by reaction with an ammonium source such as NH_4OAc. Another way to synthesise substituted terpyridine compounds is based on 4'-[[(trifluoromethyl)sulfonyl]oxy]-2,2':6',2"-terpyridine (**65**). It has been shown that triflate derivatives undergo Pd catalysed reaction with the formation of a new C-C bond. The reaction is called Sonogashira cross-coupling. Compound (**65**) possesses great potential to react as a precursor for a wide range of substituted terpyridines.

Scheme 27 shows a few examples where (**65**) has been employed as a precursor. Reaction between (**65**) and phenyl acetylene, catalysed by $[Pd(PPh_3)_2Cl_2]$, resulted in the formation of 4'-(phenylethynyl)-2,2':6',2"-terpyridine (**66**).[4] Acetylene substituted (**66**) plays an important role as a ligand for ruthenium(II) complexes with prolonged lifetimes. 4'-Ferrocenyl-2,2':6',2"-terpyridine (**67**) was obtained from the reaction between (**65**) and ethynylferrocene with $Pd(PPh_3)_4$ as a catalyst.[5] The ruthenium(II) complexes of (**67**) show interesting electro- and photochemical properties, due to the redox-active ferrocenyl group. The reaction of triflate (**65**) with vinyltributyltin using the Stille procedure gave 4'-vinyl-2,2':6',2"-terpyridine (**68**).[6] The transition metal complexes of (**68**) are of interest due to their applications in polymer chemistry, chemically modified electrodes and in solar energy conversion. The last example given in Scheme 27 is the coupling reaction between (**65**) and an ethylene derivative of 2,2'-bipyridine, which gave a bridging ligand, 2,2'-bipyridine-2,2':6',2"-terpyridine (**69**).[7] Different transition metals can be coordinated to the two vacant coordination sites. The ditopic ligand can create binuclear complexes with long-range electronic coupling due to the alkyne bridge between the cationic units.
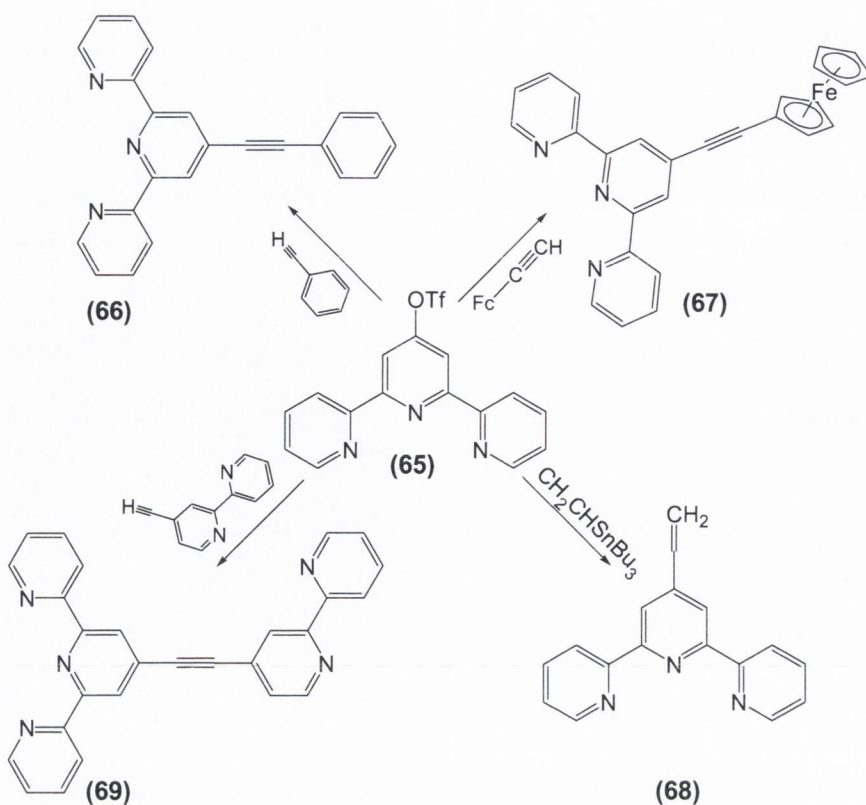
Scheme 27: The synthesis of ligands based on 4'-[[(trifluoromethyl)sulfonyl]oxy]-2,2':6',2"-terpyridine (65).[4,5,6,7]

Müllen *et al.* discovered a new series of polyaromatic hydrocarbons (PAHs). The work was based on the synthesis of systems larger than hexa-peri-hexabenzocoronene (HBC).[8,9,10] The extended PAHs are available by a two-step protocol, the synthesis of a non-planar oligophenylene precursor and planarization *via* a cyclodehydrogenation reaction. Scheme 28 shows one of the literature examples; the synthesis of arrow-like molecules.[11] The oligophenylene precursors (**72a**) and (**72b**) were obtained by Diels-Alder cycloaddition between alkyne (**70a, 70b**) and tetraphenylcyclopentadienone (**71a, 71b**) by refluxing in diphenyl ether.
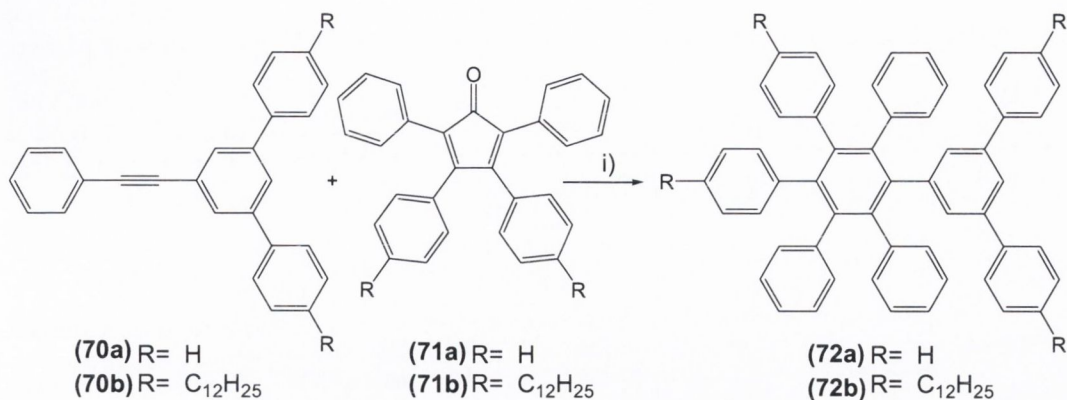
Scheme 28: The synthesis of oligophenylene precursors (72a) and (72b), i) diphenyl ether, reflux 16h.[11]

The final step in the synthesis of large PAHs is the oxidative cyclodehydrogenation of the oligophenylene precursor under Lewis acidic conditions (Scheme 29). The planarisation of (72) was obtained by using copper(II) trifluoromethanesulfonate and aluminium(III) trichloride as oxidative reagents. The four long chains substituted analogue (73) was synthesised by using iron(III) trichloride as an oxidative agent.[11]
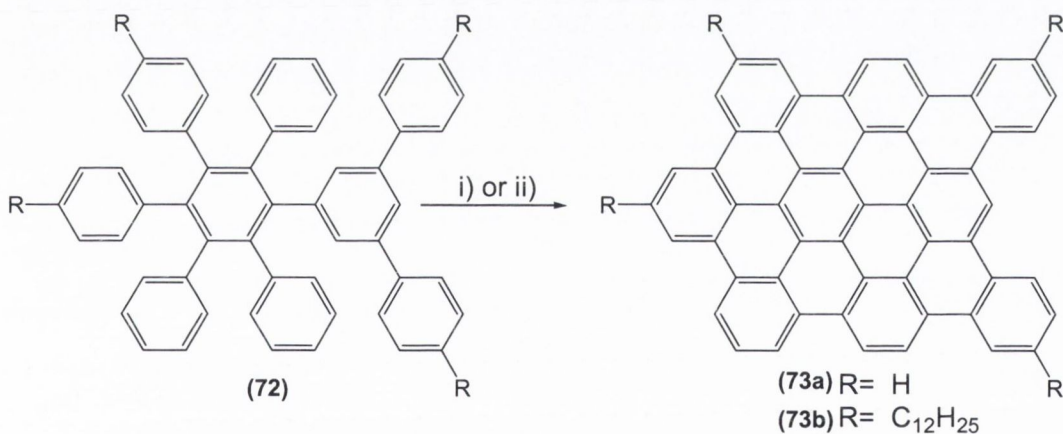
Scheme 29: The synthesis of PAHs (73a) and (73b), i) Cu(OSO$_2$CF$_3$)$_2$, AlCl$_3$, CS$_2$, 25°C, 24h, ii) FeCl$_3$, CH$_2$Cl$_2$.[11]

Iron(III) trichloride as an oxidative reagent for alkyl-substituted oligophenylenes proved to be superior to all the other reagents commonly used, such as AlCl$_3$, CuCl$_2$. FeCl$_3$ does not cause dealkylation, chlorination or migration of the alkyl group.

Due to their low solubility in common organic solvents the characterisation of planar extended PAHs causes problems. The substitution of PAHs with alkyl chains, such as four dodecyl chains in (73) increases the solubility, and allows the use of general analysis techniques like NMR spectroscopy and electrospray mass spectrometry.

Aromatic molecules such as triphenylene or HBC substituted with alkyl chains can form discotic liquid crystals and find applications for materials with one-dimensional transport processes such as energy migration, electric conductivity and photoconductivity. Extended PAHs have become increasingly important as functional materials in optoelectronic and electronics.[12]

3.1.2. Ruthenium complexes

Ruthenium(II) polypyridine complexes have attracted steady interest over the last few decades. Their unusual photophysical properties make them attractive candidates for applications as photoactive components. Polynuclear arrays composed of ruthenium(II) complexes are ideal for light-harvesting devices.[13,14,15]

The family of transition metal complexes of 2,2'-bipyridine (bpy) has been used very widely for luminescent supramolecular systems, which can undergo photoinduced energy or electron transfer processes. They show a unique combination of chemical stability, redox and photochemical properties. However complexes of bpy and phen (1,10-phenanthroline) families cause problems in the synthesis of supramolecular systems with controlled geometry.[16] The tris Ru(II) complexes of bidentate ligands exhibit two isomers, Λ and Δ forms, which are almost impossible to separate by standard methods.

The complexes of 2,2':6',2''-terpyridine (terpy) are an interesting alternative to bpy complexes. Bis-terpyridine metal complexes are intrinsically achiral and their syntheses cause less problems than that of tris-bipyridine metal complexes. The disadvantage of Ru(II) terpyridine complexes is that they exhibit less satisfactory photophysical properties, very weak luminescence and short lifetimes at room temperature compared to Ru(II) bispyridine complexes.[17]

$[Ru(tpy)_2]^{2+}$ possesses a relatively long luminescence lifetime at 155K, 800 ns,[3] however the luminescence lifetime at room temperature is quite short, 250 ps. Tridentate ligands, when coordinated to a ruthenium centre create a distortion from the ideal octahedral geometry. The N-Ru-N *trans* angles are smaller for coordinated

110

tpy than for their bpy analogous; as a consequence the ligand field strength is weaker. The weak ligand field strength reduces the energy of the dd metal-centred triplet state (^{3}MC) (Figure 79).[17] The decrease of the energy gap between ^{3}MLCT and ^{3}MC makes ^{3}MC thermally accessible from ^{3}MLCT. This facilitates non-radiative decay back to the ground state (GS) from ^{3}MC (Figure 79b).
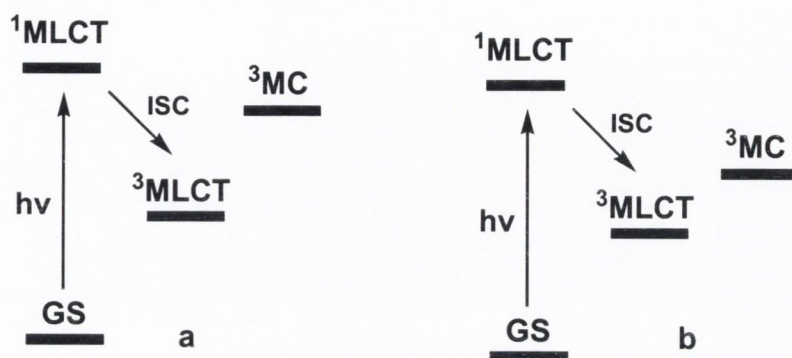
Figure 79: Energy diagrams a) for Ru(II) tris complexes of bidentate ligands, b) Ru(II) bis complexes of tridentate ligands. [17]

There are a lot of strategies used to enhance the photophysical properties of Ru(II) tridentate ligands complexes. These strategies have mostly focused on minimising non-radiative decay through the ^{3}MC to the GS transition by changing the energy levels of ^{3}MLCT and ^{3}MC.[17,18] One of the routes to enhance the photophysical properties of ruthenium(II) terpy-type complexes involves substitution with electron-withdrawing groups at the 4'-position of the terpyridine ligand.[19] The complexes with electron-withdrawing groups absorb at lower energy due to the greater stabilisation of the ligand-based LUMO orbital (compared with the metal-based HOMO orbital). It follows that the energy of ^{3}MLCT is lower and the thermal population of ^{3}MC is reduced. Figure 80 shows examples of ruthenium(II) terpy-type complexes, which emit at room temperature in acetonitrile.[20] Complex (**74**) emits with λ_{max} at 680 nm and a lifetime of 44 ns. The λ_{max} of emission for compound (**75**) appears at the same wavelength as for (**74**) but the lifetime is slightly longer (75 ns). The longest emission lifetime at room temperature for acetylene-substituted complexes 580 ns was found for the acetylene-pyrene complex (**76**) with λ_{max} 698 nm.[17,21]
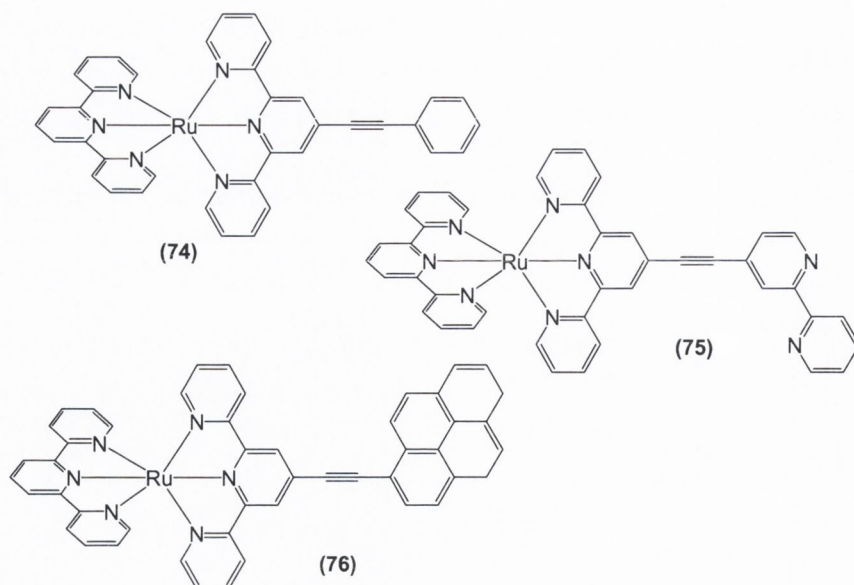
Figure 80: Examples of Ru(II)bis(terpy) complexes with acetylene-substituents.

A very promising strategy to improve the photophysical properties of terpy complexes is the bichromophoric approach.[17,21,22,23] In these systems the non-emissive triplet [3]MLCT state of an organic chromophore is supposed to be similar in energy to an emissive [3]MLCT of another chromophore with which it should be in equilibrium. To create such complexes the challenge is to choose the right components, which have to be electronically independent of one another, as they must maintain the particular properties of the various chromophores. Figure 81 shows two bichromophoric systems. In the homoleptic complex (**77**), with 5-(9-anthryl)-pyrimid-2-yl-2,2':6',2"-terpyridine(tpy-pm-An) as a ligand, the [3]An state of the anthracene unit and the [3]MLCT state of Ru(II) coordinated to a pyrimidyl-terpyridine are almost isoenergetic. The anthracene ring lies perpendicular to the pyrimidine ring, so both components keep their individual energy, giving the bichromophoric effect. [Ru(tpy-pm-An)$_2$]$^{2+}$ exhibits two luminescences at room temperature. The first emission, with a short lifetime of 6 ns is attributed to the [3]MLCT state of the pyrimidyl-terpyridine unit. Second emission with the long lifetime 1806 ns arises from the population of the [3]An state.

The same effect can be obtained when an anthracene is attached in a heteroleptic complex where pyrimidyl-terpyridine is the other ligand. In complex (**78**), the anthracene unit is substituted by a ligand, which is not involved in the [3]MLCT

112

emitting level. Complex (**78**) emits at room temperature with two lifetimes of 25 ns and 1052 nm.
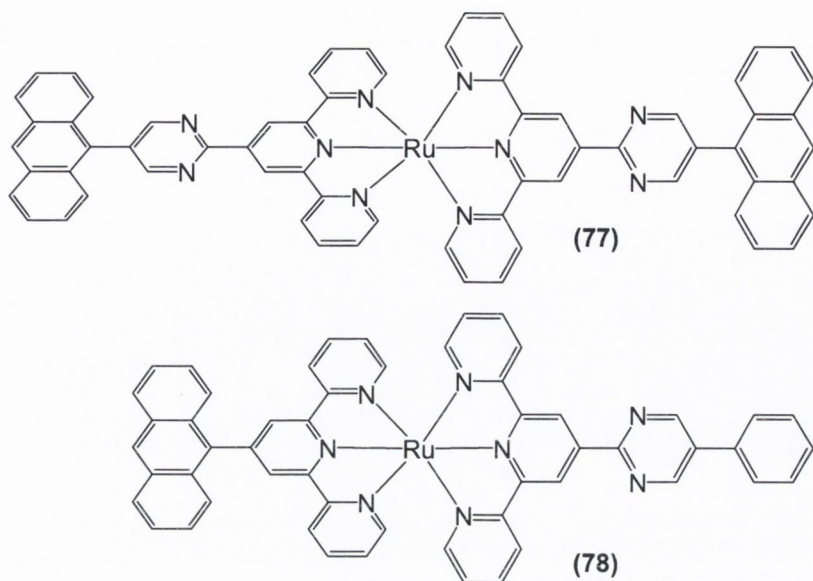
Figure 81: Bichromophoric complexes of Ru(II).[17,21,22,23]

The homoleptic Ru(II) complex (**79**), synthesised by Albano *et al.* does not emit[24]. Complex (**79**) is based on the 4'-(9-anthryl)-2,2':6',2"-terpyridine (An-tpy) ligand, in which the potentially luminescent anthracene is linked directly to the 4'-position terpyridine transition metal complex (Figure 82). The absorption spectra of [Ru(An-tpy)$_2$]$^{2+}$ is similar to the sum of the spectra for [Ru(tpy)$_2$]$^{2+}$ and anthracene (An). MLCT band λ_{max} for [Ru(An-tpy)$_2$]$^{2+}$ is observed at 485 nm (in acetonitrile). Figure 82 shows the energy diagram for [Ru(An-tpy)$_2$]$^{2+}$. Due to energy transfer by the [Ru(tpy)$_2$]$^{2+}$ unit, the potentially fluorescent S$_1$ excited state of anthracene is quenched. In [Ru(An-tpy)$_2$]$^{2+}$ the lowest ^{3}MLCT excited state of [Ru(tpy)$_2$]$^{2+}$ is quenched by the lowest excited state T$_1$ of An (^{3}An). The diagram shows that the T$_1$ level is lower in energy than the ^{3}MLCT. The lowest excited state of [Ru(An-tpy)$_2$]$^{2+}$ is based on the An moiety, if An is non-emissive then the whole-system [Ru(An-tpy)$_2$]$^{2+}$ does not emit. There is no emission for complex (**79**) even in a rigid matrix at 77K.
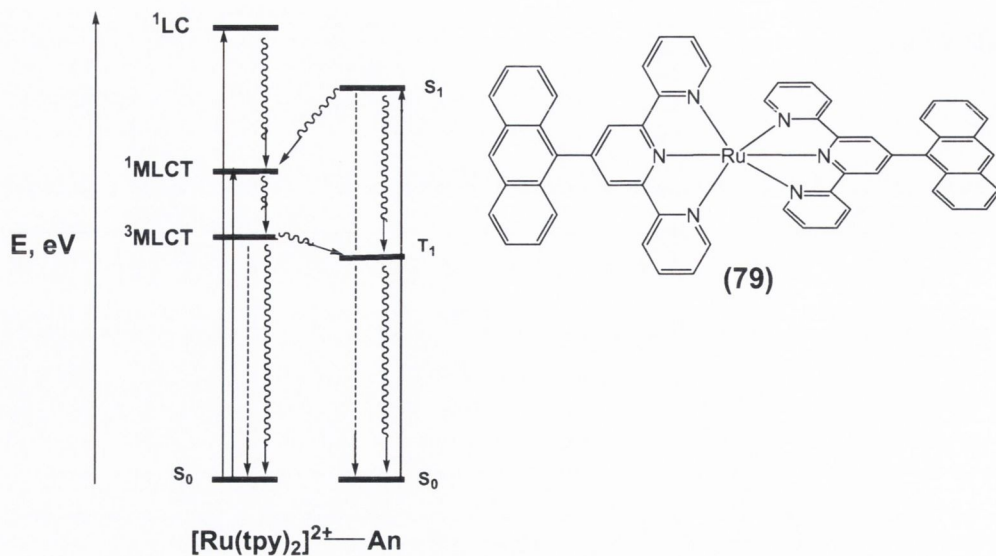
Figure 82: Energy diagram of complex [Ru(An-terpy)₂]²⁺ (79).²⁴

The aim of our work was to synthesise novel polyaromatic ligands with the tridentate terpy-like coordination side. The arrangement of the phenyl rings in those ligands makes them as precursors for planar N-containing hydrocarbons. New transition metal complexes were synthesised and their photophysical properties stablished.

3.2. Results and discussion

3.2.1. Synthesis of terpy-polyphenylene ligands

The novel polyphenyl-terpy ligand (**86**) was obtained in a Diels-Alder reaction between 4'-(phenylethynyl)-2.2':6'2"-terpyridine (**85**) and tetraphenylcyclo-pentadienone.
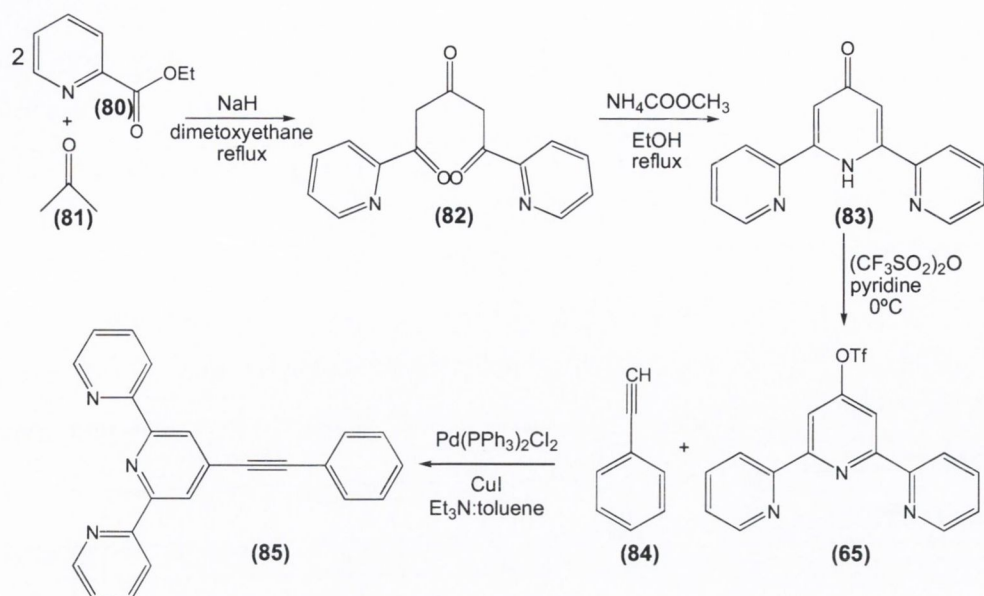
Scheme 30: The synthetic route for precursor (85).[4,6,25]

The synthesis of precursor (**85**) involves four steps and is based on a combination of literature examples (Scheme 30). The first step yields 1,5-bis(2'-pyridyl)pentane-1,3,5-trione (**82**) in a Claisen condensation of one equivalent of acetone (**81**) and two equivalents of ethyl 2-pyridinecarboxylate (**80**)[25] in dimethoxyethane. Then a suspension of sodium hydride was added and the reaction mixture was stirred at room temperature. After the exothermic reaction occurred and the colour changed to bright orange, the mixture was refluxed for 6 hrs. The reaction was cooled down, the solvent evaporated and the yellow solid washed with water. The orange filtrate was adjusted to pH 7 by the addition of diluted HCl and the yellow product precipitated out. It is important to keep the solution at pH 7. The further increase in pH causes the product to dissolve. If the pH is too low an addition of base is required to recover the product. The yellow product was obtained in 54% yield.

In the next step, triketone (**82**) was converted into 2,6-bis(2'-pyridyl)-4-pyridone (**83**) by cyclisation with ammonium acetate in ethanol. The mixture was refluxed for 6 hrs after which the volume of solvent was reduced to half. From the dark brown crude mixture the pure product was separated by recrystallisation from ethanol. The product was formed in 64% yield as a white precipitate. The triflate (**65**) was prepared by reacting (**83**) and trifluoromethanesulfonic anhydride in the presence of pyridine.[6] The mixture was stirred at 0°C for 30 min and then for 48 hrs at room temperature. It was then poured into ice-water causing a brown solid to form, the brown solid was

collected, washed with water and redissolved in hexane. Some insoluble parts were filtered off and the evaporation of solvent from the filtrate gave a white precipitate of (65) with an improved 76% yield, compared to the literature (70%).[6] In the last step to obtain compound (85), the precursor (65) was reacted with phenyl acetylene (84) in a Sonogashira cross coupling reaction using [Pd(PPh$_3$)$_2$Cl$_2$] and CuI as catalysts.[4] The reaction mixture was stirred for 3 hrs at 70°C, in an argon atmosphere. After solvent evaporation, column chromatography yielded (85) as a white product in 75% yield. Precursor (85) was characterised by ^{1}H and ^{13}C NMR spectroscopy, and mass spectrometry. All the results were consistent with available literature data.[4,6,25]

An equimolar mixture of (85) and commercially available tetraphenyl-cyclopentadieone (23) was refluxed at 280°C using benzophenone as solvent. The [2+4] Diels-Alder addition reaction of (85) and (23) gave a new terpy derivative ligand (86) (Scheme 31). The experiment was carried out in an inert atmosphere to avoid the reaction between cyclon (23) and atmospheric oxygen, which is known to result in a lactone. (This happened while reacting (6) and (23) in Chapter 1 (Scheme 9)).
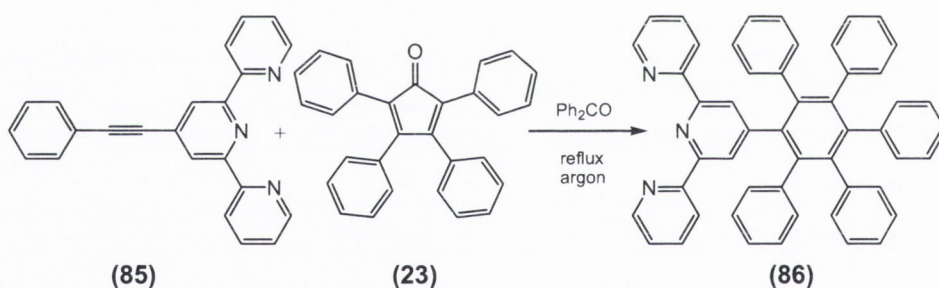
Scheme 31: The synthesis of (86).

After refluxing the mixture for 7 hrs the product (86) was obtained in 48% yield. A longer reaction time (12 and 24 hours) increased the formation of side products leading to lower yields.

Figure 83 shows the ^{1}H NMR spectrum for compound (86) and the hydrogen atom numbering. The peaks were assigned using H, H COSY, C, H COSY and nOe experiments. The spectrum consists of nine signals in the range δ 8.61-6.79. In the low field area of the spectrum are the five characteristic signals for terpy compounds, two doublets, two triplets and one singlet. The most downfield signal is the doublet assigned to H9 at δ 8.61 integrating for two hydrogen atoms. The next signal is a

116

doublet at δ 8.36, assigned to H6 and integrating for two protons. The only singlet in the spectrum is at δ 8.05, relating to the two H3 protons. The two triplets at δ 7.73 and δ 7.24 integrate for two hydrogen atoms each and are assigned to H7 and H8. The signals for phenyl ring A are well resolved. There is a doublet integrating for two protons and assigned to H18 (δ7.02). Triplet H17 at δ 6.83 is overlapping with a multiplet, another triplet related to H16 is the most upfield signal. Both triplets integrate for two hydrogen atoms each. The multiplet at δ 6.86 is related to the last two phenyl rings and integrates for fifteen hydrogen atoms.
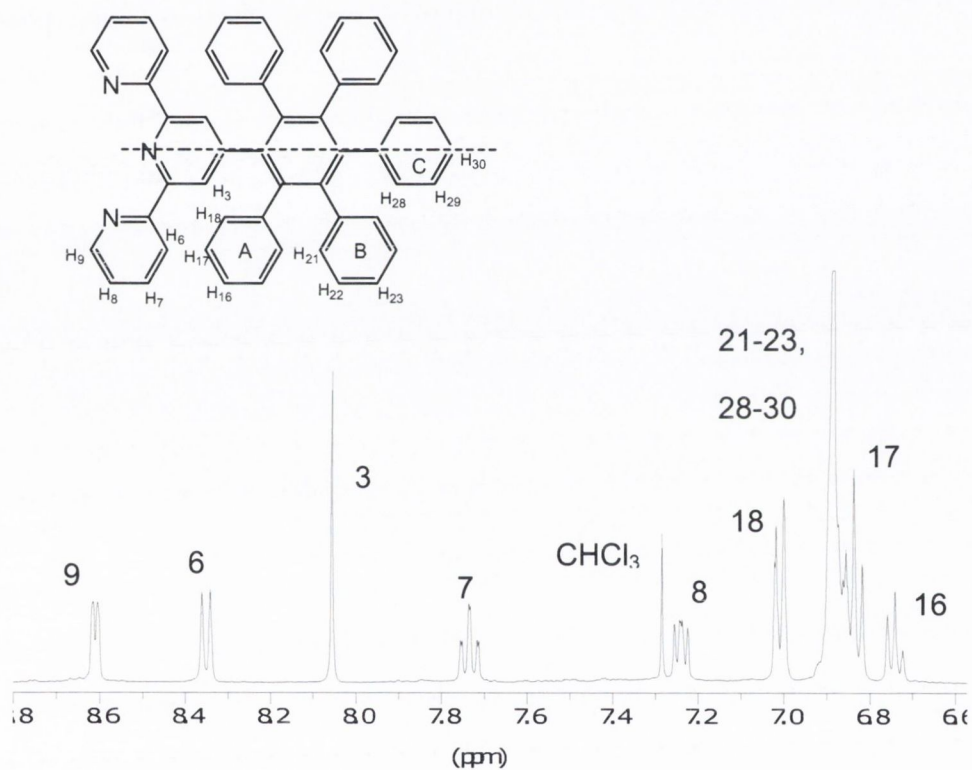
Figure 83: The ^{1}H NMR spectrum for compound (86) in CDCl₃, 400 MHz, 25°C.

The *t*-butyl derivative (89) of compound (86) was also prepared, to increase the solubility of the cyclised product. Synthesis of (89) follows that of (86).
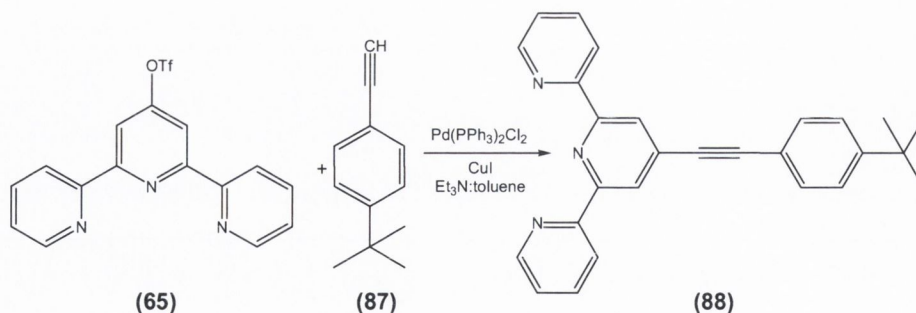
Scheme 32: Synthesis of 4'-(4-tert-butyl phenylethynyl)-2,2':6'2"-terpyridine (88).

Scheme 32 shows the synthesis for 4'-(4-*tert*-butyl phenylethynyl)-2.2':6'2"-terpyridine (**88**). The triflate (**65**) was prepared according to the synthetic route shown in Scheme 30. Compounds (**65**) and commercially available 4-*tert*-butyl phenyl acetylene (**87**) were reacted in a palladium(II) catalysed Sonogashira coupling reaction with a triethylamine/toluene solvent system. The reaction mixture was stirred at 70°C for 4.5 hrs. The solvents were then evaporated and the crude mixture was chromatographed in 2% acetone in dichloromethane. The new compound (**88**) was obtained in 75% yield as a white precipitate. (**88**) was characterised by NMR spectroscopy and mass spectrometry. Figure 84 shows the aromatic region of the ^{1}H NMR spectrum of (**88**). The spectrum consists of seven signals. Five of them are characteristic signals for terpy-like compounds (two doublets, two triplets and one singlet). Those signals are assigned to H9 (δ 8.75), H6 (δ8.65), H8 (δ 7.39) and H7 (δ 7.89) H3 (δ 8.59), respectively, each integrating for two hydrogen atoms. The most downfield signal is for proton H9 lying next to the nitrogen on the terpyridine ring. The two doublets (AB system) at δ 7.55 and δ 7.44 are assigned to H14 and H15, and they belong to the phenyl ring. There is one signal in the aliphatic region; it is a singlet at δ 1.36, integrating for nine hydrogen atoms, which belongs to the *t*-butyl group. The signals for protons H9, H6, H3, H7 and H8 for (**88**) and (**85**) have similar shifts, the *t*-butyl group does not affect them.
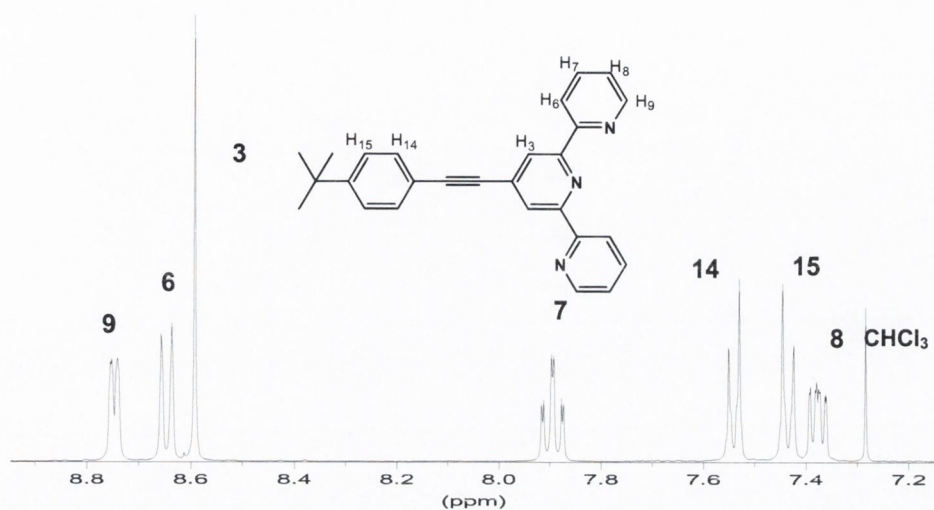
Figure 84: The aromatic region of the ^1H NMR spectrum of (88) in CDCl$_3$, 400 MHz, 25°C, with atom numbering.

The second precursor for the synthesis of (89) is 2,3,4,5-tetra-(4-*tert*-butyl-phenyl) cyclopentadienone (5) (Scheme 33). The synthesis of (5) involves a few steps, the last step being the Knoevenagel condensation between 1,2-bis-(4-*tert*-butyl-phenyl)ethane-1,2-dione and 1,3-bis-(4-tetra-butyl-phenyl)-propan-2-one in the presence of a base. All the details for this synthesis are given in Chapter 1 (Scheme 4). An equimolar mixture of (88) and (5) in benzophenone was refluxed at 280°C for 7 hrs in an inert atmosphere. The product (89) was purified by column chromatography with chloroform/methanol (30:1) solvent mixture. This yielded the product as a white precipitate in 52% yield. In this experiment it is important to keep the temperature around 280°C, as a higher temperature may cause the decomposition of the starting materials. The reaction time should not be longer than 8 hrs. After refluxing for 12 or 24 hrs, the crude mixture was more impure and the yield was much lower.

119
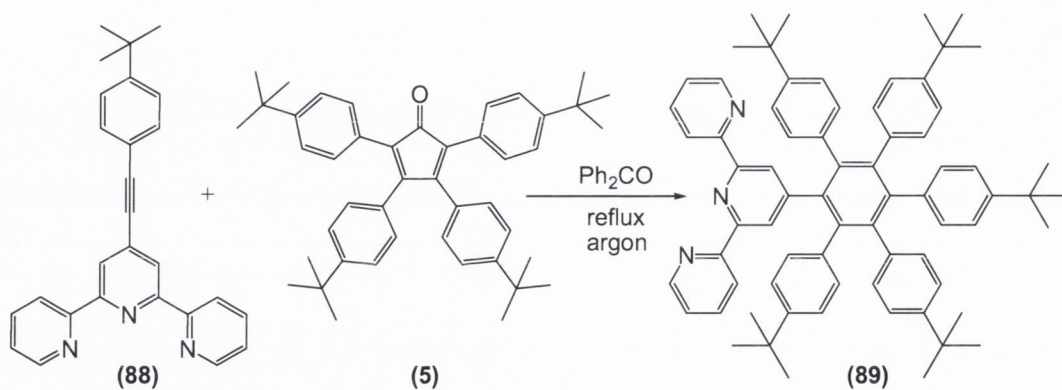
Scheme 33: The synthesis of (89).

The novel ligand (89) was identified by ^{1}H, ^{13}C NMR spectroscopy, mass spectrometry and single crystal X-ray analysis. The aromatic region of the ^{1}H NMR spectrum for (89) is shown in Figure 85. The peaks were assigned using H, H COSY, C, H COSY and nOe experiments. In general the peaks of the terpy part of the ligand are shifted upfield compared to the starting material (88). This is due to the loss of the shielding effect of the triple bond.
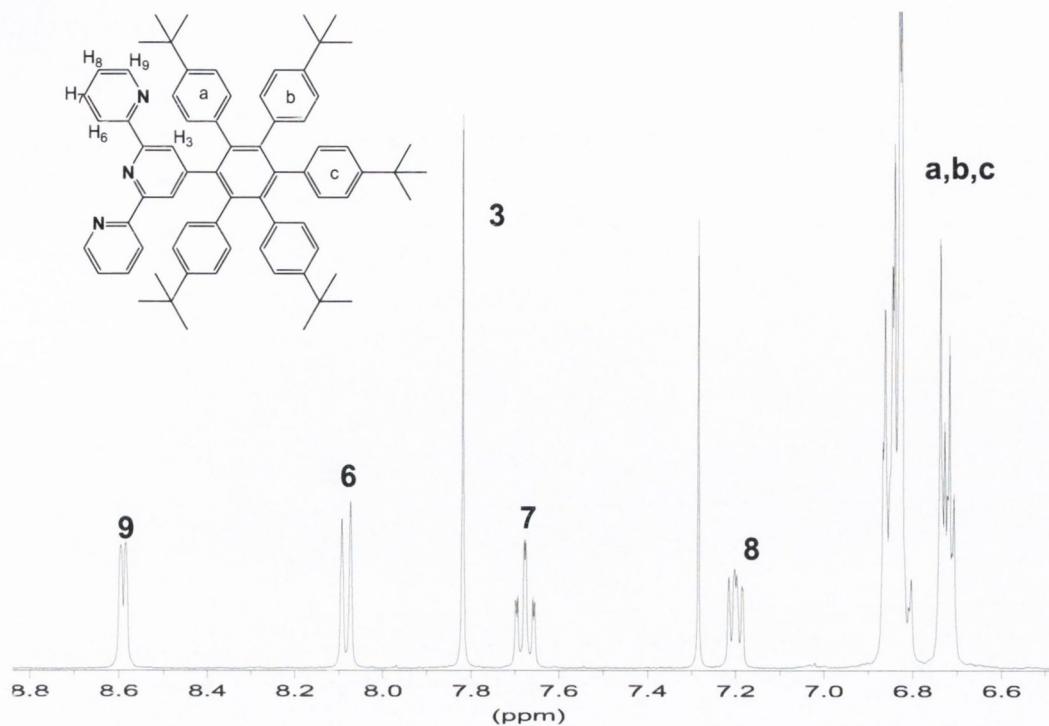
Figure 85: The aromatic region of ^1H NMR spectrum of (89) in CDCl₃, 400 MHz, 25°C, with atom numbering.

The lowest field resonance is a doublet assigned to H9 as expected from the deshielding effect of the adjacent nitrogen atom. H9 appears at δ 8.60 and integrates for two hydrogen atoms. The next doublet is at δ 8.11 and is assigned to H6, it integrates for two protons. The singlet at δ 7.83 assigned to H3 integrates for two protons. The two triplets at δ 7.67 and δ 7.20, each integrating for two hydrogen atoms are assigned to H7 and H8 respectively. Around δ 6.84-6.73 are two multiplets which integrate together for twenty-five protons. These protons are situated on the five phenyl rings around the central benzene ring. In the aliphatic region of the ^1H NMR spectrum for (89) are two singlets at δ 1.13 and δ 1.12, which are assigned to the five *t*-butyl groups and integrate for forty-five hydrogen atoms.

Crystals suitable for X-ray analysis were obtained of compounds (89) and (86). The slow evaporation of a dichloromethane solution of (89) gave white crystals. Figure 86 shows the asymmetric unit for compound (89) and significant bond distances and angles are given. The terpyridine part of (89) is bent 86.9° with respect to the central

benzene ring (C19-C23). The tilt angles for the other rings are shown in Table 17. Of the five phenyl rings substituted to the central benzene, ring 3 has the greatest tilt.
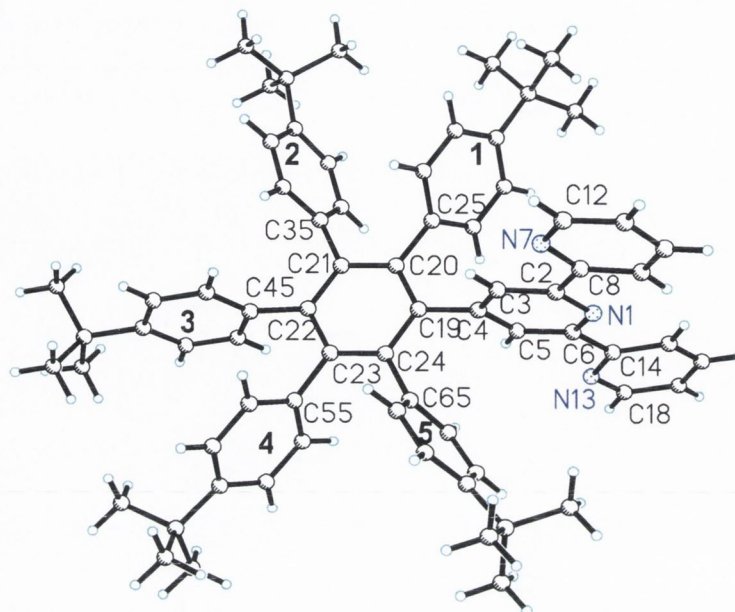
Figure 86: The molecular structure of (89) showing selected atomic labelling.

Selected bond lengths (Å): N1-C2 1.337(4), C2-C3 1.400(4), C3-C4 1.383(4), C4-C5 1.385(4), C5-C6 1.391(4), N1-C6 1.341(4), N7-C8 1.336(4), N7-C12 1.334(4), C2-C8 1.493(4), N13-C14 1.337(4), N13-C18 1.337(4), C6-C14 1.492(4), C4-C19 1.500(4), C19-C20 1.404(4), C20-C21 1.409(4), C21-C22 1.404(4), C22-C23 1.407(4), C23-C24 1.400(4), C24-C19 1.406(4), C20-C25 1.498(3), C21-C35 1.498(4), C22-C45 1.507(3), C23-C55 1.500(3), C24-C65 1.498(4). Selected bond angles (°): C2-N1-C6 117.5(2), C8-N7-C12 117.3(3), C14-N13-C18 117.5(3).

(89) shows intermolecular π-stacking at the terpy-end the molecule with distance of 3.74 Å (Figure 87).
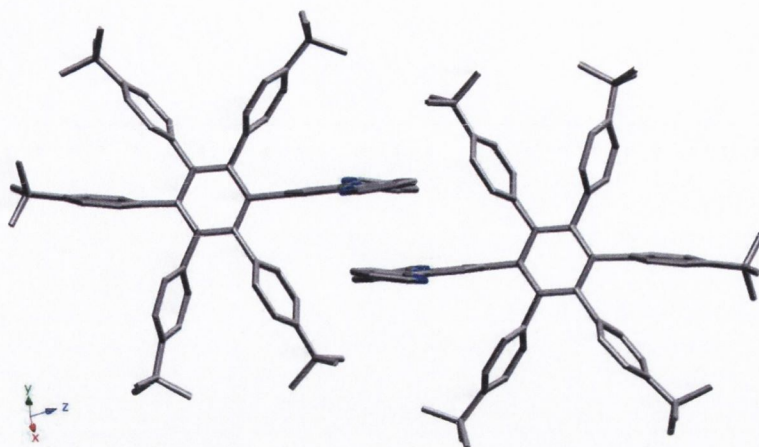
*Figure 87: The π-stacking interaction between two molecules of (**89**).*

Figure 88 shows the packing arrangement between molecules of (**89**). They create layers, which are shown in pink and blue. The molecules in the layer are organised in columns. The distance between two molecules in the column is 10.52 Å. The distance was measured between central benzene rings. The blue layer is organised in the same way as the pink and related by the inversion centre. Figure 88A shows the stacking between molecules from the blue and the pink layer. Figure 88B illustrates the organisation between the flat terpy-ends of the molecules and the perpendicular polyphenylenes.
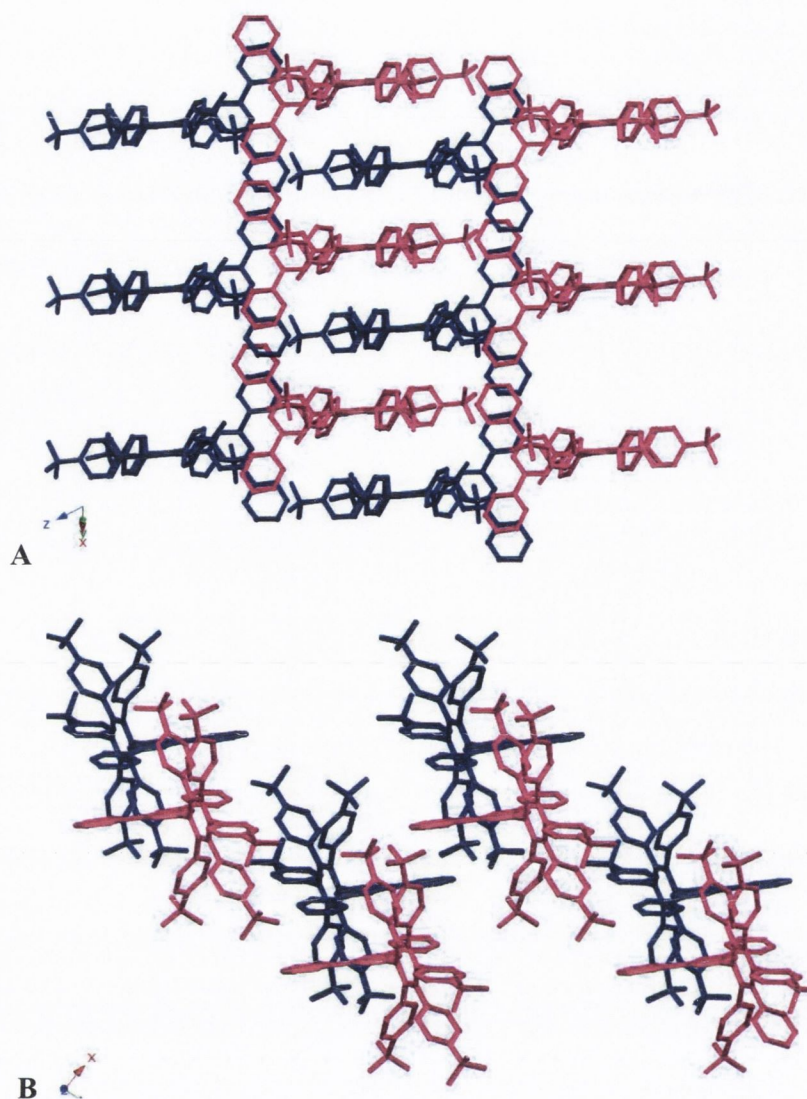
Figure 88: The perspective views of the crystal packing in compound (89).

Crystals of (**86**) suitable for X-ray diffraction were obtained by slow solvent evaporation from a chloroform solution of (**86**). The asymmetric unit contains one molecule of ligand and three molecules of chloroform (Figure 89). The significant bond distances and angles are given. The terpy end of the ligand is bent by 56.8° with respect to the central benzene ring. This angle is smaller than for ligand (**89**) where the terpy-end is almost perpendicular to the rest of the ligand. The tilt angles for the phenyl rings substituted onto the central benzene ring varies from 65° to 70°.

124
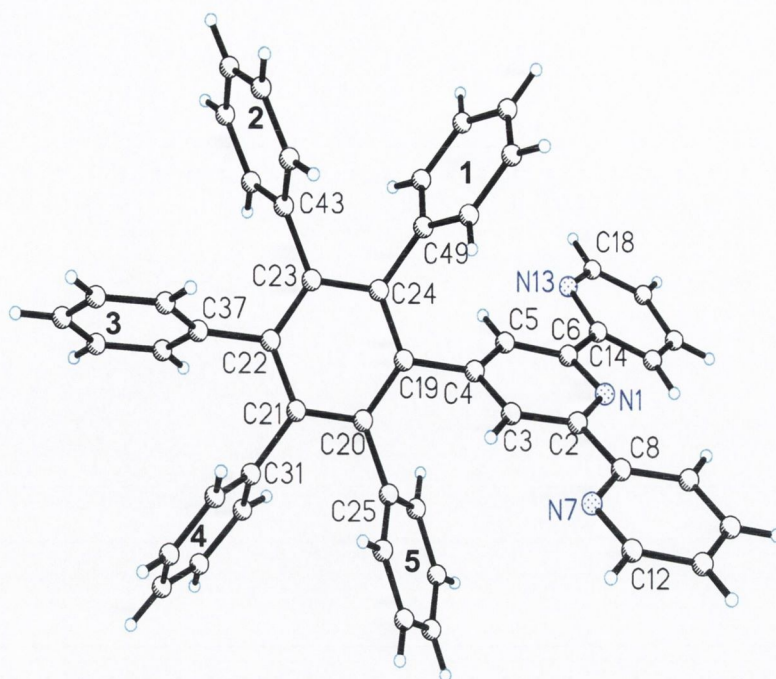
Figure 89: The X-ray crystal structure of (86) showing selected atomic labelling. The solvent molecules are omitted for clarity.

Selected bond lengths (Å): N1-C2 1.338(3), C2-C3 1.392(3), C3-C4 1.387(3), C4-C5 1.389(3), C5-C6 1.392(3), N1-C6 1.345(3), N7-C8 1.336(4), N7-C12 1.339(4), C2-C8 1.494(3), N13-C14 1.342(3), N13-C18 1.333(4), C6-C14 1.488(3), C4-C19 1.500(3), C19-C20 1.403(3), C20-C21 1.403(3), C21-C22 1.400(3), C22-C23 1.406(3), C23-C24 1.408(3), C24-C19 1.403(3), C20-C25 1.500(3), C21-C31 1.497(3), C22-C37 1.497(3), C23-C43 1.496(3), C24-C49 1.497(3). Selected bond angles (°): C2-N1-C6 117.8(2), C8-N7-C12 117.5(3), C14-N13-C18 117.0(2).

Figure 90 shows the organisation between molecules of (86), which are not involved in any π-stacking. The perspective view shows that the molecules create columns, and they are related by the inversion centre. Two molecules, each from a different column, generate pairs in a head-to-head style.
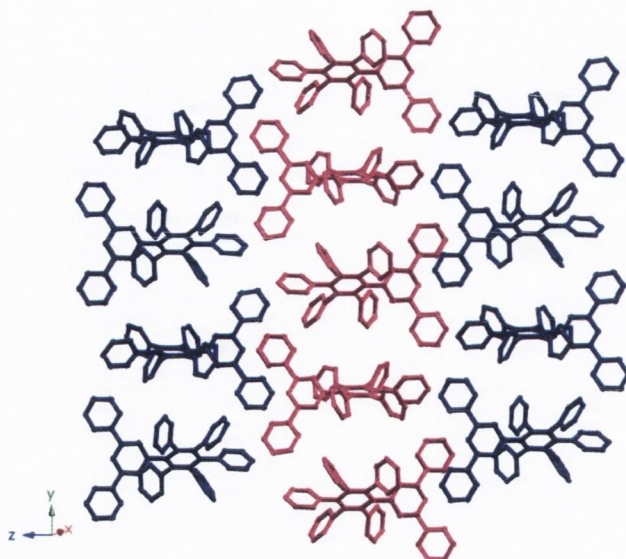
Figure 90: Perspective view of crystal packing in (86).

Table 17 gives all the tilt angles for compounds (86) and (89). For both, the angles for the terpyridine ring containing (N7) and (N13) are similar with respect to the middle ring (N1). The highest tilt angle for the phenyl rings is 82.1° for ring 3 in (89); this ring is situated *ortho* to the terpy-end.

Compound	Rings numbering							
	(N7)	(N13)	(C19)	1	2	3	4	5
	With respect to the central pyridine ring (N1)			With respect to the central benzene ring (C19-C24)				
(86)	1.8	17.0	56.8	65.2	70.1	66.5	70.1	64.5
(89)	2.6	13.5	86.9	63.7	66.5	82.1	73.1	73.2

Table 17: Tilt angles for phenyl rings and N-conataining rings in (86) and (89) in (°).

The UV-vis spectra for (86) and (89) in chloroform and acetonitrile (Figure 91) exhibit two characteristic absorption bands (Table 18). The polarity of solvent does not have an influence on the shifts of the absorption bands for (86) and (89) is blue shifted by 27 and 34 nm in acetonitrile respectively. The absorption bands at lower energy for both (86) and (89) did not show any shifts due to the polarity of the solvent.
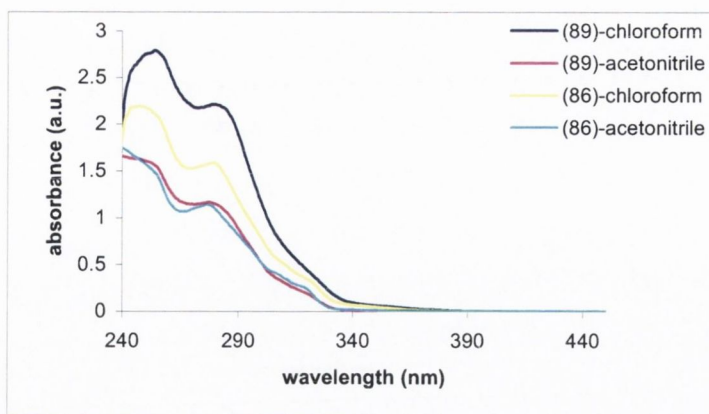
Figure 91: The absorption spectra for (86) and (89).

Compound	λ^{abs}_{max} (nm) in chloroform		λ^{abs}_{max} (nm) in acetonitrile	
(86)	277	245	275	247(br)
(89)	279	250	275	249
terpy	-	-	279	-

Table 18: Absorption data for (86) and (89).

3.2.2. Cyclisation reactions of terpy-polyphenylene ligands

Polyaromatic hydrocarbons, (PAHs) are very important in the area of molecular electronics and optoelectronics. Nitrogen containing PAHs with their extended π^* orbitals are ideal ligands for transition metal complexes. The design of tridentate Ru(II) complexes based on ligands that exhibit long-lived metal to ligand charge transfer are of great interest. The oligophenylene terpy compounds (86) and (89) are potential candidates as precursors for tridentate terpy-type polyaromatic ligands.

Müllen *et al.* synthesised the all-carbon analogue to (86) (Scheme 29).[11] Following the literature, the synthesis of the nitrogen-containing analogue of (72) was attempted. To obtain the planar terpy-arrow like molecule, with three nitrogen atoms and fifty-one aromatic carbons, a few attempts at the oxidative cyclodehydrogenation reaction were carried out of compound (86) (Scheme 34). At first the aluminium trichloride

127

and copper dichloride were used as reactants. $AlCl_3$, $CuCl_2$ and (86) in 20:20:1 ratio respectively were dissolved in degassed CS_2.[26,27] The reaction was carried out in a dry and inert atmosphere. The reaction mixture was stirred for four days at room temperature and the progress of the reaction was checked by TLC every twelve hours. The cyclisation reaction did not occur. After quenching with a diluted solution of ammonium hydroxide and extraction with chloroform, only the starting material was recovered. For the all-carbon analogue the product was obtained after twenty-four hours stirring.[11]

The next attempt at the cyclisation of (86) used iron(III) trichloride as both a Lewis acid and oxidising agent. Different ratios of the reagents and different reaction times were tested. Each time the main product was an iron(II) complex of (86) and some unidentified fractions were obtained as well. The yields for the latter fractions were too low for them to be identified by ^1H NMR spectroscopy and the mass spectrometry did not show any fragmentation.

The third attempted cyclisation reaction of (86) was carried out using molybdenum(V) pentachloride as an oxidising agent. $MoCl_5$ and starting material (86) were dissolved in dichloromethane and the reaction mixture was stirred at room temperature for 3 days under argon. In the literature example only 24 hours were required to obtain the corresponding product.[11] In the case of (86) even a longer reaction time did not help to obtain the cyclised product.
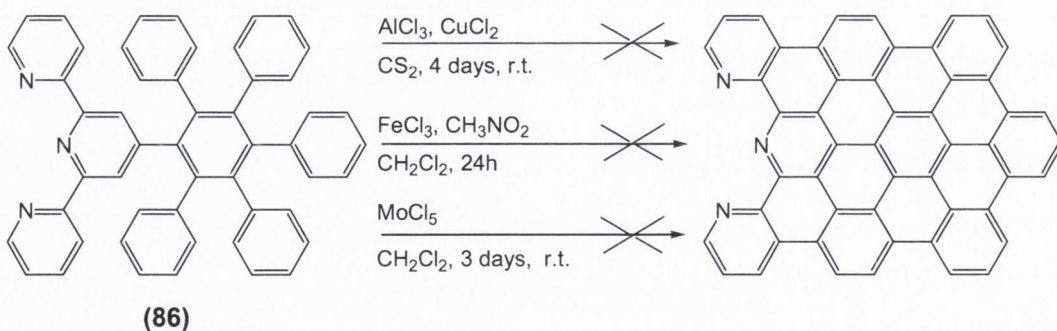
Scheme 34: The oxidative dehydrogenation of (86).

The same conditions for the cyclisation reaction were examined for precursor (89); the *t*-butyl analogue of (86). The oxidative dehydrogenation of (89) with $AlCl_3/CuCl_2$ as oxidative reagents did not result in cyclisation. The same unsatisfactory results

were obtained with MoCl$_5$ as the reagent. Different ratios and reaction times were tested, but compound (89) did not cyclise and only the starting material was recovered.

For precursor (89), iron(III) trichloride proved a helpful oxidising agent (Scheme 35). One equivalent of starting material (89) was dissolved in degassed dichloromethane. A solution of 20 equivalents of FeCl$_3$ in nitromethane was added dropwise. To help remove the HCl evolved during the reaction, a stream of argon was bubbled through the reaction mixture. After 2 hours of bubbling and stirring HCl evolution was observed. The bubbling was carried out for a further two hours, and stopped after no further HCl evolution was noticed. The mixture was left stirring at room temperature and in an argon atmosphere for 24 hours. The progress of the reaction was monitored by TLC. The reaction mixture was quenched with methanol, washed with water and extracted with chloroform. The silica column chromatography with chloroform / methanol/NH$_{3aq}$ (3:1:0.4) as eluent yielded (90) as a yellow solid in 34% yield. The partially cyclised compound (90) was characterised by ^{1}H NMR spectroscopy and mass spectrometry. The peaks were assigned using H,H COSY, C,H COSY and nOe experiments.
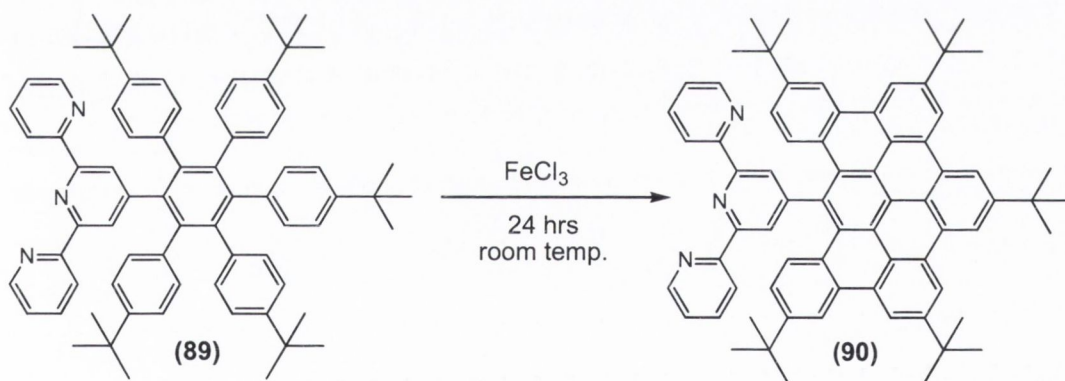
Scheme 35: Oxidative cyclisation reaction of compound (89).

The ^{1}H NMR spectrum of (90) in CDCl$_3$ consists of nine signals in the aromatic and two in the aliphatic region. The two singlets at δ 1.81 and 1.37 are assigned to the five *t*-butyl groups and they integrate for twenty-seven and eighteen hydrogen atoms, respectively. Figure 92 shows the aromatic region of the ^{1}H NMR spectrum of (90).
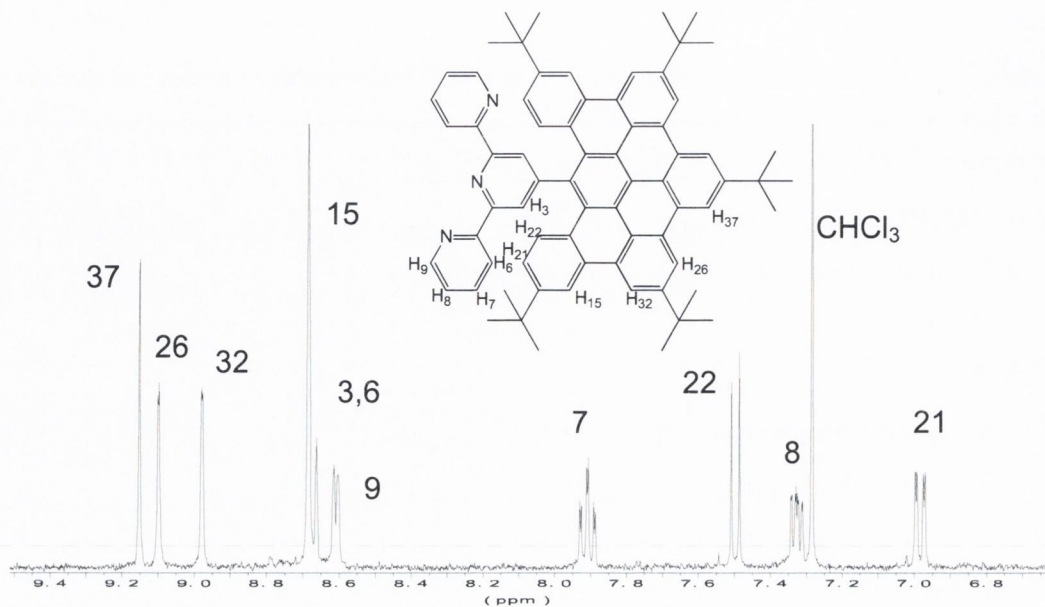
Figure 92: The aromatic region of ^1H NMR spectrum of (90) in $CDCl_3$, 400 MHz, 25°C, with atom labelling.

For the terpy-type compounds the most downfield signal is generally the one for H9, due to the deshielding effect of the nitrogen atom. For (90) it is different: the most downfield signals are four singlets related to protons on the cyclised part of the compound. They appear at δ 9.15, 9.09, 8.98, 8.68 and they are assigned to H37, H26, H32, and H15 respectively; each singlet integrates for two hydrogen atoms, however two more signals are overlapping together with singlet H15 at δ 8.68. These signals correspond to H3 (singlet) and H6 (doublet) and with H15 they integrate for six hydrogen atoms in total. The doublet at δ 8.61 integrates for two protons and is assigned to H9. The signal at δ 7.91 is a doublet of doublets integrating for two protons and is assigned to H7. The last signal from the pyridine ring relates to H8 and appears as a doublet of doublets at δ 7.32. Two doublets at δ 7.50 and δ 6.99 are related to H22 and H21 and are situated on the uncyclised phenyl ring; each signal integrates for two hydrogen atoms each.

The UV-vis absorption spectra of ligand (90) in a variety of solvents are shown in Figure 93. The spectra in methanol and acetonitrile possess the same shape and show five characteristic absorption. There are three bands in the visible region at λ_{max} 346

130

nm, 372 nm and 440 nm, which were not observed in the absorption spectra for the uncyclised compound (**89**). All wavelengths for the absorption are given in Table 19.
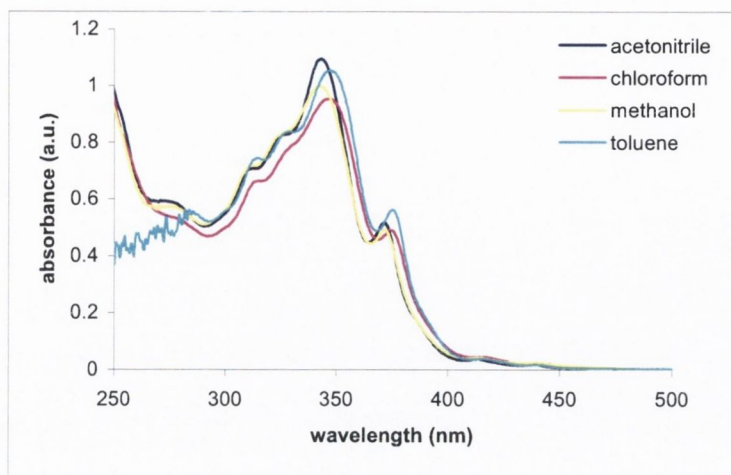
*Figure 93: Absorption spectra of (**90**) in the variety of solvents conc. 8.0*10^{-9}M.*

Figure 94 shows the emission spectra of (**90**) in acetonitrile, toluene, and chloroform at room temperature. The spectra show two emission bands. The band at higher energy is the most intense one and appears at λ_{max} 445 nm in acetonitrile and 448 nm in toluene and chloroform. The second emission band appears at λ_{max} 472 nm in acetonitrile and 475 nm in chloroform and toluene. The most intense emission is observed in acetonitrile even if the concentration (4.0*10^{-9}M) of the solution is half that of the toluene and chloroform solution (8.0*10^{-9}M). No emission was observed in methanol.
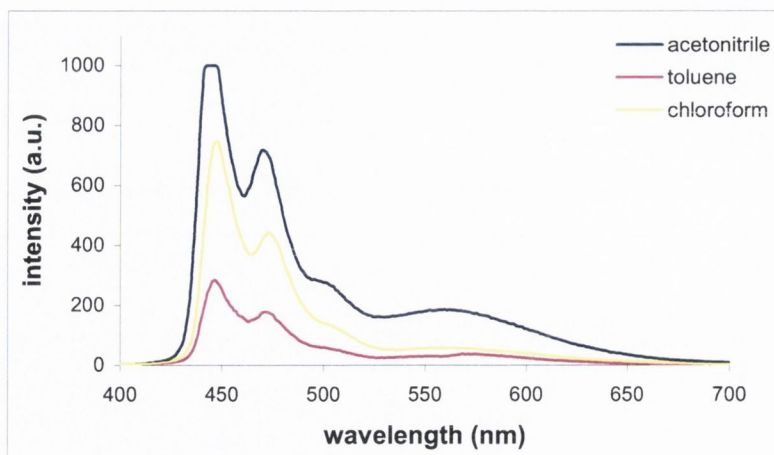
Figure 94: Emission spectra of (90) in a variety of solvents at room temp. conc.
8.0*10⁻⁹M.

Solvent	λ^{abs}_{max} (nm) of (90)					λ^{em}_{max} (nm) of (90)	
acetonitrile	439 br.	372	343	323	309	445	472
chloroform	441 br	375	347	326	310	448	475
methanol	440 br	372	346	326(br)	310(br)	-	-
toluene	440 br	375	347	311	-	448	475

Table 19: Photophysical data for (90).

Compound (90) possesses three nitrogen atoms and each one can act as a proton acceptor. The effect of protonation of the N atoms was studied (Figure 95). The protonation with CF_3SO_3H acid was carried out for (90) in an acetonitrile solution and monitored by absorption spectroscopy. To start with, up to three molar equivalents of acid (one for each N) in acetonitrile were added but no changes were observed in the absorption spectrum. Then the concentration of acid was increased by using 0.01M solution and adding gradually from 0 to 90 μl. The brown curve shows changes after addition of one drop of concentrated acid (99%) (Figure 95). Further addition of acid did not cause any modification of the spectra. 10 μl of acid (0.01M) gives 4000 equivalents for one equivalent of ligand. The addition of acid caused changes in the absorption spectrum, which means that the protonation has an electronic effect on the

132

π electron density. Three isobestic points were found at λ_{max} 281 nm, 340 nm and 366 nm. The disappearance of the absorption band at λ_{max} 372 nm suggests that this band was related to the n→π* transition in the ligand. The addition of acid moves the most intense absorption band to higher energy and further increases its intensity.
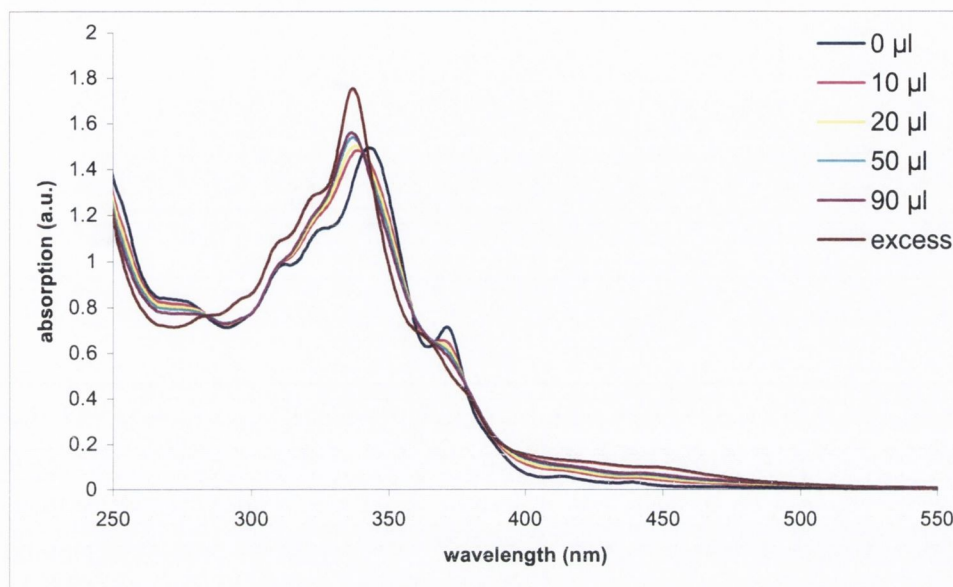
Figure 95: Absorption spectra of (90) in acetonitrile (8*10^{-9} M) on addition of 0.01M CF$_3$SO$_3$H acid in acetonitrile solution.

Figure 96 shows the emission spectra of an acetonitrile solution of (90) with the addition of 0.01M CF$_3$SO$_3$H. The gradual addition of acid decreases the intensity of the emission bands. The brown line shows that the addition of very concentrated acid quenches the emission completely.
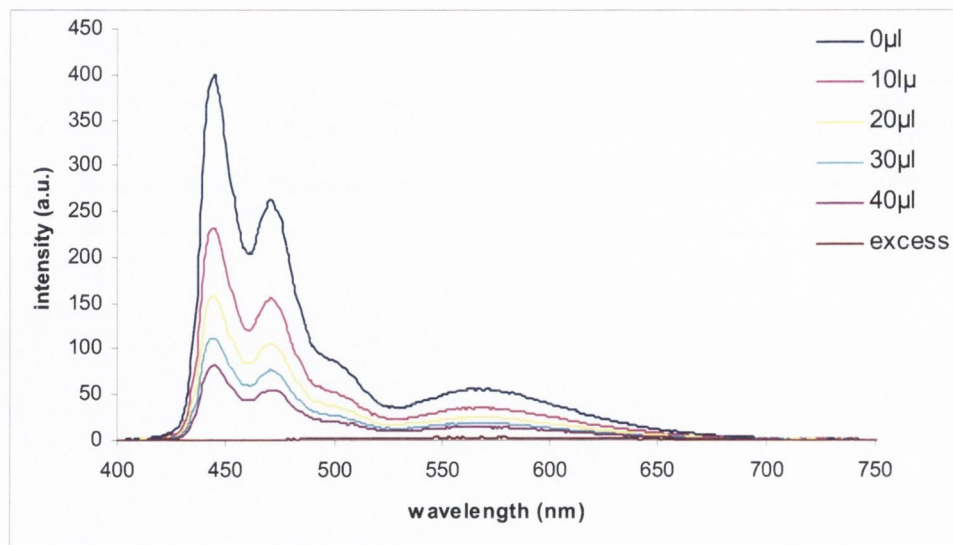
*Figure 96: Emission spectra of (**90**) in acetonitrile (8*10^{-9} M) on addition of 0.01M CF$_3$SO$_3$H acid.*

The absorption spectra of (**90**) after protonation show different features than for related compounds in the literature. Figure 97 shows the absorption and emission spectra of An-tpy (4'-(9-anthryl)-2,2':6',2"-terpyridine) (λ^{em}_{max} 422 nm) and of its protonated forms.[24] The addition of up to 1 equivalent of acid resulted in isobestic points at 309, 362, 372, 381 and 393 nm. For the addition of 1 to 2 equivalents the spectra shows isobestic points at 279, 340 and 402 nm. More than 2 equivalents of acid do not cause any additional spectral changes. According to the literature this behaviour shows that two species are formed; monoprotonated An-tpyH$^+$ and diprotonated An-tpyH$_2$$^{2+}$ (λ^{em}_{max} 532 nm).

134
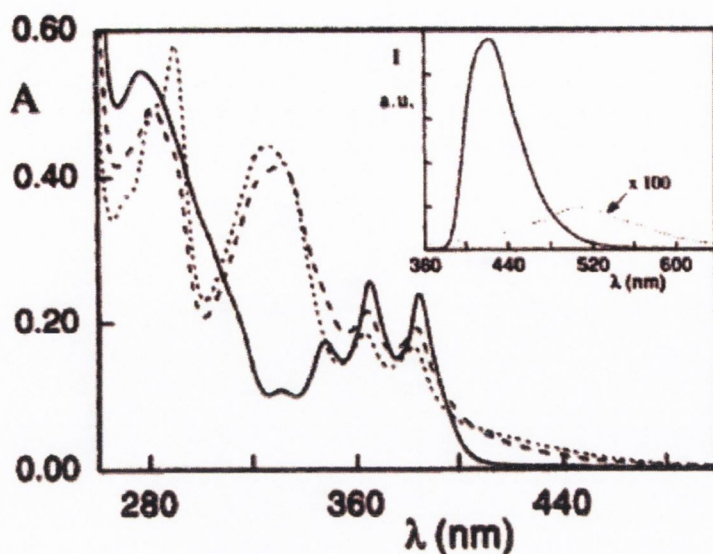
Figure 97: Absorption and emission (inset) spectra of An-terpy (full line), An-tpy-H$^+$ (dashed line) and An-terpy-2H$^+$, in acetonitrile, at room temperature. [24]

3.2.3. Ruthenium complexes of terpy-polyphenylene ligands

3.2.3.1. Synthesis and characterisation of [Ru(86)$_2$](PF$_6$)$_2$

Two equivalents of ligand (**86**) were dissolved in a 1:1 mixture of ethanol and chloroform, and argon was bubbled through the mixture for 30 min. To this solution one equivalent of ruthenium(III) trichloride was added together with three drops of N-ethylmorpholine (Scheme 36). The reaction mixture was refluxed for six hours and the colour changed from brown to orange. After cooling down a saturated solution of KPF$_6$ was added to obtain a red precipitate. Column chromatography with acetonitrile/KNO$_3$/H$_2$O (10:0.5:1.5) as the solvent system allowed the isolation of the homoleptic Ru(II) complex (**91**) in 30% yield.
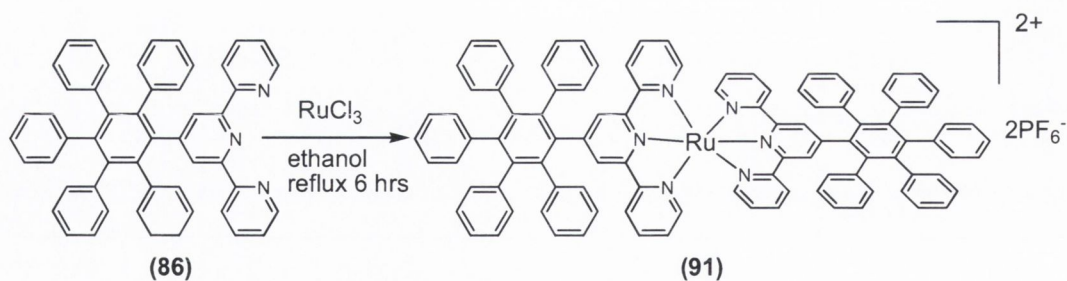
*Scheme 36: The synthesis of [Ru(**86**)₂](PF₆)₂.*

Complex (**91**) was fully characterised by ^{1}H NMR spectroscopy and mass spectrometry. The peaks were assigned using H,H COSY, C,H COSY and nOe experiments. The ^{1}H NMR spectrum of a CD_3CN solution of (**91**) is shown in Figure 98. In general the signals for complex (**91**) are in the range δ 8.13-6.60 and shifted upfield compared to the free ligand (**86**) (δ 8.63-6.76) in acetonitrile. The most downfield signal at δ 8.13 is a singlet assigned to H3, integrating for two hydrogen atoms and shifted downfield compared to H3 (δ 8.09) for the free ligand. The doublet H6 at δ 8.07 shows a large upfield shift (Δδ 0.37) compared to the free ligand and integrates for two protons. The signal at δ 8.83 integrates for two protons and is assigned to H7. The doublet at δ 7.25, triplet at δ 6.90 and the multilplet at δ 7.09-6.96 integrate for 25 hydrogen atoms and are assigned to the five phenyl rings. The doublet of doublets at δ 7.16 assigned to H8 is integrated for two protons and shifted upfield with respect to H8 for free the ligand (δ 7.37). The biggest shift upfield (Δδ 2.03) compared to (**86**) is observed for the doublet assigned to H9. This is due to the shielding effect of the pyridine ring from an other ligand.

The ESI-mass spectra of (**91**) gave a base peak at m/z = 740.24 assigned to $[Ru(\mathbf{86})_2]^{2+}$. The ½ m.u. intervals confirmed the 2+ charge of the molecular ion. Accurate mass analysis was obtained in acetonitrile and gave a peak at 1480.4730 for $(C_{102}H_{70}N_6Ru)^{2+}$, which matched the calculated value of 1480.4705.
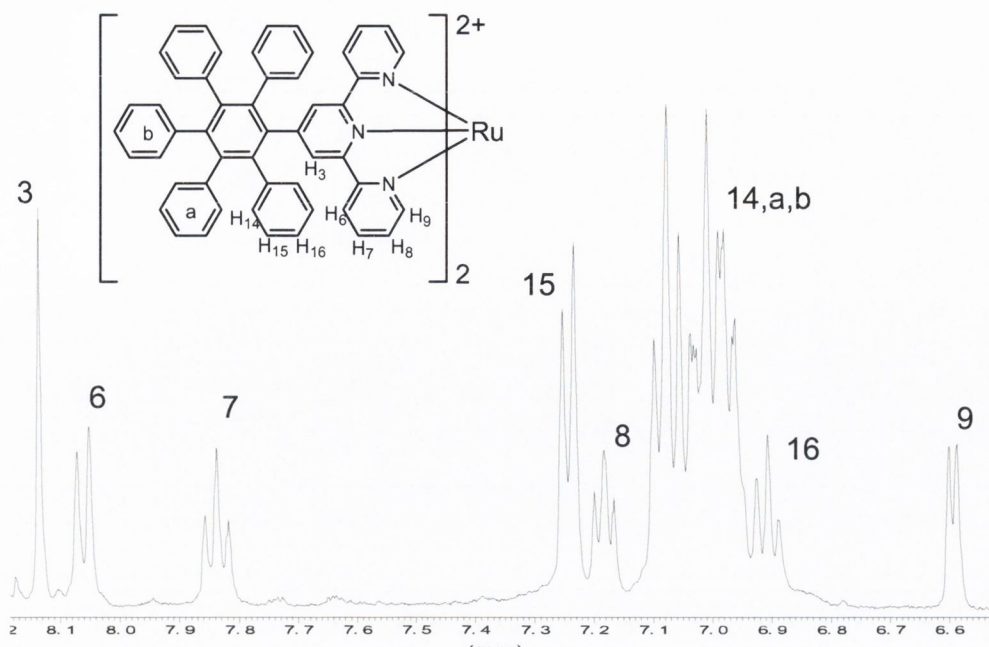
Figure 98: The ^1H NMR spectrum of (91) in CD$_3$CN, 400 MHz, 25°C, inset showing atom labelling.

The absorption spectra of Ru(II) complex (91) and of ligand (86) are shown in Figure 99. There are two spectra for (91), one in acetonitrile and the other in methanol. The spectrum in acetonitrile shows three characteristic bands. In the ultraviolet region two bands appear at λ_{max} 278 nm and 310 nm, both attributed to the π-π^* transitions ligand localised on the ligand. These bands are blue shifted with respect to uncoordinated ligand (86) (λ_{max} 246nm, 277 nm). In the complex, a new broad band is observed in the visible region at λ_{max} 486 nm. This absorption is assigned to the ^{1}MLCT d-π^* transition. The spectrum of (91) in methanol has the same shape as in acetonitrile. The LC and MLCT transitions appear at the same wavelengths irrespective of solvent (Table 20). The ^{1}MLCT transition for [Ru(86)$_2$]$^{2+}$ (λ_{max} 486 nm in acetonitrile) appeared at the lower energy with respect to [Ru(tpy)$_2$]$^{2+}$ (λ_{max} 475 nm in acetonitrile). This red shift of λ_{max} is due to better delocalisation of charge on (86), which possesses six additional phenyl rings compared to terpyridine.

Figure 99: Absorption spectra of (91) and for ligand (86), room temperature, conc. 2.2*10⁻⁵M.
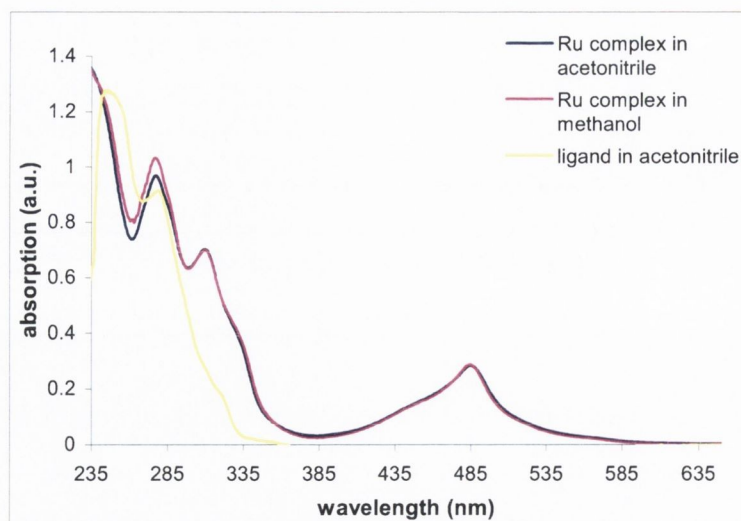
Figure 99: Absorption spectra of (91) and for ligand (86), room temperature, conc. $2.2*10^{-5}M$.

Compound	Absorption peaks λ_{max} (nm)			
ligand (86)-acetonitrile			277	246
complex (91)-acetonitrile	486	310	278	
complex (91)-methanol	485	310	277	
$[Ru(terpy)_2]^{2+}$-acetonitrile	475	307	270	

Table 20: Comparison of λ_{max} of absorption data for complex (91), ligand (86) and $[Ru(terpy)_2]^{2+}$.

Figure 100 shows the absorption spectrum for an ethanol/methanol (4:1) solution of (91) at room temperature and the emission spectrum at 77K. Complex (91) does not emit at room temperature, but when cooled down to 77K shows the emission band with λ^{em}_{max} at 607 nm. This effect is very common for Ru(II) terpy-type complexes.[3,17,18] The emission for (91) was obtained by the excitation of λ^{abs}_{max} 486 nm (ethanol/methanol 4:1) and as expected is shifted to higher energy compared to $[Ru(terpy)_2]^{2+}$ complex. $[Ru(terpy)_2]^{2+}$ shows an emission band with λ^{em}_{max} at 598 nm (at 77 K in alcohol solution).[3]

138
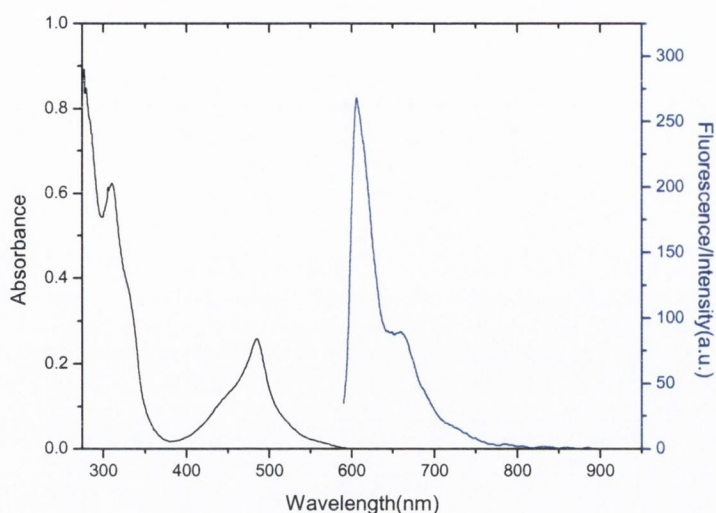
Figure 100: Absorption (at room temp) and emission (at 77K) spectra for
[Ru(86)₂](PF₆)₂ in ethano/methanol (4:1).

3.2.3.2. Synthesis and characterisation of [Ru(terpy)(89)](PF₆)₂

The first step to obtain the heteroleptic ruthenium(II) complex [Ru(terpy)(89)](PF₆)₂ (92) was the synthesis of the precursor Ru(terpy)Cl₃.[20] An equimolar mixture of terpy and RuCl₃ in ethanol was refluxed for 4 hrs. The brown insoluble solid of Ru(terpy)Cl₃ was filtered off and washed with a few portions of ethanol. Ru(terpy)Cl₃ was used as a precursor for the next step without further purification. Scheme 37 shows the synthesis of (92). An ethylene glycol solution of ligand (89) was degassed using bubbling argon. After degassing for 20 minutes an equimolar amount of Ru(terpy)Cl₃ and a few drops of N-ethyl morpholine were added. The reaction mixture was heated for 9 hrs at 92°C, then cooled down and treated with a saturated solution of KPF₆ to give a dark orange precipitate. Purification by preparative silica plates with CH₃CN/KNO₃/H₂O (10:0.5:1.5) as the solvent system allowed the isolation of (92) in 30% yield. Complex (92) was characterised by ^{1}H, ^{13}C NMR spectroscopy and mass spectrometry.

139
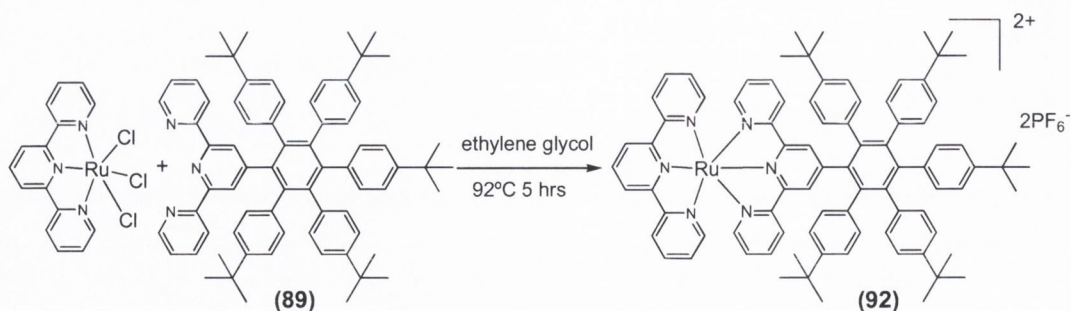
Scheme 37: The synthesis of [Ru(terpy)(89)](PF$_6$)$_2$ (92).

Complex (92) potentially possesses C$_2$ symmetry in solution, which simplifies the spectroscopic analysis. The aromatic region for the ^{1}H NMR spectrum of (92) in acetonitrile is shown in Figure 101. The spectrum shows fifteen signals: six of them belong to the tpy ligand and nine to (89). The first most downfield signal belongs to the terpy ligand. The most downfield signal, integrated for two hydrogen atoms is a doublet of doublets assigned to proton H3' at δ 8.74. The doublet of doublets at δ 8.50, triplet at δ 8.41 and triplet of doublets at δ 7.96 are assigned to H6', H4', and H7', respectively. Each signal integrates for two hydrogen atoms. The last two signals for the terpy protons appear at δ 7.34 and δ 7.04 and they are assigned to H8' and H9', respectively. Five signals, which are related to the ten protons on pyridyl rings for ligand (89), appear at δ 7.92, δ 7.84, δ 7.77, δ 7.19 and δ 7.07, and are assigned to H3, H6, H7, H8, and H9, respectively. The signals for the five phenyl rings are designated by a,b,c and they integrate for twenty five protons. The signal, which shows the greatest upfield shift when compared to the free ligand is H9. This is due to the shielding effect of the pyridyl ring of the terpy ligand. The shift was also observed for H9' in the terpy ligand. In the aliphatic region at δ 1.16 and δ 0.8 are two singlets assigned to *t*-butyl groups, and they both integrate for forty-five hydrogen atoms each.

140
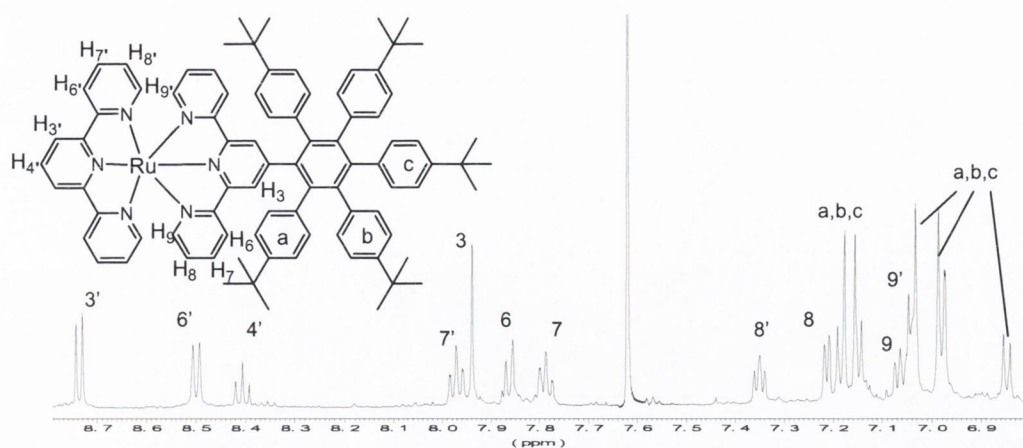
Figure 101: The aromatic region of ^1H NMR spectrum of (92) in CD_3CN, 600MHz, 25°C.

The ESI-mass spectra of (92) gave a base peak at $m/z= 651.8$ assigned to $[Ru(terpy)(89)]^{2+}$. The ½ m.u. intervals confirmed the 2+ charge of the molecular ion. Accurate mass analysis in acetonitrile gave a peak at 1304.5970 for $(C_{86}H_{86}N_6Ru)^{2+}$, in good agreement with the calculated value 1304.5957.

The absorption spectra for (92) were run in three different solvent: acetonitrile, chloroform and methanol (Figure 102). In all solvents the spectra show four characteristic bands. The three bands in the 220-370 nm region are attributed to π-π^* transitions localised on terpy ligands and (89) (for details see Table 21). The lowest energy band at λ_{max} 482 nm is a d-π^* transition, due to metal to ligand charge transfer. The MLCT band for (92) as expected slightly shifts to lower energy compared to homoleptic complex (91) (λ_{max} 486 nm). The MLCT band does not show any dependence on the polarity of the solvent.
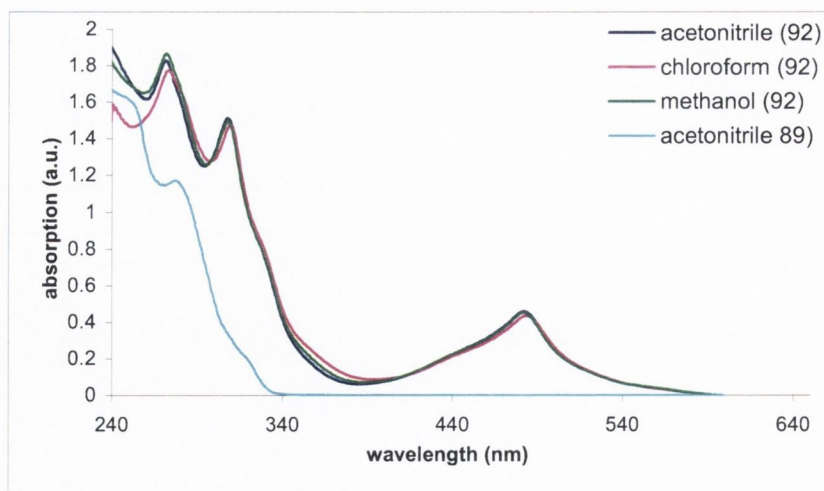
Figure 102: Absorption spectra of (92) in variety of solvents and spectrum for ligand (89) in acetonitrile.

Compound	λ_{max} absorption		
ligand (89)-acetonitrile		274	250
complex (92)-acetonitrile	482	308	271
complex (92)-chloroform	484	310	273
complex (92)-methanol	482	308	272

Table 21: λ_{max} absorption data for (92) in comparison with (89).

Figure 103 shows the absorption spectra of (92) in an ethanol/methanol (4:1) solution at room temperature, together with the emission spectra at 77K. The excitation at the 482 nm absorption band resulted in an emission band with λ_{max} at 610 nm. Both complex [Ru(terpy)(89)](PF$_6$)$_2$ and (91) do not emit at room temperature.

142
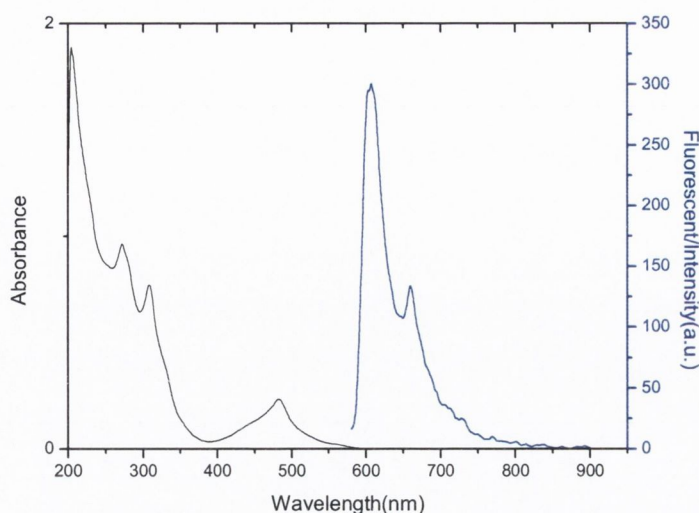
*Figure 103: Absorption (at room temp) and emission (at 77K) spectra for [Ru(terpy)(**89**)](PF₆)₂ in ethanol/methanol (4:1).*

3.2.3.3. Synthesis and characterisation of [Ru(terpy)(**90**)](PF₆)₂

The synthesis of [Ru(terpy)(**90**)](PF₆)₂ (**93**) was based on the similar complexation method as for complex (**92**). Scheme 38 shows the synthesis of (**93**). The solution of ligand (**90**) in ethylene glycol was degassed by bubbling argon through for it 30 min. Ru(terpy)Cl₃ was added and bubbling was continued for an additional 20 min. To this solution a few drops of N-ethylmorpholine were added and the reaction mixture was heated at 95°C for 7 hrs. Then the reaction mixture was cooled down and filtered. The addition of a saturated solution of KPF₆ resulted in a dark orange precipitate. Column chromatography with CH₃CN/KNO₃/H₂O (10:0.5:1.5) as the solvents system allowed isolation of (**93**) in 45% yield. Complex (**93**) was characterised by ¹H, ¹³C NMR spectroscopy and mass spectrometry.
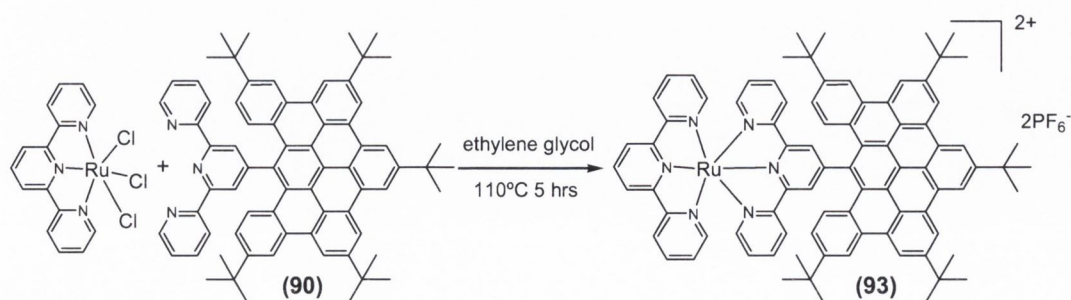
*Scheme 38: Synthesis of [Ru(terpy)(**90**)](PF₆)₂ (**93**).*

Complex (**93**) shows C_2 symmetry, which simplifies the spectroscopic analysis. The peaks were assigned using H,H COSY, C,H COSY and nOe experiments. Figure 104 shows ^1H NMR spectra of (**93**) in deuterated acetonitrile. The spectrum exhibits the expected seventeen resonances for the symmetrical (**93**): six from 2,2':6',2"-terpyridine ligand and eleven from ligand (**90**). Due to the C_2 symmetry, all the signals should integrate for two protons, the exceptions were the signal H4' which is on the axis of symmetry and integrates for one proton and signal δ 7.9 which integrates for four due to the overlapping of two peaks. The lowest field signal is 37 (δ 9.36) followed by 26 (δ 9.32) and 32 (δ 9.20), corresponding to protons H37, H26 and H32. These protons lie on the cyclised part of the ligand (**90**) (rings a,b). The same signal arrangement was observed for free ligand (**90**). The three signals that belong to partially cyclised ring c are assigned to H15, H21 and H22; they appear as a singlet (δ 8.93) and two doublets (δ 7.84, 7.28), respectively. The singlet at δ 9.09 is assigned to H3. The last four signals which belong to coordinated (**90**) are characteristic signals for pyridine rings in terpy-type ligands. They are two triplets of doublets assigned to H7 (δ 7.86) and H8 (δ 7.21), and two doublets assigned to H6 (δ 8.19) and H9 (δ 7.47). The biggest upfield shift in (**90**) on coordination compared to free ligand is observed for H9 and this is due to the shielding effect of the adjacent terpyridine ligand. The doublet at δ 8.88 assigned to H3', which belongs to terpyridine ligand, integrates for two hydrogen atoms and is shifted downfield compared to H3' (δ 8.74) for [Ru(terpy)$_2$]$^{2+}$. The doublet of doublets at δ 8.52 corresponds to H4'. The last four signals exhibit the typical arrangement for terpy-type ligands. These signals are two doublets of doublets assigned to H7' (δ 8.11) and H8' (δ 7.51), and to doublets H6' (δ 8.65) and H9' (δ 7.78). As expected due to the shielding effect of the coordinated (**90**) the biggest upfield shift compared to the free terpyridine is observed for signal H9'. In general all the signals for coordinated terpy in (**93**) are shifted downfield compared to the homoleptic complex [Ru(terpy)$_2$]$^{2+}$.

144
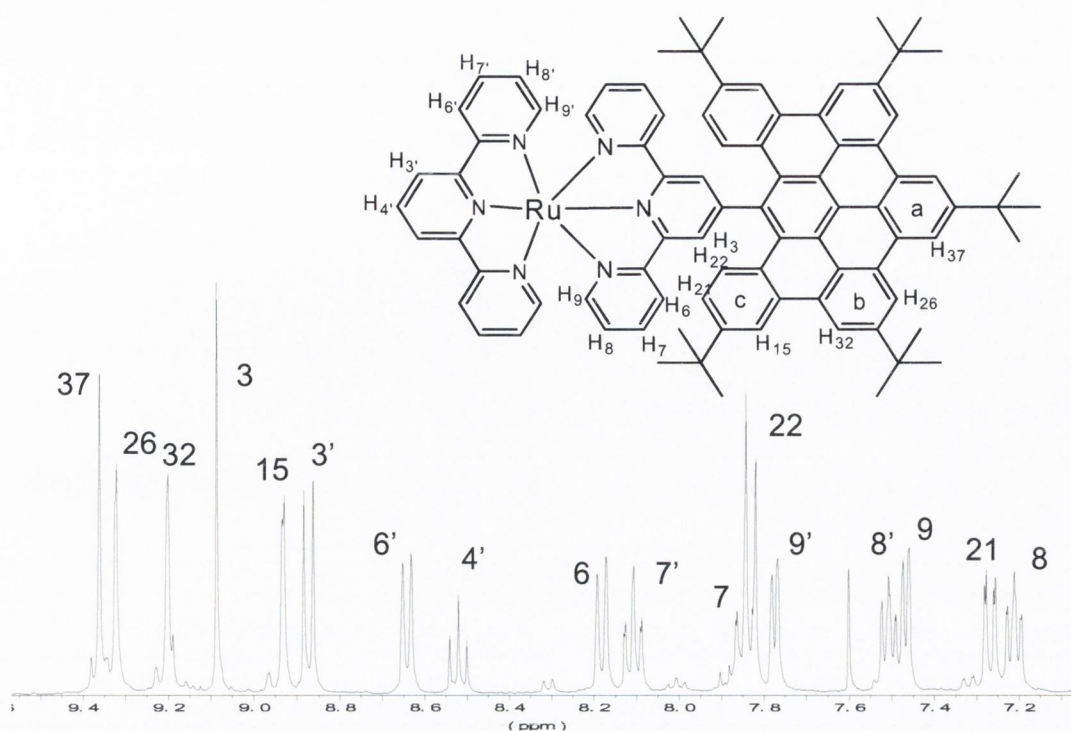
*Figure 104: The aromatic region of ^1H NMR spectrum of (**93**) in CD₃CN, 600MHz, 25°C, inset atom labelling.*

Electrospray mass spectrometry for (**93**) gave a base peak at $m/z = 648.26$ assigned to $[Ru(terpy)(\mathbf{90})]^{2+}$. The ½ m.u. intervals confirmed the 2+ charge of the molecular ion. The mass analysis was obtained in acetonitrile and gave a peak at 1297.55 for $(C_{86}H_{78}N_6Ru)^{2+}$, which matched the calculated value of 1297.71.

Figure 105 shows the UV-vis spectra for $[Ru(terpy)(\mathbf{90})](PF_6)_2$ (**93**) and for ligand (**90**) in acetonitrile. The spectrum for (**93**) exhibits five characteristic bands. There are three bands in the UV range with λ_{max} at 226, 271 and 309 nm, all corresponding to LC $\pi \rightarrow \pi^*$ transitions. The absorption bands at λ_{max} 271 and 309 nm are new compared to the free ligand. In the visible are two bands the first one at λ_{max} 338 nm, which is observed for free ligand as well; the second one is a new band more red-shifted at λ_{max} 489 nm. This transition is a metal to ligand charge transfer between the ruthenium and ligand (**90**). There is a very weak shoulder at 450 nm, which can be attributed to the MLCT from tpy ligand, (for $[Ru(tpy)_2]^{2+}$ MLCT transition appears at λ_{max} 475 nm).

145
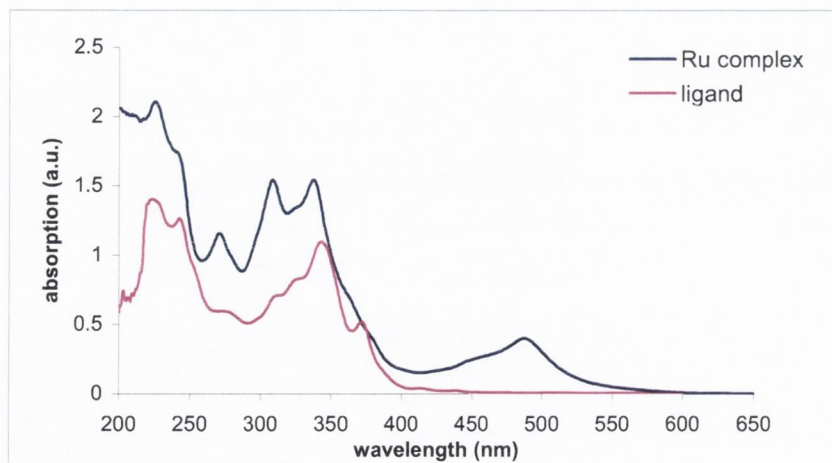
Figure 105: The absorption spectra for complex (93) conc. $9.3*10^{-5}M$ and ligand (90) in acetonitrile, room temp.

Compound	Absorption peaks λ_{max} (nm)				
ligand (90)-acetonitrile	-	438	414	243	223
complex (93)-acetonitrile	489	338	309	271	226
complex (93)-ethanol/methanol (4:1)	489	335	306	271	-
[Ru(terpy)$_2$]$^{2+}$-acetonitrile	475	-	307	270	-

Table 22: Absorption data for (93) in various solvents, ligand (90) and [Ru(terpy)$_2$](PF$_6$)$_2$ in acetonitrile.

[Ru(terpy)(90)](PF$_6$)$_2$ (93) complex does not emit at room temperature, but does at 77K. Figure 106 shows the absorption spectrum for (93) in an alcohol solution at room temperature and the emission spectrum at 77K. The spectrum in ethanol/methanol (4:1) shows four characteristic bands. The bands in the range 200-350 nm correspond to the LC transitions, while the peak at the lowest energy is assigned to the MLCT with λ_{max} 489 nm. Due to the excitation at 489 nm at 77K complex, (93) emits in the range 600-700 nm with λ_{max} 622 nm and a lifetime of 12 μs.

146
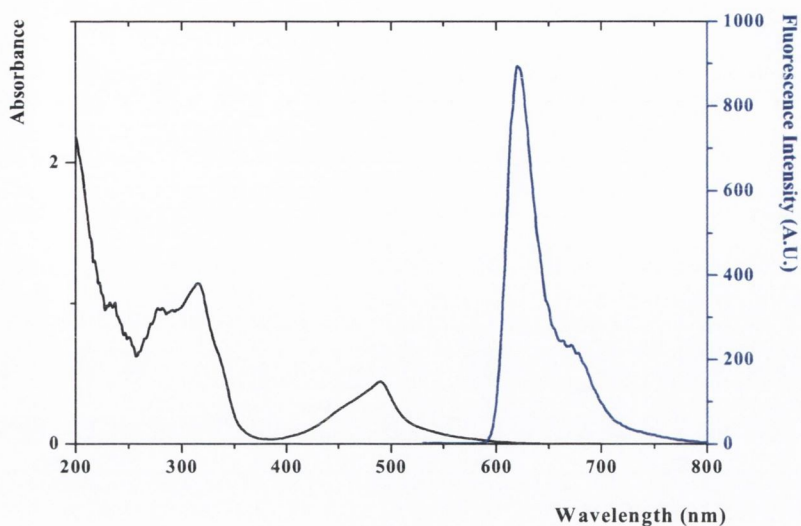
*Figure 106: Absorption spectrum (at room temp) and emission spectrum (at 77K) for [Ru(terpy)(**90**)](PF$_6$)$_2$ in ethanol / methanol (4:1).*

All presented Ru(II) complexes (**91**), (**92**) and (**93**) do not emit in room temperature. Similar behaviour was observed for others Ru(II) terpy-type complexes, such as [Ru(tpy)(pyrenyl)]$^{2+}$ ($\lambda_{max}{}^{em}$ 626 nm, at 77K) (pyrenyl- 4'-(1-pyrenyl)-2,2':6',2"-terpyridine or [Ru(tpy)(naphthyl)]$^{2+}$ ($\lambda_{max}{}^{em}$ 625 nm, at 77K) (naphthyl- 4'-(2-naphthyl)-2,2':6',2"-terpyridine.[28] This effect is attributed to the equilibration of the ^{3}MLCT state with the high-spin d-d (MC) state. The ideal octahedral geometry in Ru(II) complexes of rigid tridentate ligands is distorted which cause the weaker ligand field strength. This effectively reduces the energy of the d-d metal centred state. Then ^{3}MC state lies close to the potentially luminescent ^{3}MLCT state and thermally activated population of ^{3}MC state promotes fast radiationless decay to the ground state.

In the series of synthesised complexes (**93**) has the lowest energy absorption MLCT band with λ_{max} at 489 nm, due to the higher charge delocalisation on (**90**) compared to (**86**) or (**89**). The MLCT band for heteroleptic (**92**) with λ_{max} at 482 nm is blue shifted with respect to homoleptic complex (**91**) (MLCT, 486 nm). The absorption bands for (**91**), (**92**) and (**93**) shift in accordance with the level of the ligands conjugation in complexes. The $\lambda^{em}{}_{max}$ for homoleptic (**91**) at 607 nm is slightly blue shifted compared to (**92**) (610 nm), the literature shows both blue and red shifts with respect

147

to analogous complexes.[17,23] The lowest energy emission band as expected is for complex (93) with λ^{em}_{max} at 622 nm.

Figure 107 shows the energy-minimised structure of (93), which was calculated by using Density Functional Theory (B3LYP-functional, 6-316* basis set). The structure confirms the expected pseudo-octahedral geometry around the metal centre. The ten cyclised benzene rings of ligand (90) create a rigid platform with A and B rings slightly bent out of the plane (Figure 107a). The cyclised part of (90) does not lie in the same plane as the terpy ligand, but is bent by 121° (Figure 107b). The planar polyaromatic sheet on ligand (90) possesses great potential to create π→π stacking interactions between molecules of the complex.
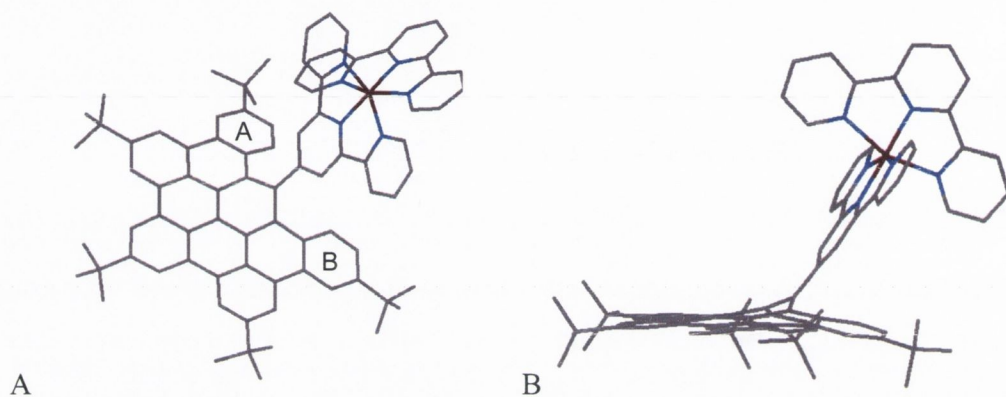
Figure 107: Stick representation of the energy-minimised structure of (93).

3.3. Conclusion.

In Chapter 3, the synthesis of two novel polyphenylene substituted terpyridine-type ligands has been described. Ligands (86) and (89) were synthesised in good yields and fully characterised. (89) is an analogue of (86) substituted with five *t*-butyl groups, to increase its solubility.

The oligophenylene all-carbon compounds undergo oxidative cyclodehydrogenation to create planar, all aromatic sheets, called PAHs.[8,9,10] The arrangement of the phenyl rings in ligands (86) and (89) makes them precursors for planar N-containing hydrocarbons. The idea was to obtain fully cyclised aromatic terpy-type ligands analogous to bidentate polyaromatic ligand N-HSB (Chapter 1). The cyclisation reaction of (86) failed despite the use of a variety of oxidising agents in different

ratios and reaction durations. However, the *t*-butyl substituted (**89**) gave a partially cyclised product (**93**) with iron(III) trichloride as an oxidative agent. (**90**) is the first terpy-type ligand with such a large polyaromatic antenna substituted in the 4'-position.

Compounds (**86**), (**89**) and (**90**) are very attractive as ligands for transition metal complexes. Three Ru(II) complexes (**91**), (**92**), and (**93**) have been synthesised and their photophysical properties studied. ^{3}MLCT bands appeared at λ_{max} 482 nm, 486 nm and 489 nm for (**92**), (**91**) and (**93**) respectively. ^{3}MLCT bands for those complexes move from higher to lower energy with the increased degree of substituted phenyl rings and planarisation in the coordinated ligands.

The ^{3}MLCT band for (**93**) was expected to appear at lower energy, due to the degree of delocalisation density on the planar ten-aromatic rings antenna. However, there was not much electronic communication between Ru(II) terpy and the aromatic platform. According to the literature, this communication could be increased by the introduction of an acetylene spacer. This should improve the photophysical properties of the Ru(II) complexes thus formed.[17,19,20]

3.4. <u>References</u>

[1] . S. Serroni, S. Campagna, R. P. Nascone, G. S. Hanan, G. J. E. Davidson, J. P. Lehn, *Chem. Eur. J.*, **1999**, 5, 3523-3527

[2] E. C. Constable, A. M. W. C. Thompson, J. Cherryman, T. Liddiment, *Inorg. Chim. Acta*, **1995**, 165-171

[3] J. P. Sauvage, J. P. Collin, J. C. Chambron, S. Guillerez, C. Coudret, *Chem. Rev.*, **1994**, 94, 993-1019

[4] S. Ott, M. Borgström, M. Kritikos, R. Lomoth, J. Bergquist, B. Åkermark, L. Hammarström, L. Sun, *Inorg. Chem.*, **2004**, 43, 4683-4692

[5] U. Siemeling, J. Vor der Brüggen, U. Vorfeld, B. Neumann, A. Stammler, H. G. Stammler, A. Brockhinke, R. Plesspw, P. Zanello, F. Laschi, F. de Biani, M. Fontani, S. Steenken, M. Stapper, G. Gurzadyan, *Chem. Eur. J.*, **2003**, 2819-2833

[6] K. T. Potta, D. Konwar, *J. Org. Chem.* **1991**, 56, 4815-4816

[7] A. Harriman, R. Zissel, *Chem. Commun.*, **1996**, 1707-1716

[8] J. Wu, M. D. Watson, N. Tchebotareva, Z. Wang, K. Müllen, *J. Org. Chem.*, **2004**, 69, 8194-8204

[9] C. S. Simpson, J. D. Brand, A. J. Berresheim, L. Przybilla, H. J. Räder, K. Müllen, *Chem. Eur. J.*, **2002**, 8, 1424-1429

[10] D. Wasserfallen, M. Kastler, W. Pisule, W. A. Hofer, Y. Fogel, Z. Wang, K. Müllen, *J. Am. Chem. Soc.*, **2006**, 128, 13334-1339

[11] F. Dötz, J. D. Brand, S. Ito, L. Gherghel, K. Müllen, *J. Am. Chem. Soc.*, **2000**, 7707-7717

[12] P. Herwig, C. W. Kayser, K. Müllen, H. W. Spiess, *Adv. Mater.*, **1996**, 8, 510-513

[13] P. A. Anderson, G. F. Strouse, J. A. Treadway, R. Keene, T. J. Meyer, *Inorg. Chem.*, 33, **1994**, 3863-3864

[14] B. Durham, J. V. Caspar, J. K. Nagle, T. Meyer, *J. Am. Chem. Soc.*, **1982**, 4803-4810,

[15] F. Barigelletti, L. De Cola, V. Balzani, P. Belser, A. von Zalewsky, F. Vögtle, F. Ebmeyer, S. Grammenudi, *J. Am. Chem. Soc.*, **1989**, 111, 4662-4668

[16] S. Campagna, S. Serroni, S. Bodige, F. M. MacDonnell, *Inorg. Chem.*, **1999**, 38, 692-701

[17] E. A. Medlycott, G. S. Hanan, *Chem. Soc. Rev.*, **2005**, 34, 133-142

[18] M. I. J. Polson, E. A. Medlycott, G. S. Hanan, L. Mikelsons, N. J. Taylor, M. Watanabe, Y. Tanaka, F. Loiseau, R. Passalacqua, S. Campagna, *Chem. Eur. J.*, **2004**, 10, 3640-3648

[19] A. C. Benniston, G. M. Chabman, A. Harriman, S. A. Rostron, *Inorg. Chem.*, **2005**, 44, 4029-4036

[20] A. C. Benniston, G. Chapman, A. Harriman, M. Mehrabi, C. A. Sams, *Inorg. Chem.* **2004**, 4227-4233

[21] E. A. Medlycott, G. S. Hanan, *Coord. Chem. Rev.*, **2006**, 1763-1782

[22] J. Wang, G. S. Hanan, F. Loiseau, S. Campagna, *Chem. Commun.*, **2004**, 2068-2069

[23] R. Passalacqua, F. Loiseau, S. Campagna, Y. Fang, G. S. Hanan, *Angew. Chem. Int. Ed.*, **2003**, 42, 1608-1611

[24] G. Albano, V. Balzani, E. C. Constable, M. Maestri, D. R. Smith, *Inorg. Chim. Acta,* **1998**, 225-231

[25] E. C. Constable, M. D. Ward, *J. Chem. Soc. Dalton*, **1990**, 1405-1409

[26] M. Müller, V. S. Iyer, C. Kübel, V. Enkelmann, K. Müllen, *Angew. Chem. Int. Ed. Engl.*, **1997**, 36, 1607-1610

[27] F. Morgenroth, K. Müllen, *Tetrahedron*, **1997**, 15349-15366

[28] H. Y. Ding, X. S. Wang, L. Q. Song, J. R. Chen, J. H. Yu, Chao-Li, B. W. Zhang, *J. of Photochem. and Photobiol. A: Chem.*, **2006**, 286-294

Part 4: Platinum(II), Palladium(II) and Iron(II) complexes.

4.1. Introduction

4.1.1. Palladium(II) and Platinum(II) complexes

Great interest has been focused on the square-planar complexes of Pt(II) and Pd(II) complexes. They receive much attention due to their applications, such as antitumor drugs[1,2] and catalysts for C-H activation.[3] For example, cis-[Pt(Cl$_2$)(NH$_3$)$_2$] is used in chemotherapy.[4,5] Pt(II) complexes are very well suited to interact with DNA by intercalation and their antitumor activity is being investigated.[6,7]

There are many examples of platinum and palladium complexes with terpyridine-type ligands. [Pt(terpy)X]$^+$ (X= Cl, NCS, OME, OH) complexes usually possess planar geometry, which is expected to discourage the distortions that promote radiationless decay. They are likely to have low-lying charge transfer states due to the extended π-systems of the terpy ligands, which gives interesting photophysical properties.

Arena *et al.* have synthesised a series of organometallic platinum polypyridine complexes: [Pt(4'-Ph-terpy)Cl]Cl (**94**), [Pt(4'-Ph-terpy)Me]Cl (**95**) and [Pt(4'-Ph-terpy)Ph]Cl (**96**) (Figure 108).[8] The absorption spectra of these complexes show that the lowest energy band assigned to metal to ligand charge transfer decreases in energy in the order Cl>Ph≈Me. The MLCT bands were found at λ$_{max}$ 410 nm, 426 nm and 430 nm for (**94**), (**95**) and (**96**) respectively. Electron donation into the terpy moiety increases from Cl to Ph and Me groups. The same behaviour was observed for unsubstituted 2,2':6',2''-terpyridine analogues to (**94**), (**95**) and (**96**).
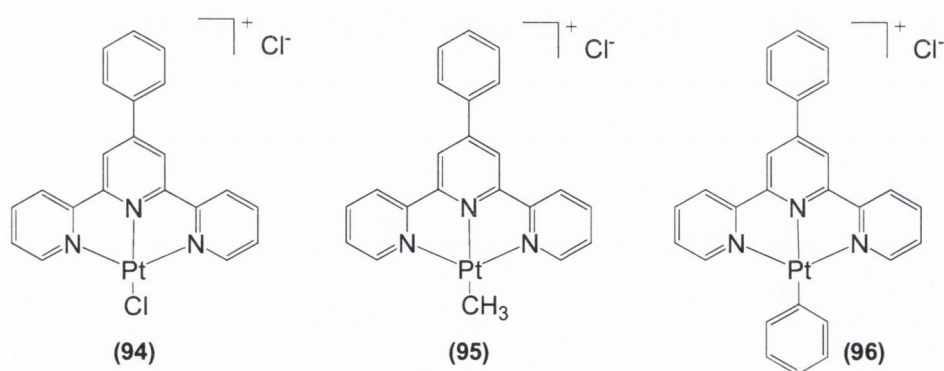
*Figure 108: The structures of [Pt(4'-Ph-terpy)Cl]Cl (**94**), [Pt(4'-Ph-terpy)Me]Cl (**95**) and [Pt(4'-Ph-terpy)Ph]Cl (**96**).[8]*

Pt(II) complexes have a tendency to create dimers in solution. This can occur in two ways: through metal-metal interaction, which results in d^8-d^8 dimers or *via* organic π-π interaction between two molecules of ligand.[9,10] The dimerisation results in a low-energy absorption at 460-550 nm, which is attributed to metal-metal to ligand charge transfer (MMLCT).[11]

In many cases the room temperature luminescence of platinum(II) polypyridine complexes can be quenched due thermal population of the low-lying MC excited state which provides the deactivation *via* molecular distortion. At low temperature the situation is different, the thermally activated quenching process is blocked and emission can be observed.[8]

Luminescence of platinum(II) polypyridine complexes at room temperature has been reported.[12,13] At room temperature the emission varies with the nature of the 4' substituent as well as the solvent. Michalec *et al.* have synthesised a series of platinum(II) complexes with electron donating substituents in 4'-position of the terpy (**97**) and (**98**), which emit at room temperature (Figure 109).[14]
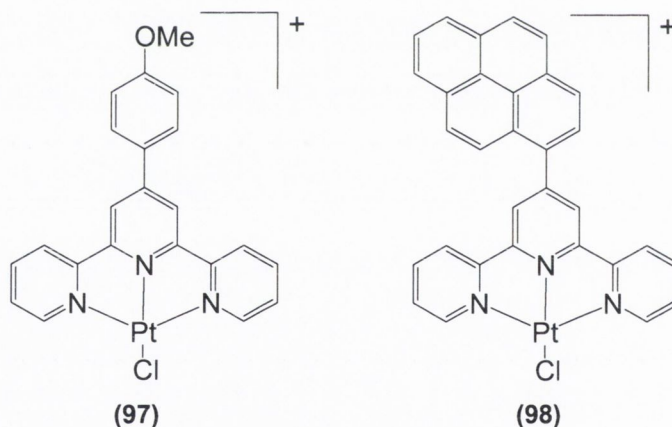
*Figure 109: Structures of complexes [Pt(4'-pMeOPh-terpy)Cl]$^+$ (**97**) and [Pt(4'-Pyre-terpy)Cl]$^+$ (**98**).[14]*

Figure 110 shows the absorption spectra for complexes [Pt(4'-Ph-terpy)Cl]$^+$ (**94**), [Pt(4'-pMeOPh-terpy)Cl]$^+$ (**97**) and [Pt(4'-Pyre-terpy)Cl]$^+$ (**98**) and emission for (**98**) in dichloromethane. The longest wavelength emission, for these complexes, comes from the pyrene substituted complex with λ_{max} 685 nm and a lifetime of 64 μs,

complex (**97**) emits around 560 nm with lifetime 5 μs.[14] (**94**) exhibits an emission in dichloromethane solution at λ_{max} 535 nm with a lifetime 85 ns. The radiative process in a pure intraligand triplet state would be strongly forbidden.[14] However, in these complexes emission is observed due to a combination of ^{3}ILCT and ^{3}MLCT states.
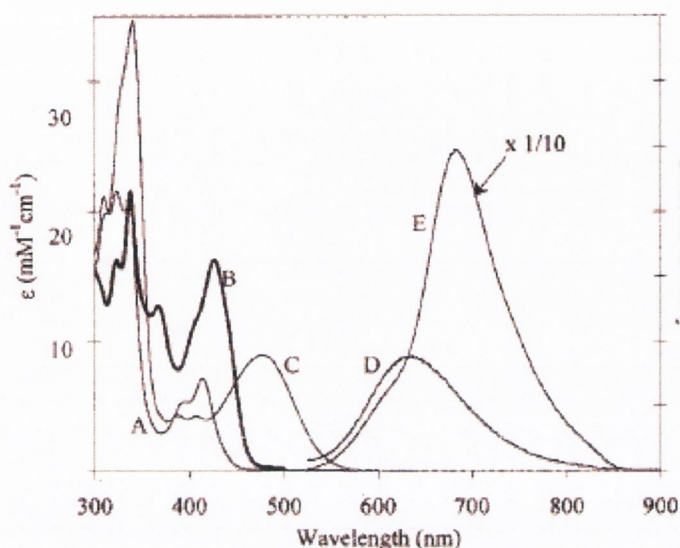
Figure 110: Absorption spectra in dichloromethane at room temperature for [Pt(4'-Ph-terpy)Cl]$^+$ (A), [Pt(4'-pMeOPh-terpy)Cl]$^+$ (B), [Pt(4'-Pyre-terpy)Cl]$^+$ (C) and emission of [Pt(4'-Pyre-terpy)Cl]$^+$ in air (D), under nitrogen (E). [14]

4.1.2. Iron Complexes.

Transition metal complexes of 2,2':6',2"-terpyridine have been explored very extensively because of their electronic, photonic, magnetic and reactive properties.[15] Transition metal ions with d^5, d^6 and d^7 electronic configuration are able to form complexes in either low-spin or high-spin electronic configuration. Iron(II) complexes with the general formula [Fe(terpy)$_2$]X$_2$ have low-spin configuration, irrespective of the counterion X. The introduction of substituents at the 4'-position of the ligand does not effect the spin state of the complex.[16]

There are a lot of examples of iron(II) complexes based on terpy-type ligands with interesting photophysical and electronic properties.[17,18,19] The reactivity of the organic ligand has a great effect on the properties of the complex. Special attention has been

155

drawn to the design of terpy-based ligands because the valuable electronic properties are dependent on the substitution of functional groups in the 4'-position.

The functionalised ligand 4'-(4'''-pyridyl)-2,2':6',2''-terpyridine (pyterpy) was synthesised by Constable *et al.*[20] The reaction of pyterpy with $[Fe(H_2O)_6][BF_4]_2$ gave the homoleptic complex $[Fe(pyterpy)_2][BF_4]_2$ (**99**). The absorption spectrum of this complex in acetonitrile shows a MLCT band at 569 nm together with the ligand based transitions n→π* or π→π* at 245, 276, 284 and 324 nm. Complex (**99**) shows a reversible Fe(II) →Fe(III) oxidation at +0.801V. The comparison of these data with data for $[Fe(terpy)_2]^{2+}$ (MLCT 552 nm and Fe oxidation at +0.77V) shows that the pyterpy ligand is a better π-acceptor then terpy. The lower energy MLCT and more positive oxidation potential of the pyterpy complex suggest that the Fe(II) state is more stabilised. It has been shown that pyterpy can still act as an electrophile after coordination to iron. On addition of acid to a methanolic solution of (**99**), protonation of the free 4'-pyridyl group occurred. The MLCT band of $[Fe(Hpyterpy)_2]^{4+}$ appeared at 594 nm, showing that the protonation of the complex lowered the energy of the π* level of the ligand.

Lopez *et al.* synthesized the novel 4'-(4'''-pyridyl-N-oxide)-2,2':6',2''-terpyridine (pyNoxterpy) ligand. The pyridyl-*N*-oxide substituent possesses unique properties as it can act as an electron acceptor or as an electron donor.[21] The homoleptic iron complex $[Fe(pyNoxterpy)_2](BF_4)_2$ (**100**) in acetonitrile showed a MLCT band at 577 nm (Figure 111), shifted to a lower energy compared with the MLCT for $[Fe(pyterpy)_2][BF_4]_2$ (569 nm). The conjugation in the pyNoxterpy ligand is higher than in pyterpy, and lowers the energy of the π* level of the ligand. The addition of acid to a solution of (**100**) gave protonation of the N-oxide groups. The MLCT band for the protonated complex moved to lower energy and appeared at 589 nm (Figure 111).
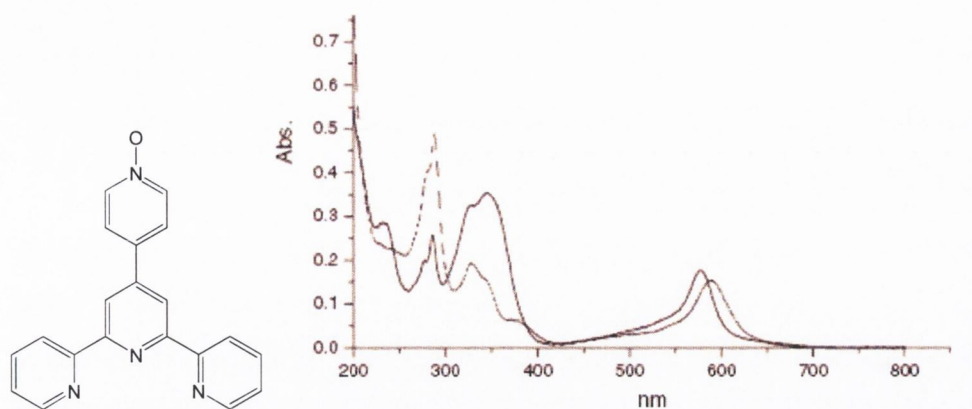
Figure 111: Absorption spectra of [Fe(pyNoxterpy)₂](BF₄)₂ in acetonitrile (solid line) and after addition of concentrated HCl (dashed line), inset shows the structure of pyNoxterpy ligand. [21]

Substitution at the 4'-position of the terpy-type ligands is very popular, however the literature shows few examples of functionalised lateral pyridyl rings. Ligands (**101**) and (**102**) due to the introduction of the steric bulk (as shown Figure 112) can create spin-crossover complexes with Fe(II) metal. The substitution of terpy with phenyl rings at the 6- and (or) 6'-positions reduces the ligand field and makes the high-spin configuration more favourable. The electronic spectra of [Fe(**101**)₂](PF₆)₂ shows both high- and low-spin species, and the purple complex shows the MLCT band around 550 nm, which is very weak compared to the MLCT of [Fe(terpy)₂]²⁺ (548 nm). The homoleptic iron(II) complex of (**102**) [Fe(**102**)₂](PF₆)₂ does not show any absorption at 548 nm and possesses an orange colour arising from the very intense absorption of a ligand π-π* at 330 nm. Once again it has been shown that the attachment of functional groups to C(4') atom of terpy, from the photophysical point of view, gives more attractive ligands for its transition metal complexes.[16]
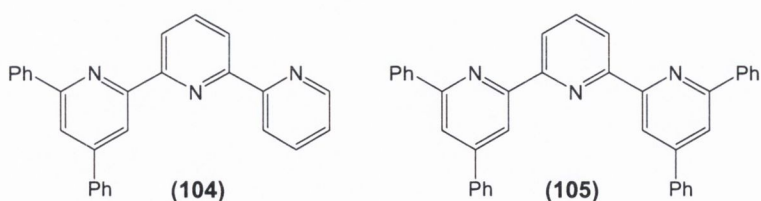
*Figure 112: The structures of ligands (**101**) and (**102**).* [16]

4.2. Results and discussion.

4.2.1. [Pt(89)Cl]Cl-(103)

4.2.1.1. Synthesis

The precursor for complex (**103**), $Pt(DMSO)_2Cl_2$, was prepared in a simple exchange reaction. K_2PtCl_4 was dissolved in water and dimethylsulfoxide was added.[22,23] The mixture was allowed to stand overnight at room temperature. Bright yellow crystals of $Pt(DMSO)_2Cl_2$ were collected by filtration in 84% yield. An equimolar mixture of $Pt(DMSO)_2Cl_2$ and (**89**) was dissolved in chloroform and heated at 55°C for 24 hrs. The deep yellow precipitate of the platinum(II) complex [Pt(**89**)Cl]Cl was recrystallised from dichloromethane and diethyl ether (Scheme 39).
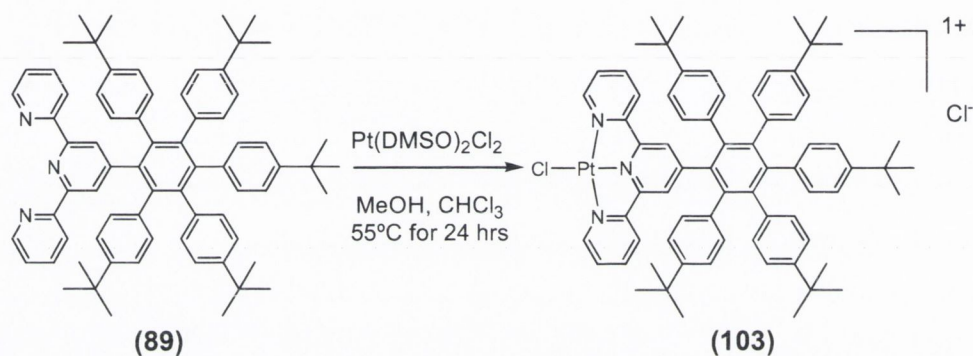
Scheme 39: Synthesis of platinum(II) complex (103).

Complex (**103**) was characterized by ^1H and ^{13}C NMR spectroscopic analysis, and by mass spectrometry. The aromatic region of the ^1H NMR spectrum for (**103**) is shown in Figure 113. As expected the most downfield signal is a doublet assigned to H9 (δ 8.53) shifted upfield with respect to H9 (δ 8.60) for free ligand (**89**). The triplet of doublets at δ 8.49 is related to H7 and integrates for two hydrogen atoms. A doublet of doublets also integrating for two protons is assigned to H6 (δ 7.97) and is shifted upfield compared to H6 (δ 8.11) for the uncoordinated ligand (**89**). The last two signals assigned to H8 and H3, which belong to the terpy part of the complex are overlapping and resonate at δ 7.67. They integrate for four hydrogen atoms. Signals at δ 7.01, 6.98, 6.89 and 6.72 are related to the five phenyl rings and are assigned to rings a, b and c, respectively. These four signals integrate for twenty hydrogen atoms in total. In the aliphatic region of the ^1H NMR spectrum for (**103**) are two singlets at δ 1.12 and δ 0.97, which are related to the five *t*-butyl groups. They integrate for forty-five protons in total.

158
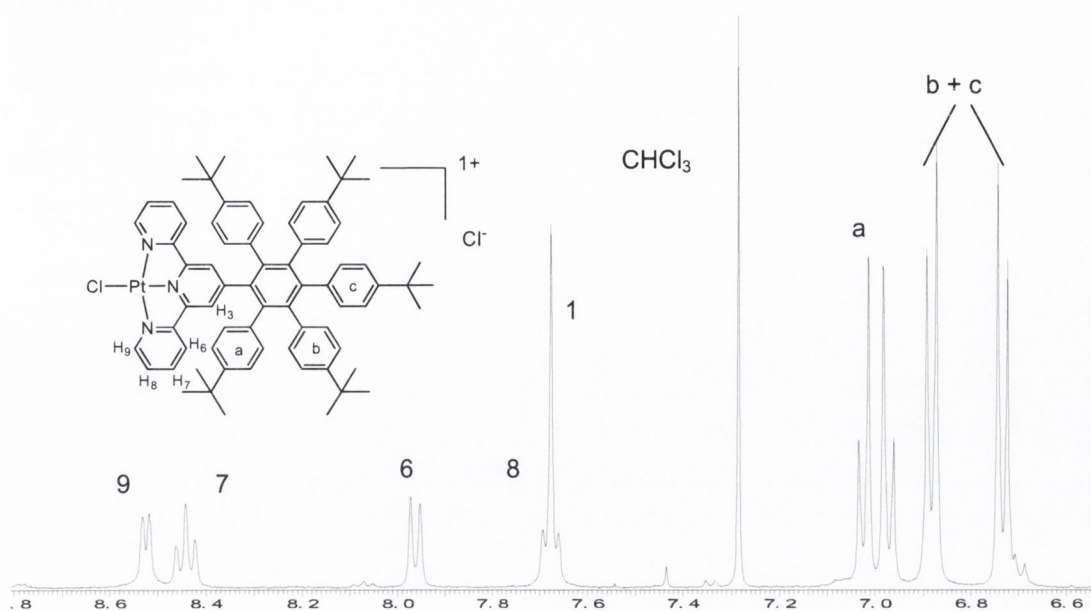
*Figure 113: The aromatic region of ^1H NMR spectrum for compound (**103**) in CDCl$_3$, 400 MHz, 25°C.*

The ESI-mass spectra of (**103**) gave a base peak at *m/z* = 1199.5 assigned to [M-Cl]$^+$. Accurate mass analysis in methanol gave a peak at 1199.5242 for (C$_{71}$H$_{75}$N$_3$ClPt)$^+$, which agrees with that calculated at 1199.5297.

4.2.1.2. Photophysical properties.

Absorption

The absorption spectra for [Pt(**89**)Cl]Cl (**103**) in various solvents (chloroform, methanol, acetonitrile) are shown in Figure 114. (**103**) shows solvatochromic behaviour. The peaks for the spectrum run in methanol (as expected for the most polar solvent) are most intense and they are blue shifted with respect to the spectra in chloroform and toluene. All data are shown in Table 23. The spectra in chloroform and methanol show four characteristic bands. These bands in the range 245-350 nm, are assigned to LC $\pi\rightarrow\pi^*$ and $\sigma\rightarrow\pi^*$ transitions. The MLCT transition between the platinum and the coordinated ligand (**89**) is the most red shifted band. This band appears at 424 nm in chloroform, at 419 nm in toluene and at 412 nm in methanol. The MLCT band assignment is based on the absence of visible band in the spectrum of free ligand and the literature examples.[8] The MLCT band for (**103**) is red-shifted

159

compared to MLCT band for [Pt(terpy)Cl]$^+$ (390 nm) or for [Pt(Ph-terpy)Cl]$^+$, which exhibits its MLCT absorption at 400 nm in acetonitrile.[24]
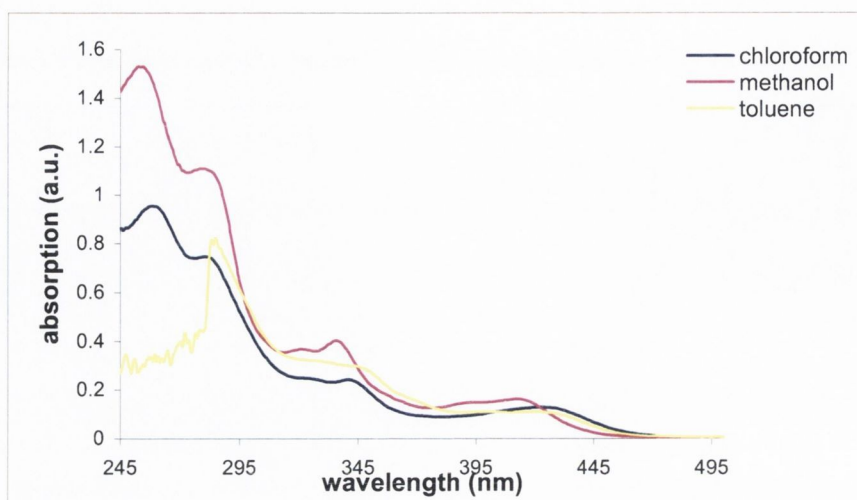
*Figure 114: The absorption spectra of (**103**) in different solvents at room temperature, conc. 3.3*10^{-5}M.*

Addition of a saturated solution of NH$_4$PF$_6$ to a methanolic solution of [Pt(**89**)Cl]Cl allowed counter-ion exchange and isolation of [Pt(**89**)Cl]PF$_6$ (**103a**) as a yellow precipitate. Figure 115 shows the absorption spectra for (**103a**) in chloroform, methanol and toluene. The overall shape of the spectra is similar to those obtained for (**103**). There is no big difference in intensities for absorption bands in different solvents. (**103a**) like (**103**) shows solvatochromic behaviour. The spectrum in methanol is shifted to higher energy. The most red-shifted band is assigned to metal to ligand charge transfer. They are at 411 nm in methanol, 425 in toluene and 425 nm in chloroform. All data are given in Table 23.

160
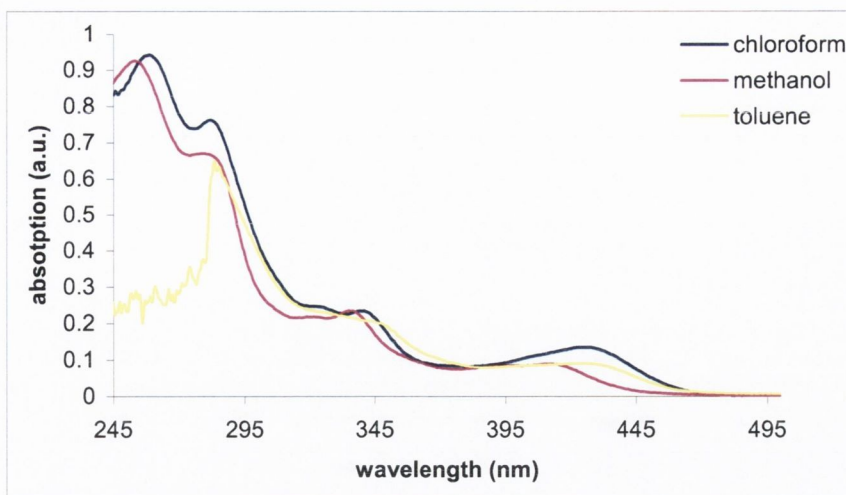
*Figure 115: The absorption spectra of (**103a**) in different solvents at room temperature.*

Absorption data λ_{max} (nm) in a variety of solvents			
Compound	**chloroform**	**methanol**	**toluene**
[Pt(**89**)Cl]Cl-(**103**)	258,280,341,424	254,278,321,336,412	247,282,419
[Pt(**89**)Cl]PF$_6$-(**103a**)	258,281,340,425	253,278,321,335,411	283,342,425

*Table 23: The absorption data for complexes (**103**) and (**103a**).*

Complexes (**103**) and (**103a**) do not show the low energy MMLCT absorption (usually around 460-550 nm). However, the broadening of absorption spectra occurs, perhaps this is connected to the aggregation of complexes in the solution. A possibility is π-π stacking through the polysryl ligands although steric bulk would also be a factor.

Emission

The change of the counterion did not cause any significant changes in the absorption spectra, but it did affect the fluorescence properties of (**103a**). Complex [Pt(**89**)Cl]PF$_6$ (**103a**) shows emission in chloroform at room temperature (Figure 116) but (**103**) does not. This emission for (**103a**) is very weak and the band is very broad with λ^{em}_{max} at 640 nm.

161
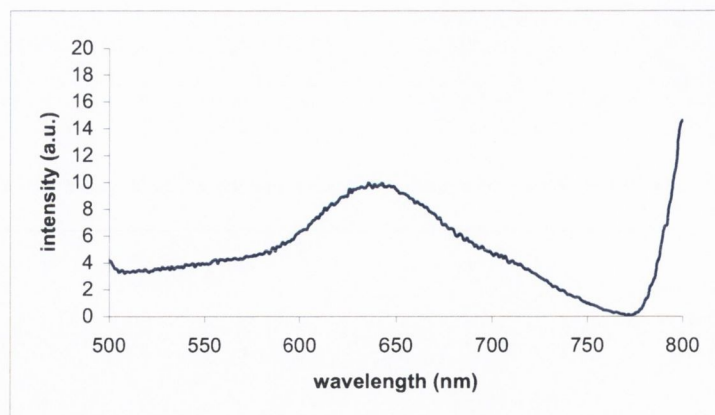
*Figure 116: Emission spectrum of (**103a**) in chloroform at room temp. conc. 3*10^{-5}M.*

The broadness and weakness of the emission of square-planar complexes of Pt(II) is a very common effect.[9,10] It is due to the presence of a low-lying d-d excited state. This d-d state is very unstable, which provide a facile deactivation *via* molecular distortion.[24]

4.2.2. [Pd(89)Cl]Cl-(104)

4.2.2.1. Synthesis

To synthesise the palladium(II) complex of ligand (**89**) a methanolic solution of $Na_2Pd_2Cl_4$ was used. One equivalent of $PdCl_2$ and two equivalents of NaCl were dissolved in methanol and heated to 50°C until all the NaCl had reacted. The resulting brown solution of $Na_2Pd_2Cl_4$ (0.056M) was used in the reaction with (**89**), with a solvent mixture of chloroform/methanol (3 ml/1 ml). Two equivalents of ligand (**89**) and one equivalent of $Na_2Pd_2Cl_4$ were mixed and refluxed for 18 hrs (Scheme 40). The yellow precipitate of pure (**104**) was obtained after recrystallisation in diethyl ether.
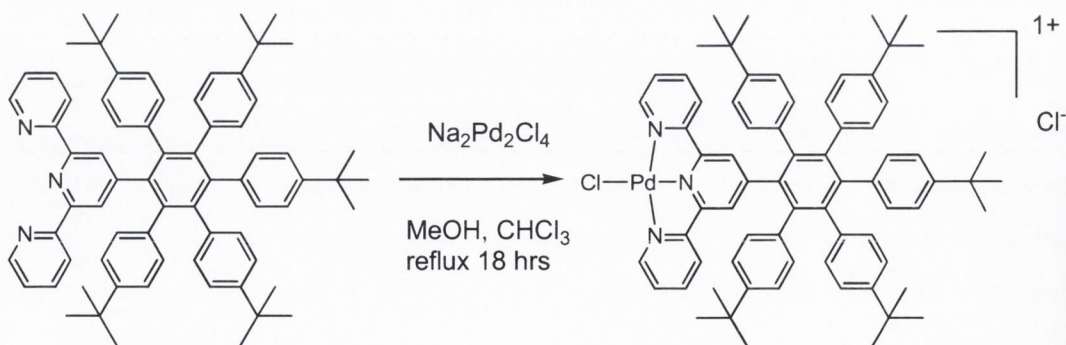
*Scheme 40: Synthesis of palladium(II) complex (**104**).*

162

Complex [Pd(**89**)Cl]Cl (**104**) was characterised by ^{1}H NMR and ^{13}C NMR spectroscopic analysis, and by mass spectrometry. To assign all the signals H,H COSY, C,H COSY and nOe experiments were carried out. The aromatic region of the ^{1}H NMR spectrum in deuterated chloroform is shown in Figure 117. The arrangement of the signals is similar to those in (**103**). Two singlets in the aliphatic region at δ 1.12 and 1.02 are assigned to the five t-butyl groups. These signals integrate for forty-five hydrogen atoms. The aromatic region of the spectrum shows eight signals. The most downfield signal is a broad doublet assigned to H9 (δ 8.79) and integrates for two hydrogen atoms. H9 is shifted downfield with respect to H9 (δ 8.60) from the uncoordinated ligand (**89**), this is due to the shielding effect of the coordinated metal. The broad triplet of doublets at δ 8.41 is related to H7 and integrates for two protons. Signals for protons H6 and H8 are overlapping at δ7.74 and they integrate for four hydrogen atoms. The singlet at δ 7.48 related to H3 is shifted upfield with respect to H3 (δ 7.83) in the free ligand (**89**). The doublets at δ7.07 and δ 6.92 integrate for eight protons and relate to phenyl ring a. The signals at δ 6.90 and δ 6.74 integrate for twelve hydrogen atoms and assigned to phenyl rings b and c.
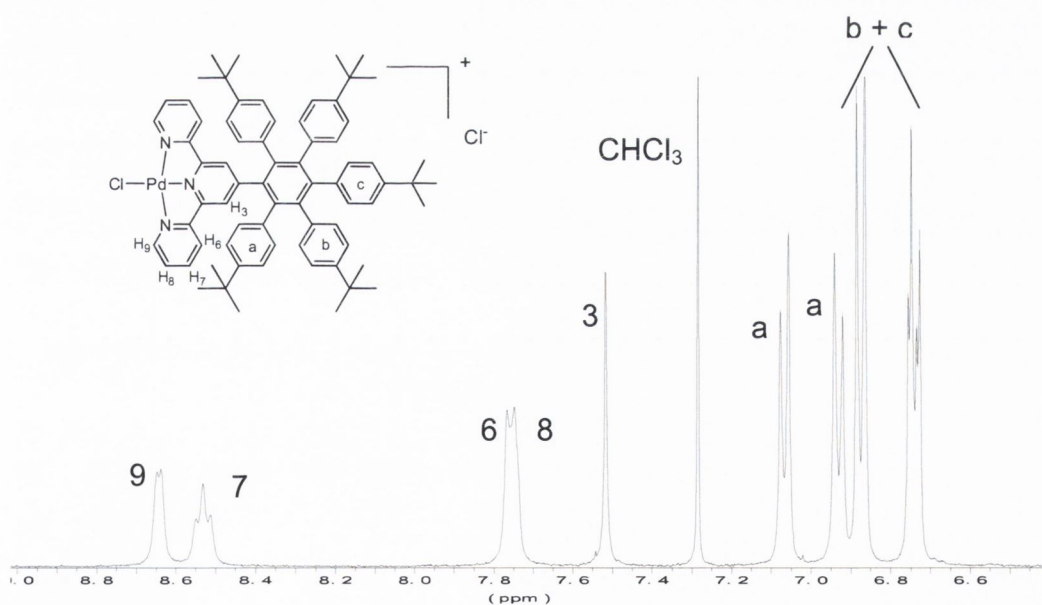
*Figure 117: The aromatic region of the ^{1}H NMR spectrum for compound (**104**), in CDCl$_3$, 400 MHz, 25°C, inset shows atoms labelling.*

163

The ESI-mass spectrum shows the parent ion at m/z 1110.47 assigned to $[\text{M-Cl}]^+$. Accurate mass analysis in methanol gave a peak at 1110.4653 for $(C_{71}H_{75}N_3ClPd)^+$, which aggress with that calculated 1110.4684.

4.2.2.2. Photophysical properties.

Figure 118 shows the absorption spectra of [Pd(**89**)Cl]Cl in chloroform and methanol. Complex (**104**) shows solvatochromic behaviour, the spectrum in methanol (more polar solvent compared to chloroform) is shifted to higher energy. The absorption bands in the UV region are attributed to LC transitions and appear at λ_{max} 282 nm and 249 nm in chloroform, and at 276 nm, 245 nm in methanol. The spectra in chloroform and methanol show very broad peak around 350-400 nm, with λ_{max} at 375 nm in chloroform and λ_{max} at 365 nm, both assigned to MLCT $d \rightarrow \pi^*$ transition between palladium and the coordinated ligand (**89**). The MLCT band is shifted to lower energy compared to the MLCT for [Pd(terpy)Cl]Cl·2H$_2$O (360 nm in water).[25] The MLCT of [Pd(terpy)Cl]$^+$ in acetonitrile solution appears at 362 nm.[26]
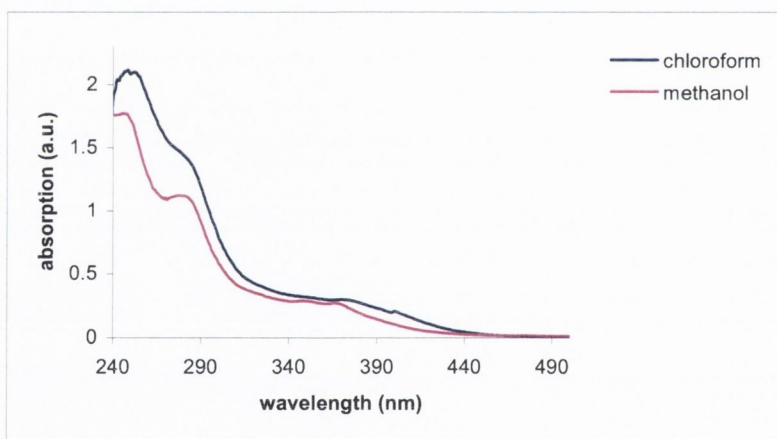
Figure 118: The absorption spectra of (104) in chloroform and methanol at room temp., conc. 7*10^{-5}M.

Complex [Pd(**89**)Cl]Cl is not emissive in ether room at temperature and 77K. The change of counterion gave interesting results for the emission for (**103**); the counterion exchange was carried out on (**104**) to give (**104a**). Figure 119 shows the absorption spectra of [Pd(**89**)Cl]PF$_6$ (**104a**) in chloroform and methanol. They are similar to the spectra of (**104**). (**104a**) also shows solvatohromic behaviour but with smaller shifts compared to (**104**). The spectrum in chloroform shows two characteristic bands: at 280 nm which are assigned to ligand centred transitions and a

very broad band at 368-400 nm, which relates to the MLCT $d \rightarrow \pi^*$ transition. In methanol there are two bands assigned to LC transitions at 276 nm and 246 nm. The MLCT transition band is broad and appears at 365 nm.

The absorption bands for (**104**) and (**104a**) are similar, with only small shifts for the LC transition: the change in counterion did not affect the absorption spectra.
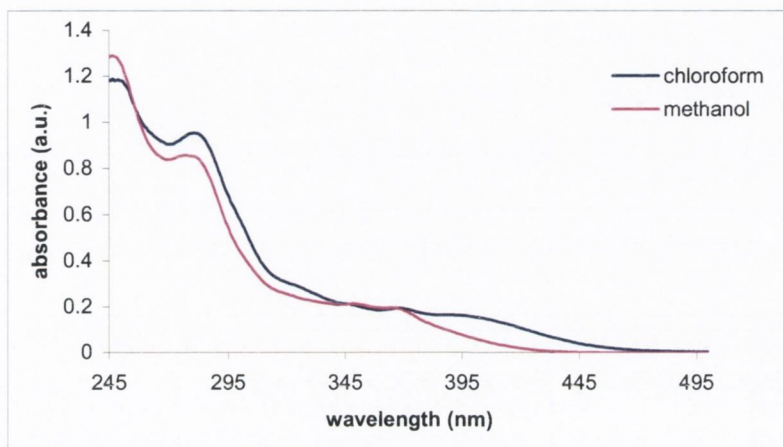
*Figure 119: Absorption spectra of (**104a**) in chloroform and methanol at room temp., conc. $5*10^{-5}M$.*

The absorption spectra for (**104**) and (**104a**) are broader than their platinum analogues. The MLCT bands for platinum complexes (**103**) and (**103a**) are shifted to lower energy with respect to the palladium complexes (**104**) and (**104a**). Similar behaviour was observed for complex [Pd(terpy)Cl]PF$_6$ and [Pt(terpy)Cl]PF$_6$ which show the MLCT absorption at 362 nm[26] and 405 nm,[14] respectively.

The change in counterion from Cl$^-$ to PF$_6^-$ has an effect on the emission spectrum. Figure 120 shows the emission spectrum of [Pd(**89**)Cl]PF$_6$ (**104a**) in chloroform in room temperature. When excited at 368 nm (**104a**) gives a broad emission band around 575 nm. The other sharp peak at 728 nm is the anti-Stokes emission peak.
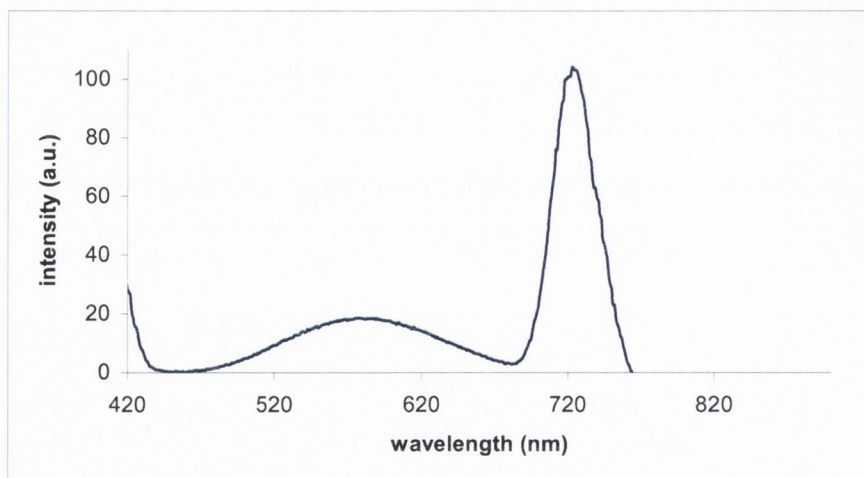
*Figure 120: Emission spectra of (**104a**) in chloroform at room temp. conc. 5*10^{-5}M.*

4.2.3. Iron(II) complexes

4.2.3.1. Synthesis

The iron(II) complex [Fe(**86**)$_2$](PF$_6$)$_2$ (**105**) was obtained as a main product during the attempted oxidative cyclodehydrogenation reaction of (**86**) (Scheme 41). In the cyclisation reaction with iron(III) chloride (as a Lewis acid catalyst and an oxidant) hydrochloric acid is evolved and a new C-C bond is created, and iron(III) is reduced to iron(II). For this reaction a large excess of FeCl$_3$ is used.[27] In this experiment with precursor (**86**) the complex (**105**) was obtained in 40% yield and a mixture of probably partially cyclised products was obtained. Due to the very low yields these products could not be isolated or characterised.
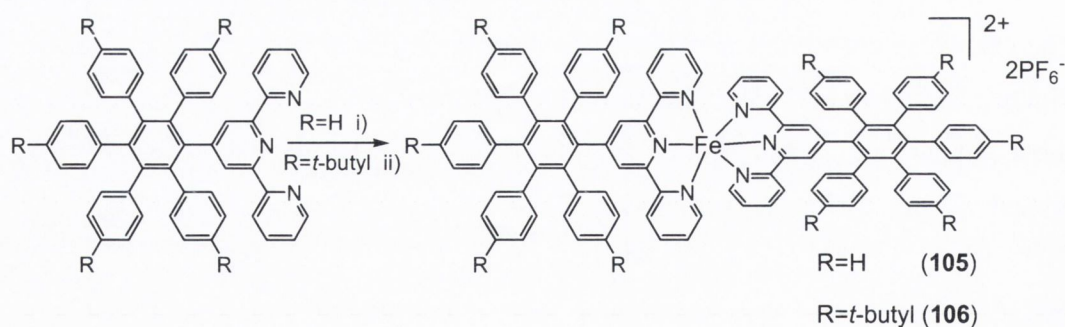
*Scheme 41: Synthesis of iron(II) complex (**105**) and (**106**), i) FeCl$_3$, ii) [Fe(H$_2$O)$_6$](BF$_4$)$_2$.*
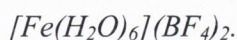
The synthesises of [Fe(**89**)$_2$](PF$_6$)$_2$ (**106**) and [Fe(**88**)$_2$](PF$_6$)$_2$ (**107**) were based on the general procedure for Fe(II) terpy complexes.[20] A methanolic solution of one

166

equivalent of $[Fe(H_2O)_6](BF_4)_2$ was added to a solution of two equivalents of (**89**) or (**88**) in methanol, respectively for (**106**) (Scheme 41) and (**107**) (Scheme 42). In both cases the deep purple solution was refluxed for 30 min. Then the mixtures were cooled down and the addition of saturated solution of KPF_6 resulted in the preparation of $[Fe(\mathbf{89})_2](PF_6)_2$ (**106**) in 75%, and $[Fe(\mathbf{88})_2](PF_6)_2$ (**107**) in 80%, respectively. Both as a deep purple precipitates.
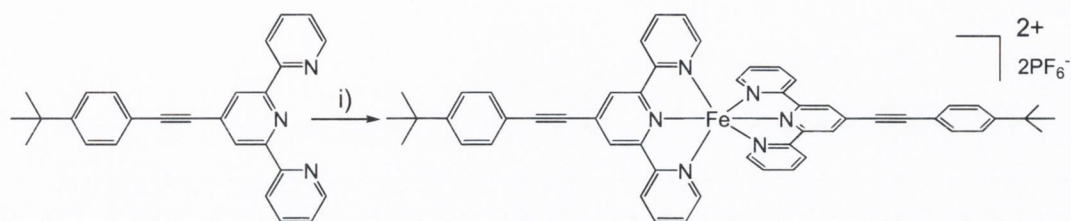
Scheme 42: Synthesis of iron(II) complex (107), i) [Fe(H₂O)₆](BF₄)₂.

Complexes (**105**), (**106**) and (**107**) were characterised by ^1H and ^{13}C NMR spectroscopic analysis, and by mass spectrometry. These homoleptic complexes possess C_2 symmetry, which simplifies the spectroscopic analysis. The signals were assigned by H,H, C,H-COSY and nOe experiments. The iron(II) complexes (**105**), (**106**) and (**107**) are low spin and diamagnetic. The diamagnetic complexes show resonances within the normal ^1H NMR spectroscopic region, between $\delta 0$ and $\delta 15$. Paramagnetic complexes would exhibit shifts in the range $(-\delta 500$ to $+500)$ and they would be high spin.

Figure 121 shows the aromatic region of ^1H NMR spectra of $[Fe(\mathbf{86})_2](PF_6)_2$ (**105**) and $[Fe(\mathbf{89})_2](PF_6)_2$ (**106**). Both complexes have the same arrangement of signals. The most downfield signal is a singlet assigned to H3 as expected, at δ 8.01 (for **105**) and δ 8.32 (for **106**). Signal H3 is integrated for four hydrogen atoms and is shifted downfield with respect to H3 for free ligand (**86** δ 8.09) and (**89** δ7.92). The most upfield peak is a doublet integrated for four protons and assigned to H9 as expected. The signal H9 appears at δ 6.26 for (**105**) and at δ 6.63 for (**106**). The shift of signal H9 with respect to H9 for the free ligand, δ 8.62 for (**86**) and at δ 8.60 for (**89**), in acetonitrile is significant. This upfield shift in the complex is due to the shielding effect of another pyridine ring. The same effect was observed in literature examples.[20,21] The doublet of doublets at δ8.07 for (**105**) is assigned to H6 and integrates for four protons. The last two signals for the terpy unit of the ligand are assigned to H7 (δ7.82) and H8 (δ7.13) and integrate for four hydrogen atoms each. In

the case of (**106**) the signals assigned to H6 and H7 are overlapping at δ7.81-7.78 and they integrate for eight hydrogen atoms. The signal related to H8 overlaps with one of the signals assigned to the phenyl rings at δ7.18. The signals related to the phenyl rings appear as a doublet of doublets at δ7.32 and as a multiplet at δ7.10-6.92 for (**105**). These signals integrate together for fifty hydrogen atoms. For (**106**) there are three doublets, one of them overlaps with the signal for H8. This and the multiplet integrate for forty hydrogen atoms.
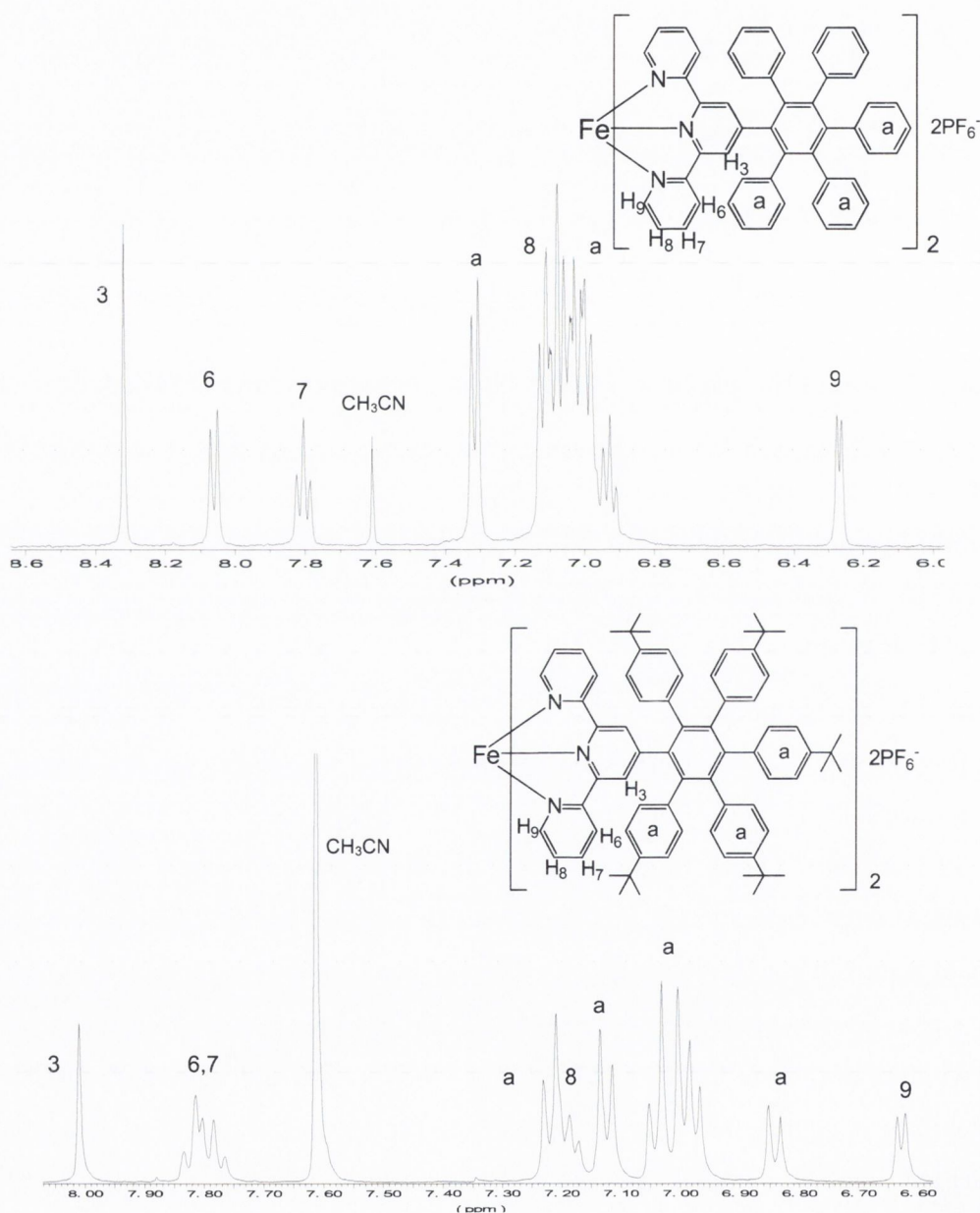
Figure 121: The aromatic region of ^1H NMR spectrum for complex (105) and (106) in CD₃CN, 400 MHz, 25°C, inserts show atom labelling.

168

Table 24 shows the ^{1}H NMR spectroscopic shifts for the iron(II) complexes [Fe(**86**)$_2$](PF$_6$)$_2$ (**105**) [Fe(**89**)$_2$](PF$_6$)$_2$ (**106**) and ligands (**86**) and (**89**).

Compound	^{1}H NMR data (ppm) in acetonitrile					
	H9	**H8**	**H7**	**H6**	**H3**	**Phenyl rings a**
Ligand (**86**)	8.62	7.38	7.86	8.44	8.09	7.06-6.76
Ligand (**89**)	8.60	7.34	7.83	8.36	7.92	6.92-6.80
[Fe(**86**)$_2$](PF$_6$)$_2$-(**105**)	6.26	7.13	7.82	8.07	8.32	7.10-6.92
[Fe(**89**)$_2$](PF$_6$)$_2$–(**106**)	6.63	7.18	7.78	7.81	8.01	7.23-6.83

*Table 24: The ^{1}H NMR data for complexes (**105**) and (**106**) together with ligands (**86**) and (**89**).*

Figure 122 shows the aromatic region of the ^{1}H NMR spectrum for homopleptic complex [Fe(**88**)$_2$](PF$_6$)$_2$ (**112**). In the aliphatic region there is one signal assigned to a *t*-butyl and it integrates for eighteen hydrogen atoms. The most shifted downfield is a singlet related to H3 at δ9.04 Δδ0.72 and Δδ1.03 respectively. This shift is due to the shielding effect of the neighbouring triple bond. The doublet of doublets at δ 8.51 is assigned to H6 and integrates for four protons. The signal at δ 7.93 is attributed to H7 and integrates for four hydrogen atoms. Two doublets at δ 7.79 and 7.67 are assigned to H14, H15 and there are related to the phenyl ring. The most upfield signal is assigned to H8, and not H9 as in [Fe(pyterpy)$_2$]$^{2+}$ complex.[20] Signal H8 (δ 7.11) integrate for four protons. The doublet of doublets assigned to H9 appears at δ7.18 and shifts downfield with respect to H9 for (**105**) and (**106**) within Δδ0.92 and Δδ0.55 respectively.
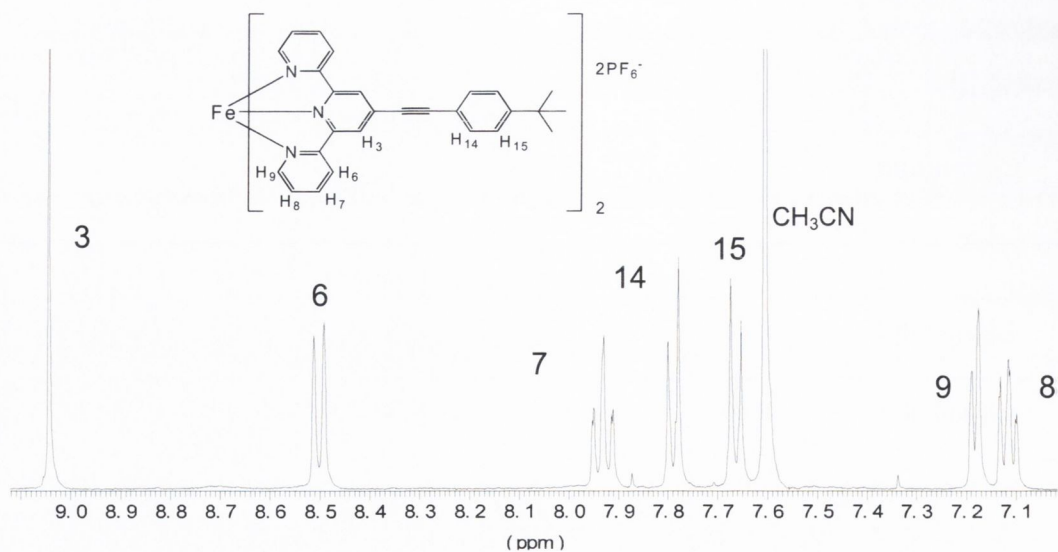
Figure 122: The aromatic region of ^1H NMR spectrum for compound (107), 600 MHz, in CD$_3$CN, 25°C, inset shows atoms labelling.

The ESI mass spectrs of (105), (106) and (107) show the molecular ion at assigned to [M-2PF$_6$]$^{2+}$ with ½ m.u. intervals in the isotopic distribution. This confirms the 2+ charge of the molecular ion. For each complex an accurate mass analysis was obtained in acetonitrile. All data are given in Table 25.

Complex	[M-2PF$_6$]$^{2+}$	Accurate mass	
		found	calculated
[Fe(**86**)$_2$](PF$_6$)$_2$ (**105**)	717.7	1435.4844	1435.4863
[Fe(**89**)$_2$](PF$_6$)$_2$ (**106**)	997.6	1996.1370	1996.1350
[Fe(**88**)$_2$](PF$_6$)$_2$ (**107**).	417.2	843.3124	834.3133

Table 25: ESI mass data for (105) in methanol, (106) and (107) in acetonitrile.

4.2.3.2. Photophysical properties of Fe(II) complexes.

Figure 123 shows the absorption spectra for complex [Fe(**86**)$_2$]PF$_6$)$_2$ (**105**) in acetonitrile , methanol and acetone (2.0*10^{-5}M). The spectra show three characteristic bands. Those in the range λ_{max} 250-350 nm are assigned to ligand centred transitions at approx. 279 nm and 322 nm. The lowest energy band is related to MLCT $d\rightarrow\pi^*$

170

transition it appears at λ_{max} 562 nm in acetonitrile, acetone, and methanol. The spectra do not show any solvent dependence. The MLCT absorption of (105) is red-shifted compared to that of $[Fe(terpy)_2]^{2+}$ λ_{max} 548 nm (acetonitrile) as expected.[16] This effect is due to better delocalisation of charge on the polyaryl substituted terpy of (86).
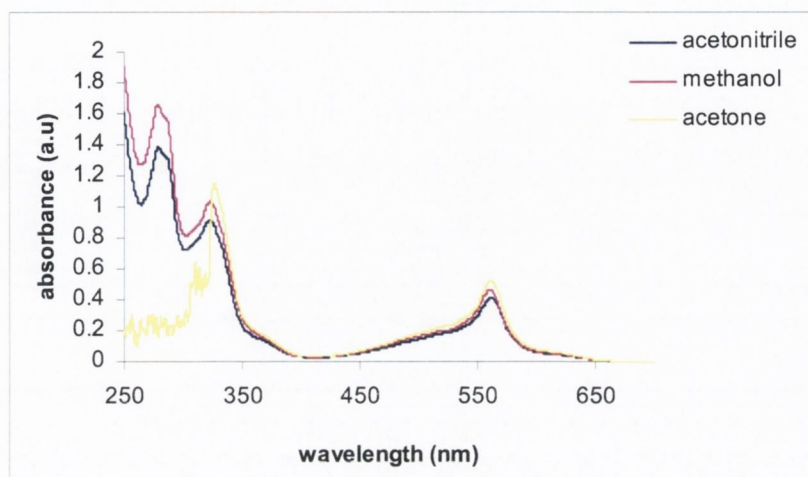
Figure 123: The absorption spectra of (105) in variety of solvents at room temperature., conc. $5.6*10^{-5}M$.

The absorption spectra for complex $[Fe(89)_2](PF_6)_2$ (106) in acetonitrile, methanol and acetone are presented in Figure 124. Like (105) it does not show any solvatochromism. The absorption in the UV region are assigned to ligand centred transitions. The band at the lowest energy is related to MLCT $d\rightarrow\pi^*$ transition. MLCT at λ_{max} 564 nm.
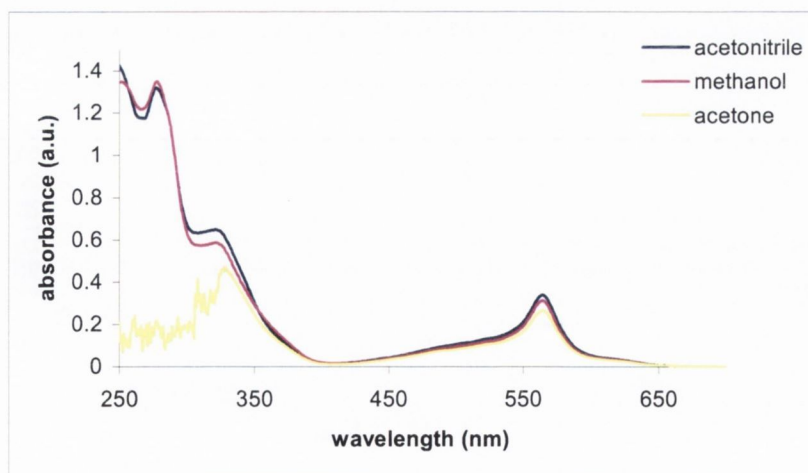
Figure 124: The absorption spectra of (106) in variety of solvents, conc. $4.2*10^{-5}M$.

171

Figure 125 shows the absorption spectra for complex [Fe(**88**)$_2$](PF$_6$)$_2$ (**107**) in acetonitrile, methanol and acetone. The absorption bands in acetone and methanol are more intense compared to spectrum in acetonitrile. Absorption bands in the range 250-350 nm are assigned to ligand centred transitions. The longest wavelength absorption is related to MLCT $d \rightarrow \pi^*$ transition and appears at λ_{max} 579 nm in acetonitrile and acetone, and at 577 nm in methanol. The MLCT transition for (**107**) is lower energy compared to that in MLCT (**105**) and (**106**), this is due to neighbouring of acetylene group in (**88**), which enhances the electron delocalisation. The MLCT band for (**107**) is of similar wavelength to that observed in the homoleptic complex [Fe(pyNoxterpy)$_2$](BF$_4$)$_2$ (577 nm) in acetonitrile,[21] but red-shifted with respect to that of [Fe(**I**)$_2$](BF$_4$)$_2$ at 556 nm (I-4'-(naphthalene-2-ylmetoxy)-2,2':6',2''-terpyridine).[28]
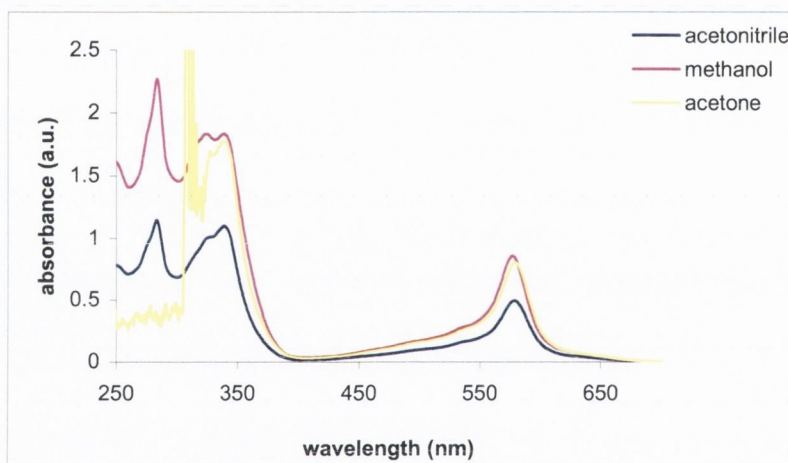
*Figure 125: Absorption spectra of (**107**) in variety of solvents at room temp. conc. 8*10^{-5}M.*

Table 26 shows the absorption data for the synthesised iron(II) complexes. The data for complexes (**105**) and (**106**) is very similar as expected, because ligand (**89**) is a *t*-butyl substituted analogue of (**86**) and *t*-butyl group are not expected to influence the absorption spectra.

Absorption data λ_{max} (nm) in variety of solvents			
Compound	acetonitrile	methanol	acetone
[Fe(**86**)$_2$](PF$_6$)$_2$-(**105**)	562	562	562
[Fe(**89**)$_2$](PF$_6$)$_2$-(**106**)	564	564	564
[Fe(**88**)$_2$](PF$_6$)$_2$-(**107**)	579	577	579

*Table 26: Absorption data for iron(II) complexes (**105**), (**106**) and (**107**).*

4.3. Conclusion

The new compounds presented in Chapter 3, (**86**), (**88**) and (**89**), have been studied as ligands for coordination chemistry with metals such as Pt(II), Pd(II) and Fe(II).

The novel square-planar complexes [Pt(**89**)Cl]Cl (**103**) and [Pd(**89**)Cl]Cl (**104**) have been synthesised. Both complexes have been fully characterised and their photophysical properties investigated. The MLCT band for (**103**) and (**104**) appears above 400 nm and is shifted to lower energy compared with the terpy or Ph-terpy analogues. This is due to the extended π-electron density created by the additional phenyl rings on (**89**), compared with terpy and Ph-terpy ligands. It has been shown that changing the counterion Cl⁻ to PF$_6$⁻ affects the photophysical properties of the complexes. (**103a**) and (**104a**) show emission in solution at room temperature. The intensity of the emission is very weak; to improve this as shown in the literature the Cl⁻ ligand coordinated directly to the metal needs to be replaced by another ligand, such as -Me or -Ph.

As future work, the Pt(II) and Pd(II) complexes of a novel ligand (**90**) (Chapter 3) might show very interesting result from the photophysical point of view. As well new complexes have been proposed (Figure 126), which should show more intense emission at room temperature compared to (**103a**) and (**104a**). Pd(II) analogues could be synthesised as well.
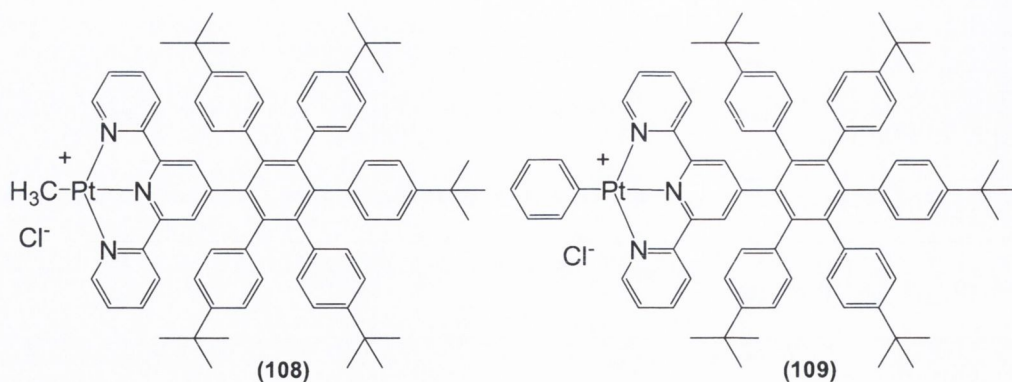
Figure 126: Suggested new Pt(II) complexes.

Three new transition metal complexes have been obtained [Fe(**86**)$_2$](PF$_6$) (**105**), [Fe(**89**)$_2$](PF$_6$)$_2$ (**106**) and [Fe(**88**)$_2$](PF$_6$)$_2$ (**107**). As expected: all three complexes show low spin configuration Fe(II). The ^{1}H NMR spectra show normal shifts within (δ 0 to 15) which is characteristic for diamagnetic complexes. The photophysical properties of (**105**), (**106**) and (**107**) have been studied. The MLCT bands of those complexes are shifted to lower energy compared to [Fe(terpy)$_2$]$^{2+}$. In the case of (**105**) and (**106**) this is due to the higher electron delocalisation on the ligands (**86**) and (**89**), which possess six additional phenyl rings compared to terpy. The MLCT for (**107**) is the most red-shifted (λ_{max} 579 nm) of the newly synthesised complexes. This suggests that substitution at the 4'-position of the terpy with phenyacetylene (**88**) lowers the ligand π^* orbital energy more readily than the presence of six phenyl rings (**86**, **89**). The new terpy-type ligand (**90**) described in Chapter 3, and its derivative with the acetylene linkage between terpy-moiety and aromatic core are ideal for creating new Fe(II) complexes. These complexes might possess very interesting photophysical properties, due to the extended aromatic surface linked to 4'-position of terpy ligand by a single or triple bond.

4.4. <u>References</u>

[1] C. S. Peyratout, T. K. Aldridge, D. K. Crites, D. R. McMillin, *Inorg. Chem.*, **1995**, 4484

[2] Ž. D. Bugarčic, G. Liehr, R. Van Eldik, *J. Chem. Soc., Dalton Trans.*, **2002**, 951-956

[3] M. Tilset, *J. Am. Chem. Soc.*, **2001**, 739

[4] J. Reedijk, *Chem. Rev.*, **1999**, 2499

[5] E. R. Jamieson, S. J. Lippard, *Chem. Rev.*, **1999**, 2467

[6] H. Q. Liu, S. M. Peng, C. M. Che, *J. Chem. Soc., Chem. Commun.*, **1995**, 509.

[7] H. Q. Liu, T.C. Cheung, C. M. Che, *Chem. Commun.*, **1996**, 1039

[8] G. Arena, G.N. Calogero, S. Campagna, L. Monsu Scolaro, V. Ricevuto, R. Romeo, *Inorg. Chem.*, **1998**, 2763-2769

[9] J. A. Bailey, M. G. Holl, R. E. Marsh, V. M. Miskowski, W. P. Schaefer, H. B. Gray, *Inorg.Chem.*, **1995**, 4591-4599

[10] A. J. Goshe, I. M. Steele, B. Bosnich, *Inorg. Chim. Acta*, **2004**, 4544-4551

[11] S. Wai, M. C. Chan, K.K. Cheung, C.M. Che, *Inorg. Chem.*, **1999**, 4262-4267

[12] D. K. Crites, C. T. Cunnigham, D. R. McMillin, *Inorg. Chim. Acta*, **1998**, 346-353

[13] H. Yip, L. Cheng, K. K. Cheung, C. M. Che, *J. Chem. Soc., Dalton Trans.*, **1993**, 2933-2938

[14] J. F. Michalec, S. A. Bejune, D. R. McMillin, *Inorg. Chem.,* **2000**, 2708-2709

[15] C. L. W. Fan, D. A. Straus, B. Lei, S. Asano, D. Zhang, J. Han, M. Meyyappan, C. Zhou, *J. Am. Chem. Soc.*, **2004**, 7750-7751

[16] E. C. Constable, G. Baum, E. Bill, R. Dyson, R. Van Eldik, D. Fenske, S. Kaderli, D. Morris, A. Neubrand, M. Neuburger, D. R. Smith, K. Wieghardt, M. Zehnder, A. D. Zuberbühler, *Chem. Eur. J.*, **1999**, 498-508

[17] S. Hwang, C. N. Moorefield, F. R. Fronczek, O. Lukoyanova, L. Echegoyen, G. R. Newkome, *Chem. Commun.*, **2005**, 713-715

[18] E. C. Constable, C. E. Housecroft, M. Neuburger, S. Scheffner, L. J. Scherer, *Dalton Trans.*, **2004,** 2635-2642

[19] G. R. Newkome, T. J. Cho, C. N. Moorfield, P. P. Mohapatra, L. A. Godinez, *Chem. Eur. J.*, **2004**, 1493-1500

[20] E. C. Constable, A. M. W. Cargill Thompson, *J. Chem. Soc., Dalton Trans.*, **1992**, 2947-2950

[21] J. Pitarch Lopez, W. Kraus, G. Reck, A. Thünemann, D. G. Kurth, *Inorg. Chim. Acta*, **2005**, 3384-3390

[22] S. Chakraborty, T. J. Wadas, H. Hester, C. Flaschenreim, R. Schmehl, R. Eisenberg, *Inorg. Chem.*, **2005**, 6284-6293

[23] J. H. Price, A. N. Williamson, R. F. Schramm, B. B. Wayland, *Inorg. Chem.*, **1972,** 1280-1284

[24] R. Büchner, C.T. Cunningham, J. S. Field, R. J. Haines, D. R. McMillin, G.C. Summerton, *J.Chem. Soc., Dalton Trans.*, **1999**, 711-717

[25] P. Castan, F. Dahan, S. Wimmer, *J. Chem. Soc., Dalton Trans.*, **1990**, 2679-2683

[26] W. Zhang, C. Bensimon, R. J. Crutchley, *Inorg. Chem.*, **1993,** 5808-5812

[27] S. P. Brown, I. Schenell, J. D. Brand, K. Müllen, H. W. Spiess, *J. Am. Chem. Soc.*, **1999**, 6712-6718

[28] H. S. Chow, E. C. Constable, C. E. Housecroft, M. Neuburger, S. Schaffner, *Dalton Trans.*, **2006**, 2881-2890

<u>Part 5</u>: Experimental

5.1. General experimental

Unless otherwise stated, reactions were carried out in air. The solvents were distilled under nitrogen and dried with appropriate drying agents using standard techniques. Flash chromatography was performed using silica gel (Aldrich) or aluminum oxide (type 507C, neutral, Fluka) as the stationary phase. Separations were undertaken in the air. The chemicals were obtained from commercial sources (mostly Aldrich, Fluka).

IR spectra were recorded on a Genesis II FTIR Spectrometer, Mattson, 1001 Fourier Drive. Spectra were recorded from KBr discs. Nuclear magnetic resonance data were recorded on a Brüker Avance DPX 400 MHz spectrometer, operating at frequencies: 400.1 MHz for ^{1}H and 100.6 MHz for ^{13}C for all cases except where indicated a Brüker Avance II 600 MHz spectrometer, Cryo Probe, operating at frequencies: 600.1 MHz for ^{1}H and 150.9 MHz for ^{13}C, both were standardised with respect to TMS.

Electrospray mass spectra were obtained on a micromass LCT electrospray mass spectrometer. Accurate mass spectra were referenced against Leucine Enkephalin (555.6 g/mol). Elementary analysis was obtained on Carlo Erba 1006 automatic analyzer at University College Dublin. Melting points were recorded on a Griffin melting point apparatus.

UV-vis absorption spectra were recorded on a Shimadzu UV-2401PC UV-vis recording spectrometer. The emission spectra were not corrected and were recorded at room temperature on Varian Fluorescence Cary Eclipse spectrophotometer. The low temperature emission was obtained using a Perkin Elmer LS 50B Luminescence spectrometer. The luminescence lifetime were measured in Dublin City University using 355 nm line of pulsed Nd: YAG laser (energy approx. 35 mJ per pulse, system response 20 ns).

Crystal data and structural experimental are summarised in Tables in Annex. Selected bond lengths and angles are given in the discussion. The remaining angles, distances, atom coordinates as well as anisotropic displacement parameters and hydrogen atom coordinates are on the enclosed CD. The single-crystal analyses were performed by Dr. Christopher Fitchett in Trinity College with a Brüker SMART APEX CCD

diffractometer using graphite monochromised Mo-K$_\alpha$ (λ=0.71073Å) radiation at the temperatures given in tables on pages 213-215. Data reduction was performed using SAINT. Intensities were corrected for Lorentz and polarisation effects and for absorption by SADABS. Space groups were determined from systematic absences and checked for higher symmetry. The structures were solved by direct methods using SHELXS and refined on F^2 using all data by full-matrix least-squares procedures with SHELX-97. All non-hydrogen atoms were refined with anisotropic displacement parameters 1.3 times the isotropic equivalent of their carrier carbons. Absolute structure determinations were based on the Flack parameter. The functions minimised were $\Sigma w(F_o^2 - F_c^2)$, with $w=[\sigma^2(F_o^2) + (aP)^2 + bP]^{-1}$, where $P= [max(F_o)^2 + 2F_c^2]/3$. In all cases, final Fourier syntheses showed no significant residual electron density in chemically sensible positions.

5.2. N-heterosuperbenzenes

Synthesis of 1,3-bis-(4-tetra-butyl-phenyl)-propan-2-one (4)[1]

The synthesis was carried out in an argon atmosphere. Ca(OH)$_2$ (2.6 g; 35.2 mmol) and Bu$_4$N$^+$HSO$_4^-$ (1.5 g; 4.4 mmol) were added to 1:1 dichloromethane/water (180 ml) and the mixture was stirred at room temperature. 4-*Tert*-butylbenzylbromide (4 g; 17.6 mmol) was added, followed by Fe(CO)$_5$ (1.16 ml; 8.8 mmol) and the reaction mixture was stirred for 5 h at room temperature, with a steam of argon bubbling through the solution. After 5 h the mixture was oxidised in air and acidified with 10% HCl solution (60 ml). The phases were separated and the aqueous phase was extracted with dichloromethane.The combined organic phases were dried over MgSO$_4$. The product (4) was purified using column chromatography (SiO$_2$, 1:1 hexane : dichloromethane) and crystallized from hexane giving white crystals. Yield 3.29g, 58%; m.p.:80-82°C.

^{1}H NMR (CDCl$_3$): δ 7.36 (d, 4H, $^3J_{HH}$=8.4, H1), 7.12 (d, 4H, $^3J_{HH}$=8.4, H2), 3.71 (s, 4H, H3), 1.33 (s, 18H, -C(CH$_3$)$_3$). **^{13}C NMR** (CDCl$_3$): δ 205.7 (1C, C=O), 149.4 (2C, C$_{quat,}$), 130.5 (2C, C$_{quat,}$), 128.7 (4C, C1), 125.1 (4C, C2), 48.1 (2C, C3), 34.0 (2C,

$C_{quat/alkyl}$), 30.9 (6C, -CH$_3$). **IR** (KBr disk, cm^{-1}): ν(C-H st, CH$_3$): 2955, ν(C=O st): 1684.

(4)
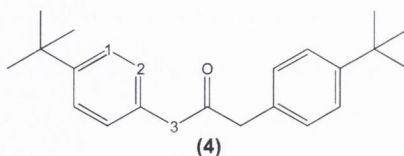
Synthesis of 1,2-bis-(4-*tert*-butyl-phenyl)ethane-1,2-dione (3)[1]

The synthesis was carried out in an argon atmosphere. 1-Bromo-4-tert-butyl-benzene (2.6 ml, 18.8 mmol) was dissolved in THF (30 ml) and the solution was cooled down to –78°C. To this a solution of *n*-BuLi (7.55 ml of 2.5M solution in hexane, 18.8 mmol) in THF (60 ml) at –78°C was added dropwise. The solution was stirred for 2 h at 195 K, then added to a solution of 1,4-dimethyl-piperazine-2,3-dione (1.32 g, 9.3 mmol) in THF (20 ml) at –78°C. The reaction mixture was stirred and allowed to warm to room temperature over 1.5 h, then stirred for a further 1 h. The reaction mixture was quenched with 5% HCl (120 ml), and the product (3) was extracted with dichloromethane. The organic phase was washed and dried over MgSO$_4$. Column chromatography (SiO$_2$, hexane/dichloromethane, 4:5), and recrystallization from hexane yielded white crystals. Yield 1.46g, 48%; m.p.:102°C.

¹H NMR (CDCl$_3$): δ 7.94 (d, 4H, $^3J_{HH}$=8.5, H$_{aryl}$), 7.55 (d, 4H, $^3J_{HH}$=8.5, H$_{ary}$), 1.36 (s, 18H, -C(CH$_3$)$_3$). **¹³C NMR** (CDCl$_3$): δ 197.3 (2C, C=O), 158.4 (2C, C$_{quat/aryl}$), 130.1 (2C, C$_{quat/aryl}$), 129.4 (4C, CH), 125.5 (4C, CH), 34.9 (2C, C$_{quat/alkyl}$), 30.5 (6C, -CH$_3$). **IR** (KBr disk, cm^{-1}): ν(C-H st, CH$_3$): 2956, ν(C=O st): 1672, 1623.

(3)
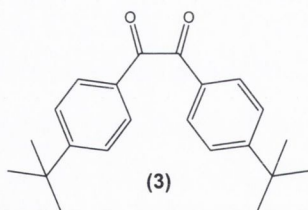
Synthesis of 2,3,4,5-tetra-(4-*tert*-butyl-phenyl) cyclopentadienone (5)[1]

(4) (200 mg, 0.62 mmol) and (3) (200 mg, 0.62 mmol) were dissolved in hot ethanol (1.5 ml), and the solution was heated close to boiling point. Then to this mixture was then slowly added a solution of KOH (17.4 mg, 0.31 mmol) in ethanol (1.5 ml), in two portions through the condenser. The mixture was heated to reflux for 20 minutes.

From the red/brown solution the solvent was evaporated, and the product (**5**) was purified by column chromatography (SiO$_2$, hexane/dichloromethane, 1:1), to produce deep red crystals. Yield 276mg, 73%; m.p.:238-240°C.

^{1}H NMR (CDCl$_3$): δ 7.26 (m, 8H, H1, H2), 7.18 (d, 4H, $^3J_{HH}$=8.5, H3 or H 4), 6.68 (d, 4H, $^3J_{HH}$=8.5, H3 or H4), 1.31, 1.18 (s, 18H, -C(CH$_3$)$_3$). **IR** (KBr disk, cm^{-1}): ν (C-H st, CH$_3$): 2960, ν (C=O st): 1707, ν (CH$_3$ δ): 1498, 1456.

(5)
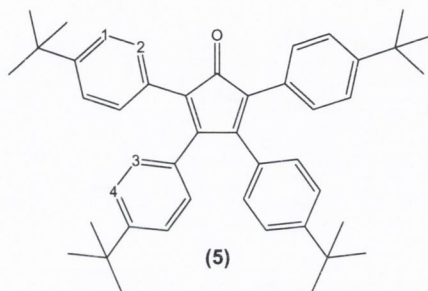
Synthesis of 2-methyl-4-pyrimidin-5-yl-but-3-yn-2-ol (21)[1]

The synthesis was carried out in an argon atmosphere. Bis(triphenylphosphine) palladium(II) dichloride (88 mg, 0.2 mmol), CuI (14 mg, 0.07 mmol), and 5-bromopyrimidine (2g, 12.6 mmol) were dissolved in diethylamine (30 ml). To this solution 2-methyl-3-butyn-2-ol (1.46 ml, 15.1 mmol) was added. The mixture was stirred for 3 h at room temperature. The diethylamine was evaporated under reduced pressure. The product was washed with water and extracted with dichloromethane, dried over MgSO$_4$, and purified using column chromatography (SiO$_2$, diethyl ether). Crystallization with ethylacetate/petroleum ether gave white crystals of (**21**). Yield 1.61g, 79 %; m.p.:114°C.

^{1}H NMR (CDCl$_3$): δ 9.15 (s, 1H, H1), 8.79 (s, 2H, H2), 2.35 (br s, -OH), 1.66 (s, 6H,-C(CH$_3$)$_2$-). **^{13}C NMR** (CDCl$_3$): δ 158.3 (2C, C$_{aryl}$), 156.3 (1C, C$_{aryl}$), 118.9 (1C, C$_{quat/aryl}$), 100.6, 75.1 (-C≡C-), 65.1 (1C, C$_{quat/alkyl}$), 30.8 (2C, -C(CH$_3$)$_2$-).

(21)
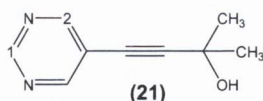
Synthesis of 5-ethynylpyrimidine (22) [1]

A toluene solution (118 ml) of (**13**) (1.51 g, 9 mmol) was heated under reflux with NaOH (300 mg, 7.5 mmol) for 2 h. The mixture was washed with water, and phases

separated. The organic phase was dried over MgSO$_4$ and purified by column chromatography (SiO$_2$, dichlomethane/methanol, 20:1). The product (**22**) was further purified *via* sublimation. Yield 614 mg, 64%; m.p.:86°C.

^{1}H NMR (CDCl$_3$): δ 9.19 (s, 1H, H1), 8.85 (s, 2H, H2), 3.42 (s, 1H, -C≡CH). **^{13}C NMR** (CDCl$_3$): δ 158.9 (2C, C$_{aryl}$), 156.8 (1C, C$_{aryl}$), 118.3 (1C, C$_{quat/aryl}$), 98.9, 84.0 (-C≡C-). **IR** (KBr disk, cm^{-1}): ν(≡C-H st,):3648, ν(C=N st): 1698, 1540, 1488, ν(γC-H):862.

(**22**)
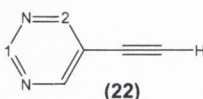
Synthesis of di-(pyrimid-3,5-yl) acetylene (6)[1]

The synthesis was carried out in an argon atmosphere. A solution of (**14**) (420 mg, 4 mmol) in triethylamine (50 ml) was added to a solution of 5-bromopyrimidine (611mg, 4 mmol), bis(triphenylphosphine)palladium(II) (300 mg, 0.6 mmol), and CuI (45 mg, 0.2 mmol) in DMF (100 ml). The reaction mixture was stirred for 1 h at 55°C, then for 24 h at room temperature. This was then washed water and the product extracted with dichloromethane. The organic phase was dried over MgSO$_4$ and purified by column chromatography (SiO$_2$, ethylacetate/chloroform, 1:1). (**6**) was recrystallized from ethylacetate/petroleum ether, to afford yellow crystals. Yield 395 mg, 54%; m.p.:168-170°C.

^{1}H NMR (CDCl$_3$): δ 9.24 (s, 2H, H1), 8.93 (s, 4H, H2). **IR** (KBr disk, cm^{-1}): ν(C=N st): 1636, 1542, 1427, ν(γC-H): 717.

(**6**)
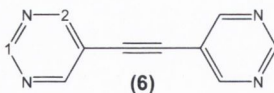
Synthesis of 1,2-dipyrimidyl-3,4,5,6-tetre-(4-tert-butylphenyl)benzene (7)[1]

A mixture of (**6**) (175 mg, 0.3 mmol), (**5**) (53 mg, 0.3 mmol), and benzophenone (2 g) was stirred in a round bottom flask attached to an air condenser. The reaction mixture was heated to reflux over a microburner for 1 h. Carbon monoxide was evolved and the colour changed from red to brown. After cooling, the product (**7**) was purified by

column chromatography (SiO$_2$, diethyl ether) and recrystallized from ethylacetate/petroleum ether to give white crystals. Yield 150mg, 68%; m.p.:306-308°C.

^{1}H NMR (CDCl$_3$): δ 8.78 (s, 2H, H1), 8.26 (s, 4H, H2), 6.95 (d, 4H, $^3J_{HH}$=8.5, H$_{aryl}$), 6.87 (d, 4H, $^3J_{HH}$=8.5, H$_{aryl}$), 6.72 (d, 4H, $^3J_{HH}$=8.5, H$_{aryl}$), 6.69 (d, 4H, $^3J_{HH}$=8.5, H$_{aryl}$), 1.11 (s, 18H, -C(CH$_3$)$_3$), 1.13 (s, 18H, -C(CH$_3$)$_3$). **IR** (KBr disk, cm^{-1}): ν (C-H st, arom): 3095, 3040, ν (C-H st, CH$_3$): 2955, ν(C=N st): 1544, 1427.

(7)
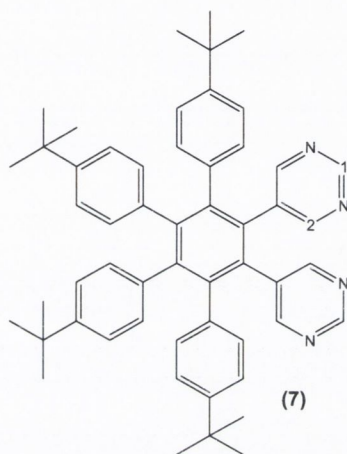
Synthesis of tetra-peri-(tert-butyl-benzo)-di-peri-(pyrimidino)-coronene (8), (N-HSB)[1]

The product was made using reaction conditions a) and b) carried out in an argon atmosphere.

a) A mixture of (**7**) (100 mg, 0.131 mmol), aluminium trichloride (278 mg, 2.08 mmol), and copper(II) chloride (282 mg, 2.01 mmol) in CS$_2$ (30 ml) was stirred for 72h at room temperature. The black solid was allowed to settle and the CS$_2$ removed using a cannula. The reaction mixture was stirred with a 10 % ammonia solution (70 ml) for 30 min. The reaction mixture was washed with water and product (**8**) was extracted with chloroform. The organic layer was dried over MgSO$_4$, and purified by chromatography (SiO$_2$, toluene/methanol, 9:1). After recrystallization from toluene/petroleum ether, orange crystals were obtained. Yield 34 mg, 35%, m.p.:>360°C.

¹H NMR (CDCl₃) (as per literature assigment): δ 9.81 (s, 2H, H aryl), 9.44 (s, 2H, H_{aryl}), 9.09 (s, 2H, H_{aryl}), 9.03 (s, 2H, H_{aryl}), 8.96 (s, 2H, H_{aryl}), 1.96(s, 18H, -C(CH₃)₃), 1.88 (s, 18H, -C(CH₃)₃). **ESI-MS** (toluene) *m/z* (MH)⁺ 751.2167 (found), 751.3840 (calcd)..

b) A solution of (**7**) (160 mg, 0.209 mmol), aluminium trichloride (996 mg, 7.43 mmol), and copper(II) trifluoromethanesulfonate (2.7 g, 7.43 mmol) in CS₂ (60 ml) was stirred for 5 days at room temperature. The brown solid was allowed to settle and the CS₂ removed using a cannula. The reaction mixture was stirred with 10 % ammonia solution (100 ml) for 1h. The reaction mixture was washed with water and extracted with chloroform. The chloroform layer was dried over MgSO₄, and column chromatographed (SiO₂, toluene/methanol, 9:1). Six side products were obtained, but there were insufficient amounts for purification and characterization.

(8)
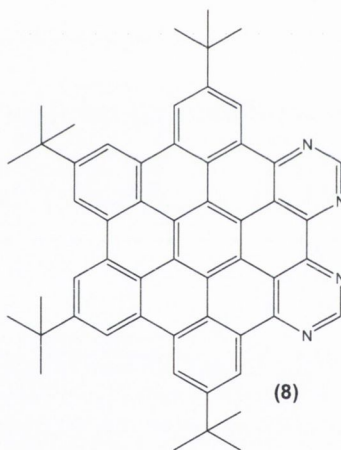
Synthesis of "half-cyclised" N-½HSB (9)[2]

The synthesis was carried out in an argon atmosphere. A solution of iron(III) trichloride (0.42 g, 2.58 mmol) in nitromethane (3 ml) was added dropwise to a stirred solution of (**7**) (0.1 g, 0.13 mmol) in dichloromethane (20 ml). Argon was bubbled through the reaction mixture during the entire reaction time. After stirring for 40 min. the reaction was quenched with methanol (20 ml), and the mixture was left stirring for another 30 min. The mixture was washed with water and product was extracted with dichloromethane, dried over MgSO₄. The half-cyclised product (**9**) was separated by

silica preparative plates using toluene/methanol (9:1) solution as a eluent. The product was obtained with 30% yield.

¹H NMR (CDCl₃): δ 10.13 (s, 2H, H1), 9.64 (s, 2H, H2), 7.84 (d, 2H, H4), 7.40 (d, 2H, H3), 7.29 (d, 2H, H5 or H6), 7.06 (d, 2H, H5 or H6).

(9)
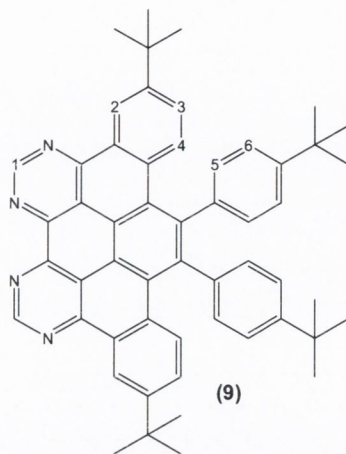
5.3. **Ruthenium(II) complexes of N-HSB (8) and N-½HSB (9).**

Synthesis of [Ru(bpy)₂(8)](PF₆)₂ (19)[3]

The synthesis was carried out in an argon atmosphere. A solution of ligand (**8**) (20 mg, 2.66×10⁻² mmol) in diethylene glycol ethyl ether (5 ml) was sonicated for 20 minutes. The brown/orange solution was degassed by bubbling a stream of argon through the flask for 30 minutes. Then [Ru(bpy)₂Cl₂]·2H₂O (15.4 mg, 2.96×10⁻² mmol) was added and the solution was degassed for another 20 minutes. The reaction mixture was heated for 20 h at 125°C. During the reaction time the colour changed from brown to green. After cooling and filtering saturated aqueous solution of NH₄PF₆ was added to the mixture to form a dark green precipitate. The precipitate was filtered, washed with water and diethyl ether. The product was purified by column chromatography (SiO₂, acetonitrile/water/KNO₃(sat.), 100:10:1), followed by anion exchange with saturated solution of NH₄PF₆. (**9**) was obtained as dark-green solid. Yield 25mg, 58%.

¹H NMR (40°C) (CDCl₃) (as per literature assigment): δ 9.98 (s, 2H, H aryl), 9.64 (s, 2H, H aryl), 9.43 (s, 4H, H aryl), 9.22 (s, 2H, H aryl), 8.57 (d, 2H, ³J_HH=7.5, H aryl), 8.50 (br d, 2H, ³J_HH=6.5, H aryl), 8.28 (t, 2H, ³J_HH=5, H aryl), 8.20 (t, 2H, ³J_HH=7, H aryl), 7.99 (m,

4H, H$_{aryl}$), 7.79 (t, 2H, $^3J_{HH}$=5.5, H$_{aryl}$), 7.33 (br s, 2H, H$_{aryl}$), 1.63 (s, 36H, -C(CH$_3$)$_3$).

ESI-MS (CH$_3$CN) *m/z* [M-2PF$_6$]$^{2+}$ 582.16 (found), 582.70 (calcd).

(19)
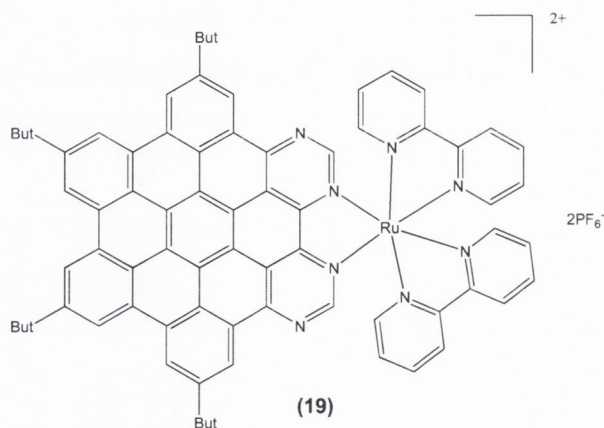
Synthesis of dichlorotetrakis(dimethyl sulfoxide)ruthenium(II), Ru(DMSO)$_4$Cl$_2$ (29)[4]

The procedure was carried out in an argon atmosphere. Ruthenium trichloride hydrate (4 g, 19 mmol) was heated to reflux in dimethyl sulfoxide (20 ml, 282 mmol) for 5 minutes. The volume of DMSO was reduced to half under high vacuum. An addition of acetone (80 ml) gave a yellow precipitate. The yellow complex (**29**) was filtered off on a sintered glass funnel, washed with acetone and diethyl ether and vacuum dried. Yield 5.42 g, 58%.

^{1}**H NMR** (CDCl$_3$) (as per literature assigment): δ 3.45 (s, 2H, H $_{alkyl}$), 3.51 (s, 4H, H $_{alkyl}$), 3.45 (s, 8H, H $_{alkyl}$), 3.34 (s, 4H, H $_{alkyl}$), 2.74 (s, 4H, H $_{alkyl}$), 2.64 (s, 2H, H $_{alkyl}$).

Synthesis of [Ru(1,10-phen)$_3$](PF$_6$)$_2$, (test reaction)

The synthesis was carried out in an argon atmosphere. 1,10-Phenanthroline (298mg, 1.6 mmol) was dissolved in ethanol, which was degassed by bubbling stream of argon through the solution using a syringe for 20 minutes. Then (**16**) (200 mg, 0.4 mmol) was added and the mixture was degassed for a further 20 minutes. The reaction mixture was heated to reflux for 26 h. The colour changed from yellow to deep orange. After cooling, the solution was filtered, and saturated NH$_4$PF$_6$ was added to afford an orange precipitate that was collected by filtration. Product [Ru(1,10-phen)$_3$](PF$_6$)$_2$ was washed with water and diethyl ether. Yield 0.309 mg, 79%.

^{1}H NMR (CDCl$_3$) (as per literature assigment): δ 8.62 (d, 2H, H $_{aryl}$), 8.27 (s, 2H, H $_{aryl}$), 8.05 (d, 2H, H $_{aryl}$), 7.65 (m, 2H, H $_{aryl}$). **ESI-MS** (CH$_3$CN) m/z [M-2PF$_6$]$^{2+}$ 320.9 (found), 320.75 (calcd).

Synthesis of [Ru(N-HSB)$_3$](PF$_6$)$_2$ (28)-route A (first attempt).

The synthesis was carried out in an argon atmosphere. The ligand (**8**) (25 mg, 3.2x10^{-2} mmol) was sonicated in diethylene glycol ethyl ether (6 ml) for 20 minutes. The brown/orange solution was degassed by bubbling a stream of argon through the flask for 30 min. Then ruthenium(III) trichloride (1.7 mg, 0.8x10^{-2} mmol) and 5 drops of N-ethylmorpholine were added. The reaction mixture was degassed for another 20 minutes then heated at 150°C for 44 h. The solution colour changed from orange/brown to khaki. After cooling and filtration the saturated aqueous solution of NH$_4$PF$_6$ was added to the mixture to obtain a greenish precipitate. Column chromatography (Al$_2$O$_3$, toluene/acetonitrile, 3:1) allowed isolation of one product, but in too small quantity for characterization.

Synthesis of [Ru(N-HSB)$_3$](PF$_6$)$_2$ (28)-route B (second attempt).

The synthesis was carried out in an argon atmosphere. A solution of ligand (**8**) (25 mg, 3.2x10^{-2} mmol) in diethylene glycol ethyl ether (5 ml) was sonicated for 20 minutes. The brown/orange solution was degassed by bubbling a stream of argon through the flask for 30 minutes. Then (**16**) (4 mg, 0.8x10^{-2} mmol) was added, the mixture was degassed and heated at 155°C for 74 h. The solvent was evaporated and the mixture was dissolved in acetonitrile. A saturated aqueous solution of NH$_4$PF$_6$ was added to obtain the green precipitate which was collected by filtration. The product (**28**) was purified by column chromatography (Al$_2$O$_3$, THF/acetonitrile/KNO$_{3(sat)}$ 12:4:0.5). Yield 3 mg, 15%.

^{1}H NMR (40°C) (CDCl$_3$): δ 9.91 (s, 2H, H $_{aryl}$), 9.82(s, 2H, H$_{aryl}$), 9.77 (s, 2H, H$_{aryl}$), 9.66 (s, 2H, H$_{aryl}$), 9.61 (s, 2H, H$_{aryl}$), 2.08 (s, 36H, -C(CH$_3$)$_3$). **ESI-MS** (CH$_3$CN) m/z [M-2PF$_6$]$^{2+}$ 1177.15 (found), 1177.95(calcd).
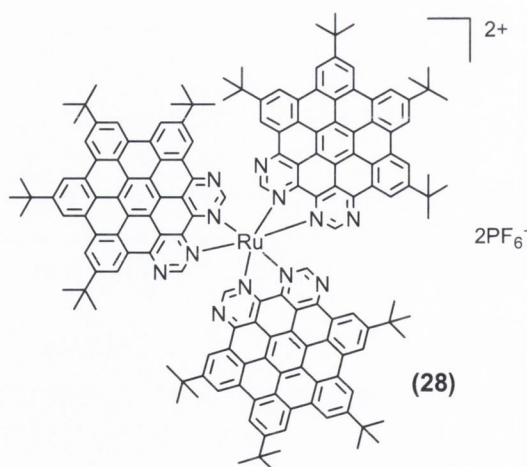
Synthesis of [Ru(9)₃](PF₆)₂ (30)

The synthesis was carried out in an argon atmosphere. A solution of (9) (32 mg, 0.042 mmol) in diethylene glycol ethyl ether (7 ml) was sonicated for 30 min. The orange solution was degassed by bubbling a stream of argon through the flask for 40 min. Then ruthenium(III) trichloride (2.2 mg, 0.011 mmol) was added and the mixture degassed for another 20 min. Then 7 drops of N-ethylmorpholine were added. The reaction mixture was stirred at 145°C for 3 days. The solvent was removed under vacuum, the mixture was dissolved in acetonitrile, filtered off and crashed out by adding a solution of saturated KPF₆. The blue complex was isolated by column chromatography (SiO₂) and preparative plates in THF/CH₃CN/KNO₃ₛₐₜ. (14:4:0.5). The ruthenium complex was obtained in 32% yield, 8 mg.

^{1}**H NMR** (CH₃CN): δ 9.56 (s, 2H, H1), 9.41 (s, 2H, H2), 7.92 (d, 2H, H4), 7.56 (d, 2H, H3), 7.39 (d, 2H, H5 or H6), 7.19 (d, 2H, H5 or H6), 1.37, 1.35 (18H, CH, C(CH₃)₃). **ESI-MS** (CH₃CN) m/z $[M-2PF_6]^{2+}$ 1184.54 (found), 1184.85 (calcd).

(30)
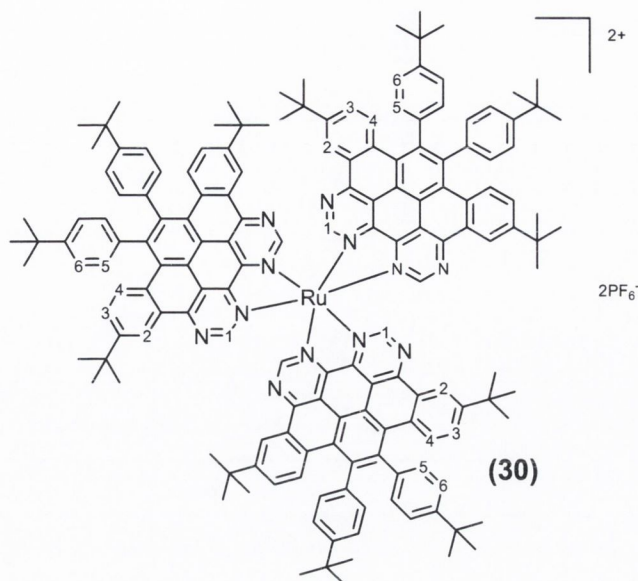
5.4. <u>New N-heterosuperbenzenes</u>

Synthesis of 1,2-dipyrimidyl-3,4,5,6-tetra-phenyl benzene (24)

The synthesis was carried out in an argon atmosphere. A mixture of tetraphenylcyclopentadieone (0.218 g, 0.57 mmol), dipyrimidyl-acetylene (0.1g, 0.57 mmol), and benzophenone (3.5 g) was stirred in a round bottom flask attached to an air condenser under an argon atmosphere. The mixture was heated to reflux at 280°C for 6 hrs. Carbon monoxide was evolved and the colour changed from red to brown. After cooling, the product (**24**) was purified by column chromatography (SiO$_2$, chloroform/ethyl acetate, 4:1). The white product was obtained in 59% yield.

^{1}H NMR (CDCl$_3$): δ 8.78 (s, 2H, H7), 8.25 (s, 4H, H5 and H9), 6.95-6.85 (m, 20H, H10 and H11). **^{13}C NMR** (CDCl$_3$): δ 157.5 (4C, CH, C5 and C9), 155.6 (2C, CH, C7), 142.2, 141.2, 138.7, 138.1, 133.4, 132.7(12C, C$_{quat}$, C$_{aryl}$), 130.6, 130.4, 127.1, 126.5, 126.1, 125.5 (20C, CH, C10,11). **ESI-MS** (MeOH) *m/z* 539.2918 [M-H]$^+$ (calcd 539.2909).

(24)

189
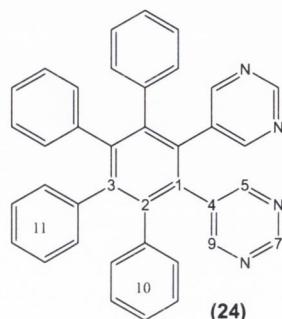
Synthesis of (25) and (26)

The synthesis was carried out in an argon atmosphere. A solution of (**24**) (0.1 g, 0.185 mmol), aluminium trichloride (0.32 g, 2.5 mmol), and copper (II) chloride (0.335 g, 2.5 mmol) in CS_2 (30 ml) was stirred for 5 days at room temperature. The black solid was allowed to settle and the CS_2 removed by cannula. The reaction mixture was stirred with a 10 % ammonia solution (70 ml). The mixture was washed with water and extracted into chloroform, the insoluble precipitate was filtered off. The organic layer from the filtrate was dried over $MgSO_4$. The insoluble brown precipitate of (**26**) was filtered off, washed with diluted potassium hydroxide, diluted hydrochloric acid, water and diethyl ether. The soluble part was purified by chromatography (SiO_2, toluene/methanol, 9:1) and gave the half-cyclised product (**25**) in 5% yield, 4.9 mg.

^{1}H NMR ($CDCl_3$): δ 10.12 (br. s, 2H, H1), 9.54 (d, 2H, J=7.52 Hz, H2), 7.81 (d, 2H, J=8.52 Hz, H5), 7.68 (t, 2H, J=7 Hz, J=7 Hz, H3), 7.38 (br. t, 2H, H4), 7.26, 7.20 (m, 10H, H6). **ESI-MS** (toluene) m/z 533.1753 [M-H]$^+$ (calcd 533.1760).

(25)
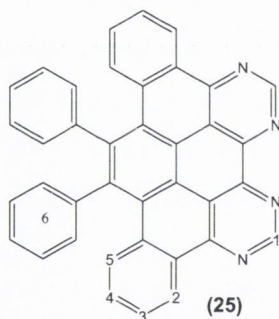
The insoluble brown precipitate (**26**) was identified by MALDI-TOF spectrometry. The analysis showed a peak for the fully-cyclised product (**26**) m/z 527.6 [M-H]$^+$ (calcd) and [M+Cu]$^+$ 591.8. Yield 78 mg, 80%.

(26)

190
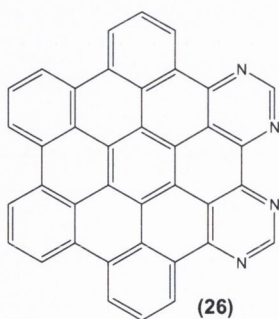
Synthesis of (25) and (27)

The synthesis was carried out in an argon atmosphere. A solution of (**24**) (0.1 g, 0.185 mmol), molybdenum pentachloride (0.606 g, 2.2 mmol), in dichloromethane (20 ml) was stirred for 5 days at room temperature, under an argon atmosphere. Then methanol (10 ml) was added and stirring was continued for an additional hour. The resulting mixture was washed with water and extracted with dichloromethane; the organic layer was dried over MgSO$_4$. The purification on silica preparative plates with toluene/methanol (9:10) as an eluent gave two main products: (**25**) and (**27**) in 32% (31 mg) and 10% (10 mg) yields respectively.

Data for (**25**): **^{1}H NMR** (CDCl$_3$): δ 10.12 (br. s, 2H, H1), 9.54 (d, 2H, J=7.52 Hz, H2), 7.81 (d, 2H, J=8.52 Hz, H5), 7.68 (t, 2H, J=7 Hz, J=7 Hz, H3), 7.38 (br. t, 2H, H4), 7.26, 7.20 (m, 10H, H6). **ESI-MS** (toluene) m/z 533.1756 [M-H]$^+$ (calcd 533.1760).

Data for (**27**): **^{1}H NMR** (CDCl$_3$): δ 9.42 (s, 2H, H1), 9.37 (s, 2H, H2), 9.32 (d, 2H, J = 4 Hz, H3), 7.66 (t, 2H, J = 8 Hz, H4), 7.43 (d, 2H, J = 8 Hz, H6), 7.28 (m, 2H, H5 and H7), 7.19 (m, 2H, H8 and H9), 6.97 (d, 2H, J = 7.3 Hz, H6). **^{13}C NMR** (CDCl$_3$): δ 158.0 (2C, CH, C1), 155.5 (2C, CH, C2), 150.4, 140.9, 140.2, 137.7, 132.3, 129.9, 129.3, 128.1, 123.1 (C$_{quat}$, 9C), 129.4 (2C, CH, C5), 129.0 (2C, CH, C8), 128.8 (2C, CH, C6), 127.4 (2C, CH, C6), 127.0 (2C, CH, C7), 125.2 (2C, CH, C3). **ESI-MS** (toluene), m/z [M-H]$^+$ 533.1777, 533. 1760 (calcd).

(25)   (27)
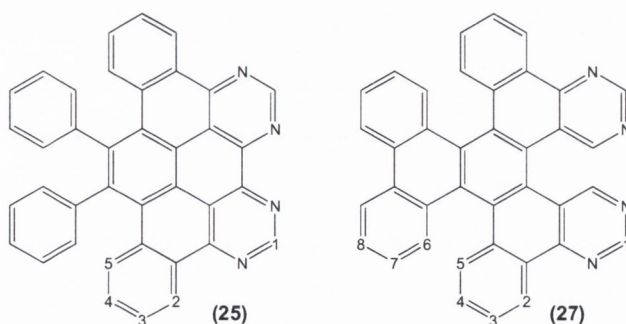
5.5. 3', 4', 5'-substitued terpyridine ligands

Synthesis of [1-(2-pyridyl)-2-phenyl]ethanone (39)[5]

The synthesis was carried out in an argon atmosphere. Benzylchloride (16.5 g, 0.13mol, 15 ml) was added dropwise to a mixture of magnesium (3.17g, 0.132 mol) in dry diethyl ether (60 ml). A gentle reflux was maintained after the addition of benzylchloride.

To this Grignard reagent 2-cyanopyridine (13.6 g, 12.6 ml, 0.132 mol) in diethyl ether (40 ml) was added dropwise. A yellow precipitate was formed, and the mixture was left stirring for 12 hrs. Then a saturated solution of ammonium chloride (200 ml) was added and product was extracted with chloroform. The layers were separated and the organic phase was dried over $MgSO_4$ and reduced to the yellow oil. The crude mixture was column chromatographed (SiO_2, Et_2O/petroleum ether (1:2)) to yield a product (39) in 40% yield (10.3 g).

^{1}H NMR ($CDCl_3$): δ 8.74 (d, 1H, H6), 8.08 (d, 1H, H3), 7.79 (ddd, 1H, H4), 7.44(ddd, 1H, H5), 7.40-7.33 (m, 5H, H$_{phenyl}$), 4.61 (s, 2H, CH_2).

(39)
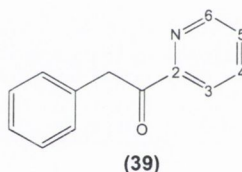
Synthesis of [2,6-di(2-pyridyl)-4-(4-pyridyl)-3,5-diphenyl]-pyridine (41)[6]

4-Pyridinecarboxaldehyde (0.696 g, 6.5 mmol) and NaOH (0.41 g, 0.007 mol, in 4 ml of water) were added in a solution of (39) (2.58 g, 0.013 mol) in ethanol (10 ml). The reaction mixture colour changed from yellow to dark orange. After 20 min. the white precipitate appeared. The mixture was stirred for 3 hrs at room temperature. The white product was filtered off, washed with cold ethanol to give the corresponding diketone in 69% yield (2.8 g).

The diketone (1.5 g, 3.1 mmol) was mixed with ammonium acetate (10.48 g) and heated to reflux in acetic acid (84 ml) for 2 days. The mixture was cooled down, quenched with a 5M NaOH aqueous solution (300 ml). The reaction mixture was extracted with dichloromethane. The organic phase was dried over $MgSO_4$ solvent

192

was evaporated. The recrystalisation from dichlomethane/diethyl ether gave (**41**) as a white precipitate. Yield 0.98 g, 68%; m.p.: 255°C

¹H NMR (CDCl₃): δ 8.51 (d, 2H, J= 5, H9), 8.21 (d, 2H, H19), 7.53 (ddd, 2H, J= 7.5 and 1.5, H7), 7.38 (d, 2H, J= 7.5, H6), 7.12 (ddd, 2H, J= 5 and 1, H8), 7.02 (m, 6H, H13, H14 and H15), 6.92 (m, 4H, H12 and H16), 6.75 (d, 2H, H18). **¹³C NMR**: δ 157.2 (2C, C$_{quat}$, C5), 155.6 (2C, C$_{quat}$, C2), 148.9 (2C, CH, C9), 148.0 (2C, CH, C19), 147.0 (1C, C$_{quat}$, C4), 145.8 (1C, C$_{quat}$, C17), 136.3 (2C, C$_{quat}$, C11), 135.2 (2C, CH, C7), 134.2 (2C, C$_{quat}$, C3), 130.3 (4C, CH, C12 and C16), 127.1 (4C, CH, C13 and C15), 126.4 (2C, CH, C14), 124.8 (2C, CH, C18), 124.5 (2C, CH, C6), 121.8 (2C, CH, C8). **ESI-MS** (MeOH) m/z 463.1934 [M-H]⁺, 631.1923 (calcd).

(**41**)
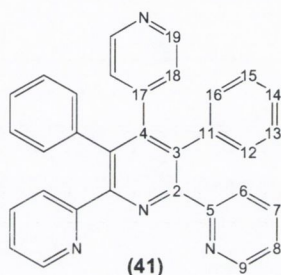
Synthesis of [2,6-di(2-pyridyl)-4-(3-pyridyl)-3,5-diphenyl]-pyridine (42)

3-Pyridinecarboxaldehyde (1.43 g, 0.013 mol) and NaOH (0.82 g, 0.0146 mol, in 8 ml of water) was added to a solution of (**39**) (5.2 g, 0.026 mol) in ethanol (20 ml). The reaction mixture colour changed from yellow to dark orange. After 20 min. the white precipitate was appeared. The mixture was stirred for 3 hrs at room temperature. The white product was filtered off, washed with cold ethanol to give the corresponding diketone in 86% yield (5.5 g).

The diketone (1.5 g, 3.1 mmol) was mixed with ammonium acetate (10.48 g) and heated to reflux in acetic acid (84 ml) for 2 days. The mixture was cooled down, quenched with 5M NaOH aqueous solution (300 ml) and the white product was extracted with dichloromethane. The organic layer was dried over MgSO₄ and solvent was evapotrated. Product (**42**) was recrystalised from dichlomethane/diethyl ether as a white precipitate. Yield 0.78 g, 55%; m.p.: 235°C

¹H NMR (CDCl₃): δ 8.52 (d, 2H, J= 5 and 1.5, H9), 8.21 (d, 1H, H20), 8.09 (s, 1H, H18) 7.53 (ddd, 2H, J= 7.5 and 1.5, H7), 7.40 (d, 2H, J= 7.5, H6), 7.13-7.09(m, 3H, J= 5, H8 and H22), 7.04 (m, 6H, H13, H14 and H15), 6.99-6.89 (m, 5H, H12, H16,

and H21). ^{13}C **NMR**: δ 157.6 (2C, C$_{quat}$, C5), 155.5 (2C, C$_{quat}$, C2), 150.5 (1C, CH, C18), 148.9 (2C, CH, C9), 147.5 (1C, CH, C20), 143.4 (1C, C$_{quat}$, C4), 137.4 (1C, CH, C22), 136.5 (1C, C$_{quat}$, C17), 135.7 (2C, CH, C7), 135.1 (2C, C$_{quat}$, C11), 133.3 (2C, C$_{quat}$, C11), 131.0 (1C, CH, C21), 127.7 (2C, CH, C14), 126.7 (4C, CH, C13, 15), 125.0 (2C, CH, C6), 122.2 (4C, CH, C12 and C16), 122.2 (2C, CH, C8). **ESI-MS** (MeOH) *m/z* 463.1923 [M-H]$^+$, 463.1923 (calcd).

(42)
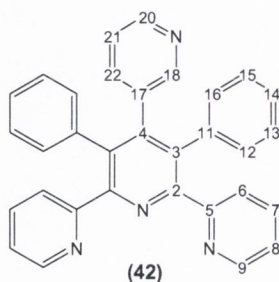
Synthesis of 1-pyridin-2-yl-2-pyridin-4-yl-ethanone (46)[7]

To a solution of diisopropylamine (3 ml, 0.022 mol) in THF (40 ml), at -78°C nBuLi (1.6M (in hexane), 14 ml, 0.022 mol) was added. The mixture was stirred for 10 min and a solution of 4-picoline (2.08 g, 2.2 ml, 0.022 mol) in THF (15 ml) was added over 20 min. The brown/orange mixture was kept at -78°C and ethyl picolinate (3.4g, 3 ml, 0.022 mol) was added (quickly). The mixture was allowed to warm slowly to 0°C, and quenched with water (80 ml). The ethyl acetate (80 ml) was poured to the yellow mixture, and the residual solid was dissolved by addition of acetic acid (1 ml). The product was extracted with ethyl acetate, and organic phase was dried over MgSO$_4$. The purification by column chromatography (SiO$_2$, CH$_2$Cl$_2$/Et$_2$O/MeOH, 10:9:1) gave a yellow product (46) in 80% yield (3.5 g).

^{1}**H NMR** (CDCl$_3$): δ 8.74 (d, 1H, H6), 8.55 (d, 2H, H10, 12), 8.08 (d, 1H, H3), 7.88 (ddd, 1H,H4), 7.52 (ddd, 1H, H5), 7.29 (d, 2H, H9, 13), 4.57 (s, CH$_2$).

(46)
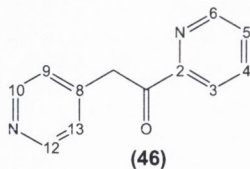
Synthesis of [2,6-di(2-pyridyl)-3,4,5-tri-(4-pyridyl)]-pyridine (51)

The 4-pyridinecarboxaldehyde (0.47 g, 4.4 mmol) and NaOH (0.384 g, 6.9 mmol, in 5 ml of water) were added to a solution of (46) (1.75 g, 8.8 mmol) in ethanol (9 ml). The reaction mixture colour changed from yellow to dark orange. After 1.5 hrs the white precipitate appeared. The mixture was stirred for 24 hrs at room temperature. The white product was filtered off, washed with cold ethanol to give the corresponding diketone in 34% yield (0.72 g).

The diketone (0.4 g, 0.82 mmol) was mixed with ammonium acetate (2.8 g) and was heated to reflux in acetic acid (22.2 ml) for 2 days. The mixture was cooled down, quenched with 5M NaOH aqueous solution (75 ml). The white product was extracted with dichloromethane. The phases were separated and the organic layer was dried over $MgSO_4$. The purification by a column chromatography (SiO_2, $CH_2Cl_2/Et_2O/MeOH$, 10:9:1) gave a white product (51) in 45% yield (0.17 g); m.p.: 278°C

^{1}H NMR ($CDCl_3$): δ 8.30 (d, 2H, J= 5, H9), 8.24 (d, 6H, H13, 15, 19), 7.72 (d, 2H, J= 7.5, H6) 7.66 (ddd, 2H J=7.5 and 2, H7), 7.14 (ddd, 2H, J= 5, H8), 6.83 (d, 4H, H12, 16), 6.73 (d, 2H, H18). **^{13}C NMR**: δ 156.4 (2C, C_{quat}, C5), 155.3 (2C, C_{quat}, C2), 148.7 (2C, CH, C19), 148.4 (4C, CH, C13, 15), 148.2 (2C, CH, C9), 146.8 (1C, C_{quat}, C4), 145.0 (1C, C_{quat}, C17), 143.9 (2C, C_{quat}, C11), 135.9 (2C, CH, C8), 131.7 (2C, C_{quat}, C3), 124.9 (4C, CH, C12. 16), 124.3 (2C, CH, C6), 124.2 (2C, CH, C18), 122.5 (2C, CH, C7). **ESI-MS** (MeOH) m/z 465.1838 [M-H]$^+$, 465.1828 (calcd).

(51)
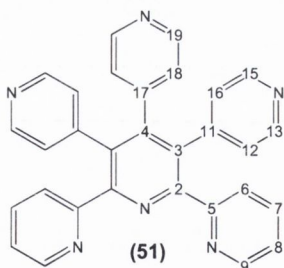
5.6. Complexes of pyridine-centred ligands

Reaction of CuI with (42)

A warm solution of copper(I) iodide (9.5 mg, 0.05 mmol) in acetonitrile (1 ml) and a solution of (42) (23.1 mg, 0.05 mmol) in methanol (1 ml) were mixed and green crystals of (53) appeared overnight. The copper complex was filtered off and washed with diethyl ether. Yield 12 mg, 35%. Anal. Calcd. for $C_{33}H_{25}N_4OCuI$ +$8CH_3CN$+H_2O+$3CH_3OH$+$CHCl_3$: C, 51.09; H, 5.18; N, 13.49; Found: C, 51.38; H, 4.22, N, 13.99.

Reaction of CuI with (51)

A warm solution of (51) (15 mg, 0.03 mmol) in methanol (0.6 ml) was added to the warm solution of copper(I) iodide (5.7 mg, 0.03 mmol) in acetonitrile (0.6 ml). A brown precipitate appeared immediately. After few days green crystals of (55) grew in the reaction mixture. The copper complex was filtered off and washed with diethyl ether. Yield 10 mg, 43%. Anal. Calcd. for $C_{31}H_{20}N_6O_2CuI$+$3CH_3CN$+$3H_2O$+ CH_3OH+$2CHCl_3$: C, 41.89; H, 3.60; N, 10.99; Found: C, 42.25; H, 2.92, N, 10.91.

Reaction of CdSO₄ with (51)

To a warm solution of $CdSO_4$ (0.018 mg, 0.086 mmol) in methanol and water (0.5 ml/1 ml), a solution of (51) (0.02 g, 0.043 mmol) in methanol (1 ml) was added. Clear crystals of (56) appeared overnight. Complex (56) was filtered off and washed with diethyl ether. Yield 17 mg, 45% Anal. Calcd. for $C_{30}H_{20}N_6O_8S_2Cd_3$+$8CH_3OH$+ CH_3CN C, 38.50; H,4.28, N, 9.40; Found: C, 41.91; H, 3.38, N, 9.57.

Reaction of La(NO₃)₃·xH₂O with (41)

A warm solution of (41) (0.023g, 0.05mmol) in methanol (1 ml) was added to a warm solution of $La(NO_3)_3$*xH_2O (0.021g, 0.05mmol) in methanol (1 ml). The white crystals (57) were obtained over night. The crystals were filtered off and washed with

196

diethyl ether. Yield 27 mg, 72 %. Anal. Calcd. for $C_{33}H_{26}N_7O_{10}La$: C, 48.35; H, 3.17, N, 11.96; Found: C, 48.05; H, 3.14, N, 11.61.

Reaction of La(NO₃)₃*xH₂O with (41)

(41) (0.023g, 0.05mmol) was dissolved in warm dichloromethane (1ml) and added to a warm solution of $La(NO_3)_3 \cdot xH_2O$ (0.021g, 0.05mmol) in acetonitrile (1ml). The white crystals of **(58)** were obtained overnight in 65% yield (25 mg). Anal. Calcd. for $C_{32}H_{22}N_7O_9La + \frac{1}{2}CH_2Cl_2$: C, 47.03; H, 2.79, N, 11.81; Found: C, 46.97; H, 2.88, N, 11.84.

Reaction of Sm(NO₃)₃*6H₂O with (41)

$Sm(NO_3)_3 \cdot 6H_2O$ (0.023g, 0.05mmol) was dissolved in warm methanol (1 ml). To this solution **(41)** (0.023g, 0.05mmol) in methanol (1 ml) was added. The mixture was cooled overnight to give white crystals of **(59)**. The crystals were washed with Et₂O. Yield 28 mg, 69%. Anal. Calcd. for $C_{33}H_{26}N_7O_{10}Sm + 2H_2O$: C, 45.72; H, 3.49, N, 11.31; Found: C, 45.57; H, 3.13, N, 11.23.

Synthesis of [Ru(41)₂](PF₆)₂ (60)

The synthesis was carried out in an argon atmosphere. Ligand **(41)** (30 mg, 0.065 mmol) was dissolved in ethylene glycol (4 ml). The solution was degassed by bubbling stream of argon through the flask for 30 minutes. Then RuCl₃ (7 mg, 0.033 mmol) and 4 drops of N-ethynylmorpholine were added. The reaction mixture was heated at 110°C for 18 hrs in an argon atmosphere. After cooling down, a saturated solution of KPF₆ was added, and deep orange precipitate was formed. Complex **(60)** was purified by column chromatography (Al₂O₃, H₂O/CH₃CN/KNO₃, 10:0.5:1.5). Yield 14 mg, 32%.

¹H NMR (CD₃CN): δ 8.30 (br.s, 4H, H19), 7.81 (dd, 4H, *J*= 4.5, and 1.5 and 1, H9), 7.48 (m, 20H, H15), 7.43 (td, 4H, H7), 7.25(td, 4H, *J*=5.5 and 1, H8), 7.17 (br.s, 4H, H18), 6.92 (dd, 4H, *J*= 8.5 H6). **¹³C NMR**: δ 157.8 (4C, C$_{quat}$, C5), 151.6 (4C, CH, C9), 148.1, 148.0 (6C, C$_{quat}$, C2, C4), 144.0 (4C, CH, C19), 138.8 (4C, CH, C7), 136.6, 134,6 (10C, C$_{quat}$, C3, C11, C17), 129.0, 128.8 (20C, CH, C15), 127.3 (4C,

CH, C18), 126.8 (4C, CH, C6), 124.8 (4C, CH, C8). **ESI-MS** (CH$_3$CN) *m/z* 513.1366 [M-2PF$_6$]$^{2+}$ (calcd 513.1368).

(60)
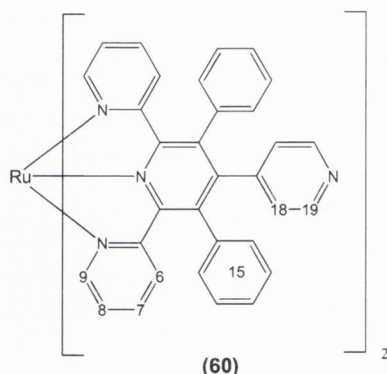
5.7. 4'-Substituted terpyridine ligands

Synthesis of 1,5-bis(2'-pyridyl)pentane-1,3,5-trione (82)[8]

A solution of acetone (1.84 ml, 25 mmol) and ethyl 2-pyridinecarboxylate (10.12 ml, 75 mmol) in 1,2-dimethoxyethane (1,2 DME) (50 ml) was added to a suspension of sodium hydride (80% dispersion in mineral oil; 3.75g) in 1,2 DME (70 ml). The mixture was stirred under an argon atmosphere at room temperature until a vigorous reaction occurred and an orange suspension was obtained. Then the mixture was refluxed for 5.5 hrs, the solvent was evaporated and 120 ml of H$_2$O added to destroy any excess of NaH. The yellow precipitate was dissolved in water to a form dark orange solution, which was filtered through celite. The filtrate was adjusted to pH7, by the addition of diluted HCl dropwise. The yellow precipitate was formed. The yellow solid was collected by filtration washed with water and dissolved in Et$_2$O. The solution was dried over MgSO$_4$. The removing of the solvent yielded a yellow product (82) in 45% yield (3.8 g).

^{1}H NMR (CDCl$_3$): δ 8.67 (d, H11), 8.12 (d, H8), 7.84 (ddd, H9), 7.40 (ddd, H10), 6.81 (s, H1).

(82)

198
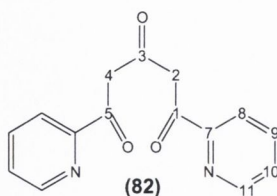
Synthesis of 2,6-bis(2-pyridyl)-4-pyridone (83)[8]

A solution of (82) (2.7g, 0.01 mol) and ammonium acetate (5.4g, 0.07 mol) in 70 ml of ethanol was heated to reflux for 6 hrs, The mixture changed colour from yellow to dark brown. The solution was concentrated to half the original volume, cooled down and a white precipitate was formed. The product was collected by filtration and washed with Et$_2$O. The recrystallisation from ethanol gave white precipitate of (83) in 64% yield (1.6 g).

^{1}H NMR (CDCl$_3$): δ 12.03 (s, NH), 8.78 (d, H9), 7.97 (d, H6), 7.89 (ddd, H7), 7.44 (ddd, H8), 7.32 (s, H3).
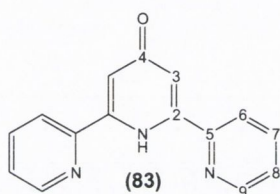
Synthesis of 4'-[[trifluoremethyl)sulfonyl]oxy]-2,2':6',2"-terpyridine (65)[9]

A solution of (83) (1g, 4 mmol) in dry pyridine (10 ml) was treated slowly at 0°C with trifluoromethanesulfonic anhydride (1.188 g, 4 mmol, 0.674 ml). The mixture was stirred at 0°C for 30 min, allowed to warm to room temperature and kept at this temperature for 48 hrs. It was then poured in to ice-water (100 g) and stirred for 0.5 hr. The creamy precipitate was filtered washed with cold water and dried. It was then dissolved in hexane and the insoluble portion was filtered off. Concentration of the mother liquor and cooling gave (65) as a white product, in 76% yield (1.17 g).

^{1}H NMR (CDCl$_3$): δ 8.74 (d, H9), 8.63(d, H6), 8.44 (s, H3), 7.90(ddd, H7), 7.42 (ddd, H8).
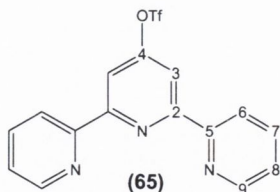
Synthesis of 4'-(phenylethynyl)-2.2':6'2"-terpyridine (85)[10]

Copper iodide (13.8 mg, 0.069 mmol) was added to a degassed solution of phenyl acetylene (0.135 g, 1.35 mmol), (65) (0.342 g, 0.9 mmol) and [Pd(PPh$_3$)$_2$Cl$_2$] (48.3

mg, 0.069 mmol) in toluene and Et$_3$N (1:1, 15 ml). The reaction mixture was stirred at 70°C for 3 hrs. The solvents were removed under vacuo and the product separated by column chromatography (SiO$_2$, DCM+2% acetone). The separation gave (85) as a white product in 88% yield (0.26 g).

^{1}**H NMR** (CDCl$_3$): δ 8.75 (d, J= 4, H9), 8.65 (d, J= 7.6, H6), 8.60 (s, H3), 7.89 (ddd, J= 7.5 and 1.5, H7), 7.61 (m, H13), 7.41 (m, H13), 7.36 (ddd, J= 5.5 and 1, H8). ^{13}**C NMR** (CDCl$_3$): δ 155.2, 155.1, 148.8, 136.5, 133.0, 131.5, 128.6, 128.0, 123.6, 122.4, 120.8.

(85)
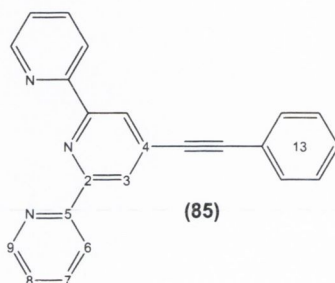
Synthesis of (2,2':6',2"-terpyrid-4yl)-pentaphenylbenzene (86)

The synthesis was carried out in an argon atmosphere. A mixture of (85) (0.3 g, 0.9 mmol), (23) (0.33g, 0.9 mmol) and benzophenone (3.5 g) was stirred and heated at 280°C for 7.5 hrs. Carbon dioxide was evolved and the colour changed from purple to brown. After cooling the product was purified by column chromatography (SiO$_2$, CHCl$_3$/MeOH, 30:1 then polarity was increased to CHCl$_3$/MeOH/NH$_{3aq}$, 10:1:1). The reaction gave (86) as a white powder in 48% yield (0.3 g).

^{1}**H NMR** (CDCl$_3$): δ 8.61 (d, J= 4, H9), 8.36 (d, J= 8, H6), 8.05 (s, H3), 7.35 (ddd, J= 7.6 and 1.5, H7), 7.24 (ddd, J= 4.5 and 1, H8), 7.02 (d, J=7, H14 and H18), 6.86(m, H15, H17, H21-H25 and H28-H30), 6.79 (t, J= 7.5, H16). ^{13}**C NMR** (CDCl$_3$): δ 155.6 (2C, C$_{quat}$, C5), 153.2 (2C, C$_{quat}$, C2), 150.6 (2C, C$_{quat}$, C4), 148.5 (2C, CH, C9), 140.5 (1C, C$_{quat}$), 140.0 (2C, C$_{quat}$), 139.9 (1C, C$_{quat}$), 139.8 (2C, C$_{quat}$), 139.4 (2C, C$_{quat}$), 139.3 (2C, C$_{quat}$), 137.7 (1C, C$_{quat}$), 136.0 (2C, CH, C7), 130.8 (CH), 126.3 (CH), 126.1 (CH), 124.8 (CH), 130.7 (4C, CH, C14 and C18), 125.1 (2C, CH, C16), 123.4 (2C, CH, C3), 122.8 (2C, CH, C8), 120.4 (2C, CH, C6).). **ESI-MS** (MeOH) m/z 690.2918 [M-H]$^+$ (calcd 690.2909).

(86)
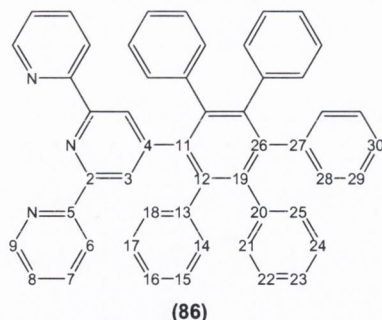
Synthesis of 4'-(4-*tert*-butyl phenylethynyl)-2.2':6'2"-terpyridine (88)

Copper iodide (25 mg, 0.125 mmol) was added to a degassed solution of 4-*tert*-butyl phenyl acetylene (0.389 g, 2.46 mmol), (**65**) (0.62 g, 1.63 mmol) and [Pd(PPh$_3$)$_2$Cl$_2$] (89 mg, 0.127 mmol) in toluene and Et$_3$N (1:1, 25 ml). The reaction mixture was stirred at 70°C for 3 hrs. The solvents were removed under vacuo and the product was separated by column chromatography (SiO$_2$, DCM+2% acetone). The separation gave (**88**) as a white product in 77% yield (0.49 g).

^{1}**H NMR** (CDCl$_3$): δ 8.75 (d, *J*=5.52, H9), 8.65 (d, *J*=8, H6), 8.59 (s, H3), 7.89 (ddd, *J*=8 and 2, H7), 7.55 (m, *J*=8.5, H14), 7.44 (m, *J*=8.5, H15), 7.37 (ddd, *J*=4.5 and 1, H8), 1.36 (s, -C(CH)$_3$). ^{13}**C NMR** (CDCl$_3$): δ 155.3 (2C, C$_{quat}$, C5), 155.0 (2C, C$_{quat}$, C2), 154.7 (1C, C$_{quat}$, C4), 151.9 (2C, CH, C9), 148.7, 133.3 (2C, C-C), 136.5 (2C, CH, C7), 123.6 (2C, CH, C3), 122.4 (2C, CH, C8), 120.8 (2C, CH, C6), 131.3, 125.1, (4C, C$_{quat}$, C$_{aryl}$), 119.0, 116.2 (4C, CH, C14,15), 34.5 (1C, C$_{quat}$, C17), 30.1 (3C, CH , -C(CH)$_3$).

(88)
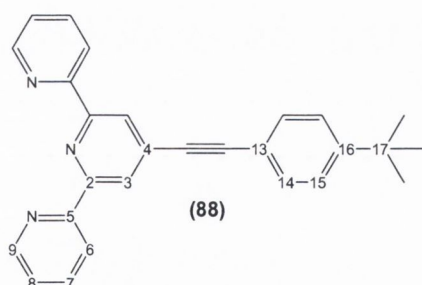
Synthesis of (2,2':6',2"-terpyrid-4yl)-penta(4-*tert*butylphenyl)benzene (89)

The synthesis was carried out in an argon atmosphere. A mixture of (**88**) (0.127 g, 0.33 mmol), (**23**) (0.2g, 0.33 mmol) and benzophenone (1.5 g) was stirred and heated at 280°C for 7.5 hrs. Carbon dioxide was evolved and colour changed from purple to brown. After cooling the product was purified by column chromatography (SiO$_2$,

CHCl₃/MeOH, 30:1gradient elution). The reaction gave (**89**) as a white powder in 56% yield (0.17 g).

¹H NMR (CDCl₃): δ 8.60 (d, J=4, H9), 8.11 (d, J=8, H6), 7.83 (s, H3), 7.67 (ddd, J=8 and 1.5, H7), 7.20 (ddd, J=4.5, H8), 6.84, 6.73(m, H14, H15, H21, H22, H25, H26, H32, H33, H36 and H37), 1.13, 1.12 (s, 45H, -C(CH₃)₃). **¹³C NMR** (CDCl₃): δ 155.1 (2C, C$_{quat}$, C5), 153.5 (2C, C$_{quat}$, C2), 150.8 (1C, C$_{quat}$, C4), 149.0 (2C, CH, C9), 147.4(C$_{quat}$), 147.0 (C$_{quat}$), 140.9 (C$_{quat}$), 140.2 (C$_{quat}$), 139.3 (C$_{quat}$), 135.7 (C$_{quat}$), 136.7 (2C, CH, C7), 131.1 (CH), 131.0 (CH), 123.0 (CH), 122.6 (CH), 124.3 (2C, CH, C3), 122.4 (2C, CH, C8), 121.0 (2C, CH, C6), 33.5 (5C, C$_{quat}$, C17, 28, 39), 30.7, 30.4 (15C, CH, C18, 19, 20, 29, 30, 31, 41, 42, 43).). **ESI-MS** (MeOH) m/z [M-H]⁺ (calcd).

(**89**)
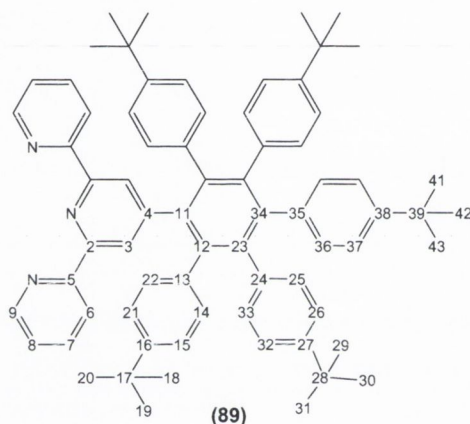
Synthesis of (90)

The synthesis was carried out in an argon atmosphere. A solution of iron(III) chloride (0.5g, 3 mmol) in nitromethane (4.5 ml) was added dropwise to a stirred solution of (**89**) (0.15g, 0.154 mmol) in dichloromethane (35 ml). Argon was bubbled though the mixture for 2 hrs. Then the mixture was stirred in an argon atmosphere for 48 hrs. The reaction mixture was quenched with methanol (50 ml), washed with water and extracted with dichlometahne. The phases were separated and the organic phase was dried over MgSO₄. The yellow product (**90**) was purified by column chromatography (SiO₂, CHCl₃/MeOH (1:1) then CHCl₃/MeOH/NH₃ₐq, (1:1:0.5)). Yield 50 mg, 32%.

¹H NMR (CDCl₃): δ 9.16 (s, H37), 9.11 (s, H26), 8.98 (s, H32), 8.69 (s, H15. H3), 8.67 (d, J= 7.5, H6), 8.62 (d, J= 4, H9), 7.91 (ddd, J= 7.5 and 1.5, H7), 7.51 (d, J= 9, H22), 7.33 (ddd, J= 6 and 1, H8), 6.98 (d, J= 8.5, H21), 1.81 (s, 27H, H29, H30, H31, H41, H42 and H43), 1.37 (s, 18H, H18, H19 and H20). **¹³C NMR** (CDCl₃): δ

202

156.2 (2C, C$_{quat}$, C5), 155.8 (2C, C$_{quat}$, C2), 155.2 (2C, C$_{quat}$, C4), 148.9 (2C, CH, C9), 148.7 (C$_{quat}$), 136.2 (2C, CH, C22), 132.0 (C$_{quat}$), 131.5 (2C, CH, C22), 130.9 (C$_{quat}$), 129.8 (C$_{quat}$), 129.3 (C$_{quat}$,), 127.3 (2C, CH, C3), 125.5 (C$_{quat}$), 124.5 (C$_{quat}$), 123.1 (2C, CH, C8), 122.7 (C$_{quat}$), 122.5 (C$_{quat}$), 122.3 (C$_{quat}$), 121.7 (2C, CH, C21), 120.8 (2C, CH, C6), 118.8 (2C, CH, C15), 118.5 (2C, CH, C37), 118.4 (2C, CH, C26), 117.5 (2C, CH, C32), 35.2, 34.3 (5C, C$_{quat}$, C17, C28 and C39), 31.5, 31.4 (9C, CH, -C(CH)$_3$), 30.7 (6C, CH, -C(CH)$_3$).). **ESI-MS** (MeOH) *m/z* 962.5399 [M-H]$^+$ (calcd 962.5413).

(90)
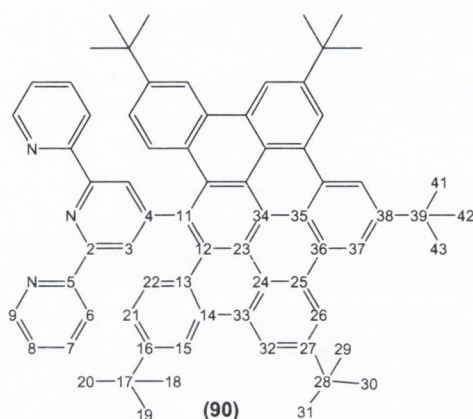
5.8. Ruthenium(II) complexes of terpyridine-type ligands

Synthesis of [Ru(86)$_2$](PF$_6$)$_2$ (91)

The synthesis was carried out in an argon atmosphere. Ligand (**86**) (50 mg, 0.73 mol) was dissolved in a 1:1 mixture of ethanol/chloroform (5 ml). The solution was degassed by bubbling stream of argon through the flask. After 30 minutes RuCl$_3$ (7.5 mg, 0.36 mol) was added, and the reaction mixture was flushed with argon for 20 min, and 4 drops of N-ethynylmorpholine were added. The reaction mixture was heated to reflux for 6 hrs. After cooling down, the mixture was filtered and the chloroform was evaporated. To the ethanol solution a saturated solution of KPF$_6$ was added and a deep orange precipitate was formed. Complex (**91**) was purified by column chromatography (Al$_2$O$_3$, CH$_3$CN/KNO$_3$/H$_2$O, 10:0.5:1.5). Yield 19 mg, 30%.

¹H NMR (CD$_3$CN): δ 8.13 (s, 4H, H3), 8.07 (dd, *J*= 8, 4H, H6), 7.83 (td, *J*= 7.5, 4H, H7), 7.25 (d, *J*= 7.5, 4H, H15), 7.18 (td, *J*= 6.5, 4H, H8), 7.09-6.96 (m, 34H, H14,

rings a,b), 6.90 (td, *J*=7, 4H, H16), 6.60 (dd, *J*=5.5, 4H, H9). **ESI-MS** (CH$_3$CN) *m/z* 740.2365 [M-2PF$_6$]$^{2+}$ (calcd 740.2352).

(91)
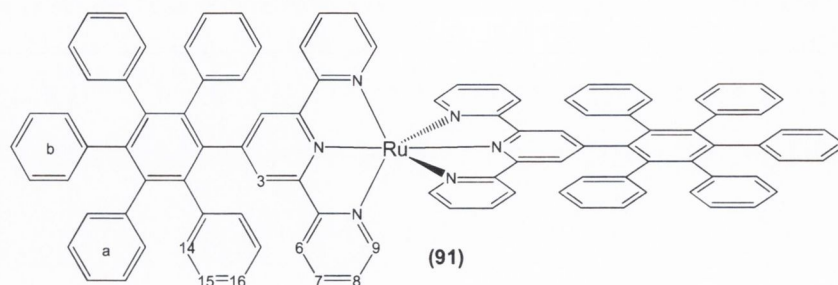
Synthesis of Ru(terpy)Cl$_3$[11]

A solution of 2,2':6',2"-terpyridine (100 mg, 0.429 mmol) and RuCl$_3$ (89 mg, 0.429 mmol) in ethanol (10 ml) was heated to reflux for 3 hrs. The mixture was cooled and Ru(terpy)Cl$_3$ was filtered off. Product was washed with few portions of ethanol. Yield 0.12 g, 66%.

Synthesis of [Ru(terpy)(89)](PF$_6$)$_2$ (92)

The synthesis was carried out in an argon atmosphere. Ligand (**89**) (20 mg, 0.021 mmol) was dissolved in ethylene glycol (4 ml) and the mixture was degassed by bubbling stream of argon through the flask for 30 min. Then Ru(terpy)Cl$_3$ (9.1 mg, 0.021 mmol) was added and the reaction mixture was heated to 92°C for 6 hrs. After cooling down, a saturated solution of KPF$_6$ was added to obtain a deep orange precipitate. Complex (**92**) was purified by silica preparative plates with (CH$_3$CN/KNO$_3$/H$_2$O, 10:0.5:1.5) as the system of solvents. Product (**92**) was isolated in 30% yield (9.7 mg).

^{1}H NMR (CD$_3$CN): δ 8.74 (dd, *J*=8, 2H, H3'), 8.50 (dd, *J*=8, 2H, H6'), 8.39 (td, *J*=8, 1H, H4'), 7.96 (td, *J*=8, 2H, H7'), 7.92 (s, 2H, H3), 7.84 (dd, *J*=7.5, 2H, H6), 7.77 (td, *J*=7.5, 2H, H7), 7.34 (td, *J*=6.5, 2H, H8'), 7.19 (td, 2H, H8), 7.16-7.08 (m, 8H and H for rings a,b,c), 7.06 (dd, 2H, H9), 7.04 (dd, 2H, H9'), 7.02 (d, *J*=8, 2H, a,b,c), 6.96 (dd, *J*=8, 6H, a,b,c), 6.84 (dd, *J*=8, 4H and H for a,b,c), 1.16, 0.8 (s, 45H, -C(CH)$_3$). **^{13}C NMR** (CD$_3$CN): δ 158.1 (C$_{quat}$, C$_{aryl}$), 157.3 (C$_{quat}$, C$_{aryl}$), 155.0 (C$_{quat}$,

C$_{aryl.}$), 152.7 (C$_{quat}$, C$_{aryl.}$), 152.3 (2C, CH, C8), 150.9 (2C, CH, C9), 149.3 (C$_{quat}$, C$_{aryl.}$), 149.0 (C$_{quat}$, C$_{aryl.}$), 148.6 (C$_{quat}$, C$_{aryl.}$), 148.3 (C$_{quat}$, C$_{aryl.}$), 143.2 (C$_{quat}$, C$_{aryl.}$), 141.1 (C$_{quat}$, C$_{aryl.}$), 140.0 (C$_{quat}$, C$_{aryl.}$), 129.6 (C$_{quat}$, C$_{aryl.}$), 128.2 (C$_{quat}$, C$_{aryl.}$), 138.0 (2C, CH, C7), 137.7 (2C, CH, C7'), 135.5 (2C, CH, C4'), 136.9, 136.5, 135.6, 131.9, 130.8, 130.6, 126.2, 123.3 (C, CH, a,b,c), 127.5 (2C, CH, C8'), 127.0 (2C, CH, C3), 124.4 (2C, CH, C6), 123.9 (2C, CH, C3'), 123.7 (2C, CH, C9'), 123.5 (2C, CH, C6), 33.7 (5C, C$_{quat}$, -C(CH)$_3$), 30.3, 30.1 (15C, CH, -C(CH)$_3$). **ESI-MS** (CH$_3$CN) m/z 652.2985 [M-2PF$_6$]$^{2+}$ (calcd 652.2979).

(92)
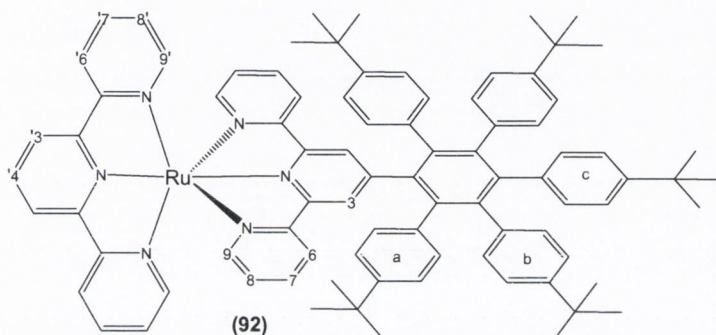
Synthesis of [Ru(terpy)(90)](PF$_6$)$_2$ (93)

Ligand (89) (20 mg, 0.021 mmol) was dissolved in ethylene glycol (4 ml) and the mixture was degassed by bubbling stream of argon through the flask for 30 min. Then Ru(terpy)Cl$_3$ (9.1 mg, 0.021 mmol) was added and the reaction mixture was heated to 92°C for 6 hrs. After cooling down, a saturated solution of KPF$_6$ was added to obtain deep orange precipitate. Complex (93) was purified by silica preparative plates with (CH$_3$CN/KNO$_3$/H$_2$O, 10:0.5:1.5) as the system of solvents. Product (92) was separated in 30% yield (9.9 mg).

^{1}H NMR (CD$_3$CN): δ 9.36 (s, 2H, H37), 9.32 (s, 2H, H26), 9.21 (s, 2H, H32), 9.09 (s, 2H, H3), 8.93 (s, 2H, H15), 8.88 (d, J=8, 2H, H3'), 8.65 (d, J=8, 2H, H6'), 8.52 (td, J=8, 1H, H4'), 8.19 (d, J=8, 2H, H6), 8.11 (td, J=7.5, 2H, H7'), 7.85 (m, 4H, H7 and H22), 7.79 (dd, J=5.5, 2H, H9'), 7.52 (td, J=6, 2H, H8'), 7.47 (dd, J=5, 2H, H9), 7.28 (dd, J=8.5, 2H, H21), 7.22 (td, J=6, 2H, H8), 1.85, 1.42 (s, 45H, -C(CH)$_3$). **^{13}C NMR** (CD$_3$CN): δ 158.3 (C$_{quat}$, C$_{aryl.}$), 158.1 (C$_{quat}$, C$_{aryl.}$), 156.0 (C$_{quat}$, C$_{aryl.}$), 155.2 (C$_{quat}$, C$_{aryl.}$), 152.8 (C$_{quat}$, C$_{aryl.}$), 152.5 (2C, CH, C9), 151.6 (2C, CH, C9'), 150.8, 150.6, 150.4 (C$_{quat}$, C$_{aryl.}$), 138.3 (2C, CH, C7'), 137.9 (2C, CH, C7), 135.9 (2C, CH,

C4'), 132.7 ($C_{quat.}$, $C_{aryl.}$), 132.0 ($C_{quat.}$, $C_{aryl.}$), 130.4 ($C_{quat.}$, $C_{aryl.}$), 130.2 ($C_{quat.}$, $C_{aryl.}$), 130.0 ($C_{quat.}$, $C_{aryl.}$), 129.7 ($C_{quat.}$, $C_{aryl.}$), 127.4 (C, $C_{quat.}$, $C_{aryl.}$), 132.0 (2C, CH, C22), 127.9 (2C, CH, C3), 127.3 (2C, CH, C8), 127.1 (2C, CH, C8'), 125.0 ($C_{quat.}$, $C_{aryl.}$), 122.9 ($C_{quat.}$, $C_{aryl.}$), 122.0 ($C_{quat.}$, $C_{aryl.}$), 121.8 ($C_{quat.}$, $C_{aryl.}$), 121.0 ($C_{quat.}$, $C_{aryl.}$), 120.3 ($C_{quat.}$, $C_{aryl.}$), 124.6 (2C, CH, C6'), 124.1 (2C, CH, C6), 123.9 (2C, CH, C3'), 122.6 (2C, CH, C21), 120.2 (2C, CH, C15), 119.8 (2C, CH, C37), 119.7 (2C, CH, C26), 118.7 (2C, CH, C32), 35.6, 35.5 (5C, $C_{quat.}$, -$C(CH)_3$), 31.0, 30.4 (15C, CH, -$C(CH)_3$). **ESI-MS** (CH_3CN) *m/z* 648.775 $[M-2PF_6]^{2+}$ (calcd 648.550).

(93)
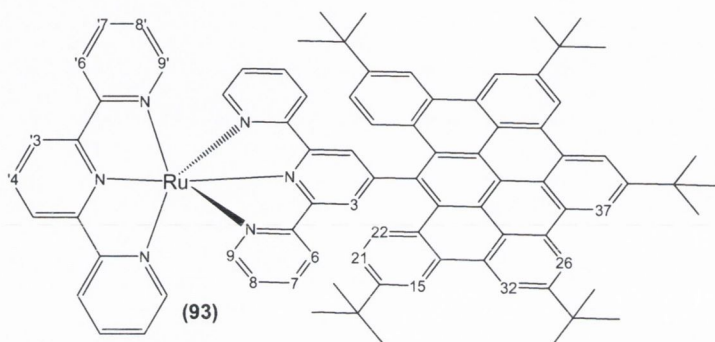
5.9. Platinium(II), Palladium(II) and Iron(II) complexes of terpyridine-type ligands

Synthesis of Pt(DMSO)$_2$Cl$_2$[12]

K_2PtCl_2 (0.1g, 0.24 mmol) was dissolved in water (1.1 ml) and dimethylsulfoxide (0.05 ml, 0.72 mmol) was added. The mixture was allowed to stand overnight at room temperature to obtaine bright yellow crystals. The complex was filtered, washed with water, ethanol and diethyl ether. Yield 85 mg, 84%. Anal. Calcd. for $C_8H_{24}O_4S_4PtCl_2$+3DMSO+2.3H_2O: C, 11.24; H, 2.81, S, 14.98; Found: C,11.24; H, 2.74, N, 14.78.

Synthesis of [Pt(89)Cl]Cl (103)

A solution of Pt(DMSO)$_2$Cl$_2$ (0.012 g, 0.028 mmol) in chloroform (2 ml) was added to a solution of ligand (89) (0.034 g, 0.037 mmol) in chloroform (2 ml). The mixture was heated at 55°C for 24 hrs. After cooling the solvent was evaporated, the crude mixture was dissolved in dichlomethane and product (103) (yellow precipitate) was crashed out by adding diethyl ether. Yield 15 mg, 35%.

^{1}H NMR (CDCl$_3$): δ 8.53 (d, J=5.5, H9), 8.49 (ddd, J=8, H7), 7.97 (d, J=8, H6), 7.67 (ddd, H8), 7.67 (s, H3), 7.01, 6.98 (d, J=8, 8H, H14, H15, H21 and H22), 6.89, 6.72 (d, J=8.5, 12H, H25, H26, H32, H33, H36 and H37), 1.12, 0.97 (s, 45H, -C(CH)$_3$). ^{13}C NMR (CDCl$_3$): δ 157.5, 151.7 (6C, C$_{quat}$, C2, 4, 5), 150.6 (2C, CH, C9), 148.8 (C$_{quat}$, C$_{aryl}$), 147.8 (C$_{quat}$, C$_{aryl}$), 147.7 (C$_{quat}$, C$_{aryl}$), 143.5 (C$_{quat}$, C$_{aryl}$), 141.4 (C$_{quat}$, C$_{aryl}$), 138.8 (C$_{quat}$, C$_{aryl}$), 136.2 (C$_{quat}$, C$_{aryl}$), 135.9 (C$_{quat}$, C$_{aryl}$), 134.0 (C$_{quat}$, C$_{aryl}$), 142.6 (2C, CH, C7), 131.0 (CH, C$_{aryl}$), 130.2 (CH, C$_{aryl}$), 130.1 (CH, C$_{aryl}$), 124.1 (CH, C$_{aryl}$), 123.0 (CH, C$_{aryl}$), 122.9 (CH, C$_{aryl}$) 128.4 (2C, CH, C8), 126.4 (2C, CH, C3), 124.6 (2C, CH, C6), 33.8, 33.6 (5C, C$_{quat}$, -C(CH)$_3$), 30.6, 30.5 (15C, CH, -C(CH)$_3$). **ESI-MS** (MeOH) m/z 1199.5242 [M-Cl]$^+$ (calcd 1199.5297).

(103)
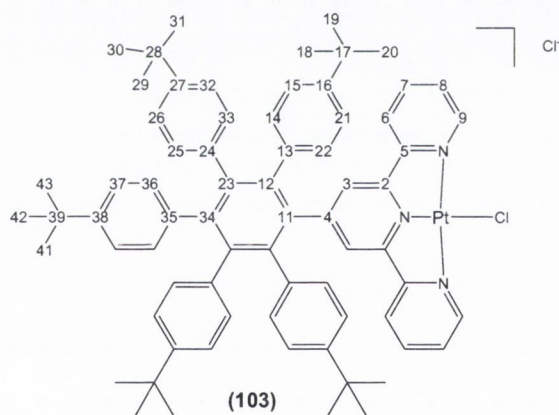
Synthesis of [Pt(89)Cl]PF$_6$ (103a)

The counterion exchange reaction was carried out in methanol. A saturated metahanolic solution of NH$_4$KP$_6$ was added to complex (103) in methanol. Complex (103a) was crashed out as yellow needles in 65% yield.

Synthesis of Na$_2$Pd$_2$Cl$_4$[6]

PdCl$_2$ (0.5 g, 2.8 mmol) and NaCl (0.33g, 5.6 mmol) were dissolved in methanol (9 ml). The mixture was heated at 50°C until all the NaCl had reacted. The brown solution was filtered off and 50 ml solution of 0.056M Na$_2$Pd$_2$Cl$_4$ in methanol was prepared in 50 ml volumetric flask.

Synthesis of [Pd(89)Cl]Cl (104)

Ligand (**89**) (0.025 g, 0.026 mmol) was dissolved in chloroform / methanol (3 ml/1 ml) and added to the solution of Na$_2$Pd$_2$Cl$_4$ (0.056M, 2.3 ml, 0.013 mmol). The reaction mixture was heated to reflux for 18 hrs. After cooling the solvent was evaporated, the crude mixture was dissolved in dichlomethane and adding diethyl ether crashed out the yellow product out. Yield 12 mg, 42%.

^{1}H NMR (CDCl$_3$): δ 8.79 (d, 2H, H9), 8.41 (br. ddd, 2H, H7), 7.74 (d, 2H, H6), 7.74 (br. ddd, 2H, H8), 7.48 (s, 2H, H3), 7.07, 6.92 (2d, J=7, J=7.5, 8H, H14, H15, H21 and H22), 6.90, 6.74 (m, J=8.5, J=8.5, 12H, H25, H26, H32, H33, H36 and H37), 1.12, 1.02 (s, 45H, -C(CH)$_3$). **^{13}C NMR** (CDCl$_3$): δ 157.3, 156.1, 152.0 (6C, C$_{quat}$, C2, 4, 5), 152.5 (2C, CH, C9), 148.9 (C$_{quat}$, C$_{aryl}$), 147.6 (C$_{quat}$, C$_{aryl}$), 147.5 (C$_{quat}$, C$_{aryl}$), 142.1 (C$_{quat}$, C$_{aryl}$), 141.3 (C$_{quat}$, C$_{aryl}$), 139.3 (C$_{quat}$, C$_{aryl}$), 136.5 (C$_{quat}$, C$_{aryl}$), 136.1 (C$_{quat}$, C$_{aryl}$), 135.7 (C$_{quat}$, C$_{aryl}$), 133.7 (C$_{quat}$, C$_{aryl}$), 143.4 (2C, CH, C7), 131.2 (CH, C$_{aryl}$), 130.4 (CH, C$_{aryl}$), 130.2 (CH, C$_{aryl}$), 124.0 (CH, C$_{aryl}$), 122.9 (CH, C$_{aryl}$), 122.8 (CH, C$_{aryl}$), 128.5 (2C, CH, C8), 126.6 (2C, CH, C3), 124.2 (2C, CH, C6), 33.8, 33.6 (5C, C$_{quat}$, -C(CH)$_3$), 30.6, 30.5 (-C(CH)$_3$). **ESI-MS** (MeOH) m/z 1110.4653 [M-Cl]$^+$ (calcd 1110.4684).

(104)

Synthesis of [Pd(89)Cl]PF$_6$ (104a)

The counterion exchange reaction was carried out in methanol. A saturated metahanolic solution of NH$_4$KP$_6$ was added to complex (**104**) in methanol. Complex (**104a**) was crashed out as a yellow precipitate in 45% yield.
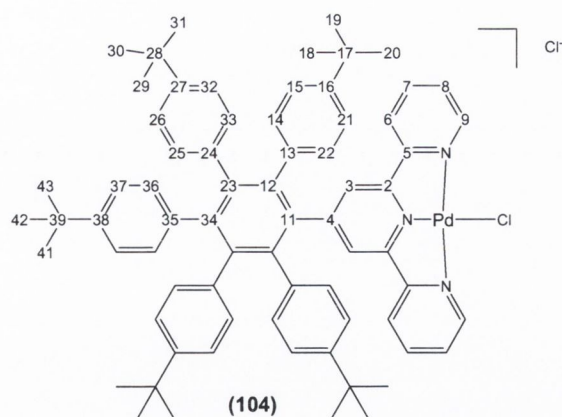
Synthesis of [Fe(86)$_2$](PF$_6$)$_2$ (105)

A solution of iron(III) chloride (0.47g, 2.9 mmol) in nitromethane (3 ml) was added dropwise to a stirred solution of (**86**) (0.1g, 0.145 mmol) in dichloromethane (20 ml). The mixture was stirred and argon was bubbled through reaction mixture for 1 hr. The reaction mixture was quenched with methanol (20 ml) and washed with water. The product was extracted into dichloromethane. The layers were separated and the organic phase was dried over MgSO$_4$. The purple product was separated by column chromatography (SiO$_2$, CHCl$_3$/MeOH, 1:1). Yield 40 mg, 40%.

^{1}H NMR (CD$_3$CN): δ 8.32 (s, 2H, H3), 8.07 (d, 2H, *J*=8 Hz, H6), 7.82 (ddd, 2H, *J*=8 Hz, *J*=8 Hz, H7), 7.32 (d, 4H and H for ring a), 7.33-6.92 (m, 25H, H8 and H for ring a). **^{13}C NMR** (CD$_3$CN): δ 157.5 (4C, C$_{quat}$, C5), 156.9 (4C, C$_{quat}$, C2), 155.9 (2C, C$_{quat}$, C4), 151.0 (4C, CH, C9), 140.4 (C$_{quat}$, C$_{aryl.}$), 139.6 (C$_{quat}$, C$_{aryl.}$), 139.3 (C$_{quat}$, C$_{aryl}$), 139.2 (C$_{quat}$, C$_{aryl.}$), 138.3 (4C, CH, C7), 130.8 (4C, CH, C8), 126.4 (4C, CH, C3), 131.4 (CH, C$_{aryl}$), 130.7 (CH, C$_{aryl}$) 126.8 (CH, C$_{aryl}$), 126.5 (CH, C$_{aryl}$), 125.9 (CH, C$_{aryl}$), 125.6 (CH, C$_{aryl}$), 125.3 (CH, C$_{aryl}$), 122.9 (CH, C$_{aryl}$). **ESI-MS** (MeOH) *m/z* 717.7422 [M-2PF$_6$]$^{2+}$ (calcd 717.7443).

(105)
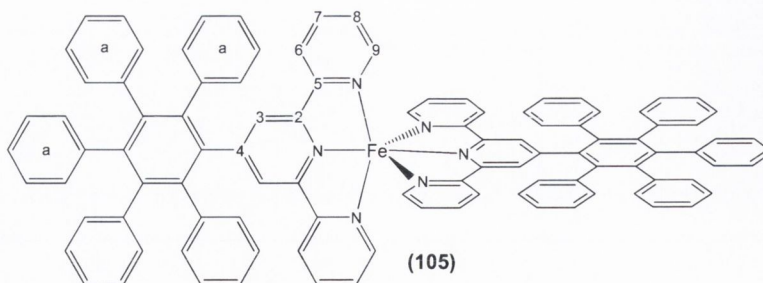
Synthesis of [Fe(89)$_2$](PF$_6$)$_2$ (106)

A solution of [Fe(H$_2$O)$_6$](BF$_6$)$_2$ (3.5 mg, 0.01 mmol) in methanol (2 ml) was added to a solution of (89) (20 mg, 0.02 mmol) in warm methanol (2 ml). The reaction mixture was heated at 50°C for 20 min. Then the purple solution was cooled down and addition of a saturated aqueous solution of KPF$_6$ resulted in the formation of (106) as a dark deep purple precipitate. Yield 19 mg, 79%.

^{1}H NMR (CD$_3$CN): δ 8.01 (s, 4H, H3), 7.81-7.78 (m, 8H, H6 and H7), 7.23-7.18 (m, 12H, H8 and H for ring a), 7.03-6.96 (m, 20H and H forring a) 6.85 (d, J=5.5, 4H and H for ring a), 6.63 (d, 4H, J=5.5, H9), 1.16, 0.71 (s, 90H, -C(CH)$_3$). ^{13}C NMR (CD$_3$CN): δ 157.1 (4C, C$_{quat}$, C5), 157.0 (4C, C$_{quat}$, C2), 151.3 (4C, CH, C9), 150.9 (2C, C$_{quat}$, C4), 149.2 (C$_{quat}$, C$_{aryl.}$), 148.4 (C$_{quat}$, C$_{aryl.}$), 148.0 (C$_{quat}$, C$_{aryl.}$), 143.2 (C$_{quat}$, C$_{aryl.}$), 140.8 (C$_{quat}$, C$_{aryl.}$), 139.5 (C$_{quat}$, C$_{aryl.}$), 136.7 (C$_{quat}$, C$_{aryl.}$), 136.6 (C$_{quat}$, C$_{aryl.}$), 136.0, (C$_{quat}$, C$_{aryl.}$), 138.6 (4C, CH, C7), 131.6, 130.5, 130.2 (20C, CH, a) 126.9 (4C, CH, C8), 126.0 (4C, CH, C3), 123.2 (4C, CH, C6), 123.6 (CH, C$_{aryl}$), 122.9 (CH, C$_{aryl}$), 122.7 (CH, C$_{aryl}$), 33.3, 29.4 (10C, C$_{quat}$, -C(CH)$_3$), 30.0, 29.9, 29.7 (30C, CH, -C(CH)$_3$). **ESI-MS** (CH$_3$CN) m/z 1996.1370 [M-2PF$_6$]$^{2+}$ (calcd 1996.1350).

(106)
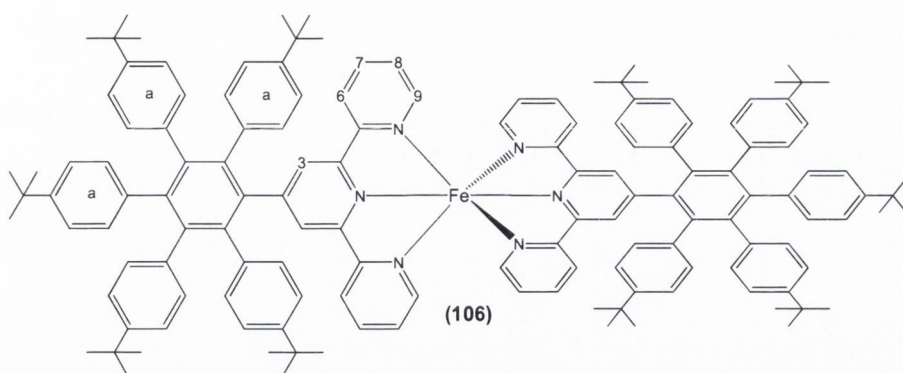
Synthesis of [Fe(88)₂](PF₆)₂ (107)

A solution of [Fe(H₂O)₆](BF₆)₂ (13 mg, 0.08 mmol) in methanol (3 ml) was added to a solution of (88) (20 mg, 0.02 mmol) in warm methanol (3ml). The deep purple reaction mixture was heated at 50°C for 20 min. Then the mixture was cooled down and a saturated aqueous solution of KPF₆ was added to crash out the product. (107) was collected as a dark deep purple precipitate in 85%yield (25 mg).

¹H NMR (CD₃CN): δ 9.04 (s, 4H, H3), 8.51(d, 4H, J=8, H6), 7.93 (ddd, 4H, J=8, H7), 7.79 (d, 4H, J=8, H14), 7.67 (d, 4H, J=8, H15), 7.18 (d, 4H, J=5.5, H9,) 7.11 (ddd, 4H, J=6, H8,) 1.42 (s, 18H, -C(CH₃)₃). **¹³C NMR** (CD₃CN): δ 159.6 (4C, C$_{quat}$, C5), 156.9 (4C, C$_{quat}$, C2), 153.6 (4C, C$_{quat}$, C11.12), 152.7 (4C, CH, C7), 138.5 (4C, CH, C8), 132.2 (2C, C$_{quat}$, C10), 131.5 (4C, CH, C14), 127.1 (4C, CH, C6), 125.7 (4C, CH, C15), 125.5 (4C, C$_{quat}$, C13, 17), 124.6 (4C, CH, C3), 123.5 (4C, CH, C9), 97.7 (4C, CH, C15), 85.4 (4C, CH, C15), 34.3 (2C, C$_{quat}$, C17), 29.8, 29.4 (6C, CH, -C(CH)₃). **ESI-MS** (CH₃CN) m/z 843.3124 [M-2PF₆]²⁺ (calcd 834.3133).

(107)

211
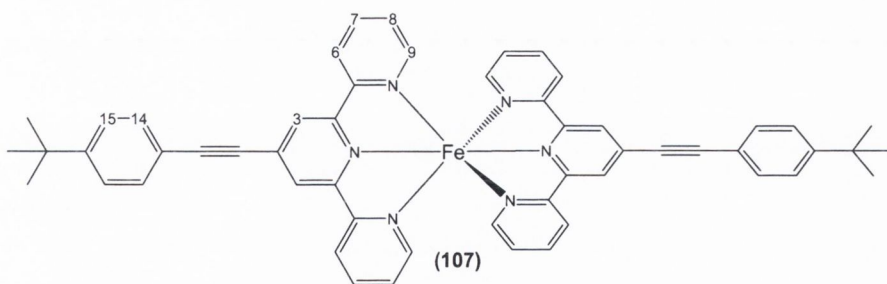
5.10. <u>References</u>

[1] S. M. Draper, D. Gregg, R. Madathil, *J. Am. Chem. Soc.*, **2002**, 124, 3486-34

[2] D. J. Gregg, E. Bothe, P. Höfer, P. Passaniti, S. M. Draper, *Inorg. Chem.,* **2005**, 44, 5654-5660

[3] S. M. Draper, D. J. Gregg, E. R. Schofield, W. R. Browne, *J. Am. Chem. Soc.*, **2004**, 126, 8694-8701

[4] I. P. Evans, A. Spencer, G. Wilkinson, *J. Chem. Soc., Dalton Trans.*, **1972**, 204-209

[5] G. M. McCann, R. A. More O'Ferrall, S. M. Walsh, *J. Chem. Soc. Perkin Trans. 2*, **1997**, 2761

[6] Cecile Ollagnier, PhD thesis, New N-and S-containing polyaryl compounds as ligands in transition metal complexes, **2005**, TCD

[7] B. D. Wade, R. Bonjouklian, L. Junkai, W. T. McMillen, P. B. Lee, S. J. Scott, J. M. Yingling, Y. J. Schulenburg, **2004**, patent number:WO2004026871

[8] E. C. Constable, M. D. Ward, *J. Chem. Soc. Dalton*, **1990**, 1405-1409

[9] A. Harriman, R. Zissel, *Chem. Commun.*, **1996**, 1707-1716

[10] S. Ott, M. Borgström, M. Kritikos, R. Lomoth, J. Bergquist, B. Åkermark, L. Hammarström, L. Sun, *Inorg. Chem.*, **2004**, 43, 4683-4692

[11] A. C. Benniston, G. Chapman, A. Harriman, M. Mehrabi, C. A. Sams, *Inorg. Chem.* **2004**, 4227-4233

[12] J. H. Price, A. N. Williamson, R. F. Schramm, B. B. Wayland, *Inorg. Chem.,* **1972**, 1280-1284

Annex

Crystal data and X-ray experimental details for **51**, **53**, **55**, **56**, **57**, **58**, **59**, **86** and **89**.

Compound	51	53	55
Empirical formula	$C_{31} H_{21} Cl_3 N_6$	$C_{34} H_{29} CuI N_4 O_2$	$C_{32} H_{27} Cu I N_6 O_2$
Formula weight	556.8	716.1	710.9
Temperature (K)	153(2)	153(2)	153(2)
Crystal system	Monoclinic	Orthorhombic	Monoclinic
Space group	P2(1)/c	P2(1)2(1)2(1)	C2/c
Unit cell dimention : a(Å)	14.6414(10)	12.7988(6)	24.1537(10)
b (Å)	10.4844(7)	14.7483(8)	17.4806(7)
c (Å)	19.5384(14)	16.0193(8)	18.6287(8)
α (°)	90	90	90
β (°)	106.2640(10)	90	119.7180(10)
γ (°)	90	90	90
Volume (Å^3)	2879.2(3)	3023.8(3)	6830.9(5)
Z	4	4	8
Density (calculated) (Mg/m^3)	1.285	1.573	1.383
Absorption coefficient (mm^{-1})	0.346	1.781	1.578
F(000)	1144	1436	2816
Crystal size (mm)	0.50 x 0.34 x 0.03	0.24 x 0.16 x 0.14	0.23 x 0.09 x 0.04
Theta range for data collection (°)	2.17 to 26.50	1.88 to 26.00	1.63 to 26.00
Reflections collected	30618	26326	29319
Independent reflections [R(int)]	5968 [0.0436]	5937 [0.0596]	6717 [0.0611]
Data / restraints / parameters	5968 / 0 / 389	5937 / 0 / 382	6717 / 0 / 430
Goodness-of-fit-on F^2	1.014	1.088	1.095
R_1[I>sigma(I)]	0.0462	0.0516	0.0730
wR$_2$ (all data)	0.1298	0.1097	0.1926

213

Compound	56	57	58
Empirical formula	$C_{30} H_{21} Cd_{2.5} N_6 O_9 S_2$	$C_{33} H_{26} N_7 O_{10} La$	$C_{33} H_{26} N_7 O_{10} Sm$
Formula weight	881.4	819.5	830.9
Temperature (K)	153(2)	153(2)	153(2)
Crystal system	Monoclinic	Monoclinic	Monoclinic
Space group	P2(1)/c	P2(1)/n	P2(1)/n
Unit cell dimention : a(Å)	19.4056(11)	13.2519(7)	13.1965(7)
b (Å)	16.6093(10)	12.6230(7)	12.6021(7)
c (Å)	18.0559(11)	20.0837(11)	19.9641(10)
α (°)	90	90	90
β (°)	93.3660(10)	92.8010(10)	92.9770(10)
γ (°)	90	90	90
Volume ($Å^3$)	5809.6(6)	3355.6(3)	3315.6(3)
Z	4	4	4
Density (calculated) (Mg/m^3)	1.008	1.622	1.665
Absorption coefficient (mm^{-1})	0.837	1.342	1.841
F(000)	1736	1640	1660
Crystal size (mm)	0.51 x 0.49 x 0.46	0.47 x 0.41 x 0.21	0.44 x 0.27 x 0.27
Theta range for data collection (°)	1.05 to 25.00	1.80 to 27.00	1.81 to 27.50
Reflections collected	60140	38826	35004
Independent reflections [R(int)]	10229 [0.0238]	7318 [R0.0252]	7606 [0.0238]
Data / restraints / parameters	10229/162/628	7318 / 0 / 464	7606 / 0 / 463
Goodness-of-fit-on F^2	3.276	1.231	1.057
R_1[I>sigma(I)]	0.1053	0.0328	0.0255
wR_2 (all data)	0.3596	0.0798	0.0706

Compound	59	86	89
Empirical formula	$C_{33} H_{24} Cl_2 La N_7 O_9$	$C_{54} H_{38} Cl_9 N_3$	$C_{73} H_{79} Cl_4 N_3$
Formula weight	872.4	1047.9	1140.2
Temperature (K)	153(2)	153(2)	153(2)
Crystal system	Monoclinic	Monoclinic	Triclinic
Space group	P2(1)/c	P2(1)/n	P-1
Unit cell dimention : a(Å)	19.4694(13)	11.5279(5)	12.2579(7)
b (Å)	9.5041(6)	17.3151(8)	16.5216(9)
c (Å)	19.0269(12)	25.3288(12)	18.2312(10)
α (°)	90	90	66.3110(10)
β (°)	102.3720(10)	95.0820(10)	70.3760(10)
γ (°)	90	90	76.7660(10)
Volume (Å^3)	3439.0(4)	5035.9(4)	3165.7(3)
Z	4	4	2
Density (calculated) (Mg/m^3)	1.685	1.382	1.196
Absorption coefficient (mm^{-1})	1.463	0.541	0.231
F(000)	1736	2144	1212
Crystal size (mm)	0.49 x 0.21 x 0.04	0.39 x 0.38 x 0.27	0.45 x 0.37 x 0.20
Theta range for data collection (°)	2.14 to 26.00	1.61 to 26.50	1.77 to 26.00
Reflections collected	38454	44768	31713
Independent reflections [R(int)]	6757 [0.0405]	10440 [0.0285]	12437 [0.0297]
Data / restraints / parameters	6757/0/469	10440/0/595	12437/0/721
Goodness-of-fit-on F^2	1.117	1.035	1.076
R_1[I>sigma(I)]	0.0502	0.0595	0.0801
wR$_2$ (all data)	0.1279	0.1707	0.2070